Université de Montréal

Surfaces nanostructurées et stimulables à base de poly-(*N*-isopropylacrylamide) : Synthèse et caractérisation

Par

Alberto Guerron

Faculté de Pharmacie

Thèse présentée en vue de l'obtention du grade de *philosophiae doctor* (Ph.D.)

en Sciences Pharmaceutiques, option Technologie Pharmaceutique

Décembre 2021

Université de Montréal

Faculté de Pharmacie

Cette thèse intitulée :

Surfaces nanostructurées et stimulables à base de poly-(*N*-isopropylacrylamide) : Synthèse et caractérisation

Présenté par

Alberto Guerron

A été évaluée par un jury composé des personnes suivantes :

Prof. Xavier Banquy
Président-rapporteur

Prof. Suzanne Giasson
Directeur de recherche

Prof. Simon Matoori
Membre du jury

Prof. Rafik Naccache
Examinateur externe

Résumé

Les revêtements polymères stimuli-sensibles permettent d'ajuster les propriétés de surface par des stimuli externes (i.e. des variations des conditions environnementales) via des changements dans leur conformation physique, la chimie de surface, ou les deux. Cette capacité permet leur utilisation comme éléments fonctionnels dans les nanotechnologies tels que des valves dans les dispositifs microfluidiques, comme lubrifiants, ou comme substrats pour la culture de tissus biologiques. Cependant, de tels revêtements souffrent généralement d'un inconvénient majeur, afin de déclencher un changement de la conformation physique du revêtement polymère (gonflement) via un stimulus, il est nécessaire de changer au moins une de ses propriétés physico-chimiques qui produit des variations simultanées des propriétés de surface (i.e. potentiel de surface, adhésion). Ce travail vise à surmonter cette limitation en étudiant une nouvelle génération de revêtements hiérarchiques fonctionnels dont les propriétés physiques et la chimie de surface peuvent être modulées indépendamment et de manière réversible en utilisant différents stimuli tels que la température et le pH. Les revêtements hiérarchiques sont constitués de matrices des microgels à base de poly-(*N*-isopropylacrylamide) bidimensionnelles fonctionnalisés en surface avec des polymères dont les dimensions caractéristiques et les propriétés de surface peuvent être contrôlées indépendamment par différents stimuli en fonction des propriétés de surface souhaitées. Ce travail démontre que les dimensions caractéristiques (i.e. diamètre hydrodynamique, épaisseur de couche) peuvent en effet être contrôlées sans affecter les propriétés de surface (i.e. potentiel de surface, adhérence) des réseaux de microgels fonctionnalisés. La réactivité des revêtements fonctionnels a été étudiée à l'aide de la Diffusion

Dynamique de la Lumière et de l'Appareil de Forces de Surface permettant de déterminer avec précision l'adhésion, la friction, le potentiel de surface, le diamètre hydrodynamique et l'épaisseur de la couche sous différents stimuli. Enfin, la capacité de ces substrats fonctionnels pour produire un détachement cellulaire déclenché par des stimuli dans le cadre de la culture cellulaire a été étudiée.

Mots-clés : Surface, revêtement polymère, matériel fonctionnel, microgel, culture cellulaire.

Abstract

Stimuli-responsive polymer coatings enable surface properties to be tuned by external stimuli (i.e. variations of environmental conditions) via changes in their physical conformation, surface chemistry, or both. This capacity enables their use as functional elements in nanotechnologies such as valves in microfluidic devices, as lubricants, or as substrates for culture of biological tissues. However, such coatings usually suffer from a major shortcoming, in order to trigger a change in the physical conformation of the polymer coating (swelling) via a stimulus, it is necessary to change at least one of its physicochemical properties which results in simultaneous variations of the surface properties (i.e. surface potential, adhesion). The present work aims to overcome this limitation by investigating a new generation of responsive hierarchical coatings whose physical properties and surface chemistry can be tuned independently and reversibly using different stimuli such as temperature and pH. The hierarchical coatings consist of two-dimensional poly-(*N*-isopropylacrylamide) microgel arrays surface-functionalized with polymers whose characteristic dimensions and surface properties can be independently controlled by different stimuli according to the desired surface properties. This work shows how the characteristic dimensions (i.e. hydrodynamic diameter, layer thickness) can indeed be controlled without affecting the surface properties (i.e. surface potential, adhesion) of the functionalized microgel arrays. The responsiveness of the functional coatings was investigated using Dynamic Light Scattering and the Surface Forces Apparatus allowing adhesion, friction, surface potential, hydrodynamic diameter, and layer thickness to be accurately determined under different stimuli.

Finally, the ability of these coatings as functional substrates to produce stimuli-triggered cell detachment during cell culture was studied.

Keywords : Surface, polymer coating, responsive material, microgel, cell culture.

Table of Contents

List of Tables

List of Figures

List of symbols and abbreviations

μ	Coefficient of friction
16-MHA	16-Mercaptohexadecanoic acid
3-MPA	3-Mercaptopropionic acid
AEMH	2-aminoethylmethacrylate hydrochloride
AFM	Atomic force microscopy
ANOVA	Analysis of variance
ATR-FTIR	Attenuated total reflection Fourier transform infrared
ATRP	Atom transfer radical polymerization
AUTES	11-aminoundecyltriethoxysilane
BCS	Bovine calf serum
BPNPs	Black phosphorus nanoparticles
BSA	Bovine serum albumin
BTA	1H-benzotriazole
D	Separation distance
d	Hydrodynamic diameter
DDS	Drug delivery systems
DLS	Dynamic Light Scattering
DMA	*N,N'*-dimethylacrylamide
DMEM	Dulbecco's modified eagle medium
DMF	Dimethylformamide
DMSO	Dimethylsulfoxide
DNA	Deoxyribonucleic acid

DSC	Differential scanning calorimetry
EBP	Electron beam polymerization
ECHETES	2-(3,4-epoxycyclohexyl)ethyltrimethoxysilane
ECM	Extracellular matrix
EDC	*N*-(3-dimethylaminopropyl)-*N'*-ethylcarbodiimide
EDTA	Ethylenediaminetetraacetic acid
EMT	Epithelial-mesenchymal transition
EPR	Enhanced permeability and retention
FBS	Fetal bovine serum
FECO	Fringes of Equal Chromatic Order
F_N	Normal force
F_S	Friction force
G	Gibbs free energy
GLA	Glutaraldehyde
H	Enthalpy
HPAM	*N*-2-hydroxyethylmethacrylamide
ITCN	Image-based tool for counting nuclei
k	Spring constant
LCST	Lower critical solution temperature
MBA	*N,N'*-methylene-*bis*-acrylamide
MCT	Mercury-cadmium-telluride
Microgel-co-PDMAEMA	PNIPAM microgels surface-functionalized with PDMAEMA
Microgel-co-PEG	PNIPAM microgels surface-functionalized with PEG
MN	Microneedles

MWCO	Molecular weight cut-off
n_{medium}	Refractive index of the medium
n_{mica}	Refractive index of mica
NHS	*N*-hydroxysuccinimidyl
NIPAM	*N*-isopropylacrylamide
NIR	Near infrared
NMP	Nitroxide-mediated polymerization
NMR	Nuclear magnetic resonance
PAA	poly(acrylic acid)
PBS	Phosphate-buffered saline
PDEAM	poly(*N,N'*-diethylacrylamide)
PDMAEMA	poly(*N,N'*-dimethylaminoethylmethacrylate)
PDMAEMA-COOH	Carboxy terminated poly(N,N'-dimethylaminoethylmethacrylate)
PDMS	Polydimethylsiloxane
PECAM-1	Platelet endothelial cell adhesion molecule-1
PEG	Polyethylene glycol
PEG-COOH	α-Carboxy ω-Hydroxy terminated polyethylene glycol
PEGMA	Polyethylene glycol methyl ether methacrylate
PEG-NHS	Methoxy polyethylene glycol succinimidyl carboxymethyl ester
$pH\text{-}Q_{imm}$	pH-triggered swelling capacity of immobilized microgels
$pH\text{-}Q_{susp}$	pH-triggered swelling capacity of microgels in suspension
PI	Polydispersity index
pK_a	Acid dissociation constant
PLA	Polylactic acid

PMAA	poly(methacrylic acid)
PNIPAM	poly(*N*-isopropylacrylamide)
PVCL	poly(*N*-vynilcaprolactone)
PVP	poly(vynil pyridine)
R	Silica disk curvature radius
RAFT	Reversible addition-fragmentation chain transfer
RDRP	Reversible deactivation radical polymerization
RGD	Arginine-glycine-aspartate
S	Entropy
s	Seconds
SAM	Self-assembled monolayer
SFA	Surface Forces Apparatus
SI	Surface Initiated
SPR	Surface plasmon resonance
TEA	Triethanolamine
TGA	Thermogravimetric analysis
$T\text{-}Q_{imm}$	Thermo-triggered swelling capacity of immobilized microgels
$T\text{-}Q_{susp}$	Thermo-triggered swelling capacity of microgels in suspension
UV	Ultraviolet
V50	2,2'-azobis-(2-methylpropylacrylamide)
VPTT	Volume phase transition temperature
W	Interaction energy
ζ	Zeta potential
θ_w	Water contact angle

λ	Wavelength

Remerciements

Je souhaite d'abord remercier ma directrice de recherche, Prof. Suzanne Giasson, pour m'avoir accueilli dans son laboratoire et qui m'a permis de travailler dans un projet qui me passionne.

Je voudrais également remercier les membres de mon comité consultatif, Prof. Xavier Banquy et Prof. Grégoire Leclair pour leurs conseils et encouragements qui m'ont donné de nouvelles perspectives sur le projet et qui m'ont permis d'avancer dans mes travaux.

Je souhaite exprimer toute ma gratitude aux membres du Jury, Prof. Xavier Banquy, Prof. Simon Matoori, et Prof. Rafik Naccache pour accepter d'évaluer ce manuscrit.

Je souligne également la précieuse contribution des coauteurs des publications incluses dans cette thèse. Prof. Valérie Gaëlle Roullin et Prof. Davide Brambilla pour leurs excellents conseils, discussions et soutiens techniques et matériels. Huu Trong Phan pour les expériences réalisées par SPR. Je suis très reconnaissant de l'aide accordé par Carolina Peñaloza-Arias pour sa disponibilité et sa patience lors de ma formation dans les techniques de culture cellulaire.

Je souhaite remercier Dre. Sylvie Descartes pour m'avoir accueilli dans son laboratoire à l'Institut National des Sciences Appliquées de Lyon. Je voudrais aussi remercier Dr. David Albertini pour avoir partagé avec moi ses exceptionnelles connaissances de la technique AFM.

Je souhaite remercie aussi les membres du groupe du Prof. Suzanne Giasson : Charly Ou, Huu Trong Phan, Laurence St-Pierre. Merci pour votre support technique au laboratoire mais encore plus pour votre amitié

et camaraderie qui m'ont encouragé tout au long de mes études. Je reconnais aussi les contributions des anciens membres du groupe. Dr. Pierre Vialar-Trarieux pour le travail qu'il a réalisé avec les microgels avant mon arrivée au groupe. Prof. Xavier Banquy, Dre. Lucie Giraud et Dr. Benoît Liberelle, qui ont mis à point plusieurs protocoles au laboratoire que j'ai pu utiliser dans le cadre de cette thèse. Un très grand merci à Dr. Changsheng Wang, pour son aide précieuse avec la technique SFA. Je remercie aussi les stagiaires qui ont travaillé au sein de notre groupe.

J'adresse mes remerciements à la Faculté de Pharmacie et au Département de Chimie de l'Université de Montréal. En Pharmacie, je tiens à souligner le soutien d'Andrée Mathieu et de l'Axe de Formulation et Analyse du Médicament. Au Département de Chimie, je remercie Patricia Moraille, Prof. Christian Pellerin, Prof. Julian Zhu et le Laboratoire de Caractérisation des Matériaux Polymères. Je veux exprimer ma gratitude aux membres de l'atelier de mécanique et d'électronique : Martin Lambert, Jean-Sébastien Meyer, Jean-François Myre, Louis Beaumont et Michel Brunette. Je remercie mes amis en Pharmacie et en Chimie : Yann, Guillaume, Pierre, Abdel, Sébastien, Cloé, Alfonso, Araceli, Anaëlle, Jean-Michel, Jordan, Hu, Pierre-Luc et à ma chère amie, collègue et partenaire d'escalade Margaux.

Merci à ma famille pour leur support inconditionnel. En particulière à mon père, Luis, et ma tante, Maria qui m'ont toujours appuyé et encouragé. Merci à mes sœurs et mon frère. Merci à Martin, Brendan, Marc et Camilo.

En fin, je remercie la personne la plus importante dans ma vie. Paule, merci de toujours m'accompagner et m'encourager. Ce travail n'aurait jamais été possible sans toi.

Chapter 1 – Introduction

1.1 Stimuli-Responsive Surfaces

Response to stimulus is a basic function of living systems. Indeed, living organisms have successfully adapted to specific, and often extremely harsh, environments through millions of years that enable them to survive and thrive. To sustain life, nature has developed complex molecular assemblies and interfaces with specific chemical function and structure which are able to respond to changing conditions in their surroundings. Examples in nature of surfaces and interfaces that exhibit an stimuli-responsive behavior are abundant. Echinoderms show light-responsiveness by changing the colour of their skin at night.[1] Chameleons posses an exceptional camouflage ability that enables them to adapt the patterns and colours of their skin according to their surroundings to hide from predators.[2] But perhaps a more relatable example, at least to all the readers of this text, is the multi-stimuli-responsiveness of the human skin.

The human skin is a multi-layered structure that responds to variations in the environment such as temperature, pressure, light, and the presence of microorganisms. Skin is the largest organ that humans posses, an average-sized person has 1.8 m^2 of skin which weights, on average, 4 kg.[3] The skin is composed of several layers, a basal dermis layer of connective tissue that contains the blood vessels, hair follicles and sweat glands and an upper epidermis made up of epithelial cells and pigmented melanocytes.[4] The skin is also one of the most versatile organs in the body. It is capable of maintaining a temperature of approximately 32 °C (depending on age, sex and weight) by responding to temperature variations via the secretion of sweat, if the temperature rises, or through the erection of the hairs of the skin to keep a layer of warm air close to the skin in cold

environments.[5] Its elastic nature makes it resistant to shock, pressure and deformation while maintaining its original shape.[3] It also plays a metabolic role by synthesizing vitamin D when exposed to UV irradiation, which is vital for ossification and production of testosterone.[3] Further, the skin is able to perceive physical stimuli and transmit it to the brain through an intricate network of sensorial receptors.[3] Because the responsive structure of human skin (and other creatures found in nature) is composed of bio-macromolecules or bio-polymers such as collagen, proteins, polysaccharides and nucleic acids, considerable effort has been dedicated to replicating these structures in the laboratory.

Scientists have focused on the synthesis of polymers that mimic biopolymers to develop a variety of materials that serve industrial and scientific applications. Ideally, synthetic polymers should exhibit abilities beyond providing structural support, such as mediating an active and dynamic participation between the material and its surroundings. To do so, it is possible to incorporate multiple functional groups in the polymer structure that are susceptible to change in character (e.g. charge, polarity, conformation) in response to small changes in environmental conditions and are synergistically amplified to produce significant differences in the macroscopic properties of materials. However, specific challenges exist in mimicking biological systems, where structural and compositional gradients across wide length scales are necessary to obtain coherent and deliberate behaviors.

1.2 Surface functionalization with polymers

Polymers offer an expansive range of surface functionalization possibilities seemingly limited only by the imagination. In fact, polymers are ubiquitous in products used everyday such as rubber and are also major components of living beings because polymers make up DNA and diverse types

of proteins.[6] Theoretical research into polymeric materials began in earnest in the 19th and 20th centuries with the recognized polymeric nature of rubber used during the industrial revolution.[7] Fundamental knowledge on the field was later established with Staudinger's macromolecular theory which established that polymers are composed of many elementary units (monomers) covalently bound together and was further supported by experiments performed by Carothers who first synthesized nylon.[8–10] The motivation behind using polymers for surface modification is the ability to customize the surface properties in a specific and sophisticated manner according to the required application. In other words, the wide commercial availability as well as widespread knowledge of polymerization pathways of a plethora of polymeric compounds allow making a choice that takes into consideration the desired properties of the final material such as porosity of the structure,[11,12] wettability,[13–15] chemical and biological stability,[16–18] mechanical[19–21] and thermal resistance[22,23] as well as biocompatibility and biodegradation characteristics.[24–26] Further, different approaches are available to immobilize polymers on different types of surfaces according to the properties of the substrate and the characteristics of the polymer layer that are needed.

The main methods for functionalizing the surface of substrates with polymeric materials are "grafting to", "grafting from", and "grafting through" techniques. The "grafting to" approach takes advantage of reactive sites on the surface to directly attach a polymer chain onto a substrate. "Grafting to" can be applied either through chemisorption by forming a chemical bond between reactive sites on the surface of the substrate and a reactive functional group on the polymer, or by physisorption via physical interactions. A typical example of surface functionalization by using "grafting to" via chemisorption involves polymers end-functionalized

with sulfur atoms to form covalent attachments of thiols and disulfides groups to metal surfaces such as Ag, Au, and Cu through metal-thiolate bonds.[27–30] Moreover, it is also possible to form covalent bonds between organic groups and metal surfaces through metal-carbon linkages using aryl diazonium, as well as metal-carbene and metal-nitrene π bonds formed via diazo derivatives or metal-acetylide and metal vinylidene bonds formed with acetylene derivatives.[30] However, the "grafting to" approach does not provide high surface coverage of the polymers due to the steric hindrance that arises from the presence of polymers chains already attached to the surface that prevent the diffusion of other polymer chains close to the remaining reactive sites on the substrate.[31] Similarly, if the polymer chain has several functional groups able to form bonds or attractive interactions with the substrate, it is unlikely that polymer chains are immobilized in a direction orthogonal to the surface but are rather deposited lengthwise on the substrate and thus occupy additional space and increase the steric hinderance. During "grafting to" through physisorption, polymer immobilization happens via physical interactions such as electrostatic, van der Waals or dipole attractions. This method is relatively simpler than chemisorption, however, since no covalent bonds are formed with the surface the grafting stability is weaker.[32,33]

The "grafting from" immobilization approach involves immobilizing initiators on a surface and growing polymer chains from them. This process is also called surface initiated (SI) polymerization. Several polymerization pathways may be applied in this technique; mainly, reversible deactivation radical polymerization (RDRP), reversible addition-fragmentation chain transfer (RAFT), nitroxide-mediated polymerization (NMP) or atom transfer radical polymerization (ATRP).[34] The advantage of this technique over the "grafting to" methodology is that it is possible to obtain a densely packed polymer layer on the surface.[35–38] It is also a viable

method to fabricate multilayered core/shell architectures on nanoparticles with customizable polymer layer thicknesses.[34] Finally, in the "grafting through" approach, monomers are covalently bound to the surface and are copolymerized with free monomers in solution to form a homogeneous and continuous layer whose thickness can be adjusted by regulating the conditions of the polymerization process and the density of monomers initially anchored to the surface.[39–41] One of the most powerful aspects of polymer functionalization of substrates is the ability to create responsive materials for which one or more properties can be modulated by external stimuli.

1.2.1 Stimuli-responsive polymers

Responsive polymers can modulate their physical and/or chemical properties through changes in their surrounding environment. These polymers, also known as smart or intelligent materials, respond to a variety of stimuli such as variations in the pH,[42] light irradiation,[43] the presence of small molecules and biomolecules[44,45] or temperature[46,47] depending on their physicochemical properties. Inspiration for progress in polymer science has often been provided by observations in the natural world. For example, the exceptional lubrication and load-bearing capacity provided by the synovial fluid in mammalian articulations, which is mainly composed of the polymers hyaluronic acid and lubricin.[21,48] Nonetheless, replicating the outstanding performance of these naturally occurring structures in the laboratory is no simple task given the complexity of physical arrangements as well as the constant and subtle interplay with the environment that surround them. To confront some of these challenges, the development of stimuli-responsive polymers focuses on creating networks capable of inducing minimal molecular, yet orchestrated changes that lead to significant and specific physicochemical responses to external stimuli.

The design of polymeric materials considers the energetic and spatial restrains involved in producing a response from a polymer. For instance, the mobility of the segments of a polymer chain is higher in suspension, compared to immobilized on surfaces, or crosslinked to form gels, due to increasing spatial restrictions.[49] Segment interactions within these spatial restrictions determine the energy requirements of the system to undergo a transition from an initial state to a final state upon applying a stimulus. For polymers suspended in solution, stimuli-triggered responses are easy to achieve due to favorable energy inputs from Brownian motion that positively contribute to the displacement of solvent molecules from the polymer segments.[50] The phase separation of polymer chains across the lower critical solution temperature (LCST) serves as an example. At temperatures below the LCST, favorable hydrogen-bonding between the polymer and the solvent produce a negative free energy ($\Delta G < 0$) and homogeneous mixing.[51] On the contrary, above the LCST, phase separation takes place as the enthalpy (ΔH) overcomes the entropic energy (ΔS) contribution and results in unfavorable free energy for the system which phase-separates. Linear polymers anchored to a surface by one end of the chain (as may take place with the "grafting to" and "grafting from" methods) experience different restrictions to their freedom of movement along the chain. Thus, segments closer to the anchoring point need a higher energy input to undergo stimuli-triggered responses because less space and free volume are available to do so compared to segments further from the surface which have more energetically favorable freedom of movement for rearrangement. Stimuli-triggered responsiveness of end-anchored polymer chains is an entropic process (ΔS) where the disorder of the anchored chains has a more significant contribution to the free energy (ΔG) than the conformational variations produced from changes in enthalpy (ΔH).[52] Stimuli-responsive gels

synthesized from polymers undergo physicochemical changes triggered by variations in the conditions of the environment in a similar manner than end-grafted polymer chains (ΔS contributes to ΔG to a greater extent than ΔH). The reason is that gels are usually crosslinked either by chemical (through covalent bonds)[53] or physical (via hydrogen-bonding, hydrophobic, van der Waals or $\pi - \pi$ stacking interactions)[54] means to retain their structural integrity and which restrain the mobility of the polymer segments when a stimulus is applied. Once that energy considerations involved in the polymer response are established, it is possible to consider the different types of stimuli that can be used to obtain a desired behavior.

Due to the wide variety of functional groups that can be incorporated into polymer segments it is possible to obtain versatile structures that respond to single or multiple triggers either punctually or in a gradient. However, in this section only a few of these triggers are discussed: variations in pH, light irradiation, and temperature. pH-responsive polymers have ionizable functional groups in their structures which allows them to donate or accept protons upon sensing pH changes in the surrounding environment. By changing the degree of ionization, the electrostatic repulsions along the polymer chain vary, which influences the hydrophobicity of the polymer as it extends or collapses via the approach or separation of the backbone segments of the chain.[55–60] pH-responsive polymers can be divided into two categories: polyacids and polybases. Polyacids have pK_a values of roughly 5 and donate protons to the surrounding solution and swell under basic pH conditions.[55–60] Some examples of polyacids include poly(acrylic acid) (PAA) and poly(methacrylic acid) (PMAA). On the contrary, polybases accept protons from the surrounding solution and extent under acidic pH conditions. Some of the most used polybases contain amino groups, such as poly(*N,N'*-dimethylaminoethylmethacrylate) (PDMAEMA) or in poly(vinyl pyridine) (PVP).

Additionally, polymers containing acetal/ketal functional groups may also be categorized as pH-sensitive, although their pH-responsive mechanism takes place via linkage cleaving rather than by changes in ionization.[61–63] Photo-responsive polymers contain photo-chromic functional groups in their structures that allow them to respond to light irradiation through three main mechanisms. The most widely known photo-responsive molecule is azobenzene, which undergoes a trans-to-cis photoisomerization upon light irradiation that induces a photo-chromic transition.[64] Light irradiation may also produce shrinking and extending through ionization-mediated molecular rearrangements, as it happens with lecuo and spiropyran derivatives.[65–67] The final photo-responsive mechanism takes place through dimerization, for example, with the photo-reactive molecule cinnamate which dimerizes upon being exposed to UV irradiation.[68,69] Controlling polymer responses through pH and irradiation offers the means to develop versatile smart materials.

Thermo-sensitive polymers are a useful choice when developing smart materials because temperature can be controlled internally (within the polymer network) or externally (by changing the temperature of the surrounding environment) allowing polymers to respond in either a localized or generalized fashion. Some polymers exhibit an LCST, which is the lowest temperature at which temperature-induced mixing occurs. Below a certain temperature, polymer chains and solvent molecules are in a single homogeneous phase whereas above it, phase separation driven by entropy takes place. Several polymeric molecules exhibit an LCST, such as: poly(*N*-vynilcaprolactone) (PVCL), poly(*N,N'*-diethylacrylamide) (PDEAM) or PDMAEMA.[70–72] However, the most widely studied thermo-responsive polymer is poly-(*N*-isopropylacrylamide) (PNIPAM) that exhibits an LCST at roughly 32 °C which is conveniently close to the physiological

temperature.[73] In fact, the reason behind the predominance of PNIPAM in the development of smart materials is its wide commercial availability and relative ease to modulate its properties by incorporating different monomers in its structure. For example, incorporating hydrophilic or hydrophobic monomers into the PNIPAM chains allows to either rise or decrease the LCST of the resulting polymer, respectively.[74,75] Similarly, additional stimuli-responsive monomers can be incorporated in PNIPAM chains to obtain multi-stimuli responsive polymers, e.g., thermo- and pH-responsive materials.[46,76,77] Further, the extensive amount of research involving PNIPAM (including in our research group)[78–80] provides a solid foundation of acquired knowledge on the properties and responsive behavior of PNIPAM to build upon. These reasons illustrate the rational behind the decision of selecting PNIPAM as the keystone polymer of the present work.

1.2.3 Remarks on the properties of poly(*N*-isopropylacrylamide)

PNIPAM is synthesized by radical polymerization from the *N*-isopropylacrylamide (NIPAM) monomer, which was first prepared in the 1950's.[81,82] This molecule has a vinyl group in its structure that enables polymerization, an amide functional group that gives the molecule a hydrophilic character and makes it water-soluble, and an isopropyl group that provides the molecule with its hydrophobic properties. Once the NIPAM monomer is polymerized, the thermo-responsive properties of PNIPAM are govern by the interactions between the amide and isopropyl functional groups and the water molecules in the solvent. These interactions are directed by the energy considerations mentioned previously, whereby the solubility of PNIPAM changes across the LCST. In other words, at temperatures below the LCST, hydrogen bonding interactions between water molecules and the amide function are favorable and the polymer is soluble while at temperatures above the LCST the hydrogen bonds become partially disturbed, which makes

the hydrophobic character of the isopropyl groups more dominant as the polymer chains fold into themselves during the coil-to-globule transition and the mixture phase-separates.[83–89] Nonetheless, the transition to the hydrophobic state is not absolute, even at temperatures well beyond the LCST, because the amide groups retain some of their hydrophilic functionality.[90] The LCST is often determined by finding the cloud point of the polymer suspension and the endothermic transition peak by differential scanning calorimetry;[91,92] however, the transition is also closely dependant on the mass fraction of the polymer in solution.[73] Moreover, for PNIPAM chains arranged in an ordered network such as in hydrogels or microgels, the change of phase is referred to as the Volume Phase Transition Temperature (VPTT) which also depends on the concentration.[83–89] The LCST and VPTT are often used interchangeably in the literature, probably because, at low polymer concentrations, both take place within a similar temperature range.[93,94] Nonetheless, in the context of this work it is important to make this distinction given that the entirety of the study was performed using PNIPAM microgels. Therefore, the characteristics of the different conformations that PNIPAM may adopt during synthesis must be addressed.

The method of preparation of PNIPAM and its final conformation have a significant impact on the properties and responsive behavior of the product. Linear PNIPAM chains have been prepared by several methods, including free radical polymerization in aqueous[89,95–98] as well as organic solutions[99–101], via redox in aqueous media,[102–104] by ionic polymerization,[105] or by ionizing radiation-induced polymerization.[106,107] In addition to linear chains, the conformation of PNIPAM can be arranged into ordered networks to create hydrogels, microgels, thin films or membranes. However, the most common conformations of PNIPAM found in the literature (aside from linear chains) are in the form of hydrogels and microgels due to their exceptional customizability,

capacity to carry and transport payloads within the polymer network, and fine-tuned multi-responsive properties.

In general, stimuli-responsive gels are formed by physical and/or chemical crosslinking of polymer chains and are described as semi-solid materials used to immobilize a solvent within their networks. Gels can be further classified according to the nature of the solvent they retain: organogels contain organic solvents while hydrogels hold aqueous solvents due to the hydrophilic nature of its polymeric components.[108] Moreover, hydrogels may be synthesized in the form of spherical particles denominated nanogels if their diameter is less than 100 nm; microgels for diameters between 100 nm and 100 µm and macrogels for diameters greater than 100 µm.[109] The diffusion rate for a spherical particle is inversely proportional to the diameter according to the Stokes-Einstein diffusion principle, and the time required for a stimulus to reach the centre of a gel sphere is proportional to the square of the diameter.[109–112] Therefore, nanogels provide the fastest response time when exposed to a stimulus but are more challenging to manipulate and analyse precisely because of their small size. Consequently, microgels represent a practical compromise between ease of manipulation and response time. Another advantage of microgels over hydrogels is the ability to immobilize discrete particles on a surface (as opposed to a continuous layer) via physisorption or chemisorption. In fact, if a continuous hydrogel layer immobilized on a substrate sustains damage through applied mechanical force, it is likely to propagate throughout the polymer layer,[113] as opposed to a microgel coating where the damage may be contained to single microgels or a reduced number of neighboring microgel particles.[42] The swelling behavior of PNIPAM hydrogels and microgels may be controlled via temperature variations in a similar manner than linear chains; however, due to the more restricted mobility of

the polymer chains (due to the crosslinking in the polymer network), the energy requirements vary slightly and according to the considerations mentioned previously. Finally, the phase transition across the VPTT may produce changes to the properties of the PNIPAM microgels other than the associated hydrophilicity. For example, as the microgels shrink with increasing temperature, the refractive index of the microgels approaches that of the polymer as water is expelled from the network,[84] the elasticity of the particles changes as the Young's modulus increases,[87] and (in the case of functionalized PNIPAM microgels) the density of functional groups at the surface increases, which could result in more significant electrophoretic mobilities in ionizable microgels.[96]

1.2.4 Remarks on the properties of polyethylene glycol (PEG)

Polyethylene glycol (PEG) is a benchmark in polymer science and a polymer of choice in biomedical applications. Even though PEG is not a stimuli-responsive polymer, the properties that it imparts to functional materials make it extremely useful and a centrepiece of this project. Its importance is due to its high structural flexibility, amphiphilicity and high hydration capacity.[114] PEGs were first synthesized in the 1850's via cationic or anionic polymerization (depending on the catalyst type) of ethylene glycol and a century later they had become commonplace in applications ranging from anti-freeze, lubricants for medical devices, food additives, laxatives and for coatings destined for dermatological applications, suppositories, tablets and pills.[115] Starting in the 1970's the term PEGylation began being used to refer to the conjugation of PEG to biomolecules or immobilized on the surface of nanoparticles or bioimplants.[116] Even though PEG is usually recognized as a biocompatible molecule, PEG can undergo oxidation in biological

environments and fluids which limit its long-term use.[117,118] Similarly, PEG may also accumulate in healthy cells and compromise their viability.[115,119]

Because of the repeating ethylene oxide units, the backbone of PEG is highly polar which increases the hydrophilicity of the polymer chain and makes it soluble in most organic and inorganic solvents.[120] PEG has traditionally been used for protein and nucleic acid purification;[121,122] conjugation with proteins[123,124] and for drug delivery systems.[124–128] Further, non-specific adsorption of biomolecules on nanoparticles and biomedical implants may adversely affect the chemistry of conjugated drugs, or cause aggregation or charge neutralization which typically leads to the removal of the nanoparticles from the bloodstream.[129–131] A potential solution to this challenge is immobilizing PEG chains on the surface of nanoparticles which has been shown to improve solubility and increase retention and circulation time.[129–131] Immobilizing PEG chains on the surface of such materials also provides anti-fouling properties via steric hinderance that repels proteins from the surface as well as by making the interphase of the material electrically neutral and thus reducing the electrostatic interactions with the charged proteins.[132–134] Additionally, because of its hydrophilic nature, immobilizing PEG chains on a surface creates a hydration layer difficult to displace and which inhibits protein deposition.[135] The presence of a hydration layer at the surface is also useful in tribological studies, whereby it is possible to reduce friction and wear between two PEG-functionalized surfaces in shear via aqueous lubrication.[136,137]

1.3 Selected applications of PNIPAM in biomedicine

The popularity and commercial availability of PNIPAM in its different polymeric conformations have translated into widespread use in diverse fields such as biomedicine, surface engineering, microfluidics, or photonics. Introducing the myriad of applications that PNIPAM may be used for

is beyond the scope of this work. Instead, some examples within the most relevant fields of interest of this project are discussed. Hence, this section presents some examples of applications of PNIPAM to drug delivery systems, lubrication applications and cellular culture.

1.3.1 Drug delivery applications involving PNIPAM

A stimuli-responsive polymeric vehicle suitable for delivery of therapeutic agents in the body must conform to conditions found in biological environments or *in vivo*. Ideally, the system must be easy to deliver; capable to carry payloads to a specific site and to release it in response to a stimulus; and be composed of non-toxic, biocompatible and biodegradable components. PNIPAM is an excellent candidate for the development of drug delivery systems (DDS) because its LCST (or VPTT) is close to the physiological temperature upon which it undergoes a sharp phase transition. Further, when arranged into ordered networks, i.e. hydrogels or microgels, it is able to entrap water in its interstitial space and create a polymer matrix permeable to small molecule drugs, proteins, or cells for delivery to specific sites of the body.[138] Despite these advantages, PNIPAM DDS still confront several challenges. For instance, low biodegradability, weak mechanical strength, relatively low drug loading capacity and burst release of drug molecules.[85,139–141] To confront some of these challenges, a common approach is to forego of pure PNIPAM structures and instead synthesize PNIPAM-based hybrid materials by incorporating inorganic nanoparticles, organic molecules, or other polymers during preparation.[142,143] Some examples of DDS that use PNIPAM to improve their performance include inorganic nanoparticles, micelles, hydrogels and microgels.

Functionalizing inorganic nanoparticles with PNIPAM improves the colloidal stability in suspension. Inorganic nanoparticles synthesized from metals are extensively used in biomedicine

for diagnosis, therapy and bioimaging. These particles range between 2 – 100 nm in diameter and display unique electronic, mechanical, chemical, optical, and magnetic properties.[144–147] Above all, these particles are particularly useful as vehicles because they can easily traverse biological barriers and enter cells via endocytosis to deliver therapeutic agents in a targeted fashion or to perform hyperthermia treatments.[148,149] For example, the passive accumulation of nanoparticles in tumor tissue increases with decreasing nanoparticle diameter in agreement with the enhanced permeability and retention (EPR) effect, whereby the tumor blood vessels become more permeable and facilitate the incorporation of nanometric-sized materials.[150,151] Delivery specificity of nanoparticles can be further improved by functionalizing the surface of the nanoparticles with ligands such as folic acid for recognition by the folate receptor that is often overexpressed on the surface of cancer cells or with arginine-glycine-aspartate (RGD) peptides to target the integrins on the endothelium of tumors.[152–154] However, the efficacy of inorganic nanoparticles as DDS is compromised by poor colloidal stability that may lead to particle aggregation and premature clearance by the body.[149,155] Numerous reports have established that diverse polymer matrices improve the long-term stability of nanoparticles against aggregation.[156–159] More specifically, functionalizing the surface of Au nanoparticles with PNIPAM chains or with reticulated PNIPAM layers that form a continuous shell or corona around the nanoparticles also improves colloidal stability via steric repulsions arising from the highly hydrated polymer even in extreme pH environments, in solutions with elevated ionic strength or after removing the citrate that typically stabilizes gold nanoparticles.[160–164] In another example, incorporating PNIPAM on the surface of Au nanoparticles enabled the modification of their optical properties with temperature, which could be useful in designing bioimaging techniques.[165]

Significant improvements to the stability and tunability of the optical properties of Au nanoparticles expand their applicability and relevance in the field of biomedicine.

PNIPAM in amphiphilic block copolymers form the core segment of micelles above the LCST due to the hydrophobic interactions between the dehydrated polymer chains.[166–168] For instance, PEG-*b*-PNIPAM block copolymers self-assemble into micelles in water above the physiological temperature and can encapsulate both hydrophilic and hydrophobic drugs in the interior of the particle; upon decreasing the temperature, the micelles disassemble and release their payload.[169] PNIPAM-based micelles composed of different polymer blocks may offer additional advantages. For example, micelles formed from PNIPAM copolymerized with *N*,*N'*-dimethylacrylamide block polylactic acid (poly(NIPAM-*co*-DMA)-*b*-PLA), can be internalized by the cells by endocytosis above the LCST to deliver therapeutic agents.[170] Further, the biodegradability of PNIPAM copolymerized with *N*-2-hydroxyethylmethacrylamide oligolactates block PEG (poly(NIPAM-*co*-HPAM-lactate)-*b*-PEG) micelles can be tuned so the micelle degrades after 24 hours, a relatively fast time that is useful for delivery of biologically active molecules.[171] The use of micelles as DDS is attractive because they exhibit a sharp and significant change of properties associated with relatively small changes in environmental temperature.

PNIPAM hydrogels have a crosslinked (either physically or chemically) porous network structure that swells with water below the VPTT that permits loading therapeutic agents and shrink above the VPTT to release the therapeutic agents according to the diffusion coefficient within the network. Because of the low viscosity of PNIPAM hydrogels below the transition temperature, they can be easily injected subcutaneously and form a gel network in situ at physiological temperature, constituting a drug depot for gradual release.[172,173] After increasing the

temperature, the release of the encapsulated payload from the hydrogel network may happen quickly ('burst effect') and be followed by a sustained, linear release.[174,175] To decrease the burst release effect, PNIPAM hydrogels can be copolymerized with dextran or with carboxymethyl chitosan which shows a more sustained and controlled release of therapeutic agents from the hydrogel network upon changing temperature.[176,177] PNIPAM hydrogels have also been used for oral delivery of insulin and calcitonin (acid labile drugs), in this case, the polymer network protects the drugs during passage through the stomach for release in the intestine.[178,179] Finally, PNIPAM hydrogels can also be used for transdermal delivery of pharmaceutical agents. For instance, hydrogels can be shaped into microneedle (MN) arrays that penetrate the skin. PNIPAM MNs can then be loaded with insulin as well as black phosphorus nanoparticles (BPNPs) such that when the arrays are exposed to near infrared (NIR) irradiation, BPNPs convert light to heat causing the PNIPAM network to shrink and release insulin to the body.[180] In another example, a wearable device (similar in shape to an adhesive bandage) composed of an electrospun heating element placed beneath PNIPAM hydrogel sheets demonstrated gradual and on-demand release of a hydrophilic model molecule (methylene blue) upon heating the device by applying a voltage through the heating elements.[181] Transdermal DDS are an excellent strategy to deliver therapeutic agents in a convenient and painless manner which increases patient compliance and quality of life.

The use of PNIPAM microgels as DDS offers important advantages over hydrogels because they combine the interstitial space available for drug loading characteristic to hydrogels with the high mobility of discrete nanoparticles. Like hydrogels, microgels can be modified chemically to improve their retention and circulation time, to make them biodegradable, to increase their drug

loading capacity and to tailor the drug release kinetics according to the desired application. In addition, the rate of microgel response vis-à-vis external stimuli is faster than for bulk gels.[109–112] These qualities make microgels versatile and powerful vehicles for therapeutic agents destined to different sites in the body.[182,183] The Serpe group, for instance, developed a drug reservoir device meant to be implanted and made of PNIPAM copolymerized with acrylic acid microgels, PNIPAM-*co*-PAA, sandwiched between two layers of gold and whose release dynamics could be controlled on demand via changes in temperature, pH and the thickness of the top gold layer.[184,185] In a different example, PNIPAM microgels copolymerized with PAA and surface-functionalized with folic acid ligands were loaded with doxorubicin, an anti-cancer drug, in order to demonstrate the *in vitro* tumor-targeted delivery ability of this vehicle.[186] The microgel particles exhibited specific binding with the folate receptors overexpressed in tumor tissues, the release of doxorubicin was mediated via temperature and was observed to improve when in the vicinity of the more acidic extracellular matrix (ECM) of cancer cells.[186] This study also illustrates the advantage of highly mobile microgel particles over stationary hydrogels as DDS. The previous examples involving PNIPAM microgels employed a release of the therapeutic agent at temperatures above the VPTT. However, in some clinical applications, such as in dermatology, it is preferable to decrease the temperature than raising it to avoid causing damage to healthy tissue.[187,188] This represents an important challenge because the release dynamics of therapeutic agents from a swollen PNIPAM microgel, i.e. below the VPTT, take place through passive diffusion, a much slower release mechanism.[189,190] A proposed alternative is to synthesize a PNIPAM microgel surrounding vaterite ($CaCO_3$) microcrystal templates with mesoporous cavities.[191] After the template is dissolved in mild acidic conditions, a therapeutic agent (dextran was used as a

model molecule) can be loaded inside the mesopores of the PNIPAM microgel which becomes entrapped once the temperature is raised above the VPTT and releases from the polymeric network upon cooling. This is a promising approach because it can be customized to respond to additional stimuli such as pH, irradiation or ionic strength and the pore size can be modulated to encapsulate molecules with a wide range of molecular weights.

1.3.2 Applications of PNIPAM to cellular culture

Cellular culture is a fundamental technique in the biomedical sciences, in cancer research and in regenerative medicine. Typically, cells are grown on culture dishes, flasks or multi-well plates made of borosilicate glass, polystyrene, polycarbonate, or polydimethylsiloxane (PDMS).[192] Once cells are ready to harvest, the standard procedures to achieve it involve enzymatic digestion of binding proteins at the cell-substrate interface that make up the ECM using, for example, trypsin-EDTA, or by crude mechanical scrapping.[193,194] However, these detachment methods have significant drawbacks, particularly, nonspecific enzymatic proteolysis compromises regular cell function because critical cellular receptors in the membranes are damaged during this process which may impair subsequent cell adhesion, proliferation as well as survival.[195–197] In addition, enzymatic treatment also acts on cell-cell junctions so the integrity of confluent cell layers is lost and continuous cell monolayers can not be harvested for tissue transplant. On the contrary, coating thermo-responsive PNIPAM on cellular culture substrates offers a gentler and more efficient detachment alternative because the polymer changes its physicochemical properties, namely the polymer layer thickness and wettability, across a well defined transition temperature close to the temperature of cellular incubation that may be used to trigger spontaneous cellular detachment.[198,199] In this section, the factors leading to cell adhesion on substrates are presented,

the role of PNIPAM on developing substrates that promote thermo-triggered cellular detachment are then discussed, and lastly a number of examples are introduced to illustrate its potential applications to cellular culture.

Protein adsorption on culture substrates precedes cellular adhesion and it depends on electrostatic attractions, the wettability of the surface, and steric impediments. Protein adsorption is a critical step in cell adhesion and proliferation because proteins bind with integrin and proteoglycan receptors on the cell membranes and the ECM.[200,201] Proteins are composed of amino acids with a variety of side groups that are either positively or negatively charged, polar or non-polar, which makes these macromolecules both amphiphilic and amphoteric.[202] Therefore, proteins can interact with the substrate through a variety of physicochemical phenomena governed by interfacial energy differences, increases of entropy and electrostatic attractions or repulsions.[202–204] Interfacial energy differences lead to protein adsorption on a surface when the Gibbs free energy decreases, which usually happens when a hydrophobic surface (or a hydrophobic polymer layer coating a substrate) in contact with an aqueous phase drives protein adsorption to increase the entropy in the water phase.[202] In addition, hydrophilic surfaces that contribute to a low interfacial energy with the surrounding aqueous phase also lead to the adsorption of a layer of water molecules at the interphase that creates a repulsive barrier via hydration forces that is difficult to displace by hydrophobic molecules.[205] Electrostatic interactions may lead to protein adsorption if the net charge of the surface is opposite to the net charge of the proteins; in general, positively charged surfaces produce more significant protein adsorption.[206] Coating hydrophilic macromolecules or polymers of a certain chain length on a substrate disfavours protein adsorption because such protein deposition would force the

extended chains to switch from a state of high freedom of mobility to a more reduced and compressed state, which decreases the entropy and raises the Gibbs free energy.[207] The physicochemical nature of the substrate, the charge density and wetting properties determine whether protein adsorption and subsequent cell adhesion and proliferation are viable. Conveniently, these characteristics can be modulated through rational design of PNIPAM coatings.

When the temperature moves across the LCST or VPTT of a PNIPAM layer coating a substrate, the coil-to-globule conformational change is accompanied by variations to the polymer layer thickness, wettability and charge density if PNIPAM bears ionizable functional groups.[96] Sakurai, Okano et al. first demonstrated that this behavior can be exploited to produce cellular detachment from culture substrates to obtain confluent cell monolayers without using enzymatic digestion.[208] Since then, numerous PNIPAM conformations such as brushes,[209] microgels,[210,211] and hydrogels[212,213] have been studied for their potential thermo-triggered cell detachment ability of various cell lines.[210,214–217] Similarly, diverse fabrication methods have been employed to create PNIPAM brushes on cellular culture substrates, the most important ones include: electron beam polymerization (EBP);[218] via UV irradiation;[219,220] surface-initiated atom transfer radical polymerization (SI-ATRP);[221] or surface-initiated reversible addition-fragmentation chain transfer (SI-RAFT).[222] On the other hand, surface functionalization has also been obtained via electrostatic attractions for PNIPAM microgels[210,211] and hydrogels.[213] Despite the significant advancements in surface fabrication, cellular attachment/detachment mechanisms remain complex processes that are heavily dependent on surface properties, cell type and environmental conditions.[223] Nevertheless, the wide range of fabrication opportunities offer ample room to

customize the nature of the substrates according to specific cell lines and incubation protocols to obtain suitable thermo-triggered cellular detachment.

A variety of cells grown on PNIPAM-functionalized substrates spontaneously detach following a decrease in temperature because the polymer coating changes its conformation and hydration state.[224,225] Cells are initially seeded on PNIPAM-functionalized substrates at 37 °C when PNIPAM chains are collapsed and exhibit a rather hydrophobic character which facilitates protein adsorption and later cell adhesion through integrin binding with substrate-immobilized proteins. Once temperature decreases beneath the phase-transition temperature of PNIPAM, the polymer chains adopt a more extended, coil-like conformation, and the polymer layer becomes more hydrated which leads to cell detachment from the substrate through two distinct but interdependent steps. First, decreasing the temperature does not affect the bindings between the cells and the ECM.[226] In fact, the hydration of the polymer layer beneath the transition temperature has a greater impact on the protein conformation in the ECM and the strength of the bonds between the ECM and the PNIPAM layer.[227] Second, successful cell detachment requires morphological changes by the cytoskeleton of the cells, from spread and flattened when adhered to spherical prior to detachment.[228] The cytoskeleton of cells attached to a substrate exert tension forces trough actin-based fibers in equilibrium with focal adhesion points formed with the ECM, when the temperature decreases and the ECM-PNIPAM bonding weakens, the tension equilibrium is disturbed and mechanotransduction signaling is relayed to the nuclei which produces morphological changes that promote detachment.[229–231] This transformation implicates metabolic energy inputs by the cells; therefore, the cell type, temperature variation, adsorbed

proteins and surface properties determine the thermo-triggered cell detachment ultimately observed.[225,232]

Cells recovered from thermo-responsive PNIPAM substrates have been shown to positively contribute to the fields of tissue engineering and regenerative medicine. As an example, **Fig. 1.1** shows a cell sheet suitable for graft transplantation obtained from a thermoresponsive PNIPAM-functionalized substrate.[233] Because cells can be retrieved as monolayers that include the ECM, they can attach more easily to native tissue during transplant without the need for sutures and with less incidence of graft rejection.[234–236] For example, PNIPAM substrates are used to produce tissues for corneal epithelial reconstruction that result in successful restoration of visual capacity.[237–239] In addition, several monolayers of cell sheets cultured on PNIPAM-functionalized substrates can be stacked together for future use in cartilage and periodontal regeneration therapy.[240,241] PNIPAM cellular culture substrates are also essential during the production of three-dimension tissue printing.[242–245]

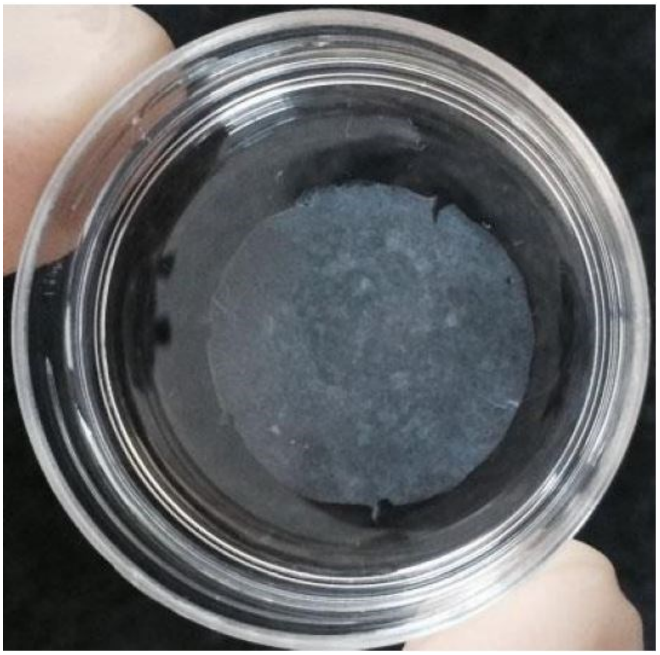

Figure 1.1. Cell sheet recovered from a thermoresponsive PNIPAM-functionalized cell culture dish. Reproduced with permission from.[233]

1.3.3 Applications of PNIPAM for lubrication

Friction forces are ubiquitous in daily life and industrial processes and there are instances when it is desirable to increase or decrease their magnitude. For example, friction makes seemingly trivial activities such as walking, grasping objects, and driving cars possible. On the other hand, large amounts of energy are lost to friction and mechanical equipment sustains wear damage from friction stress. In humans, friction plays a major role in the health of articulations and joints which are lubricated by the synovial fluid composed of water and naturally occurring biopolymers such as hyaluronic acid and lubricin.[21,48] However, if cartilage or joints are damaged and must be replaced by artificial implants, the bulk properties of the materials as well as the interfacial tribological behavior are paramount to the usefulness of the implant and the quality of life of the

patient. For instance, high friction, wear, and corrosion of artificial joints in aqueous environments may produce aseptic loosening after joint replacement surgery which causes pain and discomfort and may lead to loss of mobility.[246,247] Because water is an abundant, low-cost, and environmentally friendly lubricant found in nature, more sophisticated materials that use hydration lubrication as an advantage must be studied. PNIPAM is one of such materials because below the LCST, hydrogen bonding between the amide groups and water molecules forms a hydration layer surrounding PNIPAM. Above the LCST, the hydrogen bonding between PNIPAM and water is broken, and the hydration layer disappears. This behavior has been exploited to modulate the tribological properties with temperature between surfaces functionalized with PNIPAM brushes, hydrogels and microgels in relative motion.

PNIPAM linear chains grafted by one end to a surface and surrounded by a good solvent stretch out into the bulk of the solution to form a brush-like structure that reduces friction. The tribological properties of polymer brushes can be modulated by controlling the chain grafting density, the chain length, the chain stiffness, the solvent quality, and the degree of cross-linking between the chains.[248] In general, the best way to reduce friction between two surfaces is to keep them separated during sliding. In hydrodynamic lubrication, lubricants are used to improve the normal force generated while sliding and thus avoid contact between the surfaces. Under more drastic conditions, for example at low velocities or at high normal applied forces between the surfaces, the lubrication is in the boundary regime. In this regime, the separation between the surfaces is reduced to a few nanometers and the friction force and wear rate increase. When PNIPAM brushes are in a stretched conformation below the LCST, the solvent is absorbed within the polymer layer and forms a hydration layer that keeps the surfaces separated and adhesion

and friction low.[249] In addition to the hydration layer, the polymer backbones also contribute to keeping the surfaces separated through steric repulsions and allows them to bear normal loads in the order of hundreds of megapascals.[250] At this stage, PNIPAM chains strongly anchored to the substrate, through covalent bonds, for instance, contribute to low friction forces by decreasing the amount of chains sheared away from the surface.[250] Similarly, friction forces can be kept low by ensuring a suitably high chain grafting density in order to decrease the interpenetration of polymer chains which could produce draft while sliding.[248] On the contrary, when the temperature increases above the LCST of PNIPAM and the polymer chains change conformation from coil to globule, the hydration layer disappears, and hydrophobic polymer-polymer attractions increase adhesion and friction forces between the sliding surfaces.[250] Friction can also be controlled isothermally via the quality of the solvent, otherwise known as the co-non-solvency effect. For example, in pure water or in pure ethanol at room temperature, PNIPAM brushes are swollen, and the associated friction forces are low. However, in a mixture of 10-90 % ethanol-water, also at room temperature, the friction coefficient was found to be two orders of magnitude (roughly 120 times) higher.[251] PNIPAM structures arranged in a hydrogel conformation also exhibit similar temperature-dependent tribological tunability.

Hydrogels are a promising platform for biotribological studies given their close resemblance to biological connective tissues such as cartilage and corneal stroma.[252] Unlike isotropic materials whose response to strain is linear-elastic and may be described using Hooke's law,[253] hydrogels exhibit multiple responses with strain. First, a linear-elastic regime for low strains governed by the water content imbedded in the polymer network which leads to; second, the failure of the material which is determined by the crosslink density of the gel.[254] Further, when hydrogels are

fully swollen they can sustain large strains without permanent damage, however, relatively low applied stress can lead to permanent failure.[254,255] The tribological properties of PNIPAM hydrogels have been shown to be temperature-dependent, i.e. low friction below the VPTT and high friction above the VPTT, and follow the hydration-dehydration behavior across the VPTT previously discussed.[256] In addition, friction forces can be controlled via the co-non-solvency effect with PNIPAM hydrogels with similar results as those obtained with PNIPAM brushes.[257] On both of these examples, however, hydrogels were not synthesized entirely from PNIPAM but rather as composite gels, or double-network structured gels, in an effort to improve the poor mechanical strength that prevents high load-bearing.[258] In fact, upon sliding on PNIPAM hydrogels during tribological experiments, it is common to observe failures or cracks that propagate through the polymer network.[113] In addition, hydrogels have a slower reaction time to an applied stimulus than nano- or microgels.[109–112] Hence, tribological studies that involve PNIPAM often use microgel structures for their robustness and fast response time.

Compared to hydrogels, microgels have a larger surface area and offer a faster and localized response to external stimuli due to their discrete particle distribution. In addition, the damage incurred to a microgel coating during sliding does not propagate like it does on hydrogel coatings and can be limited to individual microgels.[42] PNIPAM microgels improve lubricity during sliding through several ways. Microgel particles are highly deformable, which combined with the high water content in their interior allows them to sustain relatively high applied normal loads.[79,259] The smaller the microgel particle size, the higher the number of microgel particles that are found within the contact area of two surfaces sliding in relative motion which decreases friction forces and wear.[260] Further, “free” microgels, i.e. microgels that are not surface-immobilized but in

suspension, may act as bearings during sliding due to their spherical shape and reduce friction forces through their rolling motion.[260] As was observed with PNIPAM brushes and hydrogels, when the temperature raises above the VPTT of PNIPAM microgels, the associated friction forces raise as well due to the dissipation of the hydration layer.[79] However, interesting modifications can be done to the microgel system in order to improve friction with temperature variations. For example, the typical paradigm to trigger the phase transition of PNIPAM microgels is to raise the temperature of the surrounding environment. This approach is easily accomplished in the laboratory; however, it is not so practical if a localized response is desired. Chen et al. proposed synthesizing a microgel shell surrounding gold nanoparticle cores to take advantage of the photothermal capacity of gold nanoparticles to trigger the shrinking of the PNIPAM shell via NIR irradiation to increase the friction force.[261] Two more groups succeeded in obtaining lower friction forces close to and even above the VPTT of PNIPAM microgels, however in both cases additives acting in synergy with PNIPAM contributed to better lubrication.[259,262] For instance, friction forces were measured for PNIPAM microgels in bovine calf serum (BCS) to better recreate the tribological environment *in vivo*.[259] Three friction regimes were identified; first, below the VPTT, hydrodynamic lubrication kept friction forces low. Second, close to the VPTT, proteins in the BCS adsorbed onto the increasingly hydrophobic PNIPAM microgel network which contributed to lower friction forces. Lastly, above the VPTT, proteins in the BCS and PNIPAM microgels precipitated from suspension and surface rugosity increased which produced higher friction forces.[259] In a different study, PNIPAM microgels were copolymerized with PEG methyl ether methacrylate (PEGMA) (PNIPAM-*g*-PEG) in an effort to retain a higher water content above the transition temperature and promote lower friction forces. Even though friction forces with

PNIPAM-*g*-PEG microgels increased above the VPTT, when 1H-benzotriazole (BTA), an anticorrosive agent, was added, friction forces were observed to decrease above the VPTT due to adsorption of BTA on the microgels which led to more efficient boundary lubrication.[262] PNIPAM microgels are a promising platform for controlling the tribological properties of materials, however, their performance remains inadequate beyond the VPTT and finer-tuned materials are necessary.

1.4 Challenges with PNIPAM-based functional coatings for modulation of surface properties

As was described in the introduction, the surface is of utmost importance because it is at the boundary between the material and the environment. Thus, the surface's chemical nature, physical conformation and topography, stability, and capacity to respond to external stimuli determine the range of possible interactions that take place with the surroundings. By functionalizing the surface through chemistry by using macromolecules such as stimuli-responsive polymers, properties like surface adhesion or wettability can be modulated through a variety of external stimuli such as light, pH or temperature. Hence, this type of functionalization confers a responsive or smart behavior to the surface that boosts versatility and adaptability through diverse environmental conditions. PNIPAM, a thermo-responsive molecule, undergoes a coil-to-globule transition across its LCST which is associated to a hydrophilic-to-hydrophobic transition. In other words, to trigger a change in the physical conformation of PNIPAM, it is necessary to modulate its physicochemical properties and the two changes are linked and interdependent.

The interplay between the physical conformation and hydrophilicity/hydrophobicity changes are at the heart of what makes PNIPAM a widely used polymer. Indeed, there are many instances where the simultaneous modulation of the physicochemical properties is suitable to a variety of applications. For example, the change in conformation and hydrophilicity with temperature is part of what makes drug loading and releasing with PNIPAM-based hydrogels or microgels a simple process. Similarly, by modulating the hydrophilic/hydrophobic behavior of a PNIPAM coating via the temperature of the environment, the adhesion and detachment of proteins and cells on a substrate can be controlled. Further, it is possible to control the friction forces between two surfaces in relative motion by changing the layer thickness and hydrophilicity of a PNIPAM coating, which determines if the lubrication is either in the hydrodynamic or in the boundary regime. However, it is not always desirable to produce a simultaneous change in the physical conformation (swelling) and on the surface chemistry properties (wettability, surface potential, adhesion) of a PNIPAM layer. In other words, this exact behavior can represent a challenge, rather than an advantage, in a different set of applications. For instance, if the objective is to be able to control the flow rate of a fluid inside of a capillary tube, i.e., in a microfluidics device, via the swelling of a PNIPAM layer, the surface adhesion will inevitably change as well.[263] Hence, even though the flow rate can be controlled by the thermo-triggered swelling of the PNIPAM layer, the functional surface becomes susceptible to non-specific adsorption of proteins or cells in biological or otherwise complex samples which may compromise the overall performance of the device.[264,265] Similarly, it could be advantageous to develop an anti-fouling polymer coating capable of preventing protein deposition or the formation of biofilm across a temperature range both below and above the LCST/VPTT of PNIPAM. Ideally, such a material should provide a fine-

tuned and independent control of the conformation or swelling of the polymer layer and of its surface properties.

1.5 General working hypothesis and objectives

1.5.1 General working hypothesis

By synthesising a hierarchical structure composed of a microgel surface-functionalized with polymer chains it is possible to control the surface properties and the swelling behavior independently.

1.5.2 Objectives

The general objective of this work is to be able to independently control the surface properties of a polymer layer, such as the surface potential or the adhesion, and the physical properties, i.e., the swelling/shrinking behavior.

To achieve this goal, the proposed platform is composed of surface-immobilized thermoresponsive microgels synthesized from PNIPAM and whose swelling can be controlled via temperature variations. The surface of the microgels is functionalized with polymer chains of different natures: a pH-responsive PDMAEMA polymer chain and a non pH-responsive polymer chain, PEG (used as a control). It is expected, upon changing the temperature, to be able to control only the swelling behavior of the microgels without affecting the surface properties provided by the polymer chains. The surface properties of the polymer layer should be modulated with pH without affecting the degree of swelling of the microgels. Hence, the project is divided into four specific objectives: (i) preparation and characterization of surface-functionalized microgels (ii) demonstration that physical conformation and surface properties of the surface-functionalized

microgels can be controlled independently in suspension and immobilized on a surface, (iii) application of the independent control of the swelling and surface properties to the control of the tribological properties in the nano- and mesoscales and, (iv) application of surface-functionalized microgels to promote initial cell-substrate adhesion while favoring a temperature-triggered cell detachment.

i) Preparation and characterization of surface-functionalized microgels.

Cationic PNIPAM microgels have been previously prepared and their stimuli-responsive behavior, stability and mechanical properties characterized, including by members of our group and by collaborators.[78,79,95,96,266] However, an independent control of the swelling and wettability properties remains elusive. Core/shell PNIPAM based microgels have been designed to improve the hydrophilicity of the PNIPAM above the VPTT.[267–270] These are generally synthesized via a two-staged seeding polymerization which produces a continuous polymer shell on the microgel cores. However, such a synthesis approach results in an increase of the VPTT, a widening of the breadth of transition, and the thermoresponsiveness becomes linear.[271–273] Instead, by using a "grafting to" approach, end-functionalized PDMAEMA (pH-responsive) and PEG (pH-unresponsive) polymer chains were used to form covalent bonds with the amine groups on the surface of the microgels via peptide-coupling.

ii) Demonstration that physical conformation and surface properties of the surface-functionalized microgels can be controlled independently in suspension and immobilized on a surface.

The independent control of the swelling ability and the surface properties of bare microgels and microgels functionalized with PDMAEMA (microgel-co-PDMAEMA) and microgels functionalized

with PEG (microgel-co-PEG) was verified by modifying the temperature and the pH of the environment surrounding the particles both in suspension and immobilized on a substrate. In suspension, the Dynamic Light Scattering (DLS) technique was used to characterize the hydrodynamic diameter to evaluate the swelling and the surface potential, expressed as the zeta potential, as an indicator of a surface property. Meanwhile, once bare and surface-functionalized microgels were immobilized on a substrate, the Surface Forces Apparatus (SFA) technique was used to evaluate the polymer layer thickness and adhesion in the static mode.

iii) Application of the independent control of the swelling and surface properties to the control of the tribological properties in the nano- and mesoscales.

The ability to independently control the swelling and adhesion of the polymer layer, and therefore the friction forces between two surfaces in relative motion was explored. In addition, this study aims to expand the knowledge on the mechanical and tribological properties of PNIPAM microgels used for lubrication applications by determining if a continuum of friction forces exists between the nano- and the mesoscales. Thus, the variations in the tribological behavior of bare and surface-functionalized microgels with temperature and pH was studied in the nanoscale using the SFA in the dynamic mode and using a custom-made tribometer for analysis in the mesoscale.

iv) Application of surface-functionalized microgels to promote initial cell-substrate adhesion while favoring a temperature-triggered cell detachment.

PNIPAM-based polymer coatings have been successfully used to develop functional substrates for cell culture applications capable of producing spontaneous thermo-triggered cellular detachment.[170,214,274] However, a wide variability of results exists due to the wide range of surface

fabrication methods, culture protocols and cell lineages used.[210,212,275–277] In addition, the inability of PNIPAM coatings (including in the microgel conformation) to produce thermo-triggered cell and protein detachment has also been reported.[211,278] Hence, in this section, the cell lineages, culture protocols and fabrication techniques were kept constant so as to isolate the effect of the substrate, coated with either bare or surface-functionalized microgels, on cellular detachment with variations in temperature and pH.

1.6 Structure of the thesis

In addition to chapter 1 which serves as the introduction, the present thesis is composed of one chapter of methodology, three chapters of results and discussions, one chapter of general discussion and one chapter of general conclusions and perspectives. The three chapters of results and discussions are presented in a mixed format addressing the objectives previously established. In other words, chapter 3 is presented as a published article, chapter 4 compiles the results and discussions obtained for the tribology section of the thesis which are not intended for publication, and chapter 5 is in the format of a submitted article. Chapter 6 is an overall discussion of all acquired results and compares them to those reported in the literature. Finally, the conclusion in chapter 7 summarizes the key findings of the present work, evaluates the challenges encountered and proposes future perspectives.

Chapter 3 addresses objectives (i) and (ii) of this thesis. It centers on the surface-functionalization of the thermo-responsive PNIPAM microgels and analyses the potentials and limitations associated with independently controlling the swelling behavior and the surface properties both in suspension and immobilized on a substrate. This section was published as an article: Guerron, A., Giasson, S. (2021) **Multiresponsive Microgels: Toward an Independent Tuning of Swelling**

and Surface Properties. *Langmuir, 37(38)*, 11212-11221. All experimental work, data processing and writing was done by Alberto Guerron, with the advice of Pr. Suzanne Giasson.

Chapter 4 deals with objective (iii), the impact of independently controlling the swelling ability and surface properties on the tribological properties of microgel-coated substrates in the nano- and mesoscales. Studies on the nanoscale were done using the SFA at Pr. Suzanne Giasson's laboratory at the University of Montreal and those in the mesoscale were done using a custom-made tribometer in collaboration with Dr. Sylvie Descartes at the Contact and Structure Mechanics Laboratory (LaMCoS) at the National Institute of Applied Sciences of Lyon, France. All experimental work, data processing and writing was done by Alberto Guerron, with the advice of Pr. Suzanne Giasson and Dr. Sylvie Descartes. This collaborative work was made possible thanks to the financial support of the International Research Group – Controlled Multifunctional Materials.

In chapter 5 the potential of bare and surface-functionalized microgels to develop cell culture dishes with the ability to produce stimuli-triggered cellular detachment was explored (objective iv). This project was done in collaboration with several research groups of the Medicament Formulation and Analysis Axis (AFAM) at the Faculty of Pharmacy of the University of Montreal and the results are part of a publication: Guerron, A., Phan, H. T., Peñaloza-Arias, C., Brambilla, D., Roullin, V. G., Giasson, S. (2022) **Selectively triggered cell detachment from PNIPAM microgel functionalized substrates**, submitted to Colloids and Surfaces B: Biointerfaces. The majority of the experimental work was done by Alberto Guerron, with the exception of the surface plasmon resonance (SPR) experiments that were done by Huu Trong Phan. Carolina Peñaloza-Arias trained Alberto Guerron in cell culture techniques. All data processing and writing was done by Alberto

Guerron, with the advice of Pr. Davide Brambilla, Pr. Valérie Gaëlle Roullin and Pr. Suzanne Giasson.

Chapter 6 constitutes a general discussion of the work performed in this thesis. The results are evaluated, critiqued, and compared to the state of the art to position this work in the context of other research groups.

Finally, chapter 7 serves as a conclusion of this work. Potential perspectives and applications for the developed microgels are proposed.

1.8 References

(1) Aizenberg, J.; Tkachenko, A.; Weiner, S.; Addadi, L.; Hendler, G. Calcitic Microlenses as Part of the Photoreceptor System in Brittlestars. *Nature* **2001**, *412*, 819–822.

(2) Stevens, M.; Merilaita, S. Animal Camouflage: Current Issues and New Perspectives. *Philos. Trans. R. Soc. B* **2009**, *364*, 423–427.

(3) Agache, P.; Lihoreau, T.; Mac-Mary, S.; Fanian, F.; Humbert, P. The Human Skin: An Overview. In *Agache's Measuring the Skin*; Humbert, P., Fanian, F., Maibach, H., Agache, P., Eds.; Springer, Cham, 2017; pp 1–4.

(4) Padya, B.; Pandey, A.; Pisay, M.; Koteshwara, K. B.; Chandrashekhar, R.; Bhat, K.; Biswas, S.; Mutalik, S. Stimuli-Responsive and Cellular Targeted Nanoplatforms for Multimodal Therapy of Skin Cancer. *Eur. J. Pharmacol.* **2021**, *890*, 173633.

(5) Maxwell, S. S. A Case of Voluntary Erection of the Human Hair. *Arch. Dermatol.* **2003**, *139*, 1117.

(6) Morris, P. J. *Polymer Pioneers: A Popular History of the Science and Technology of Large Molecules*, 5th ed.; Chemical Heritage Foundation: Philadelphia, 2005.

(7) Dove, M. A Revisionist Review of Tropical Deforestation and Development. *Environ. Conserv.* **1993**, *20*, 17–24.

(8) Staudinger, H. *From Organic Chemistry to Macromolecules: A Scientific Autobiography Based on My Original Papers*, 1st ed.; Wiley: New York, 1970.

(9) Mülhaupt, R. Hermann Staudinger and the Origin of Macromolecular Chemistry. *Angew. Chemie Int. Ed.* **2004**, *93*, 1054–1063.

(10) Kauffman, G. Wallace Hume Carothers and Nylon, The First Completely Synthetic Fiber. *J. Chem. Educ.* **1988**, *65*, 803–808.

(11) Cashin, V.; Eldridge, D.; Yu, A.; Zhao, D. Surface Functionalization and Manipulation of Mesoporous Silica Adsorbents for Improved Removal of Pollutants: A Review. *Environ. Sci. Water Res. Technol.* **2018**, *4*, 110–128.

(12) Linares, N.; Serrano, E.; Rico, M.; Balu, A. M.; Losada, E.; Luque, R.; Garcia-Martinez, J. Incorporation of Chemical Functionalities in the Framework of Mesoporous Silica. *Chem. Commun.* **2011**, *47*, 9024–9035.

(13) Gilcreest, V.; Carroll, W.; Rochev, Y.; Blute, I.; Dawson, K.; Gorelov, A. Thermoresponsive Poly(N-Isopropylacrylamide) Copolymers: Contact Angles and Surface Energies of Polymer Films. *Langmuir* **2004**, *20*, 10138–10145.

(14) Zhang, Q.; Xia, F.; Sun, T.; Song, W.; Zhao, T.; Liu, M.; Jiang, L. Wettability Switching between High Hydrophilicity at Low PH and High Hydrophobicity at High PH on Surface Based on PH-Responsive Polymer. *Chem. Commun.* **2008**, *10*, 1199–1201.

(15) Liao, K.-S.; Fu, H.; Wan, A.; Batteas, J.; Bergbreiter, D. Designing Surfaces with Wettability That Varies in Response to Solute Identity and Concentration. *Langmuir* **2009**, *25*, 26–28.

(16) Liberelle, B.; Banquy, X.; Giasson, S. Stability of Silanols and Grafted Alkylsilane Monolayers on Plasma-Activated Mica Surfaces. *Langmuir* **2008**, *24*, 3280–3288.

(17) Yang, W.; Liu, C.; Chen, Y. Stability of Polydopamine Coatings on Gold Substrates Inspected by Surface Plasmon Resonance Imaging. *Langmuir* **2018**, *34* (12), 3565–3571. https://doi.org/10.1021/acs.langmuir.7b03143.

(18) Wichaita, W.; Kim, Y.-G.; Tangboriboonrat, P.; Thérien-Aubin, H. Polymer-Functionalized

Polymer Nanoparticles and Their Behavior in Suspensions. *Polym. Chem.* **2020**, *11*, 2119–2128.

(19) Campbell, K.; Erck, R.; Swita, M.; Cosimbescu, L. Multifunctional Tunable Polymethacrylates for Enhanced Shear Stability and Wear Prevention. *Appl. Polym. Mater.* **2020**, *2* (7), 2839–2848.

(20) Qi, H.; Zhang, G.; Chang, L.; Zhao, F.; Wang, T.; Wang, Q. Ultralow Friction and Wear of Polymer Composites under Extreme Unlubricated Sliding Conditions. *Adv. Mater. Interfaces* **2017**, *4* (13).

(21) Faivre, J.; Shrestha, B.; Burdynska, J.; Xie, G.; Moldovan, F.; Delair, T.; Benayoun, S.; Laurent, D.; Matyjaszewski, K.; Banquy, X. Wear Protection without Surface Modification Using a Synergistic Micture of Molecular Brushes and Linear Polymers. *ACS Nano* **2017**, *11*, 1762–1769.

(22) Prasad Tiwari, A.; Bhattarai, D. P.; Maharjan, B.; Ko, S. W.; Kim, H. Y.; Park, C. H.; Cheol, &; Kim, S. Polydopamine-Based Implantable Multifunctional Nanocarpet for Highly Efficient Photothermal-Chemo Therapy. https://doi.org/10.1038/s41598-019-39457-y.

(23) Jouenne, S. Polymer Flooding in High Temperature, High Salinity Conditions: Selection of Polymer Type and Polymer Chemistry, Thermal Stability. *J. Pet. Sci. Eng.* **2020**, *195*, 107545–107560.

(24) Tiwari, N.; Nawale, L.; Sarkar, D.; Badiger, M. Carboxymethyl Cellulose-Grafted Mesoporous Silica Hybrid Nanogels for Enhanced Cellular Uptake and Release of Curcumin. *Gels* **2017**, *3*, 8–23.

(25) Pan, Y.-J.; Chen, Y.-Y.; Wang, D.-R.; Wei, C.; Guo, J.; Lu, D.-R.; Chu, C.-C.; Wang, C.-C. Redox/PH Dual Stimuli-Responsive Biodegradable Nanohydrogels with Varying Responses to Dithiothreitol and Glutathione for Controlled Drug Release. *Biomaterials* **2012**, *33* (27), 6570–6579. https://doi.org/10.1016/J.BIOMATERIALS.2012.05.062.

(26) Yang, J.; Yamato, M.; Kohno, C.; Nishimoto, A.; Sekine, H.; Fukai, F.; Okano, T. Cell Sheet Engineering: Recreating Tissues without Biodegradable Scaffolds. *Biomaterials* **2005**, *26*, 6415–6422.

(27) Li, C.; Zhaoyang, C. W.; Jiang, N.; Lin, W.; Li, D. Synthesis of Thiol-Terminated Thermoresponsive Polymers and Their Enhancement Effect on Optical Limiting Property of Gold Nanoparticles. *Eur. Polym. J.* **2019**, *113*, 404–410.

(28) Zhang, L.; Wei, Z.; Meng, M.; Ung, G.; He, J. Do Polymer Ligands Block the Catalysis of Metal Nanoparticles? Unexpected Importance of Binding Motifs in Improving Catalytic Activity. *J. Mater. Chem. A* **2020**, *8*, 15900–15908.

(29) Hao, B.; Lu, G.; Zhang, S.; Li, Y.; Ding, A.; Huang, X. Gold Nanoparticles Standing on PEG/PAMAM/Thiol-Functionalized Nanographene Oxide as Aqueous Catalysts. *Polym. Chem.* **2020**, *11*, 4094–4104.

(30) Azharuddin, M.; Zhu, G.; Das, D.; Ozgur, E.; Uzun, L.; Turner, A.; Patra, H. A Repertoire of Biomedical Applications of Noble Nanoparticles. *Chem. Commun.* **2019**, *55*, 6964–6996.

(31) Wieszczycka, K.; Staszak, K.; Wozniak-Budych, M.; Litowczenko, J.; Maciejewska, B.; Jurga, S. Surface Functionalization - The Way for Advanced Applications of Smart Materials. *Coord. Chem. Rev.* **2021**, *436*, 213846–213874.

(32) Gurumoorthy, A.; Khan, K. H. Polymers at Interfaces: Biological and Non-Biological Applications. *Recent Res. Sci. Technol.* **2011**, *3*, 80–86.

(33) Lin, J.-H.; Chen, H.-W.; Wang, K.-T.; Liaw, F.-H. A Novel Method for Grafting Polymers on Carbon Blacks. *J. Mater. Chem.* **1998**, *8*, 2169–2173.
(34) Zoppe, J.; Ataman, N. C.; Mocny, P.; Wang, J.; Moraes, J.; Klok, H.-A. Surface-Initiated Controlled Radical Polymerization: State-of-the-Art, Opportunities, and Challenges in Surface and Interface Engineering with Polymer Brushes. *Chem. Rev.* **2017**, *117*, 1105–1318.
(35) Zhang, X.; Liu, J.; Qian, C.; Kan, J.; Jin, C. Effect of Grafting Method on the Physical Property and Antioxidant Potential of Chitosan Film Functionalized with Gallic Acid. *Food Hydrocoll.* **2019**, *89*, 1–10.
(36) Le, A.; Liang, R.; Zhong, M. Synthesis and Self-Assembly of Mixed-Graft Block Copolymers. *Chem. - A Eur. J.* **2019**, *25*, 8177–8189.
(37) Lee, J.; Lopez, G.; Améduri, B.; Seo, M. Synthesis of Heterograft Copolymers with a Semifluorinated Backbone by Combination of Grafting-through and Grafting-from Polymerizations. *Macromolecules* **2020**, *53*, 2811–2821.
(38) Solimando, X.; Kennedy, E.; David, G.; Champagne, P.; Cunningham, M. Phosphorus-Containing Polymers Synthesised via Nitroxide-Mediated Polymerisation and Their Grafting on Chitosan by Grafting to and Grafting from Approaches. *Polym. Chem.* **2020**, *25*, 4133–4143.
(39) Madkour, M.; Bumajdad, A.; Al-Sagheer, F. To What Extent Do Polymeric Stabilizers Affect Nanoparticles Characteristics? *Adv. Colloid Interface Sci.* **2019**, *270*, 38–53.
(40) Cazzoti, J.; Fritz, A.; Garcia-Valdez, O.; Smeets, N.; Dubé, M.; Cunningham, M. Graft Modification of Starch Nanoparticles Using Nitroxide-Mediated Polymerization and the Grafting from Approach. *Carbohydr. Polym.* **2020**, *228*, 115384–115393.
(41) Biehl, P.; Schacher, F. Surface Functionalization of Magnetic Nanoparticles Using a Thiol-Based Grafting-Through Approach. *Surfaces* **2020**, *3*, 116–131.
(42) Giraud, L.; Bazin, G.; Giasson, S. Lubrication with Soft and Hard Two-Dimensional Colloidal Arrays. *Langmuir* **2017**, *33*, 3610–3623.
(43) Gorelikov, I.; Field, L.; Kumacheva, E. Hybrid Microgels Photoresponsive in the Near-Infrared Spectral Range. *J. Am. Chem. Soc.* **2004**, *126*, 15938–15939.
(44) Hu, J.; Zhang, G.; Liu, S. Enzyme-Responsive Polymeric Assemblies, Nanoparticles and Hydrogels. *Chem. Soc. Rev.* **2012**, *41*, 5933–5949.
(45) Uljin, R. Enzyme-Responsive Materials: A New Class of Smart Biomaterials. *J. Mater. Chem.* **2006**, *16*, 2217–2225.
(46) Liu, L.; Du, P.; Zhao, X.; Zeng, J.; Liu, P. Independent Temperature and PH Dual-Stimuli Responsive Yolk/Shell Polymer Microspheres for Controlled Release: Structural Effect. *Eur. Polym. J.* **2015**, *69*, 540–551.
(47) Wang, X.; Yan, S.; Song, L.; Shi, H.; Yang, H.; Luan, S.; Huang, Y.; Yin, J.; Khan, A. F.; Zhao, J. Temperature-Responsive Hierarchical Polymer Brushes Switching from Bactericidal to Cell Repellency. *ACS Appl. Mater. Interfaces* **2017**, *9*, 40930–40939.
(48) Faivre, J.; Shrestha, B.; Xie, G.; Delair, T.; Laurent, D.; Matyjaszewski, K.; Banquy, X. Unraveling the Correlations between Conformation, Lubrication and Chemical Stability of Bottlebrush Polymers at Interfaces. *Biomacromolecules* **2017**, *18*, 4002–4010.
(49) Urban, M. Stratification, Stimuli-Responsiveness, Self-Healing, and Signaling in Polymer Networks. *Prog. Polym. Sci.* **2009**, *34*, 679–687.

(50) Perrin, J. *Brownian Motion and Molecular Reality*; Dover: New York, 2005.
(51) Liu, F.; Urban, M. Recent Advances and Challenges in Designing Stimuli-Responsive Polymers. *Prog. Polym. Sci.* **2010**, *35*, 3–23.
(52) Xia, F.; Zhu, Y.; Feng, L.; Jiang, L. Smart Responsive Surfaces Switching Reversibly between Super-Hydrophobicity and Super Hydrophilicity. *Soft Matter* **2009**, *5*, 275–281.
(53) Cellesi, F.; Tirelli, N.; Hubbell, J. A. Towards a Fully-Synthetic Substitute of Alginate: Development of a New Process Using Thermal Gelation and Chemical Cross-Linking. *Biomaterials* **2004**, *25*, 5115–5124.
(54) Kamath, K.; Park, K. Biodegradable Hydrogels in Drug Delivery. *Adv. Drug Deliv. Rev.* **1993**, *11*, 59–84.
(55) Connal, L.; Li, Q.; Quinn, J.; Tjipto, E.; Caruso, F.; Qiao, G. PH-Responsive Poly(Acrylic Acid) Core Cross-Linked Star Polymers: Morphology Transitions in Solution and Multilayer Thin Films. *Macromolecules* **2008**, *41*, 2620–2626.
(56) Li, G.; Song, S.; Guo, L.; Ma, S. Self-Assembly of Thermo- and PH-Responsive Poly(Acrylic Acid)-b-Poly(N-Isopropylacrylamide) Micelles for Drug Delivery. *J. Polmer Sci. Part A* **2008**, *46*, 5028–5035.
(57) Binks, B.; Murakami, R.; Armes, S.; Fujii, S.; Schmid, A. PH-Responsive Aqueous Foams Stabilized by Ionizable Latex Particles. *Langmuir* **2007**, *17*, 8691–8694.
(58) Munoz-Bonilla, A.; Fernandez-Garcia, M.; Haddleton, D. Synthesis and Aqueous Solution Properties of Stimuli-Responsive Triblock Copolymers. *Soft Matter* **2007**, *3*, 725–731.
(59) Hu, L.; Chu, L.-Y.; Yang, M.; Wang, H.-D.; Niu, C. Preparation and Characterization of Novel Cationic PH-Responsive Poly(N,N'-Dimethylamino Ethyl Methacrylate) Microgels. *J. Colloid Interface Sci.* **2007**, *311*, 110–117.
(60) Liu, F.; Urban, M. Dual Temperature and PH Responsiveness of Poly(2-(N,N-Dimethylamino)Ethyl Methacrylate-Co-n-Butylacrylate) Colloidal Dispersions and Their Films. *Macromolecules* **2008**, *41*, 6531–6539.
(61) Gillies, E.; Fréchet, J. PH-Responsive Copolymer Assemblies for Controlled Release of Doxorubicin. *Bioconjug. Chem.* **2005**, *16*, 361–368.
(62) Chen, W.; Meng, F.; Li, F.; Ji, S.-J.; Zhong, Z. PH-Responsive Biodegradable Micelles Based on Acid-Labile Polycarbonate Hydrophobe: Synthesis and Triggered Drug Release. *Biomacromolecules* **2009**, *10*, 1727–1735.
(63) Heffernan, M.; Murthy, N. Polyketal Nanoparticles: A New PH-Sensitive Biodegradable Drug Delivery Vehicle. *Bioconjug. Chem.* **2005**, *16*, 1340–1342.
(64) Sun, S.; Liang, S.; Xu, W.-C.; Xu, G.; Wu, S. Photoresponsive Polymers with Multi-Azobenzene Groups. *Polym. Chem.* **2019**, *10*, 4389–4401.
(65) Ishikawa, M.; Kitamura, N.; Masuhara, H.; Irie, M. Size Effect on Photoinduced Volume Change of Polyacrylamide Microgels Containing Triphenylmethane Leuco Cyanide. *Macromol. Rapid Commun.* **2003**, *12*, 687–690.
(66) Sakai, H.; Ebana, H.; Sakai, K.; Tsuchiya, K.; Ohkubo, T.; Abe, M. Photo-Isomerization of Spiropyran-Modified Cationic Surfactants. *J. Colloid Interface Sci.* **2007**, *316*, 1027–1030.
(67) Sumaru, K.; Kameda, M.; Kanamori, T.; Shibo, T. Characteristic Phase Transition of Aqueous Solution of Poly(N-Isopropylacrylamide) Functionalized with Spirobenzopyran. *Macromolecules* **2004**, *37*, 4949–4955.
(68) Lendlein, A.; Jiang, H.; Junger, O.; Langer, R. Light-Induced Shape-Memory Polymers.

Nature **2005**, *434*, 879–882.
(69) Gupta, P.; Trenor, S.; Long, T.; Wilkes, G. In-Situ Photo-Cross-Linking of Cinnamate Functionalized Poly(Methyl Methacrylate-Co-2-Hydroxyethylacrylate) Fibers during Electrospinning. *Macromolecules* **2004**, *37*, 9211–9218.
(70) Marsili, L.; Dal Bo, M.; Eisele, G.; Donati, I.; Berti, F.; Toffoli, G. Characterization of Thermoresponsive Poly-N-Vinylcaprolactam Polymers for Biological Applications. *Polymers* **2021**, *13*, 2639–2654.
(71) Watanabe, R.; Takaseki, K.; Katsumata, M.; Matsushita, D.; Ida, D.; Osa, M. Characterization of Poly(N,N-Diethylacrylamide) and Cloud Points in Its Aqueous Solutions. *Polym. J.* **2016**, *48*, 621–628.
(72) Gurdag, G.; Cavus, S. Synthesis and Swelling Behavior of Poly(2-Dimethylaminoethyl Methacrylate-Co-N-Hydroxymethyl Acrylamide) Hydrogels. *Polym. Adv. Technol.* **2006**, *17*, 878–883.
(73) Halperin, A.; Kroger, M.; Winnik, F. Poly(N-Isopropylacrylamide) Phase Diagrams: Fifty Years of Research. *Angew. Chemie Int. Ed.* **2015**, *54*, 15342–15367.
(74) Crespy, D.; Rossi, R. Temperature-Responsive Polymers with LCST in the Physiological Range and Their Applications in Textiles. *Polym. Int.* **2007**, *56*, 1461–1468.
(75) Liu, R.; Fraylich, M.; Saunders, B. Thermoresponsive Copolymers: From Fundamental Studies to Applications. *Colloid Polym. Sci.* **2009**, *287*, 627–643.
(76) Efthimiadou, E. K.; Tapeinos, C.; Tziveleka, L.-A.; Boukos, N.; Kordas, G. PH- and Thermo-Responsive Microcontainers as Potential Drug Delivery Systems: Morphological Characteristic, Release and Cytotoxicity Studies. *Mater. Sci. Eng. C* **2014**, *37*, 271–277. https://doi.org/10.1016/J.MSEC.2014.01.024.
(77) Cheng, R.; Meng, F.; Deng, C.; Klok, H.-A.; Zhong, Z. Dual and Multi-Stimuli Responsive Polymeric Nanoparticles for Programmed Site-Specific Drug Delivery. *Biomaterials* **2013**, *34*, 3647–3657.
(78) Vialar, P.; Merzeau, P.; Giasson, S.; Drummond, C. Compliant Surfaces under Shear: Elastohydrodynamic Lift Force. *Langmuir* **2019**, *35*, 15605–15613.
(79) Vialar, P.; Merzeau, P.; Barthel, E.; Giasson, S.; Drummond, C. Interaction between Compliant Surfaces: How Soft Surfaces Can Reduce Friction. *Langmuir* **2019**, *35*, 15723–15728.
(80) Ou, C.; Wang, C.-S.; Giasson, S. Enhanced Swelling Using Photothermal Responsive Surface-Immobilized Microgels. *J. Appl. Polym. Sci.* **2021**, *138*, 50973–50988.
(81) Shearer, N.; Coover, H. Amide Rodent Repellent Compositions. US2790744A, 1954.
(82) Specht, E. H.; Neuman, A.; Neher, H. T. Preparation of Acrylamides. US2773063A, 1956.
(83) Work, W.; Horie, K.; Hess, M.; Stepto, R. F. T.; Work, W. Definitions of Terms Related to Polymer Blends, Composites, and Multiphase Polymeric Materials. *Pure Appl. Chem.* **2004**, *76*, 1985–2007.
(84) Schild, H. G. Poly(N-Isopropylacrylamide): Experiment, Theory and Application. *Prog. Polym. Sci.* **1992**, *17*, 163–249.
(85) Haq, M. A.; Su, Y.; Wang, D. Mechanical Properties of PNIPAM Based Hydrogels: A Review. *Mater. Sci. Eng. C* **2017**, *70*, 842–855.
(86) Vihola, H.; Laukkanen, A.; Valtola, L.; Tenhu, H.; Hirvonen, J. Cytotoxicity of Thermosensitive Polymers Poly(N-Isopropylacrylamide), Poly(N-Vinylcaprolactam) and

Amphiphilically Modified Poly(N-Vynilcaprolactam). *Biomaterials* **2005**, *26*, 3055–3064.
(87) Sierra-Martín, B.; Laporte, Y.; South, A. B.; Lyon, A.; Fernández-Nieves, A. Bulk Modulus of Poly(N-Isopropylacrylamide) Microgels through the Swelling Transition. *Phys. Rev. E* **2011**, *84*, 011406–011410.
(88) Burmistrova, A.; Richter, M.; Eisele, M.; Üzüm, C.; von Klitzig, R. The Effect of Co-Monomer Content on the Swelling/Shrinking and Mechanical Behavior of Individually Adsorbed PNIPAM Microgel Particles. *Polym.* **2011**, *3*, 1575–1590.
(89) Sierra-Martín, B.; Retama, J. R.; Laurenti, M.; Fernández-Barbero, A.; López Cabarcos, E. Structure and Polymer Dynamics within PNIPAM-Based Microgel Particles. *Adv. Colloid Interface Sci.* **2014**, *205*, 113–123.
(90) Pelton, R. Poly(N-Isopropylacrylamide) (PNIPAM) Is Never Hydrophobic. *J. Colloid Interface Sci.* **2010**, *348*, 673–674.
(91) Cao, Y.; Zhang, C.; Shen, W.; Cheng, Z.; Yu, L.; Ping, Q. Poly(N-Isopropylacrylamide)-Chitosan as Thermosensitive in Situ Gel-Forming Systems for Ocular Drug Delivery. *J. Control. Release* **2007**, *120*, 186–194.
(92) Geever, L.; Devine, D.; Nugent, M.; Kennedy, J.; Lyons, J.; Hanley, A.; Higginbotham, C. Lower Critical Solution Temperature Control and Swelling Behaviour of Physically Crosslinked Thermosensitive Copolymers Based on N-Isopropylacrylamide. *Eur. Polym. J.* **2006**, *42*, 2540–2548.
(93) Zhuo, R.-X.; Li, W. Preparation and Characterization of Macroporous Poly(N-Isopropylacrylamide) Hydrogels for the Controlled Release of Proteins. *J. Polmer Sci. Part A* **2003**, *41*, 152–159.
(94) Zhao, Z.; Li, Z.; Xia, Q.; Xi, H.; Lin, Y. Fast Synthesis of Temperature-Sensitive PNIPAAm Hydrogels by Microwave Irradiation. *Eur. Polym. J.* **2008**, *44*, 1217–1224.
(95) Leon-Lopez, T.; Ortega-Vinuesa, J.; Bastos-Gonzalez, D.; Elaissari, A. Cationic and Anionic Poly-(N-Isopropylacrylamide) Based Submicron Gel Particles: Electrokinetic Properties and Colloidal Stability. *J. Phys. Chem. B* **2006**, *110*, 4629–4636.
(96) Perez-Fuentes, L.; Drummond, C.; Faraudo, J.; Bastos-Gonzalez, D. Anions Make the Difference: Insights from the Interaction of Big Cations and Anions with Poly(N-Isopropylacrylamide) Chains and Microgels. *Soft Matter* **2015**, *11*, 5077–5086.
(97) Suzuki, D.; McGrath, J.; Kawaguchi, H.; Lyon, A. Colloidal Crystals of Thermosensitive, Core/Shell Hybrid Microgels. *J. Phys. Chem. C* **2007**, *111*, 5667–5672.
(98) Santos, A. M.; Elaissari, A.; Martinho, J. M. G.; Pichot, C. Synthesis of Cationic Poly(Methyl Methacrylate)-Poly(N-Isopropyl Acrylamide) Core-Shell Latexes via Two-Stage Emulsion Copolymerization. *Polymer* **2005**, *46*, 1181–1188.
(99) Winnik, F. Phase Transition of Aqueous Poly-(N-Isopropylacrylamide) Solutions: A Study by Non-Radiative Energy Transfer. *Polymer* **1990**, *31*, 2125–2134.
(100) Winnik, F. Fluorescence Studies of Aqueous Solutions of Poly(N-Isopropylacrylamide) below and above Their LCST. *Macromolecules* **1990**, *23*, 233–242.
(101) Kungwatchakun, D.; Irie, M. Photoresponsive Polymers. Photocontrol of the Phase Separation Temperature of Aqueous Solutions of Poly[N-Isopropylacrylamide-Co-N-(4-Phenylazophenyl)Acrylamide]. *Macromol. Rapid Commun.* **1988**, *9*, 243–246.
(102) Inomata, H.; Goto, S.; Saito, S. Phase Transition of N-Substituted Acrylamide Gels. *Macromolecules* **1990**, *23*, 4887–4888.

(103) Inomata, H.; Yagi, Y.; Otake, K.; Konno, M.; Saito, S. Spinodal Decomposition on an Aqueous Solution of Poly(N-Isopropylacrylamide). *Macromolecules* **1989**, *22*, 3494–3495.
(104) Chiklis, C. K.; Grasshoff, J. M. Swelling of Thin Films. Acrylamide-N-Isopropylacrylamide Copolymers in Water. *J. Polmer Sci. Part A* **1970**, *8*, 1617–1626.
(105) Otsu, T.; Kennedy, J. Hydrogen Transfer Polymerization with Anionic Catalysts and the Problem of Anionic Lsomerization Polymerization. *J. Macromol. Sci. Part C* **1972**, *6*, 237–283.
(106) Uenoyama, S.; Hoffman, A. Synthesis and Characterization of Acrylamide-N-Isopropyl Acrylamide Copolymer Grafts on Silicone Rubber Substrates. *Int. J. Radiat. Appl. Instrumentation. Part A* **1988**, *32*, 605–608.
(107) Zurakowska-Orszagh, J. Solid-State Polymerization of N-Substituted Acrylamides: 2. *Polymer* **1978**, *19*, 720–726.
(108) Esposito, C.; Kirilov, P.; Roullin, G. V. Organogels, Promising Drug Delivery Systems: An Update of State-of-the-Art and Recent Applications. *J. Control. Release* **2018**, *271*, 1–20.
(109) Kawaguchi, H. Thermoresponsive Microhydrogels: Preparation, Properties and Applications. *Polym. Int.* **2014**, *63* (6), 925–932.
(110) Edward, J. T. Molecular Volumes and the Stokes-Einstein Equation. *J. Chem. Educ.* **1970**, *47*, 261–270.
(111) Kawaguchi, H. Functional Polymer Microspheres. *Prog. Polym. Sci.* **2000**, *25* (8), 1171–1210.
(112) Tanaka, T.; Fillmore, D. J. Kinetikcs of Swelling of Gels. *J. Chem. Phys.* **1979**, *70* (3), 1214–1218.
(113) Giasson, S.; Lagleize, J. M.; Rodriguez-Hernandez, J.; Drummond, C. Boundary Lubricant Polymer Films: Effect of Cross-Linking. *Langmuir* **2013**, *29* (42), 12936–12949.
(114) Harris, M.; Chess, R. Effect of Pegylation on Pharmaceuticals. *Nat. Rev. Drug Discov.* **2003**, *2*, 214–221.
(115) Knop, K.; Hoogenboom, R.; Fischer, D.; Schubert, U. Poly(Ethylene Glycol) in Drug Delivery: Pros and Cons as Well as Potential Alternatives. *Angew. Chemie Int. Ed.* **2010**, *49*, 6288–6308.
(116) Wilson, C.; Clegg, R.; Leavesley, D.; Pearcy, M. Mediation of Biomaterial-Cell Interactions by Adsorbed Proteins: A Review. *Tissue Eng.* **2005**, *11*, 1–18.
(117) Ostuni, E.; Chapman, R.; Holmlin, E.; Takayama, S.; Whitesides, G. A Survey of Structure-Property Relationships of Surface That Resist the Adsorption of Protein. *Langmuir* **2001**, *17*, 5605–5620.
(118) Li, L.; Chen, S.; Jiang, S. Protein Interactions with Oligo(Ethylene Glycol) (OEG) Self-Assembled Monolayers: OEG Stability, Surface Packing Density and Protein Adsorption. *J. Biomater. Sci.* **2012**, *18*, 1415–1427.
(119) Duncan, R.; Gaspar, R. Nanomedicine(s) under the Microscope. *Mol. Pharm.* **2011**, *8*, 2101–2141.
(120) Pasut, G.; Veronese, F. State of the Art in PEGylation: The Great Versatility Achieved after Forty Years of Research. *J. Control. Release* **2012**, *161*, 461–472.
(121) Polson, A.; Potgieter, G. M.; Largier, J. F.; Mears, G. E. F.; Joubert, F. J. The Fractionation of Protein Mixtures by Linear Polymers of High Molecular Weight. *Biochim. Biophys. Acta - Gen. Subj.* **1964**, *82*, 463–475.
(122) Zeppezauer, M.; Brishammar, S. Protein Precipitation by Uncharged Water-Soluble

Polymers. *Biochim. Biophys. Acta - Gen. Subj.* **1965**, *94*, 581–583.
(123) Hurwitz, E.; Klapper, L.; Wilcheck, M.; Yarden, Y.; Sela, M. Inhibition of Tumor Growth by Poly(Ethylene Glycol) Derivatives of Anti-ErbB2 Antibodies. *Cancer Immunol. Immunother.* **2000**, *49*, 226–234.
(124) Veronese, F. Peptide and Protein PEGylation: A Review of Problems and Solutions. *Biomaterials* **2001**, *22*, 405–417.
(125) Kolate, A.; Baradia, D.; Patil, S.; Vhora, I.; Kore, G.; Misra, A. PEG - A Versatile Conjugating Ligand for Drugs and Drug Delivery Systems. *J. Control. Release* **2014**, *192*, 67–81.
(126) Greenwald, R.; Chloe, Y.; McGuire, J.; Conover, C. Effective Drug Delivery by PEGylated Drug Conjugates. *Adv. Drug Deliv. Rev.* **2003**, *55*, 217–250.
(127) Cheng, J.; Teply, B.; Sherifi, I.; Sung, J.; Luther, G.; Gu, F.; Nissenbaum, E.; Radovic-Moreno, A.; Langer, R.; Farokhzad, O. C. Formulation of Functionalized PLGA-PEG Nanoparticles for in Vivo Targeted Drug Delivery. *Biomaterials* **2007**, *28*, 869–876.
(128) Veronese, F.; Pasut, G. PEGylation, Succesful Approach to Drug Delivery. *Drug Discov. Today* **2005**, *10*, 1451–1458.
(129) Owens, D.; Peppas, N. A. Opsonization, Biodistribution, and Pharmacokinetics of Polymeric Nanoparticles. *Int. J. Pharm.* **2006**, *307*, 93–102.
(130) Karmali, P.; Simberg, D. Interactions of Nanoparticles with Plasma Proteins: Implications on Clearance and Toxicity of Drug Delivery Systems. *Expert Opin. Drug Deliv.* **2011**, *8*, 343–357.
(131) Jeon, S. I.; Lee, J. H.; Andrade, J. D.; De Gennes, P. G. Protein-Surface Interactions in the Presence of Polyethylene Oxide: I. Simplified Theory. *J. Colloid Interface Sci.* **1991**, *142*, 149–158.
(132) Dobrovolskaia, M.; McNeil, S. Immunological Properties of Engineered Nanomaterials. *Nat. Nanotechnol.* **2007**, *2*, 469–478.
(133) Banerjee, I.; Pangule, R.; Kane, R. Antifouling Coatings: Recent Developments in the Design of Surfaces That Prevent Fouling by Proteins, Bacteria, and Marine Organisms. *Adv. Mater.* **2010**, *23*, 690–718.
(134) Shih, Y.-J.; Chang, Y.; Quemener, D.; Yang, H.-S.; Jhong, J.-F.; Ho, F.-M.; Higuchi, A.; Chang, Y. Hemocompatibility of Polyampholyte Copolymers with Well-Defined Charged Bias in Human Blood. *Langmuir* **2014**, *30*, 6489–6496.
(135) Chen, S.; Li, L.; Zhao, C.; Zheng, J. Surface Hydration: Principles and Applications towards Low-Fouling/Nonfouling Biomaterials. *Polymer* **2010**, *51*, 5283–5293.
(136) Kobayashi, M.; Koide, T.; Hyon, S.-H. Tribological Characteristics of Polyethylene Glycol (PEG) as a Lubricant for Wear Resistance of Ultra-High-Molecular-Weight Polyethylene (UHMWPE) in Artificial Knee Join. *J. Mech. Behav. Biomed. Mater.* **2014**, *38*, 33–38.
(137) Spencer, N. Aqueous Lubrication with Poly(Ethylene Glycol) Brushes. *Tribol. Online* **2014**, *9*, 143–153.
(138) Lü, S.; Li, B.; Sun, Z.; Liu, M.; Wang, Q. Thermoresponsive Injectable Hydrogel for Three-Dimensional Cell Culture: Chondroitin Sulfate Bioconjugated with Poly(N-Isopropylacrylamide) Synthesized by RAFT Polymerization. *Soft Matter* **2011**, *22*, 10763–10772.
(139) Alexander, A.; Ajazuddin; Khan, J.; Saraf, S.; Saraf, S. Polyethylene Glycol (PEG)-Poly(N-Isopropylacrylamide) (PNIPAAm) Based Thermosensitive Injectable Hydrogels for

Biomedical Applications. *Eur. J. Pharm. Biopharm.* **2014**, *88*, 575–585.
(140) Wang, J.; Lin, L.; Cheng, Q.; Jiang, L. A Strong Bio-Inspired Layered PNIPAM-Clay Nanocomposite Hydrogel. *Angew. Chemie Int. Ed.* **2012**, *51*, 4676–4680.
(141) Tokarev, I.; Minko, S. Stimuli-Responsive Hydrogel Thin Films. *Soft Matter* **2009**, *5*, 511–524.
(142) Wang, C.; Flynn, N. T.; Langer, R. Controlled Structure and Properties of Thermoresponsive Nanoparticle-Hydrogel Composites. *Adv. Mater.* **2004**, *16*, 1074–1079.
(143) Gaharwar, A. K.; Peppas, N. A.; Khademhosseini, A. Nanocomposite Hydrogels for Biomedical Applications. *Biotechnol. Bioeng.* **2014**, *111*, 441–453.
(144) Alivisatos, P. The Use of Nanocrystals in Biological Detection. *Nat. Biotechnol.* **2004**, *22*, 47–52.
(145) Rosi, N.; Mirkin, C. Nanostructures in Biodiagnosis. *Chem. Rev.* **2005**, *105*, 1547–1562.
(146) Michalet, X.; Pinaud, F.; Bentolila, L.; Tsay, J.; Doose, S.; Li, J. J.; Sundaresan, G.; Wu, A. M.; Gambhir, S. S.; Weiss, S. Quantum Dots for Live Cells, in Vivo Imaging, and Diagnostics. *Science (80-.).* **2005**, *307*, 538–544.
(147) Lee, N.; Hyeon, T. Designed Synthesis of Uniformly Sized Iron Oxide Nanoparticles for Efficient Magnetic Resonance Imaging Contrast Agents. *Chem. Soc. Rev.* **2012**, *41*, 2575–2589.
(148) Liu, Y.; Ballauff, M. Thermosensitive Core-Shell Microgels: From Colloidal Model Systems to Nanoreactors. *Prog. Polym. Sci.* **2011**, *36*, 767–792.
(149) Peer, D.; Karp, J. M.; Hong, S.; Farokhzad, O. C.; Margalit, R.; Langer, R. Nanocarriers as an Emerging Platform for Cancer Therapy. *Nat. Nanotechnol.* **2007**, *2* (12), 751–760. https://doi.org/10.1038/nnano.2007.387.
(150) Maeda, H.; Greish, K.; Fang, J. The EPR Effect and Polymeric Drugs: A Paradigm Shift for Cancer Chemotherapy in the 21st Century. *Adv. Polym. Sci.* **2006**, *193*, 103–121.
(151) Maeda, H. The Enhanced Permeability and Retention (EPR) Effect in Tumor Vasculature: The Key Role of Tumor-Selective Macromolecular Drug Targeting. *Adv. Enzyme Regul.* **2001**, *41* (1), 189–207. https://doi.org/10.1016/S0065-2571(00)00013-3.
(152) Kohler, N.; Sun, C.; Fichtenholtz, A.; Gunn, J.; Fang, C.; Zhang, M. Methotrexate-Immobilized Poly(Ethylene Glycol) Magnetic Nanoparticles for MR Imaging and Drug Delivery. *Small* **2006**, *2*, 785–792.
(153) Liong, M.; Lu, J.; Kovochich, M.; Xia, T.; Ruehm, S. G.; Nel, A. E.; Tamanoi, F.; Zink, J. I. Multifunctional Inorganic Nanoparticles for Imaging, Targeting, and Drug Delivery. *ACS Nano* **2008**, *2*, 889–896.
(154) Taylor, K. M. L.; Rieter, W. J.; Lin, W. Manganese-Based Nanoscale Metal-Organic Frameworks for Magnetic Resonance Imaging. *J. Am. Chem. Soc.* **2008**, *130*, 14358–14359.
(155) Cabral, H.; Nishiyama, N.; Kataoka, K. Supramolecular Nanodevices: From Design Validation to Theranostic Nanomedicine. *Acc. Chem. Res.* **2011**, *44*, 999–1008.
(156) Satapathy, S.; Bhol, P.; Chakkarambath, A.; Mohanta, J.; Samantaray, K.; Bhat, S.; Panda, S.; Mohanty, P.; Si, S. Thermo-Responsive PNIPAM-Metal Hybrids: An Efficient Nanocatalyst for the Reduction of 4-Nitrophenol. *Appl. Surf. Sci.* **2017**, *420*, 753–763.
(157) Singh, R.; Bhol, P.; Mandal, D.; Mohanty, P. Stimuli-Responsive Photoluminescence Soft Hybrid Microgel Particles: Synthesis and Characterizations. *J. Phys. Condens. Matter* **2020**, *32*, 044001–044010.

(158) Zhang, J.; Xu, S.; Kumacheva, E. Polymer Microgels: Reactors for Semiconductor, Metal, and Magnetic Nanoparticles. *J. Am. Chem. Soc.* **2004**, *126*, 7908–7914.
(159) Brändel, T.; Sabadasch, V.; Hannappel, Y.; Hellweg, T. Improved Smart Microgel Carriers for Catalytic Silver Nanoparticles. *ACS Omega* **2019**, *4*, 4636–4649.
(160) Álvarez-Puebla, R.; Contreras-Cáceres, R.; Pastoriza-Santos, I.; Pérez-Juste, J.; Liz-Marzán, L. Au@pNIPAM Colloids as Molecular Traps for Surface-Enhaced, Spectroscopic, Ultra-Sensitivity Analysis. *Angew. Chem.* **2009**, *121*, 144–149.
(161) Kamzabek, D.; Le Dé, B.; Coche-Guérente, L.; Miomandre, F.; Dubacheva, G. Thermoresponsive Fluorescence Switches Based on Au@pNIPAM Nanoparticles. *Langmuir* **2021**, *37*, 10971–10978.
(162) Bhol, P.; Mohanty, P. Smart Microgel-Metal Hybrid Particles of PNIPAM-Co-PAA@AgAu: Synthesis, Characterizations and Modulated Catalytic Activity. *J. Phys. Condens. Matter* **2021**, *33*, 084002–084015.
(163) Kwon, Y.; Choi, Y.; Jang, J.; Yoon, S.; Choi, J. NIR Laser-Responsive PNIPAM and Gold Nanorod Composites for the Engineering of Thermally Reactive Drug Delivery Nanomedicine. *Pharmaceutics* **2020**, *12*, 204–222.
(164) Li, H.-J.; Li, P.-Y.; Li, L.-Y.; Haleem, A.; He, W.-D. Gold Nanoparticles Grafted with PLL-b-PNIPAM: Interplay on Thermal/PH Dual/Response and Optical Properties. *Molecules* **2018**, *23*, 921–934.
(165) Lance, K.; Coronado, E.; Zhao, L.; Schatz, G. C. The Optical Properties of Metal Nanoparticles: The Influence of Size, Shape, and Dielectric Environment. *J. Phys. Chem. B* **2002**, *107*, 668–677.
(166) Virtanen, J.; Holappa, S.; Lemmetyinen, H.; Tenhu, H. Aggregation in Aqueous Poly(N-Isopropylacrylamide)-Block-Poly(Ethylene Oxide) Solutions Studied by Fluorescence Spectroscopy and Light Scattering. *Macromolecules* **2002**, *35*, 4763–4769.
(167) Motokawa, R.; Morishita, K.; Koizumi, S.; Nakahira, T.; Annaka, M. Thermosensitive Diblock Copolymer of Poly(N-Isopropylacrylamide) and Poly(Ethylene Glycol) in Water: Polymer Preparation and Solution Behavior. *Macromolecules* **2005**, *38*, 5748–5760.
(168) Zhang, W.; Shi, L.; Wu, K.; An, Y. Thermoresponsive Micellization of Poly(Ethylene Glycol)-b-Poly(N-Isopropylacrylamide) in Water. *Macromolecules* **2005**, *38*, 5743–5747.
(169) Qin, S.; Geng, Y.; Discher, D.; Yang, S. Temperature-Controlled Assembly and Release from Polymer Vesicles of Poly(Ethylene Oxide)-Block-Poly(N-Isopropylacrylamide). *Adv. Mater.* **2006**, *18*, 2905–2909.
(170) Akimoto, J.; Nakayama, M.; Sakai, K.; Okano, T. Thermally Controlled Intracellular Uptake System of Polymeric Micelles Possessing Poly(N-Isopropylacrylamide)-Based Outer Coronas. *Mol. Pharm.* **2010**, *7*, 926–935.
(171) Rijcken, C.; Veldhuis, T.; Ramzi, A.; Meeldijk, J.; Nostrum, C.; Hennink, W. E. Novel Fast Degradable Thermosensitive Polymeric Micelles Based on PEG-Block-Poly(N-(2-Hydroxyethyl)Methacrylamide-Oligolactates). *Biomacromolecules* **2005**, *6*, 2343–2351.
(172) Xie, B.; Jin, L.; Luo, Z.; Yu, J.; Shi, S.; Zhang, Z.; Shen, M.; Chen, H.; Li, X.; Song, Z. An Injectable Thermosensitive Polymeric Hydrogel for Sustained Release of Avastatin to Treat Posterior Segment Disease. *Int. J. Pharm.* **2015**, *490*, 375–383.
(173) Tan, R.; She, Z.; Wang, M.; Fang, Z.; Liu, Y.; Feng, Q. Thermo-Sensitive Alginate-Based Injectable Hydrogel for Tissue Engineering. *Carbohydr. Polym.* **2012**, *87*, 1515–1521.

(174) Okuyama, Y.; Yoshida, R.; Sakai, K.; Okano, T.; Sakurai, Y. Swelling Controlled Zero Order and Sigmoidal Drug Release from Thermo-Responsive Poly(N-Isopropylacrylamide-Co-Butyl Methacrylate) Hydrogel. *J. Biomater. Sci.* **1993**, *4*, 545–556.
(175) Jones, D.; Lorimer, C.; McCoy, C.; Gorman, S. Characterization of the Physicochemical, Antimicrobial, and Drug Release Properties of Thermoresponsive Hydrogel Copolymers Designed for Medical Device Applications. *J. Biomed. Mater. Res.* **2008**, *85B*, 417–426.
(176) Zhang, L.; Wang, L.; Guo, B.; Ma, P. Cytocompatible Injectable Carboxymethyl Chitosan/N-Isopropylacrylamide Hydrogels for Localized Drug Delivery. *Carbohydr. Polym.* **2014**, *103*, 110–118.
(177) Andrei, M.; Turturica, G.; Stanescu, P.; Teodorescu, M. Thermosensitive Injectable Hydrogels from Poly(N-Isopropylacrylamide)-Dextran Aqueous Solutions: Thermogelation and Drug Release Properties. *Soft Mater.* **2016**, *14*, 169–169.
(178) Serres, A.; Baudys, M.; Kim, S. W. Temperature and PH-Sensitive Polymers for Human Calcitonin Delivery. *Pharm. Res.* **1996**, *13*, 196–201.
(179) Ramkissoon-Ganorkar, C.; Liu, F.; Baudys, M.; Kim, S. W. Effect of Molecular Weight and Polydispersity on Kinetics of Dissolution and Release from PH/Temperature-Sensitive Polymers. *J. Biomater. Sci.* **2012**, *10*, 1149–1161.
(180) Fan, L.; Zhang, X.; Liu, X.; Sun, B.; Li, L.; Zhao, Y. Responsive Hydrogel Microcarrier-Integrated Microneedles for Versatile and Controllable Drug Delivery. *Adv. Healthc. Mater.* **2021**, *10* (2002249–2002257).
(181) Evanghelidis, A.; Beregoi, M.; Diculescu, V.; Galatanu, A.; Ganea, P.; Enculescu, I. Flexible Delivery Patch Systems Based on Thermoresponsive Hydrogels and Submicronic Fiber Heaters. *Sci. Rep.* **2018**, *8*, 17555–17565.
(182) Motornov, M.; Roiter, Y.; Tokarev, I.; Minko, S. Stimuli-Responsive Nanoparticles, Nanogels and Capsules for Integrated Multifunctional Intelligent Systems. *Prog. Polym. Sci.* **2010**, *35*, 174–211.
(183) Mura, S.; Nicolas, J.; Couvreur, P. Stimuli-Responsive Nanocarriers for Drug Delivery. *Nat. Mater.* **2013**, *12*, 991–1003.
(184) Gao, Y.; Zago, G.; Jia, Z.; Serpe, M. Controlled and Triggered Small Molecule Release from a Confined Polymer Film. *ACS Appl. Mater. Interfaces* **2013**, *5*, 9803–9808.
(185) Guo, S.; Gao, Y.; Wei, M.; Zhang, Q.; Serpe, M. Controlled Release Kinetics from a Surface Modified Microgel-Based Reservoir Device. *J. Mater. Chem. B* **2015**, *3*, 2516–2521.
(186) Campora, S.; Mohsen, R.; Passaro, D.; Samir, H.; Ashraf, H.; Al-Mofty, S.; Diab, A.; El-Sherbiny, I.; Snowden, M.; Ghersi, G. Functionalized Poly(N-Isopropylacrylamide)-Based Microgels in Tumor Targeting Drug Delivery. *Gels* **2021**, *7*, 203–220.
(187) Yanagisawa, O.; Homma, T.; Okuwaki, T.; Shimao, D.; Takahashi, H. Effects of Cooling on Human Skin and Skeletal Muscle. *Eur. J. Appl. Physiol.* **2007**, *100*, 737–745.
(188) Utsunomiya, M.; Nitta, K.; Sawagichi, H.; Yoshikawa, A.; Karasuno, H.; Morozumi, K.; Allison, G. T.; Fujiwara, T.; Abe, K. Changes in Blood Flow, Temperature and Muscle Endurance in Association with Cryotherapy. *J. Phys. Ther. Sci.* **2010**, *22*, 43–49.
(189) Guan, Y.; Zhang, Y. PNIPAM Microgels for Biomedical Applications: From Dispersed Particles to 3D Assemblies. *Soft Matter* **2011**, *7*, 6375–6384.
(190) Zhang, Y.; Guan, Y.; Zhou, S. Permeability Control of Glucose-Sensitive Nanoshells. *Biomacromolecules* **2007**, *8*, 3842–3847.

(191) Vikulina, A.; Feoktistova, N.; Balabushevich, N.; von Klitzig, R.; Volodkin, D. Cooling-Triggered Release from Mesoporous Poly(N-Isopropylacrylamide) Microgels at Physiological Conditions. *ACS Appl. Mater. Interfaces* **2020**, *12*, 57401–57409.
(192) Lerman, M.; Lembong, J.; Muramoto, S.; Gillen, G.; Fisher, J. The Evolution of Polystyrene as a Cell Culture Material. *Tissue Eng.* **2018**, *24*, 359–372.
(193) Zheng, Q.; Iqbal, S.; Wan, Y. Cell Detachment: Post-Isolation Challenges. *Biotechnol. Adv.* **2013**, *31*, 1664–1675.
(194) Canavan, H.; Cheng, X.; Graham, D.; Ratner, B.; Castner, D. Cell Sheet Detachment Affects the Extracellular Matrix: A Surface Science Study Comparing Thermal Liftoff, Enzymatic and Mechanical Methods. *J. Biomed. Mater. Res. Part A* **2005**, *75A* (1), 1–13.
(195) Waymouth, C. Autoclavable Medium AM 77B. *J. Cell Physiol.* **1979**, *100* (3), 548–550.
(196) Revel, J. P.; Hoch, P.; Ho, D. Adhesion of Culture Cells to Their Substratum. *Exp. Cell Res.* **1974**, *84* (1–2), 207–218.
(197) Osunkoya, B. O.; Frances, C.; Mottram, C.; Isoun, M. Synthesis and Fate of Immunological Surface Receptors on Cultured Burkitt Lymphoma Cells. *Int. J. Cancer* **1969**, *4* (2), 159–165.
(198) Mano, J. Stimuli-Responsive Polymeric Systems for Biomedical Applications. *Adv. Eng. Mater.* **2008**, *10* (6), 515–568.
(199) Mendes, P. Stimuli-Responsive Surfaces for Bio-Applications. *Chem. Soc. Rev.* **2008**, *37* (11), 2361–2580.
(200) Yamada, K.; Geiger, B. Molecular Interactions in Cell Adhesion Complexes. *Curr. Opin. Cell Biol.* **1997**, *9*, 76–85.
(201) Grinnell, F. Cellular Adhesiveness and Extracellular Substrata. *Int. Rev. Cytol.* **1978**, *53*, 65–144.
(202) Norde, W.; Lyklema, J. Why Proteins Prefer Interfaces. *J. Biomater. Sci.* **1990**, *2*, 183–202.
(203) Malmsten, M. Affinity of the Adhesion Proteins. In *Biopolymers at Interfaces*; Malmsten, M., Ed.; CRC Press: Boca Raton, 2005; pp 19–42.
(204) Salloum, D.; Schlenoff, J. Protein Adsorption Modalities on Polyelectrolyte Multilayers. *Biomacromolecules* **2004**, *5*, 1089–1096.
(205) Israelachvili, J.; Pashley, R. Molecular Layering of Water at Surfaces and Origin of Repulsive Hydration Forces. *Nature* **1983**, *306*, 249–250.
(206) Andrade, J. D.; Hlady, V. Protein Adsorption and Materials Biocompatibility: A Tutorial Review and Suggested Hypotheses. In *Biopolymers/Non-Exclusion HPLC*; Springer Berlin Heidelberg, 1986; pp 1–63.
(207) Szleifer, I. Polymers and Proteins: Interactions at Interfaces. *Curr. Opin. Solid State Mater. Sci.* **1997**, *2*, 337–344.
(208) Yamada, N.; Okano, T.; Sakai, H.; Karikusa, F.; Sawasaki, Y.; Sakurai, Y. Thermo-Responsive Polymeric Surfaces; Control of Attachment and Detachment of Cultured Cells. *Die Makromol. Chemie, Rapid Commun.* **1990**, *11* (11), 571–576.
(209) Xue, C.; Choi, B.-C.; Choi, S.; Braun, P.; Leckband, D. Protein Adsorption Modes Determine Reversible Cell Attachment on Poly(N-Isopropyl Acrylamide) Brushes. *Adv. Funct. Mater.* **2012**, *22* (11), 2394–2401.
(210) Xia, Y.; Gu, Y.; Zhou, X.; Xu, H.; Zhao, X.; Yaseen, M.; Lu, J. R. Controllable Stabilization of Poly(N-Isopropylacrylamide)-Based Microgel Films through Biomimetic Mineralization of Calcium Carbonate. *Biomacromolecules* **2012**, *13*, 2299–2308.

(211) Wei, J.; Cai, J.; Li, Y.; Wu, B.; Gong, X.; Ngai, T. Investigation of Cell Behaviors on Thermo-Responsive PNIPAM Microgel Films. *Colloids Surf., B.* **2015**, *132*, 202–207.
(212) Nash, M.; Carroll, W.; Foley, P.; Maguire, G.; O'Connell, C.; Gorelov, A.; Beloshapkin, S.; Rochev, Y. Ultra-Thin Spin Coated Crosslinkable Hydrogels for Use in Cell Sheet Recovery-Synthesis, Characterisation to Appliocation. *Soft Matter* **2012**, *8* (14), 3889–3899.
(213) Haraguchi, K.; Takehisa, T.; Ebato, M. Control of Cell Cultivation and Cell Sheet Detachment on the Surface of Polymer/Clay Nanocomposite Hydrogels. *Biomacromolecules* **2006**, *7* (11), 3267–3275.
(214) Okano, T.; Yamada, N.; Sakai, H.; Sakurai, Y. A Novel Recovery System for Cultured Cells Using Plasma-Treated Polystyrene Dishes Grafted with Poly(N-Isopropylacrylamide). *J. Biomed. Mater. Res.* **1993**, *27*, 1243–1251.
(215) Yu, Q.; Zhang, Y.; Chen, H.; Zhou, F.; Wu, Z.; Huang, H.; Brash, J. Protein Adsorption and Cell Adhesion/Detachment Behavior on Dual-Responsive Silicon Surfaces Modified with Poly(N-Isopropylacrylamide)-Block-Polystyrene Copolymer. *Langmuir* **2010**, *26* (11), 8582–8588.
(216) Zhao, T.; Chen, H.; Zheng, J.; Yu, Q.; Wu, Z.; Yuan, L. Inhibition of Protein Adsorption and Cell Adhesion on PNIPAAm-Grafted Polyurethane Surface: Effect of Graft Molecular Weight. *Colloids Surf., B.* **2011**, *85* (1), 26–31.
(217) Pan, G.; Guo, Q.; Ma, Y.; Yang, H.; Li, B. Thermo-Responsive Hydrogel Layers Imprinted with RGDS Peptide: A System for Harvesting Cell Sheets. *Angew. Chemie Int. Ed.* **2013**, *52*, 6907–6911.
(218) Kumashiro, Y.; Fukumori, K.; Takahashi, H.; Nakayama, M.; Akiyama, Y.; Yamato, M.; Okano, T. Modulation of Cell Adhesion and Detachment on Thermo-Responsive Polymeric Surfaces through Observation of Surface Dynamics. *Colloids Surf., B.* **2013**, *106*, 198–207.
(219) Ito, Y.; Chen, G.; Guan, Y.; Imanishi, Y. Patterned Immobilization of Thermoresponsive Polymer. *Langmuir* **1997**, *13*, 2756–2759.
(220) Nash, M.; Healy, D.; Carroll, W.; Elvira, C.; Rochev, Y. Cell and Cell Sheet Recovery from PNIPAM Coatings; Motivation and History to Present Day Approaches. *J. Mater. Chem.* **2012**, *22*, 19376–19389.
(221) Yu, Q.; Zhang, Y.; Chen, H.; Wu, Z.; Huang, H.; Cheng, C. Protein Adsorption on Poly(N-Isopropylacrylamide)-Modified Silicon Surfaces: Effects of Grafted Layer Thickness and Protein Size. *Colloids Surf., B.* **2010**, *76* (2), 468–474.
(222) Conzatti, G.; Cavalie, S.; Combes, C.; Torrisani, J.; Carrere, N.; Tourrette, A. PNIPAM Grafted Surfaces through ATRP and RAFT Polymerization: Chemistry and Bioadhesion. *Colloids Surf., B.* **2017**, *151*, 143–155.
(223) Bauer, S.; Schmuki, P.; von der Mark, K.; Park, J. Engineering Biocompatible Impant Surfaces: Part I: Materials and Surfaces. *Prog. Mater. Sci.* **2013**, *58*, 261–326.
(224) Nagase, K.; Yamato, M.; Kanazawa, H.; Okano, T. Poly(N-Isopropylacrylamide)-Based Thermoresponsive Surfaces Provide New Types of Biomedical Applications. *Biomaterials* **2018**, *153*, 27–48.
(225) Okano, T.; Yamada, N.; Okuhara, M.; Sakai, H.; Sakurai, Y. Mechanism of Cell Detachment from Temperature-Modulated, Hydrophilic-Hydrophobic Polymer Surfaces. *Biomaterials* **1995**, *16*, 297–303.
(226) Grinnell, F.; Lang, B.; Phan, T. Binding of Plasma Fibronectin to the Surfaces of BHK Cells in Suspension at 4 °C. *Exp. Cell Res.* **1982**, *142*, 499–504.

(227) Kushida, A.; Yamato, M.; Konno, C.; Kikuchi, A.; Sakurai, Y.; Okano, T. Temperature-Responsive Culture Dishes Allow Nonenzymatic Harvest of Differentiated Madin-Darby Canine Kidney (MDCK) Cell Sheets. *J. Biomed. Mater. Res.* **2000**, *51*, 216–223.
(228) Maniotis, A.; Chen, C.; Ingber, D. Demonstration of Mechanical Connections between Integrins, Cytoskeletal Filaments, and Nucleoplasm That Stabilize Nuclear Structure. *Proc. Natl. Acad. Sci.* **1997**, *94*, 849–854.
(229) Dalby, M. Topographically Induced Direct Cell Mechanotransduction. *Med. Eng. Phys.* **2005**, *27*, 730–742.
(230) Ingber, D. Cellular Tensegrity: Defining New Rules of Biological Design That Govern the Cytoskeleton. *J. Cell Sci.* **1993**, *104*, 613–627.
(231) Ge, C.; Xiao, G.; Jiang, D.; Franceschi, R. Critical Role of the Extracellular Signal-Regulated Kinase-MAPK Pathway in Osteoblast Differentiation and Skeletal Development. *J. Cell Biol.* **2007**, *176*, 709–718.
(232) Chen, G.; Imanishi, Y.; Ito, Y. Effect of Protein and Cell Behavior on Pattern-Grafted Thermoresponsive Polymer. *J. Biomed. Mater. Res.* **1998**, *42*, 38–44.
(233) Ohki, T.; Yamato, M.; Ota, M.; Takagi, R.; Kondo, M.; Kanai, N.; Okano, T.; Yamamoto, M. Application of Regenerative Medical Technology Using Tissue-Engineered Cell Sheets for Endoscopic Submucosal Dissection of Esophageal Neoplasms. *Dig. Endosc.* **2015**, *27*, 182–188.
(234) Vacanti, J. P. Beyond Transplantation: Third Annual Samuel Jason Mixter Lecture. *Arch. Surg.* **1988**, *123* (5), 545–549.
(235) Langer, R.; Vacanti, J. P. Tissue Engineering. *Science (80-.).* **1993**, *260*, 920–926.
(236) Vacanti, C.; Vacanti, J. P. The Science of Tissue Engineering. *Orthop. Clin. North Am.* **2000**, *31* (3), 351–355.
(237) Nishida, K.; Yamato, M.; Hayashida, Y.; Watanabe, K.; Yamamoto, K.; Adachi, E.; Nagai, S.; Kikuchi, A.; Maeda, N.; Watanabe, H.; Okano, T.; Tano, Y. Corneal Reconstruction with Tissue-Engineering Cell Sheets Composed of Autologous Oral Mucousal Epithelium. *N. Engl. J. Med.* **2004**, *351*, 1187–1196.
(238) Ide, T.; Nishida, K.; Yamato, M.; Sumide, T.; Utsumi, M.; Nozaki, T.; Kikuchi, A.; Okano, T.; Tano, Y. Structural Characterization of Bioengineered Human Corneal Endothelial Cell Sheets Fabricated on Temperature-Responsive Culture Dishes. *Biomaterials* **2006**, *27*, 607–614.
(239) Nishida, K.; Yamato, M.; Hayashida, Y.; Watanabe, K.; Maeda, N.; Watanabe, H.; Yamamoto, K.; Nagai, S.; Kikuchi, A.; Tano, Y.; Okano, T. Functional Bioengineered Corneal Epithelial Sheet Grafts from Corneal Stem Cells Expanded Ex Vivo on a Temperature-Responsive Cell Culture Surface. *Transplantation* **2004**, *77*, 379–385.
(240) Akizuki, T.; Oda, S.; Komaki, M.; Tsuchioka, H.; Kawakatsu, N.; Kikuchi, A.; Yamato, M.; Okano, T.; Ishikawa, I. Application of Periodontal Ligament Cell Sheet for Periodontal Regeneration: A Pilot Study in Beagle Dogs. *J. Periodontal Res.* **2005**, *40*, 245–251.
(241) Iwata, T.; Yamato, M.; Tsuchioka, H.; Takagi, R.; Mukobata, S.; Washio, K.; Okano, T.; Ishikawa, I. Periodontal Regeneration with Multi-Layered Periodontal Ligament-Derived Cell Sheets in Canine Model. *Biomaterials* **2009**, *30*, 2716–2723.
(242) Wüst, S.; Müller, R.; Hofmann, S. Controlled Positioning of Cells in Biomaterials - Approaches Towards 3D Tissue Printing. *J. Funct. Biomater.* **2011**, *2*, 119–154.

(243) Zhou, F.; Hong, Y.; Liang, R.; Zhang, X.; Liao, Y.; Jiang, D.; Zhang, J.; Sheng, Z.; Xie, C.; Peng, Z.; Zhuang, X.; Bunpetch, V.; Zou, Y.; Huang, W.; Zhang, Q.; Alakpa, E. V.; Zhang, S.; Ouyang, H. Rapid Printing of Bio-Inspired 3D Tissue Constructs for Skin Regeneration. *Biomaterials* **2020**, *258*, 120287–120302.
(244) Haleem, A.; Javaid, M.; Khan, R. H.; Suman, R. 3D Printing Applications in Bone Tissue Engineering. *J. Clin. Orthop. Trauma* **2020**, *11*, S118–S124.
(245) Dogan, E.; Bhusal, A.; Cecen, B.; Miri, A. 3D Printing Metamaterials towards Tissue Engineering. *Appl. Mater. Today* **2020**, *20*, 100752–100765.
(246) Aibinder, W. R.; Schoch, B.; Schleck, C.; Sperling, J. W.; Cofield, R. H. Revisions for Aseptic Glenoid Component Loosening after Anatomic Shoulder Arthroplasty. *J. Shoulder Elb. Surg.* **2017**, *26*, 443–449.
(247) Lee, B.-S.; Cho, H.-I.; Bin, S.-I.; Kim, J.-M.; Jo, B.-K. Femoral Component Varus Malposition Is Associated with Tibial Aseptic Loosening After TKA. *Clin. Orthop. Relat. Res.* **2018**, *476*, 400–407.
(248) Singh, M. K. Polymer Brush Based Tribology. In *Tribology in Materials and Applications. Materials Forming, Machining and Tribology*; Katiyar, J., Ramkumar, P., Rao, T., Davim, J., Eds.; Springer, Cham, 2020; pp 15–32.
(249) Chen, Q.; Kooij, S.; Sui, X.; Padberg, C.; Hempenius, M.; Schön, P. M.; Vancso, G. J. Collapse from the Top: Brushes of Poly(N-Isopropylacrylamide) in Co-Nonsolvent Mixtures. *Soft Matter* **2014**, *10*, 3134–3142.
(250) Liu, Y.; Xiao, Y.; Luo, J. Preparation of Poly (N-Isopropylacrylamide) Brush Bonded on Silicon Substrate and Its Water-Based Lubricating Property. *Sci. China Technol. Sci.* **2012**, *55*, 3352–3358.
(251) Yu, Y.; Cirelli, M.; Kieviet, B. D.; Kooij, S.; Vancso, G. J.; de Beer, S. Tunable Friction by Employment of Co-Non-Solvency of PNIPAM Brushes. *Polymer* **2016**, *102*, 372–378.
(252) Gong, J. P. Friction and Lubrication of Hydrogels - Its Richness and Complexity. *Soft Matter* **2006**, *2* (7), 544–552.
(253) Sadd, M. *Elasticity: Theory, Applications, and Numerics*; Elsevier: Amsterdam, 2009.
(254) Nakayama, A.; Kakugo, A.; Gong, J. P.; Osada, Y.; Takai, M.; Erata, T.; Kawano, S. High Mechanical Strength Double-Network Hydrogel with Bacterial Cellulose. *Adv. Funct. Mater.* **2004**, *14*, 1124–1128.
(255) Huang, T.; Xu, H.; Jiao, K.; Zhu, L.; Brown, H. R.; Wang, H. A Novel Hydrogel with High Mechanical Strength: A Macromolecular Microsphere Composite Hydrogel. *Adv. Mater.* **2007**, *19*, 1622–1626.
(256) Chang, D.; Dolbow, J.; Zauscher, S. Switchable Friction of Stimulus-Responsive Hydrogels. *Langmuir* **2007**, *23*, 250–257.
(257) Wu, Y.; Cai, M.; Pei, X.; Yongmin, L.; Zhou, F. Switching Friction with Thermal-Responsive Gels. *Macromol. Rapid Commun.* **2013**, *34*, 1785–1790.
(258) Han, L.; Yin, J.; Wang, L.; Chia, K.-K.; Cohen, R.; Rubner, M.; Ortiz, C.; Boyce, M. Tunable Stimulus-Responsive Friction Mechanisms of Polyelectrolyte Films and Tube Forests. *Soft Matter* **2012**, *8*, 8642–8650.
(259) Xu, Y.; Bao, Y.; Liu, Z.; Zheng, Q.; Dong, Y.; Song, R.; Yang, B. Temperature-Sensitive Tribological Performance of Titanium Alloy Lubricated with PNIPAM Microgels. *Appl. Surf. Sci.* **2022**, *572*, 151392–151406.

(260) Xu, Y.; Liu, Z.; Dearn, K.; Dong, Y.; You, T.; Hu, X. Thermo-Tribological Behaviour of Microgels for Improved Aqueous Lubrication for Steel/UHMWPE Contact. *Tribol. Int.* **2019**, *130*, 63–73.
(261) Chen, Z.; Feng, Y.; Zhao, N.; Shi, J.; Liu, G.; Liu, W. Near-Infrared Photothermal Microgel for Interfacial Friction Control. *ACS Appl. Mater. Interfaces* **2021**, *3*, 4055–4061.
(262) Liu, G.; Wang, X.; Zhou, F.; Liu, W. Tuning the Tribological Property with Thermal Sensitive Microgels for Aqueous Lubrication. *ACS Appl. Mater. Interfaces* **2013**, *5*, 10842–10852.
(263) Kieviet, B. D.; Schön, P. M.; Vancso, G. J. Stimulus-Responsive Polymers and Other Functional Polymer Surfaces as Components in Glass Microfluidic Channels. *Lab Chip.* **2014**, *14*, 4159–4170.
(264) Zhao, Y.; Wen, J.; Sun, H.; Pan, D.; Huang, Y.; Bai, Y.; Shao, L. Thermo-Responsive Separation Membrane with Smart Anti-Fouling and Self-Cleaning Properties. *Chem. Eng. Res. Des.* **2020**, *156*, 333–342.
(265) D'Eramo, L.; Chollet, B.; Leman, M.; Martwong, E.; Li, M.; Geisler, H.; Dupire, J.; Kerdraon, M.; Vergne, C.; Monti, F.; Tran, Y.; Tabeling, P. Microfluidic Actuators Based on Temperature-Responsive Hydrogels. *Microsystems Nanoeng.* **2018**, *4*, 17069–17076.
(266) Meunier, F.; Elaissari, A.; Pichot, C. Preparation and Characterization of Cationic Poly(n-Isopropylacrylamide) Copolymer Latexes. *Polym. Adv. Technol.* **1995**, *6*, 489–496.
(267) Bradley, M.; Vincent, B. Poly(Vinylpyridine) Core/Poly(N-Isopropylacrylamide) Shell Microgel Particles: Their Characterization and the Uptake and Release of an Anionic Surfactant. *Langmuir* **2008**, *24*, 2421–2425.
(268) Bai, Y.; Zhang, Z.; Zhang, A.; Chen, L.; He, C.; Zhuang, X.; Chen, X. Novel Thermo- and PH-Responsive Hydroxypropyl Cellulose- and Poly (L-Glutamic Acid)-Based Microgels for Oral Insulin Controlled Release. *Carbohydr. Polym.* **2012**, *89*, 1207–1214.
(269) Raju, R.; Bandyopadhyay, S.; Sharma, A.; Villa Gonzalez, S.; Carlsen, P. H.; Gautun, O. R.; Glomm, W. R. Synthesis, Characterization and Drug Loading of Multiresponsive p[NIPAm-Co-PEGMA] (Core)/p[NIPAm-Co-AAC] (Shell) Nanogels with Monodisperse Size Distributions. *Polymers* **2018**, *10*, 309–323.
(270) Liu, L.; Zeng, J.; Zhao, X.; Tian, K.; Liu, P. Independent Temperature and PH Dual-Responsive PMAA/PNIPAM Microgels as Drug Delivery Systems: Effect of Swelling Behavior of the Core and Shell Materials in Fabrication Process. *Colloids Surf., A* **2017**, *526*, 48–55.
(271) Zeiser, M.; Freudensprung, I.; Hellweg, T. Linearly Thermoresponsive Core-Shell Microgels: Towards a New Class of Nanoactuators. *Polymer* **2012**, *53*, 6096–6101.
(272) Cors, M.; Wrede, O.; Genix, A.-C.; Anselmetti, D.; Oberdisse, J.; Hellweg, T. Core-Shell Microgel-Based Surface Coatings with Linear Thermoresponse. *Langmuir* **2017**, *33*, 6804–6811.
(273) Sabadasch, V.; Wiehemeier, L.; Kottke, T.; Hellweg, T. Core-Shell Microgels as Thermoresponsive Carriers for Catalytic Palladium Nanoparticles. *Soft Matter* **2020**, *16*, 5422–5430.
(274) Kikuchi, A.; Okano, T. Nanostructured Designs of Biomedical Materials: Applications of Cell Sheet Engineering to Functional Regenerative Tissues and Organs. *J. Control. Release* **2005**, *101*, 69–84.
(275) Cheng, X.; Canavan, H.; Stein, J.; Hull, J.; Kweskin, S.; Wagner, M.; Somorjai, G.; Castner, D.; Ratner, B. Surface Chemical and Mechanical Properties of Plasma-Polymerized N-

Isopropylacrylamide. *Langmuir* **2005**, *21* (17), 7833–7841.
(276) Mizutani, A.; Kikuchi, A.; Yamato, M.; Kanazawa, H.; Okano, T. Preparation of Thermoresponsive Polymer Brush Surfaces and Their Interaction with Cells. *Biomaterials* **2008**, *29* (13), 2073–2081.
(277) Matsuzaka, N.; Nakayama, M.; Takahashi, H.; Yamato, M.; Kikuchi, A.; Okano, T. Terminal-Functionality Effect of Poly(N-Isopropylacrylamide) Brush Surfaces on Temperature-Controlled Cell Adhesion/Detachment. *Biomacromolecules* **2013**, *14* (9), 3164–3171.
(278) Cheng, X.; Canavan, H.; Graham, D.; Castner, D.; Ratner, B. D. Temperature Dependent Activity and Structure of Adsorbed Proteins on Plasma Polymerized N-Isopropylacrylamide. *Biointerphases* **2006**, *1* (1), 61–72.

Chapter 2 – Experimental Methodology

2.1 Methodology – main experimental techniques

Throughout this work a variety of experimental techniques were necessary to manipulate products and to obtain data. The most important one, however, is the Surface Forces Apparatus (SFA) technique, used extensively to study the swelling and surface properties of microgel-coated surfaces. The majority of the results discussed in chapters 3 and 4 derive directly from experiments using the SFA and led to the determination that the developed functional substrates were suitable to be used in the study reported in chapter 5. In addition, a custom made tribometer (tribo-brush) was used to investigate the tribological properties of microgel-coated surfaces in the mesoscale for which the experimental protocol described in chapter 3 had to be modified. While other analytical techniques presented in this work are commonly available in research laboratories, the SFA and the tribo-brush are highly specialized tools used for a very specific set of applications. Therefore, the methodology section focuses in describing these techniques and does not delve into the fundamentals of operation of the secondary instrumentation techniques that were used as a support.

2.1.1 The Surface Forces Apparatus

The SFA was initially developed by Tabor, Winterton and Israelachvili in the 1970's and it allows to measure the interaction forces between two surfaces as a function of their separation distance.[1–3] Prior to their work, direct measurement of intermolecular forces had been reported by Derjaguin et al. in 1954 who used an electro-torsion balance (based on a design originally conceived by Coulomb in 1785 to measure electrical forces)[4] to measure van der Waals forces

between two glass surfaces down to a separation distance of 100 nm due to the high rugosity of glass.[5] Today, the SFA is the only technique capable of simultaneously measure force and the absolute separation distance between two surfaces (**Fig. 2.1**).[6] By using the SFA, it is possible to measure the normal and lateral forces between two surfaces across a controlled liquid or vapor medium. A major advantage of the SFA is the exceptional resolution and sensitivity that it offers. The normal and lateral distance resolutions are about 0.1 nm and 1 µm, respectively, while the force sensitivity is about 10^{-8} N.[7] Further, it allows to visualize the contact between two surfaces in real-time to study time- and rate-dependent effects, and to measure the refraction index as well as the contact area between the surfaces.[8,9]

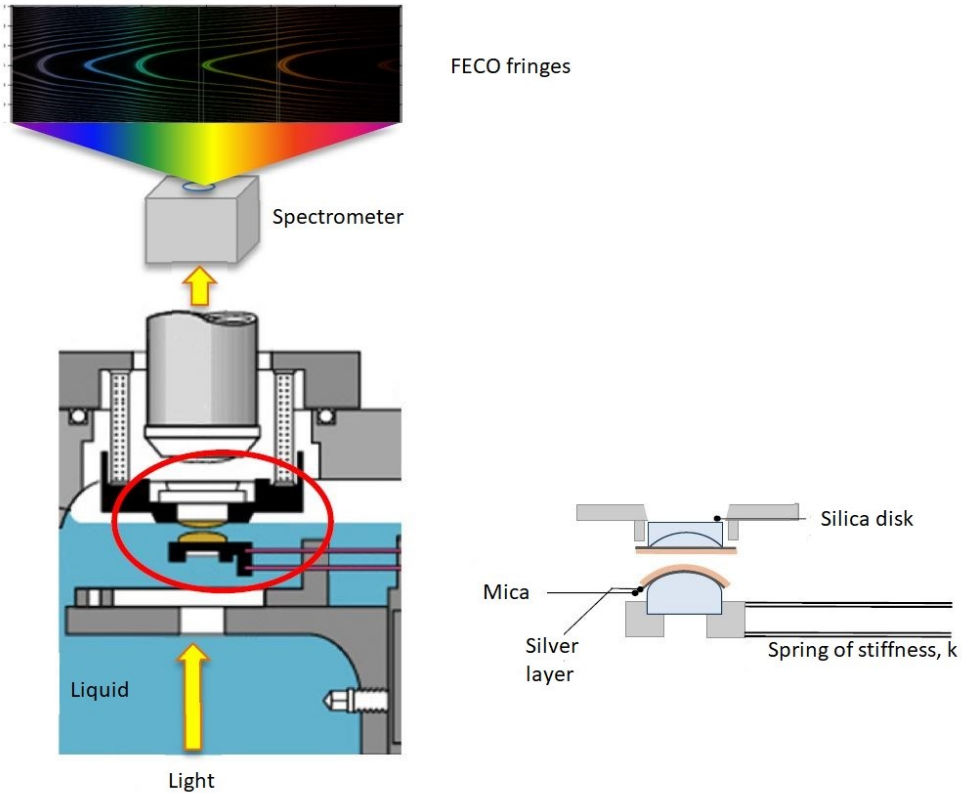

Figure 2.1. Schematic representation of the surface forces apparatus. Adapted and reproduced with permission from[10].

The most common substrate used in the SFA is muscovite mica due to its transparency and remarkably smooth surface and malleability that makes it easy to manipulate.[6,7,11] Mica surfaces are cleaved manually to obtain sheets a few micrometers thick, which makes them transparent enough to be used in optical interferometry. The system to be investigated, be it polymers, biomolecules, or thin films, is immobilized on the mica or suspended in a liquid and studied between the two mica surfaces. The mica sheets are glued onto half-cylindrical fused-silica disks (radius, R = 2 cm) and mounted in the SFA in a crossed-cylinder configuration such that the curbed axes of the cylinders are perpendicular to each other (**Fig. 2.2**). This configuration allows to have a single point of contact between the surfaces given that it is mathematically equivalent to a sphere-on-a-plane configuration when the separation distances (D) are much smaller than the curvature (R) of the surfaces according to the Derjaguin approximation,[7] a condition that is respected in SFA experiments. This set-up also provides additional experimental advantages compared to, for example, two parallel plates: alignment is easier to achieve, and different points of contact along the axes of the silica disks can be studied by simply displacing the disks laterally. This is useful, for example, to verify repeatability of measurements at different regions of a pair of mica sheets or to avoid debris or contamination. Further, the normal force, F_N, between cylindrical surfaces is related to the interaction energy between flat surfaces, W, according to the Derjaguin approximation,[7] $F_N(D)/R = 2\pi W$, which makes it easy to compare the experimental data with model predictions. For this reason, and to be able to quantitatively compare data from different experimental set-ups, the normal force data are usually presented normalized by R.

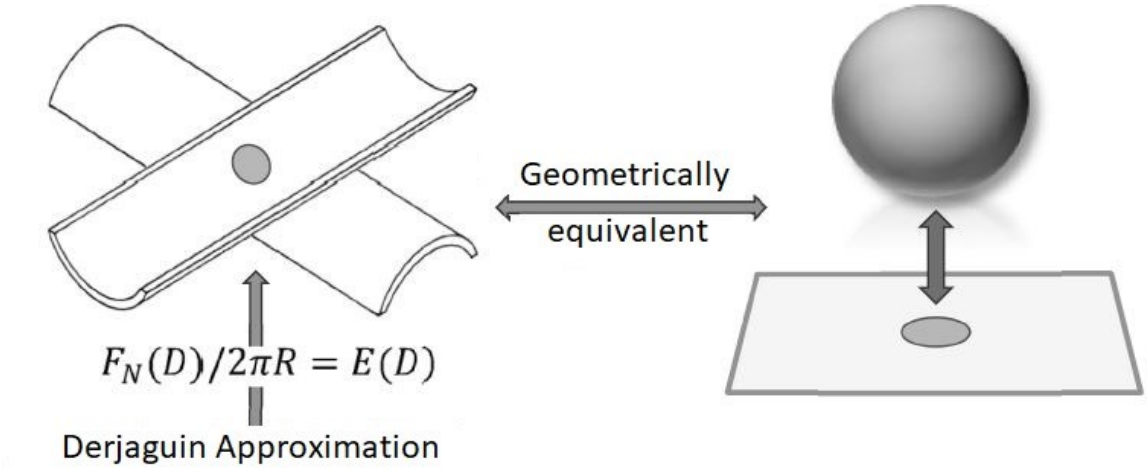

Figure 2.2. Schematic representation of the crossed-cylinder geometry of the silica disks and mathematical equivalent geometry. Adapted and reproduced with permission from[10].

The separation distance between the two surfaces is controlled by three distinct mechanisms of increasing sensitivity. A coarse micrometer allows positioning to about 1 µm, the fine micrometer (which deflects a helical spring that in turn bends a stiffer double-cantilever spring by 1/1000 of this amount) allows positioning to about 1 nm. Finally, a piezoelectric crystal tube which expands or contracts vertically when a voltage is applied, is used for positioning to 0.1 nm.

2.1.1.1 Measurement of the separation distance (*D*)

Measurement of the separation distance with subnanometer resolution is done by optical interferometry. First, the mica sheets are coated with a layer of silver approximately 50 nm thick before they are glued onto the curved silica disks (silvered sides down). The mica surfaces, the material confined between them, and the semitransparent, highly reflective silver layers on their backsides form a Fabry-Perot interferometer. White light is passed through the lower surface, and the wavelengths that interfere constructively after multiple reflections between the silver

layers emerge through the top surface. The emerging light is collimated onto the slit of a grating spectrometer and can be observed directly with an eyepiece or recorded with a camera for further analysis.[12] The resulting pattern is called Fringes of Equal Chromatic Order (FECO) and the shape of these fringes is directly related to the geometry of the contact area.[6,13] For example, when the surfaces are in physical contact, they appear flattened due to the elastic deformation of the substrate (**Fig. 2.3**). On the contrary, when the surfaces are not in contact, the fringes are round (**Fig. 2.3**). The wavelength interference pattern at the adhesive contact between bare mica surfaces in air or in dry nitrogen gas is used as $D = 0$. This distance is measured from a fringe of order n and of wavelength λ_n^0. Introducing a material confined between the mica surfaces increases the separation distance, D, between the front sides of the mica surfaces as well as the optical path which causes the fringes to shift to larger wavelengths with respect to λ_n^0. Hence, the separation distance between two mica surfaces of identical thickness can be calculated with the following equation:[7,8]

$$\tan\left(\frac{2\pi D}{\lambda_n^D}\right) = \frac{2\bar{n}\sin\left[\frac{1-\lambda_n^0/\lambda_n^D}{1-\lambda_n^0/\lambda_{n-1}^0}\pi\right]}{(1+\bar{n}^2)\cos\left[\frac{1-\lambda_n^0/\lambda_n^D}{1-\lambda_n^0/\lambda_{n-1}^D}\pi\right] \pm (\bar{n}^2-1)}$$

where the positive (+) sign represents odd fringes of order n and the negative (-) sign represents even fringes of order n-1. $\bar{n} = \frac{n_{mica}}{n_{medium}}$; where n_{mica} corresponds to the refractive index of mica and n_{medium} the refractive index of the medium between the two mica surfaces at wavelength λ_n^D. λ_n^0 and λ_{n-1}^0 correspond to the wavelengths of the even and odd FECO fringes, respectively, when the surfaces are in adhesive mica-mica contact in air (or nitrogen gas). λ_n^D and λ_{n-1}^D

correspond to the wavelengths of the even and odd FECO fringes, respectively, when the surfaces are at a separation distance *D*.

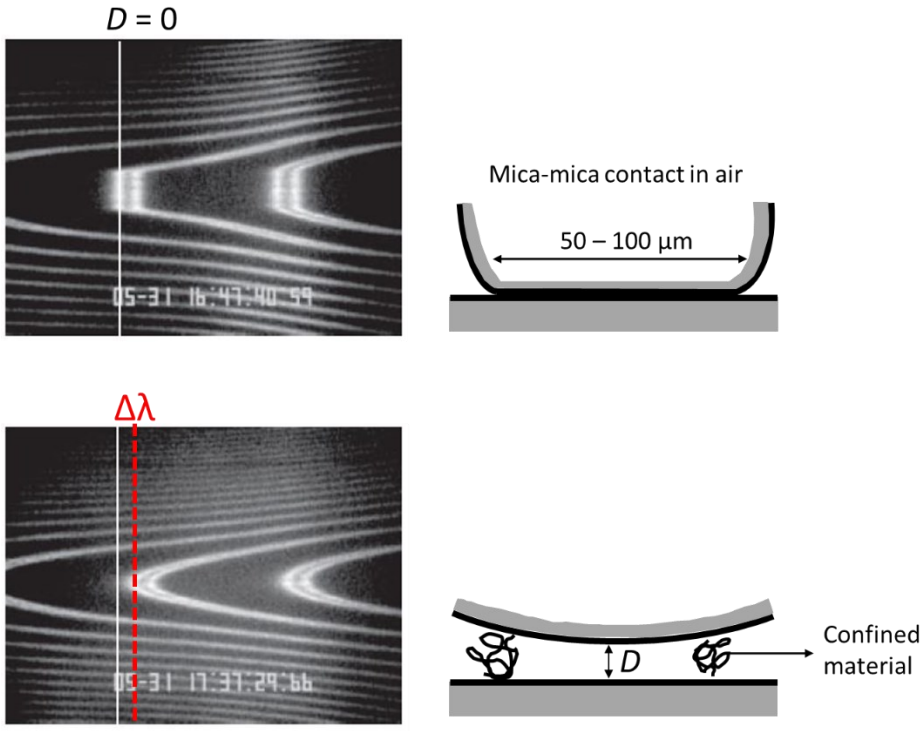

Figure 2.3. Principle of the measurement of the separation distance by using FECO. The variation in wavelength, Δλ, allows the determination of the separation distance, *D*, and the shape of the fringes indicate geometrical changes incurred upon physical contact. Adapted and reproduced with permission from[14].

2.1.1.2 Measurement of the normal force, F_N

The interaction forces in a direction normal to the surfaces are determined from the deflection of a double-cantilever spring supporting the lower surface (**Fig. 2.1**). A double cantilever beam is used to minimize tilting or sliding of the surfaces during the experiment. The spring constant, *k*, is determined by placing small weights on one of its ends and measuring the resulting deflection

with an optical microscope. During a normal force, F_N, measuring experiment, the deflection of the spring is monitored by observing the variation in wavelength of the FECO as the surfaces are moved toward or away from one another using the fine or piezoelectric displacement controls. At large separation distances, when no force is detected and there is no deflection of the springs, each incremental approaching or separating step imposed by the displacement controls, $\Delta D_{imposed}$, produces a measured displacement of equal magnitude, $\Delta D_{measured}$. Therefore, the deviation in distance, $\Delta D = \Delta D_{imposed} - \Delta D_{measured}$, is zero and the normal force is null according to Hooke's law, $\Delta F_N(D) = k\Delta D$. However, if interaction forces, either attractive or repulsive, are exerted on the surfaces the spring will experience a deflection and thus the imposed and measured distances are no longer the same, $\Delta D_{imposed} \neq \Delta D_{measured}$, and the magnitude of the interaction force is calculated by using Hooke's law (**Fig. 2.4**). Further, if the gradient of a force vs. distance curve, dF/dD, exceeds k, force measuring is no longer possible due to mechanical instability which is manifested by a spontaneous jump from one stable region to the next. Therefore, the precision in determining F_N depends on the spring constant, k, as well as on the resolution of measuring the change in separation distance, ΔD. By using this principle, it is possible to construct a force profile, where F_N is measured at each incremental approaching or separating step. Force profiles are typically reported normalized by R, the radius of the silica disks, in accordance with the Derjaguin approximation.

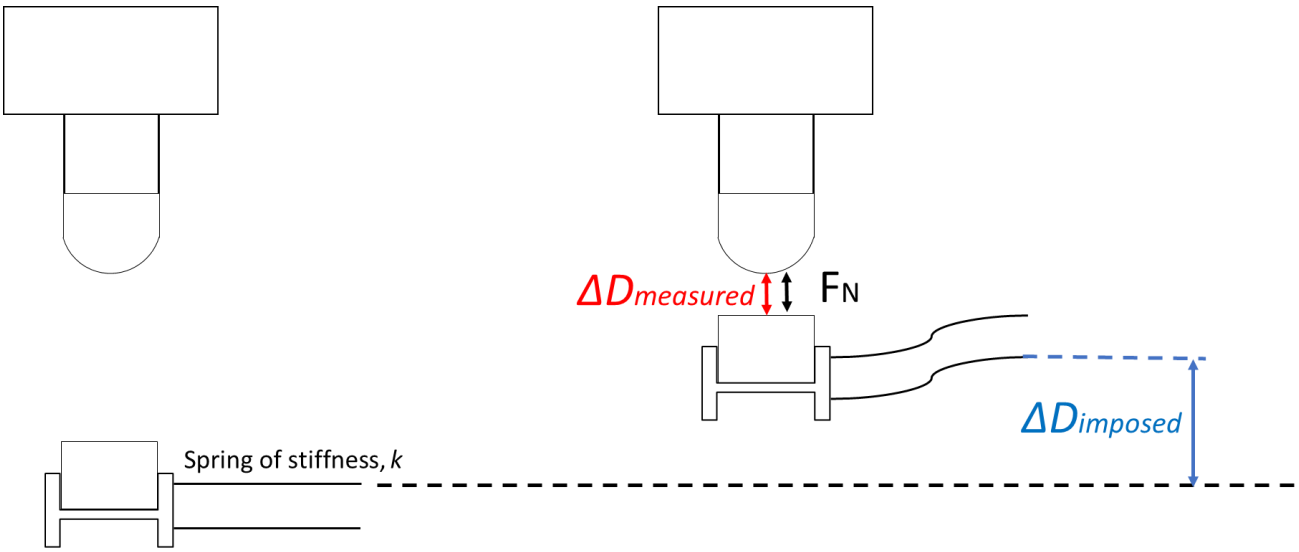

Figure 2.4. Principle of the determination of the normal force from Hooke's law. This diagram depicts a repulsive force between the two surfaces.

2.1.1.3 Measurement of the lateral force, F_S

The lateral force, F_S, or friction force between two surfaces at different applied normal loads can also be measured with the SFA.[6,15] To measure F_S, the top silica disk is mounted onto a support coupled to vertical force measuring springs coupled to strain gauges arranged in a Wheatstone bridge configuration. Sliding is generated by the action of a single-axis, motor-driven, horizontal micrometer which produces a displacement of the top surface at a controlled velocity and over a desired displacement distance (**Fig. 2.5**). The strain experienced by the friction gauges is transmitted to an amplifier as an output signal generated in volts (V). This signal is converted to Newtons through a calibration curve of the form $F_S = cV$, where the constant c is determined experimentally by placing small weights on the friction measuring springs and measuring the voltage output corresponding to each applied weight. The sensitivity in measuring F_S depends on the stiffness of the measuring springs and on the sensitivity of the strain gauges.

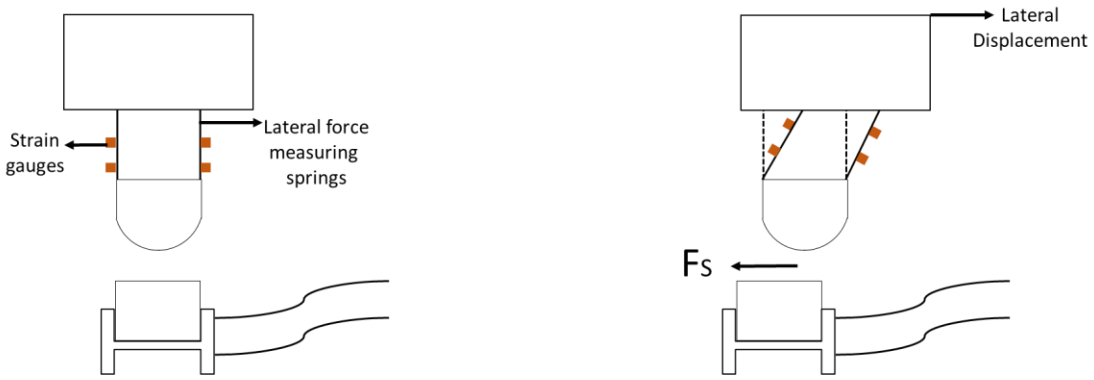

Figure 2.5. Schematic representation of the experimental set-up used to measure the lateral force, F_S, using the SFA.

2.1.1.4 Analysis of the FECO fringes

The geometry of the FECO fringes can be used to identify when two surfaces come into physical contact as well as to measure the contact area between two surfaces with a precision of approximately 1 µm.[7] In addition, the shape of the fringes is correlated to the topography of the surface and represents the shape of the surface or of any thin film trapped between. This characteristic is useful to identify any damage imparted to the surface as soon as it occurs (**Fig. 2.6**).

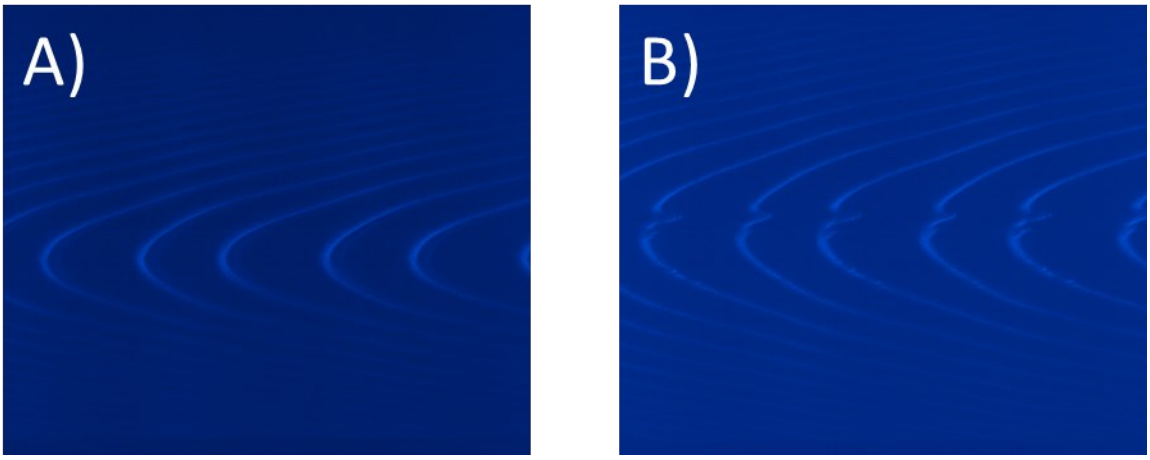

Figure 2.6. FECO fringes of the apex of the contact between two identical mica surfaces coated with PNIPAM microgels. The shape of the contacts shows A) no damage to the polymer layer or the mica substrate at low applied normal loads, and B) damage to the surfaces at high applied normal loads.

2.1.2 Experimental methodology used for the tribo-brush

Microgel synthesis and surface functionalization with PEG-NHS 5 kDa and PDMAEMA-COOH 4.8 kDa polymer brushes was achieved as described in chapter 3.[16]

2.1.2.1 Covalent attachment of microgels on silicon wafers and borosilicate lenses

2.1.2.1.1 Activation of the silicon wafers and borosilicate lenses

Silicon wafers were cut into 3 cm by 2 cm rectangles with a diamond-tip pencil. Then, silicon wafers and borosilicate lenses were sonicated in ethanol for 10 minutes before activating the surfaces by sonicating for 10 minutes in a saturated sodium hydroxide solution prepared in 1:1 ethanol:water. After the first alkaline sonication, the surfaces were thoroughly rinsed with milli-Q water and sonicated for an additional 10 minutes in the saturated sodium hydroxide solution. The surfaces were thoroughly rinsed with milli-Q water before sonicating for 10 minutes in milli-

Q water. Finally, the surfaces were rinsed in anhydrous ethanol and immediately used for aminoalkylsilane functionalization.

2.1.2.1.2 Aminoalkylsilane functionalization of silicon wafers and borosilicate lenses

Aminoalkylsilane monolayers were grafted to silicon wafers and borosilicate lenses substrates via self-adsorption from solution immediately after activation. A solution of 2-(3,4-epoxycyclohexyl)ethyltrimethoxysilane (ECHETES) at a 50 mM concentration was prepared in anhydrous ethanol and stirred for 10 minutes. After mixing, freshly activated silicon wafers and borosilicate lenses were immersed in the ECHETES solution for 2 hours. The resulting epoxy-functionalized surfaces were thoroughly rinsed with anhydrous ethanol. ECHETES grafting was completed by annealing the substrates for 1 hour at 120 °C under atmospheric pressure.

2.1.2.1.3 Microgel immobilization on ECHETES-functionalized substrates

Microgels were immobilized on ECHETES-functionalized substrates via a covalent bond between the microgel amine groups and the epoxy function. ECHETES-functionalized silicon wafers and borosilicate lenses were immersed in 0.1 % (w/v) bare or surface-functionalized microgel suspensions at 37 °C for one hour. Then, the samples were rinsed with milli-Q water and dried under a stream of nitrogen gas.

2.1.2.2 Friction measurements with the tribo-brush

Tribological tests were performed using a tribo-brush as described in previous publications.[17,18] Microgel-coated silicon wafers are attached to a movable stage connected to a displacement table by tension gauges. A single axis motion controller imparts the reciprocating motion on the displacement table while the tension gauges measure the lateral forces. A microgel-coated borosilicate lens is fixed onto a static support directly above the silicon wafer and the surfaces

are brough to a separation distance of ca. 1 mm with the aid of a coarse micrometer. The surfaces were then carefully brought into physical contact with a fine micrometer. The normal applied load is tuned with the fine micrometer and measured by tension gauges. A schematic of the components of the tribo-brush is shown in **Fig. 2.7**.

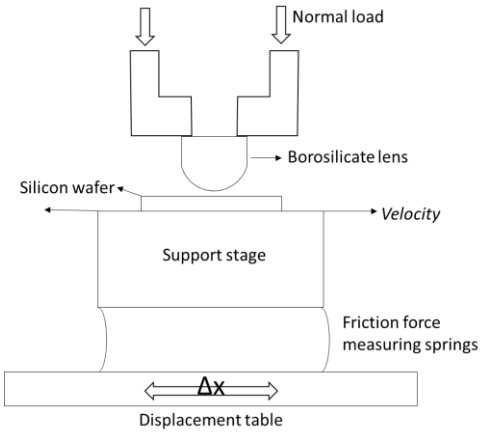

Figure 2.7. Scheme of the experimental set up for dynamic force measuring experiments in the mesoscale using the tribo-brush.

The tests were performed at sliding speeds between 4 – 8 µm/s over a sliding distance of 200 µm using normal loads between 0.05 – 1.0 N across milli-Q water adjusted to a specific pH. A 3-cycle reciprocating motion was imposed using a single axis motion controller. For all samples, friction measurements were performed at a minimum of two contact positions. Results reported herein were done in duplicate for bare microgel and microgel-co-PEG.

2.1.2.3 Topographical characterization by Atomic Force Microscopy

Atomic Force Microscopy (AFM) imaging was carried out using a Multimode microscope equipped with a Nanoscope V extended controller (Digital Instruments, Santa Barbara, CA). The imaging

was performed in dry air (30 % relative humidity) at 25 °C and 24 hours after the preparation of the surfaces. The PeakForce tapping-mode was employed using an ACTA silicon probe from APP Nano with a resonance frequency of 200 – 400 kHz. AFM images were treated and analyzed using Nanoscope Analysis software (version 1.4). The surface density of immobilized microgels was determined using Particle Analysis mode of the Nanoscope Analysis software and averaged over different surface areas of 10 µm x 10 µm and 5 µm x 5 µm scan size.

2.2 References

(1) Tabor, D.; Winterton, R. H. S. The Direct Measurement of Normal and Retarded van Der Waals Forces. *Proc. R. Soc. A* **1969**, *312*, 435–450.

(2) Israelachvili, J.; Tabor, D. The Measurement of Van Der Waals Dispersion Forces in the Range 1.5 to 130 Nm. *Proc. R. Soc. A* **1972**, *331*, 19–38.

(3) Israelachvili, J.; Adams, G. Measurement of Forces between Two Mica Surfaces in Aqueous Electrolyte Solutions in the Range 0-100 Nm. *J. Chem. Soc., Faraday Trans. 1* **1978**, *74*, 975–1001.

(4) Coulomb, C. A. Premiere Mémoire Sur l'Électricité et Le Magnétisme. *Hist. l'Académie R. des Sci.* **1785**, 569–577.

(5) Derjaguin, B. V.; Titijevskaia, A. S.; Abricossova, I. I.; Malkina, A. D. Investigations of the Forces of Interaction of Surfaces in Different Media and Their Applications to the Problem of Colloid Stability. *Discuss. Faraday Soc.* **1954**, *18*, 24–41.

(6) Israelachvili, J.; Min, Y.; Akbulut, M.; Alig, A.; Carver, G.; Greene, W.; Kristiansen, K.; Meyer, E.; Pesika, N.; Rosenberg, K.; Zeng, H. Recent Advances in the Surface Forces Apparatus (SFA) Technique. *Reports Prog. Phys.* **2010**, *73*, 036601–036617.

(7) Israelachvili, J. *Intermolecular & Surface Forces*, Second.; Academic Press Limited: London, 1992.

(8) Tadmor, R.; Chen, N.; Israelachvili, J. Thickness and Refractive Index Measurements Using Multiple Beam Interference Fringes (FECO). *J. Colloid Interface Sci.* **2003**, *264*, 548–553.

(9) Israelachvili, J. Thin Film Studies Using Multiple-Beam Interferometry. *J. Colloid Interface Sci.* **1973**, *44*, 259–272.

(10) Giraud, L. Intéractions et Propriétés Physico-Chimiques Des Surfaces Modèles de Biomatériaux, Université de Montréal, 2016.

(11) Israelachvili, J.; McGuiggan, P. M. Adhesion and Short-Range Forces Between Surfaces. Part I: New Apparatus for Surface Force Measurements. *J. Mater. Res.* **2011**, *5*, 2223–2231.

(12) Grünewald, T.; Helm, C. A. Computer-Controlled Experiments in the Surface Forces Apparatus with a CCD-Spectrograph. *Langmuir* **1996**, *12*, 3885–3890.

(13) Faghihnejad, A.; Zeng, H. Hydrophobic Interactions Between Polymer Surfaces: Using Polystyrene as a Model System. *Soft Matter* **2012**, *8*, 2746–2759.

(14) Lin, Q.; Gourdon, D.; Sun, C.; Holten-Andersen, N.; Anderson, T.; Waite, H.; Israelachvili, J. Adhesion Mechanisms of the Mussel Foot Proteins Mfp-1 and Mfp-3. *Proc. Natl. Acad. Sci.* **2007**, *104*, 3782–3786.

(15) Israelachvili, J.; McGuiggan, P. M.; Homola, A. M. Dynamic Properties of Molecularly Thin Liquid Films. *Science (80-.).* **1988**, *240*, 189–191.

(16) Guerron, A.; Giasson, S. Multiresponsive Microgels: Towards an Independent Tuning of Swelling and Surface Properties. *Langmuir* **2021**, *37*, 11212–11221.

(17) Popa, M.; Peditto, F.; Sfarghiu, A.-M.; Berthier, Y.; Descartes, S. A Tribological Approach to Understand the Behavior of Oral-Care Silica during Tooth Brushing. *Biotribology* **2016**, *6*, 1–11.

(18) Trunfio-Sfarghiu, A. M.; Berthier, Y.; Meurisse, M.-H.; Rieu, J.-P. Multiscale Analysis of the

Tribological Role of the Molecular Assemblies of Synovial Fluid. Case of a Healthy Joint and Implants. *Tribol. Int.* **2007**, *40*, 1500–1515.

Chapter 3 – Multiresponsive microgels : toward an independent tuning of swelling and surface properties

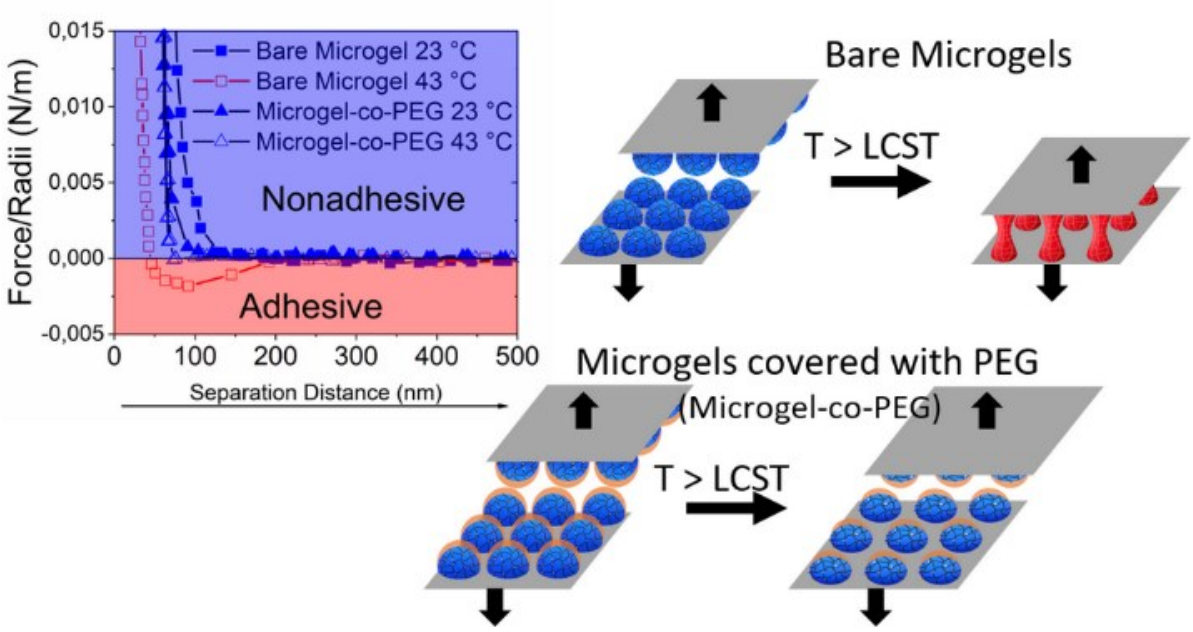

3.1 General Introduction to Chapter 3

Stimuli-responsive polymers are powerful tools to develop surfaces capable of interacting with their surroundings and adapting their properties in response to internal, or external triggers such as temperature, light, pH or ionic strength.[1,2] Among the wide range of molecules available, thermo-responsive PNIPAM is one of the most versatile and widespread options. The popularity of PNIPAM lies on its ability to undergo a sharp coil-to-globule conformational transition at its LCST which is found at roughly 32 °C, upon which the polymer changes from a highly hydrated state to a rather hydrophobic one.[3–5] This transition is immensely useful and, unsurprisingly, has been exploited in diverse applications ranging from microfluidics, to photonics, to the biomedicine field.[6–8] Nonetheless, this property can also represent a challenge, rather than an advantage, if the objective is to control the swelling degree of a polymer layer while at the same time keeping the surface properties, for example the wettability, constant.

The central hypothesis of this work is that, by synthesizing a hierarchical structure composed of a thermo-responsive PNIPAM microgel surface-functionalized with either pH-responsive or pH-insensitive polymer chains, it is possible to control the surface properties and the swelling behavior independently.

In this chapter, we demonstrate the ability to independently modulate the swelling of PNIPAM microgels without affecting the surface properties governed by the polymer chains grafted on its surface. First, a pH-responsive polymer chain (PDMAEMA) and a pH-insensitive polymer chain (PEG) were grafted to the microgel surface by forming a covalent bond between the amino functional groups on the microgels and a carboxyl group on the end-functionalized polymers via peptide coupling. The grafting was verified spectroscopically by using NMR and ATR-FTIR. Then,

the possibility of controlling the swelling and the surface potential independently was assessed in suspension by using DLS and changing the temperature and the pH of the media surrounding the bare and surface-functionalized microgels. Once that the desired behavior was demonstrated in suspension, the microgels were immobilized on a substrate and the properties of the microgel layers were studied by using the SFA technique. The swelling was evaluated by measuring the variation in layer thickness and adhesion was used as an indicator of the surface properties. Both parameters were studied as a function of temperature and pH.

This study is the subject of a publication included in the Journal of the American Chemical Society, *Langmuir*, published on the 15th of September 2021 and titled: *Multiresponsive Microgels: Toward an Independent Tuning of Swelling and Surface Properties*.[9] The entirety of the experimental work and data processing was done by Alberto Guerron. The article was written by Alberto Guerron with the advice of Pr. Suzanne Giasson.

3.2 Abstract

Dual-responsive poly-(*N*-isopropylacrylamide) (PNIPAM) microgels surface-functionalized with, polyethylene glycol (PEG) or poly-2-dimethylaminoethyl methacrylate (PDMAEMA), were developed to enable the swelling behavior of the microgels to occur independently of the surface properties provided by the polymers. The thermo-triggered swelling and pH-triggered surface properties of the microgels were investigated in aqueous suspension using Dynamic Light Scattering and on substrates using the Surface Forces Apparatus. Grafting polymer chains on the microgel surface did not impede the thermo-triggered swelling behavior of the microgels in suspension and immobilized on substrates. An unprecedented decoupling of the swelling behavior and surface properties could be obtained. More particularly, the thermo-triggered swelling behavior of the PNIPAM underlying microstructure could be tuned below and above the phase transition temperature with no change in the surface potential and adhesion provided by the surface non-responsive PEG.

3.3 Introduction

Stimuli-responsive materials have been intensively studied over the past several decades for a wide range of potential applications such as microfluidics,[10] drug delivery systems,[11] biomedicine[12,13] and lubrication.[14,15] Polymers are often used as responsive surface coatings because of their flexibility and ability to respond to different stimuli. Indeed, such materials are capable of altering their chemical and/or physical properties in response to external stimuli such as variations in pH,[16] light,[17] ionic strength[15,18] or temperature.[19,20] Depending on the external stimuli, the polymer can undergo physical and/or chemical modifications giving rise to changes in macroscopic properties of the surface such as variations in the polymer coating thickness, adhesion, friction or wettability.[16,21–25] However, as chemical and physical changes in the polymer properties are usually not decoupled, the targeted response can arise with other undesired responses. For instance, the important thermo-triggered volume phase transition of poly-(*N*-isopropylacrylamide) (PNIPAM) microgels is associated with a hydrophilicity/hydrophobicity transformation. Indeed, PNIPAM microgels exist in a highly swollen and hydrated state below the volume phase transition temperature, VPTT, (ca. 32 – 35 °C) and undergo a sharp volume transition above the VPTT expelling water and forming a rather hydrophobic network.[3] The phase transition of a variety of polymers can be favorable for developing multiresponsive structures useful for applications such as actuators,[26,27] anti-fouling,[20,28,29] drug delivery systems,[30–32] self-healing surfaces[33,34] or photonics.[35,36] But it can also be problematic when a change in the swelling behavior of a polymer coating is required with no change in the surface properties (i.e. wettability, adhesion) such as in microfluidics.[37,38] Such challenges can be overcome using functional multiresponsive PNIPAM-based hydrogels

incorporating hydrophilic polymers or oligomers into or at the surface of the PNIPAM gel. For example, Shi et al. have developed structured copolymer hydrogel substrates for immunoassay exhibiting thermo-responsiveness while minimizing the change in surface wettability.[29] Nonetheless, the extent of the swelling response as well as the independent control of the swelling and wettability properties remains elusive. Core/shell PNIPAM-based microgels can also be designed to improve surface hydrophilicity of the PNIPAM above the VPTT.[32,39–41] These are generally prepared by a two staged seeding polymerization providing a continuous polymer shell on the microgel cores. However, such synthesis approach leads to important changes in the swelling behavior of the PNIPAM-based microgels. Particularly, the VPTT increases, and the breadth of transition widens and becomes linear with temperature.[42–44]

Herein, we present the synthesis and characterization of unprecedented dual thermo- and pH-responsive microgels whose swelling behavior and surface properties can be decoupled. We used a site-specific grafting-to, as opposed to a grafting-from approach or a two-staged seeding polymerization, to minimize the impact on the VPTT of the PNIPAM microgels. The microgels are based on cationic thermosensitive poly-(*N*-isopropylacrylamide) microgels which are surface-functionalized with responsive or non-responsive polymers as illustrated in **Fig. 3.1**. The thermo-triggered swelling and pH-triggered surface properties of the microgels in suspension and on substrates were investigated by dynamic light scattering (DLS) and using the Surface Forces Apparatus (SFA).

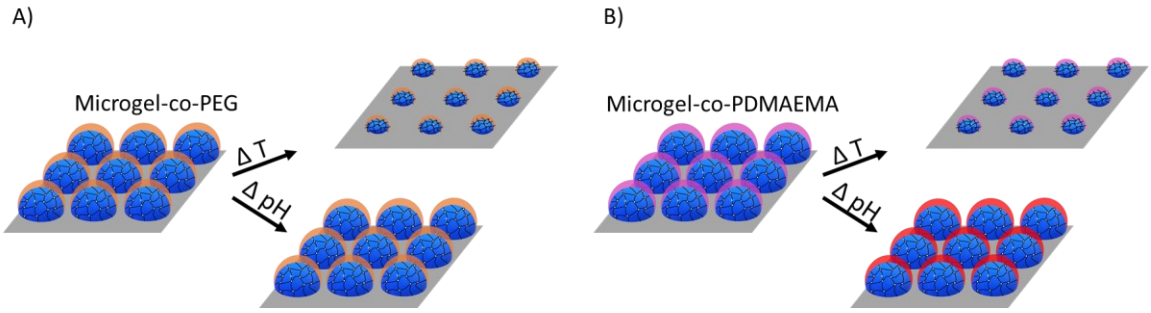

Figure 3.1. Illustration of the concept for independent control of swelling and surface properties using thermo-responsive PNIPAM microgels surface-functionalized with A) pH-insensitive PEG and B) pH-sensitive PDMAEMA.

3.4 Materials and Methods

Ruby mica sheets were purchased from S & J Trading Inc. (Glen Oaks, NY, USA). Plasma Prep II from SPI Supplies was used to activate freshly cleaved mica surfaces using 5.0 grade argon from Praxair Technology Inc. (Mississauga, ON, Canada). Milli-Q quality water was obtained from a Millipore Gradient A10 purification system (resistance 18.2 MΩcm, TOC $<$ 3 ppb). Silicon wafers were obtained from University Wafer Co (100 mm diameter, boron-doped (100) orientation, one side polished). *N*-isopropylacrylamide (NIPAM), 2-aminoethylmethacrylate hydrochloride (AEMH), 2,2'-azobis-(2-methylpropylacrylamide) (V50), triethanolamine (TEA), *N*-hydroxysuccinimidyl (NHS), *N*-(3-dimethylaminopropyl)-*N*'-ethylcarbodiimide (EDC), glutaraldehyde (GLA), sodium cyanoborohydride ($NaBH_3CN$) and Whatman 1 filter paper were purchased from Sigma-Aldrich (St. Louis, MO, USA). 11-aminoundecyltriethoxysilane (AUTES) was purchased from Gelest Inc. (Morrisville, PA, USA). Sodium hydroxide and *N,N'*-methylene-*bis*-acrylamide (MBA) were obtained from EMD Chemicals Inc. (Gibbstown, NJ, USA). Hydrochloric

acid, sulphuric acid and hydrogen peroxide were purchased from Anachemia (Lachine, QC, Canada). Carboxy terminated Poly(*N,N*-dimethylaminoethylmethacrylate) (PDMAEMA-COOH) 4800 g/mol, PI = 1.14 and α-Carboxy ω-Hydroxy terminated polyethylene glycol (PEG-COOH), 14300 g/mol, PI = 1.10, were purchased from Polymer Source (Dorval, QC, Canada). Methoxy polyethylene glycol succinimidyl carboxymethyl ester (PEG-NHS), 5000 g/mol, PI = 1.05 and 10000 g/mol, PI = 1.05, were obtained from JenKem (Plano, TX, USA). UV cured Norland optical adhesive 81 was purchased from Norland Products Inc. (Cranbury, NJ, USA). Dialysis cellulose membrane was obtained from Spectrum Laboratories Inc. (Rancho Dominguez, CA, USA). Anhydrous and 95% ethanol were purchased from Commercial Alcohols (Brampton, ON, Canada). All chemical products were used as received without further purification.

3.4.1 Microgel Synthesis

Synthesis of PNIPAM microgels was carried out using a well-established protocol thoroughly described in a previous publication.[3] Briefly, NIPAM was combined inside a three-necked round-bottomed flask with MBA and AEMH. The reagents in the three-necked flask were diluted in 40 mL of milli-Q water, the flask was connected to a condenser and heated gently to 80 °C while degassing with a stream of nitrogen gas. V50 was diluted separately in 10 mL of milli-Q water, heated gently to 80 °C and degassed with nitrogen gas. After thorough dilution and heating the V50 solution was added to the three-necked flask and the reaction was monitored for 4 hours. The concentrations of NIPAM, MBA, AEMH and V50 correspond to 94.2 %, 2.9 %, 1.5 % and 1.4 % (w/w), respectively. Following polymerization, the resulting colloidal suspension was cooled down before filtering with a Whatman 1 filter paper. Then, it was transferred to a 6000 – 8000 g/mol cellulose membrane and dialyzed against 100 times the volume of distilled water for 72

hours changing the dialysis wash every 12 hours. The concentration of the microgels in the resulting suspension (1 % w/v) was determined by measuring the weight difference before and after drying. The microgel suspensions were stored at 7 °C. Due to the low concentration of AEMH used in the initial feed, it was challenging to determine the final content of amino groups in the microgels. However, previous reports on the same cationic microgels suggest that the AEMH monomer conversion is completed after 12 – 15 minutes.[4] Moreover, increasing the concentration of AEMH in the initial feed has shown to result in a steeper initial conversion rate of the monomer and an uneven distribution of primary amines in the microgel.[4] For 1.5 % w/w AEMH, an amount of 171 µmol of the primary amines per gram of microgels was determined with 20 % of these amines located at the microgel surface.[4]

3.4.2 Surface functionalization of microgels

Microgels whose surface was functionalized with PDMAEMA (microgel-co-PDMAEMA) were prepared from an aqueous solution of 0.5 mM of PDMAEMA-COOH with 10 mM of NHS and 10 mM of EDC and stirred for 10 minutes at 7 °C inside a glass bottle covered in tin foil to block light out. After proper diluting and cooling, the microgel suspension was added to that solution to obtain a 0.1 % (w/v) microgel concentration. The suspension was left to react overnight at 7 °C with constant stirring and protected from external light.

For the microgels surface-functionalized with PEG, three different PEG chain lengths were investigated (5, 10 and 14.3K). Microgels functionalized with PEG-NHS 5k and 10k were prepared from an aqueous solution of 0.5 mM of PEG-NHS with 100 mM of TEA. The microgel suspension was added to the polymer solution at 0.1 % (w/v) microgel concentration and left to react overnight with constant stirring at room temperature. Microgels surface-functionalized with PEG-

COOH 14.3k were prepared from an aqueous solution of 0.5 mM of PEG-COOH with 10 mM of NHS and 10 mM of EDC and stirred for 10 minutes at 7 °C inside a glass bottle covered in tin foil to block light out. The microgel suspension was then added to the polymer solution at 0.1 % (w/v) microgel concentration and the solution was left to react overnight at 7 °C with constant stirring and protected from external light. The reported results correspond to microgel-co-PEG using PEG-NHS 5k unless otherwise stated. All functionalized samples were purified by dialysis following the coupling reaction in 25000 g/mol cellulose membranes against 100 times the volume of distilled water for 72 hours and changing the dialysis wash every 12 hours.

3.4.3 Microgel immobilization on mica substrates

Physisorption and covalent attachment were used to immobilize the microgels on mica surfaces. Microgel immobilization via physisorption was done by immersing freshly cleaved mica substrates in 0.1 % (w/v) bare or functionalized microgel suspensions at 37 °C for one hour. Then, samples were rinsed with milli-Q water and dried under a stream of nitrogen gas. Functionalization of the mica surfaces was required prior to covalent attachment. First, water/argon plasma was used to produce silanol groups on the mica surfaces as previously reported.[45] Briefly, freshly cleaved mica surfaces were placed inside a plasma chamber under a vacuum pressure of 0.5 mTorr. Argon and water vapor were introduced at partial pressures of 80 and 300 mTorr, respectively. Plasma activation was performed for 5 minutes at 40 W, followed by an additional 5 minutes in the plasma chamber under vacuum (0.5 mTorr). Activated mica surfaces were removed from the chamber and were immediately used for surface functionalization with aminoalkylsilane AUTES.

Aminoalkylsilane monolayers were grafted to mica substrates via self-adsorption from solution. A solution of 1 mM AUTES was prepared in anhydrous ethanol and stirred for 10 minutes. After

mixing, freshly activated mica surfaces were immersed in the AUTES solution for 20 minutes. The resulting amino-functionalized surfaces were thoroughly rinsed with anhydrous ethanol. The AUTES grafting was completed by annealing the surfaces for 1 hour at 120 °C under atmospheric pressure. Then, the surfaces bearing AUTES monolayers were immersed in a 0.1 % (w/w) aqueous solution of glutaraldehyde for 30 minutes, allowing the coupling reaction between the AUTES amine group and the glutaraldehyde carbonyl function to occur in the presence of $NaBH_3CN$.[46,47] After the coupling reaction, the substrates were thoroughly rinsed with milli-Q water prior to microgel immobilization. Microgels were immobilized on glutaraldehyde-functionalized mica substrates via covalent bonds between the microgel amine groups and the glutaraldehyde carbonyl functions. A 0.1 % (w/v) aqueous suspension of bare or functionalized microgels was prepared and heated gently to 37 °C in a water bath. Glutaraldehyde-functionalized mica substrates were then immersed in the microgel suspension and kept in the solution for 1 hour. Then, mica substrates were thoroughly rinsed with milli-Q water and dried under nitrogen.

3.4.4 Spectroscopic characterization by NMR and ATR-FTIR

Proton magnetic resonance was performed with a Bruker Avance 700 NMR. The dialyzed bare or functionalized microgels were diluted by a factor of 10 with deuterated water and approximately 1 mL of the microgel suspension was placed inside an NMR vial. Supplementary spectroscopic analysis was performed by ATR-FTIR. A milliliter of microgel suspension was placed on an aluminum foil sheet and evaporated in a stove at 120 °C for 1 hour prior to analysis by infrared microscopy using a Digilab FTS 7000 spectrometer coupled to a Digilab UMA 600 microscopic infrared. Measurements were done with a germanium ATR crystal and detected with a MCT detector with a 4 cm^{-1} resolution.

3.4.5 Polymer layer thickness determination

The thickness of surface-immobilized polymer layers was determined in air at 25 °C using a J.A. Woollam Co., INC. M-2000V ellipsometer at 75° angle of incidence. Silicon wafers were cut into 6 cm^2 pieces with a diamond-tip pencil and sonicated in ethanol for 10 minutes before activating in a piranha solution (H_2SO_4:H_2O_2 = 70:30 v/v) for 45 minutes. After activation, surfaces were rinsed with ethanol and dried with nitrogen prior to immersing in a 1 mM AUTES solution in anhydrous ethanol for 20 minutes. After silanization, the surfaces were rinsed with ethanol, dried with nitrogen, and annealed at 120 °C for 1 hour. Then, the substrates were immersed in a PEG-NHS 5k solution according to the grafting protocol described previously (S*urface functionalization of microgels***)** in the presence and absence of the coupling agent TEA.

3.4.6 Hydrodynamic diameter and zeta potential determination

The hydrodynamic diameter and zeta potential of bare and functionalized microgels in suspensions were determined using a Zetasizer Nano ZS 3600 (Malvern Instruments, U.K.) and a folded capillary cell DTS 1070 (Malvern Instruments, U.K.). The results were acquired and analyzed using Zetasizer Software (version 7.11). The dialyzed suspensions were diluted tenfold with distilled water prior to analysis and pH was adjusted with 1 M hydrochloric acid or sodium hydroxide solutions.

3.4.7 Water contact angle measurements

The water contact angle was determined on the surface-immobilized microgels using a FTA2000 dynamic contact angle analyzer (First Ten Angstrom). Surfaces were prepared according to the protocol previously described (*Microgel immobilization on mica substrates)***.** All measurements were carried out in the static mode. A droplet (3-5 µL) of milli-Q water of a given pH was deposited

on the surfaces and the contact angle was determined using the FTA32 Video software. The contact angle was measured at least on three different locations on three independently prepared substrates.

3.4.8 Surface force measurements

The interaction forces between two microgel-bearing surfaces were measured as a function of the separation distance, *D*, using the Surface Forces Apparatus (SFA 2000). The protocol for measuring interaction forces using the SFA has been previously well described.[48,49] Briefly, silver-backed mica surfaces were glued silver side down onto the cylindrical disks (radius of 2 cm) using Norland 81 UV cured glue. The two disks were mounted in the SFA chamber in a cross-cylinder configuration and were brought into adhesive contact in air to set the contact separation distance ($D = 0$) between the two mica surfaces. The SFA disks were then dismounted under a laminar-flow cabinet and microgel immobilization was performed according to the chemisorption protocol previously described (*Microgel immobilization on mica substrates*). After the microgel grafting, the disks were reinstalled and the SFA chamber was filled with an aqueous solution of defined ionic strength (0.1 mM Na_2SO_4) or pH ($4 < pH < 10$) and left at a given temperature for several hours allowing the temperature to stabilize. The force profiles were determined using a cantilever, supporting the lower surface, of stiffness 588 ± 15 N/m.

3.4.9 Topographical characterization by Atomic Force Microscopy

Atomic Force Microscopy (AFM) imaging was carried out using a Multimode microscope equipped with a Nanoscope V extend controller (Digital Instruments, Santa Barbara, CA). The imaging was performed in dry air (30 % relative humidity) at 25 °C and 24 hours after the preparation of the surfaces. The PeakForce tapping-mode was employed using an ACTA silicon probe from APP Nano

with a resonance frequency of 200-400 kHz. AFM images were treated and analyzed using Nanoscope Analysis software (version 1.4). The surface density of immobilized microgels was determined using Particle Analysis mode of the Nanoscope Analysis software.

3.5 Results and Discussion

The results are divided in three sections: (i) the characterization of the surface-functionalized microgels using NMR, FTIR and ellipsometry to assess the coupling reaction between the end functional groups of the polymers (PEG and PDMAEMA chains) and the primary amines of the microgel; (ii) the analysis of the hydrodynamic diameter and zeta potential to assess the independent control with temperature and pH; and (iii) the responsiveness of the microgels immobilized on substrates to assess the same independent control of swelling and surface properties.

3.5.1 Characterization of the microgels in aqueous suspension

In neutral media at 24 °C, the bare microgels have a hydrodynamic diameter of ca. 225 nm (**Fig. 3.2A**) and a surface potential of ca. 12 mV (**Fig. 3.3**). These characteristic properties are in agreement with previously reported studies on the same microgels.[3,4,21,50,51] The positive surface potential results from the ionizable primary amine moieties (apparent pK_a of 7.0 – 7.5)[52,53] brought by the initiator (V50) and the AEMH monomers. The surface charge density provided by the amino groups on the bare microgels prepared in our study ($4.6x10^{-4}$ C/m^2) was estimated from the zeta potential measurements using the Grahame equation derived from the Gouy-Chapman theory.[54–57] This result is in agreement with published work on the same cationic

microgels.[4] The charge density was found to decrease two-fold for microgel-co-PDMAEMA and 35-fold for microgel-co-PEG.

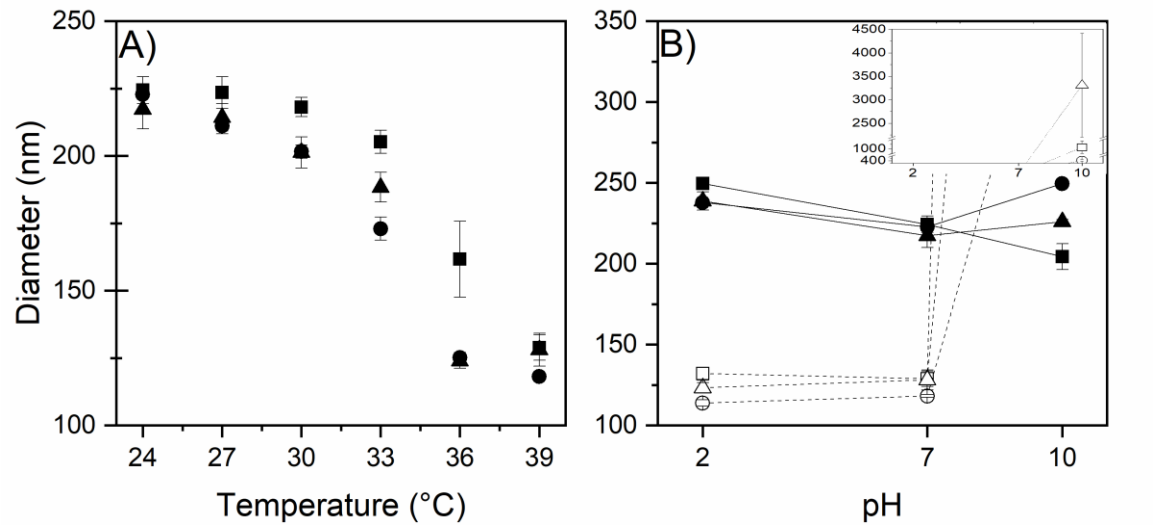

Figure 3.2. Hydrodynamic diameter as a function of A) temperature in neutral media and B) pH of bare microgel (■), microgel-co-PDMAEMA (●) and microgel-co-PEG (▲) in aqueous suspension (0.1 % w/v). In B) open and filled symbols correspond to diameters obtained at 39 °C (above the VPTT) and at 24 °C (below the VPTT), respectively. Inset shows the size of aggregated microgels at pH 10. Error bars represent the standard deviation of three independent experiments.

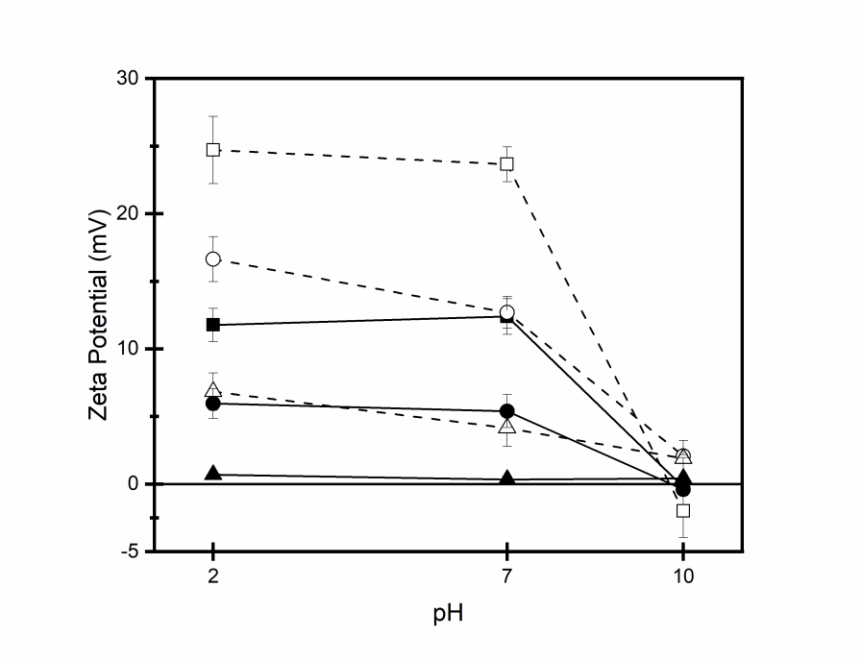

Figure 3.3. Zeta potential of bare microgels (■), microgel-co-PDMAEMA (●) and microgel-co-PEG (▲) in aqueous suspension (0.1 % w/v) of different pH. Filled and open symbols represent measurements at 24 ˚C and 39 ˚C, respectively. Error bars represent the standard deviation of three independent experiments.

Spectroscopic analysis was performed on the microgels to assess their surface functionalization with PEG and PDMAEMA. The NMR spectrum of the bare microgels (**Fig. 3.4**) shows two peaks characteristic of the isopropyl group: one at 1.1 ppm corresponding to methyl groups and one at 3.8 ppm corresponding to CH bonds. The coupling between the functional carboxyl end groups of the polymer chains (PEG and PDMAEMA) and the primary amines of the microgels is expected to occur through a peptide bond. However, the NMR signal of that peptide bond cannot be discerned (**Fig. 3.4**) because PNIPAM has a high content of amide groups relative to primary amines. Therefore, the expected change in the NMR spectrum caused by the peptide bond is buried by the major amide band. Nevertheless, resonance bands characteristic of PEG and PDMAEMA are observed in the spectra of microgel-co-PEG and microgel-co-PDMAEMA. For

microgel-co-PEG, the peak at 3.6 ppm corresponds to the methylene unit in the repeating group ($–OCH_2CH_2–$). For microgel-co-PDMAEMA, the peaks at 4.1 ppm and 2.4 ppm correspond to the O-CH_2 groups in the side chain and the methyl groups bonded to the tertiary amine of PDMAEMA, respectively.[58] As the NMR spectra were collected after the purification steps described in *Materials and Methods*, the results suggest that the polymer chains are covalently grafted to the microgel. To support the NMR results, the bare and functionalized microgels were also characterized by ATR-FTIR (**Fig. 3.S.1**). The ATR-FTIR results also indicate that PEG and PDMAEMA chains are found in the samples and do not conclusively demonstrate the formation of peptide bonds between the polymer chain ends and the microgels. In fact, the low content of amine groups (1.5 % w/w AEMH) makes the identification of the coupling between polymer chains and the microgel as well as the polymer grafting density unlikely to be conclusive. To overcome this limitation, ellipsometry was used to indirectly assess the attachment of PEG-COOH on an amino-functionalized substrate mimicking the microgel surface. The change in the layer thickness after the polymer grafting was determined with and without the coupling agents (see *Materials and Methods* for experimental details). In the absence of the coupling agents, no increase in thickness was measured relative to that of the immobilized amino-functionalized layer. In contrast, when the reaction took place in the presence of the coupling agents, an increase in the layer thickness of 2.8 ± 0.5 nm was measured. These results strongly suggest that the coupling between the carboxyl end groups of the polymer chains and the amino groups of the AUTES layer takes place through a covalent peptide coupling. Moreover, the decrease in the surface potential of the microgels upon polymer grafting, discussed hereafter, suggests the neutralization of the amine groups most likely resulting from a peptide bond.

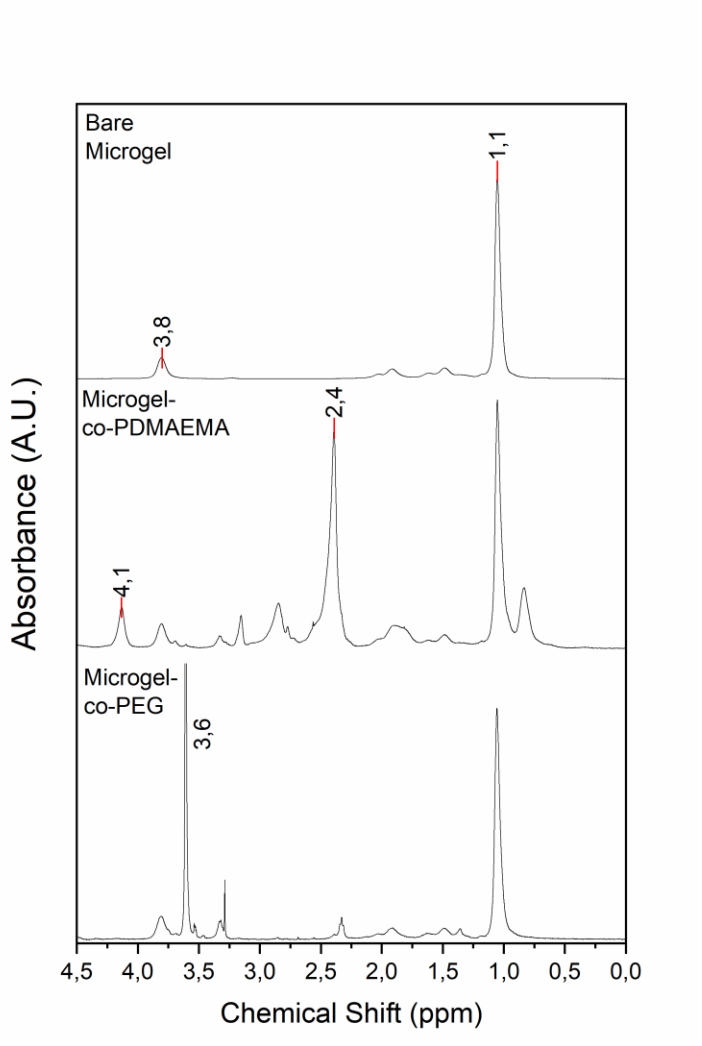

Figure 3.4. ^{1}H-NMR spectra of bare microgels, microgel-co-PEG and microgel-co-PDMAEMA 0.1 % (w/v) in deuterium solution.

3.5.2 Stability of microgels in suspension and immobilized on substrates

The stability and the potential degradation of the microgels were investigated within the pH and temperature ranges under study. The degradation of the microgels and surface-functionalized microgels with time and increasing temperature is expected to be minimal. The reason is that the carbon-carbon polymer backbone is not susceptible to hydrolysis and the amide and ester groups

in PNIPAM hydrogels (reticulated with MBA) have previously shown less than 8.5 % of degradation after 120 hours in pH 10 and pH 1 solutions at 30 °C.[59,60] AEMH is stable in acidic or neutral media when in its protonated form but hydrolyses in alkaline media.[61] However, homopolymers of AEMH have shown to slightly degrade (< 3 %) in a pH 10 solution at 50 °C after 72 hours.[61]

To verify the robustness of the attachment of the microgels on the substrates, physisorbed and covalently attached microgels on surfaces were immersed in aqueous solutions of different pH (4 < pH < 10) for 24 hours at room temperature and analyzed using AFM. 24 hours is approximately three times longer than the time required for the responsive behavior measurements reported hereafter. The microgels immobilized on mica surfaces form homogeneous layers (**Fig. 3.5** and **Fig. 3.S.2-4**) of similar grafting densities; 22.5 ± 1.3, 23.5 ± 1.9 and 24.0 ± 0.9 particles/μm^2 for the bare microgels, microgel-co-PDMA and microgel-co-PEG, respectively. No significant change in the size, the morphology and the grafting density with pH was observed for all surfaces bearing covalently attached microgels (**Fig. 3.S.5**). However, the physisorbed microgel layers immersed in pH 4 and 10 show a significant reduction in the grafting density compared to the initial coverage (**Fig. 3.S.6**). These results indicate that the physisorption of microgels is not sufficient to provide a robust surface attachment whereas covalent attachment is. The covalent attachment is expected to occur between the carboxyl groups on the substrates (provided by GLA) and the primary amines on the microgel surface. The results suggest that some surface amine groups remain available for the covalent coupling with the substrates despite the presence of PEG or PDMAEMA. These remaining surface charges are indeed responsible for the non-negligible zeta potential of the microgels measured at 39 °C, close to the grafting temperature (**Fig. 3.3**). The

robust covalent attachment also suggests that the potential steric repulsions arising between polymer chains on the microgel surface and the carboxyl-functionalized substrate do not prevent the amine groups to reach the substrate. This is probably due to the small size of the polymer chains relative to the microgel.

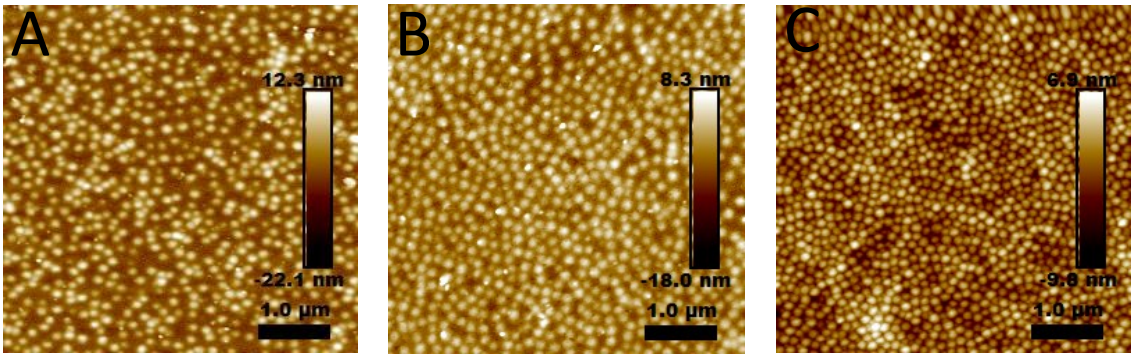

Figure 3.5. AFM images of (A) bare microgel, (B) microgel-co-PDMAEMA and (C) microgel-co-PEG covalently attached to AUTES-GLA functionalized mica substrates (24 hours after grafting) in air at 25 °C and 30 % relative humidity. PeakForce tapping mode. Image scale, 5 x 5 μm^2.

3.5.3 Tuning size and surface property of microgels in suspension

At room temperature and below the VPTT, the PNIPAM network is in its swollen and hydrophilic state. Above the VPTT, the H-bonds between the polymer and water molecules are disfavored whereas intramolecular attractive interactions prevail and induce a polymer network shrinking.[3] It is known that the volume of PNIPAM microgels can decrease up to 60 % when transitioning above the VPTT in aqueous suspensions.[3,21] The hydrodynamic diameter of all microgels (bare and surface-functionalized) decreased by roughly 50 % (ca. 225 nm to ca. 125 nm) between 24 °C and 39 °C in neutral and acid media (**Fig. 3.2A-B**). The VPTT of the bare microgels and microgel-co-PEG, determined by the tangent method, corresponds to 35 °C while that of microgel-co-

PDMAEMA is slightly less (34 °C) (**Fig. 3.S.7**). The VPTT of the microgel-co-PEG is not affected by the molecular weight of the grafted PEG (**Fig. 3.S.8A**).

To evaluate the thermo-triggered swelling capacity of the microgels in suspension, the following arbitrary swelling ratio, $T\text{-}Q_{susp}$, was used:

$$T\text{-}Q_{susp} = d_{swollen}/d_{collapsed} \quad (1)$$

where $d_{swollen}$ and $d_{collapsed}$ are the hydrodynamic diameters at 24 °C and 39 °C. $d_{collapsed}$ was determined at 39 °C since the variation in the microgel size above that temperature is not significant (**Fig. 3.2A-B**, **Fig. 3.S.7**). The values of $T\text{-}Q_{susp}$ are reported in **Table 3.1** for all microgels and at different pH values. The swelling ratio of the bare microgels (ca. 1.8) is slightly lower than previously reported.[3,4] The values of $T\text{-}Q_{susp}$, for surface-functionalized microgels range from 1.70 to 2.10 depending on the pH, showing that the surface functionalization of the microgels does not impede their thermo-responsiveness. For pH > 7, all microgels aggregated above the VPTT (**Fig. 3.2B**, inset) most probably due to the low degree of ionization of the amine groups making the NIPAM/NIPAM attractions dominant. In acid conditions, the microgels did not aggregate above the VPTT. This is explained by the presence of the surface charges (**Fig. 3.3**) which most probably provide sufficient electrostatic repulsions between the microgels to keep them dispersed. These results show that the swelling behavior can be thermo-triggered independently of the surface chemistry.

Table 3.1. Thermo-triggered swelling ratios of microgels in suspension, T-Q_{susp}, as defined by equation 1 and immobilized on a surface, T-Q_{imm}, as defined by equation 3 of bare microgel, microgel-co-PDMAEMA and microgel-co-PEG at different pH.

	Bare Microgel		Microgel-co-PDMAEMA		Microgel-co-PEG	
pH	*T-Q_{imm}*	*T-Q_{susp}*	*T-Q_{imm}*	*T-Q_{susp}*	*T-Q_{imm}*	*T-Q_{susp}*
2 – 4*	1.78 ± 0.37	1.89 ± 0.06	2.22 ± 0.21	2.10 ± 0.04	1.86 ± 0.27	1.93 ± 0.07
7	1.78 ± 0.40	1.74 ± 0.07	2.38 ± 0.46	1.89 ± 0.02	1.77 ± 0.10	1.70 ± 0.10
10	1.23 ± 0.15	Aggregated	2.32 ± 0.14	Aggregated	1.61 ± 0.02	Aggregated

* pH 2 is for the microgels in suspension and pH 4 for surface-immobilized microgels.

As the underlying PNIPAM structure of the microgels contains pH-sensitive amine groups, the effect of pH on the swelling behavior was also investigated (**Fig. 3.2B**). A decrease in the degree of ionization of the amine groups (AEMH) with increasing pH should induce a decrease in the electrostatic repulsions within the network and therefore produce a microgel shrinking. To determine the swelling triggered by variations in pH (between pH 2 and 10) at constant temperature, the following arbitrary swelling ratio in suspension, *pH-Q_{susp}*, was used:

$$pH\text{-}Q_{susp} = d_{pH\ 2}/d_{pH\ 10} \qquad (2)$$

where $d_{pH\ 2}$ and $d_{pH\ 10}$ are the hydrodynamic diameters at pH 2 and 10. The values of *pH-Q_{susp}*, reported in **Table 3.2**, range from 1.02 to 1.22. The largest pH-triggered swelling was observed with the bare microgels. These results indicate that despite the presence of primary amines in the microgels, the pH-triggered swelling is significantly less than the thermo-triggered swelling (**Table 3.1** – **3.2**).

Table 3.2. pH-triggered swelling ratios of microgels in suspension, pH-Q_{susp}, as defined by equation 2, and immobilized on a surface, pH-Q_{imm}, as defined by equation 4, at different temperatures.

	Bare Microgel		Microgel-co-PDMA		Microgel-co-PEG	
Temperature (°C)	*pH-Q_{imm}*	*pH-Q_{susp}*	*pH-Q_{imm}*	*pH-Q_{susp}*	*pH-Q_{imm}*	*pH-Q_{susp}*
23 – 24*	1.74 ± 0.24	1.22 ± 0.05	1.27 ± 0.11	0.95 ± 0.03	1.02 ± 0.04	1.05 ± 0.03
39 – 43**	1.20 ± 0.24	Aggregated	1.32 ± 0.11	Aggregated	0.89 ± 0.12	Aggregated

* 23 °C and 24 °C correspond to the lowest recorded temperature of the aqueous medium surrounding the surface-immobilized microgels and of the microgels suspension, respectively.

** 39 °C and 43 °C correspond to the highest recorded temperature of the microgels suspension and the aqueous medium surrounding the surface-immobilized microgels, respectively.

Surface potential was used as an arbitrary parameter to evaluate the ability of tuning the surface properties of the microgels. The variation in the surface potential of the microgels as a function of pH at different temperatures is reported in **Fig. 3.3**. Below the VPTT (24 °C), a decrease in the surface potential of 12 mV and 6 mV with increasing pH is observed for the bare microgels and microgel-co-PDMAEMA respectively. This is explained by the surface amine groups whose degree of ionization decreases with increasing pH. However, the surface potential of microgel-co-PEG (5k – 14.3k) did not show any significant pH-dependence, suggesting the absence of pH-sensitive surface groups (**Fig. 3.3**, **Fig. 3.S.8B**). This result suggests the neutralization of the primary amines of the microgels upon peptide coupling (**Fig. 3.3**). However, for the microgels carrying surface charges (bare microgels and microgel-co-PDMAEMA), the thermo-triggered volume phase transition is also associated with a variation in zeta potential as significant as that triggered by the

pH (**Fig. 3.3**). This is explained by the size reduction of the microgels with increasing temperature (**Fig. 3.2A-B**), which gives rise to an increase in the surface charge density of the particles (**Fig. 3.3**). Nevertheless, the results suggest that the surface potential is pH-dependent for the charged microgels (bare microgels and microgel-co-PDMAEMA) at constant temperature and pH-insensitive for the neutral microgel-co-PEG.

Water contact angle (θ_w) measurements were carried out to assess the surface property changes with pH. Upon variations in pH, the degree of charges of the microgels bearing weakly ionizable groups should be altered giving rise to wettability changes between hydrophilicity at low pH and hydrophobicity at high pH. However, the contact angle is not only dependent on the surface chemistry of the outermost layer but also on the surface roughness. In fact, significant differences in θ_w at pH 2 have been reported between rough (ca. 79°) and flat (ca. 10°) PDMAEMA surfaces.[62] In addition, only a small change in the water contact angle (5°) over a large pH range was reported on a flat PDMAEMA surface.[62] Therefore, the measurements were carried out at constant temperature (to eliminate surface roughness changes caused by the volume phase transition) and the reported results (**Fig. 3.S.9**) are for qualitative comparison only. On the bare microgel, a slight increase in θ_w with increasing pH was observed as expected from the decrease in the degree of ionization of the amine groups. However, on the microgel-co-PEG layers, no significant change in θ_w with pH was observed which agrees with the non-significant change in surface potential with pH observed in suspension (**Fig. 3.3**). In addition, a slightly larger θ_w on the microgel-co-PDMAEMA, relative to bare microgel, was observed. These results agree with the θ_w values reported for PDMAEMA functionalized surfaces (between 60° and 110° depending on temperature and pH)[62–64] and confirm the surface functionalization of the microgels.

In summary, the surface potential of the microgels in a highly hydrated state (below the VPTT) can be tuned with pH via surface functionalization independently of the swelling. More particularly, microgels surface-functionalized with the pH-sensitive PDMAEMA allows the surface potential to be tuned with pH. Conversely, functionalizing microgels with the pH-insensitive PEG makes the surface potential, the wettability, and the swelling of the cationic microgels insensitive to pH.

3.5.4 Tuning size and surface property of microgels immobilized on substrates

The responsiveness of the surface-immobilized microgels was assessed by measuring the interaction forces between two opposing microgel-bearing substrates as a function of separation distance under different conditions of temperature and pH. The resulting force profiles are illustrated in **Fig. 3.6** with each curve being the most representative of three independent and reproducible experiments (**Fig. 3.S.10**). The interaction range is related to the microgel layer thickness and the amplitude of the force on separating the surfaces to the adhesion between two microgel layers. The force profiles measured on approaching the surfaces are purely repulsive for all microgels regardless of the pH and the temperature. Repulsions between dense and neutral polymer layers in good solvent generally originate from an osmotic repulsion effect brought about by compression of the polymer chains. Such steric repulsions become non-negligible at separation distances about twice the unperturbed thickness of the polymer layer and increase progressively with compression due to the overlap of the polymer network. The electrostatic interactions which might arise from the ionizable amine groups are expected to be negligible due to the low surface

potential (< 25 mV, **Fig. 3.3**) and to the short Debye length (ca. 18 nm for 0.1 mM Na_2SO_4 in aqueous solution). Therefore, the unperturbed thickness of the microgel layers was defined as half the distance between two microgel-bearing surfaces at which the repulsive forces become non-negligible (at F/R = 1 mN/m).

(A)

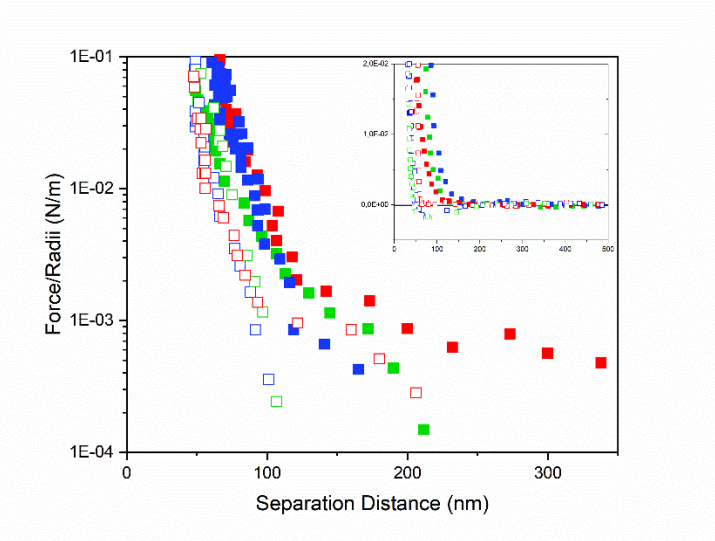

(B)

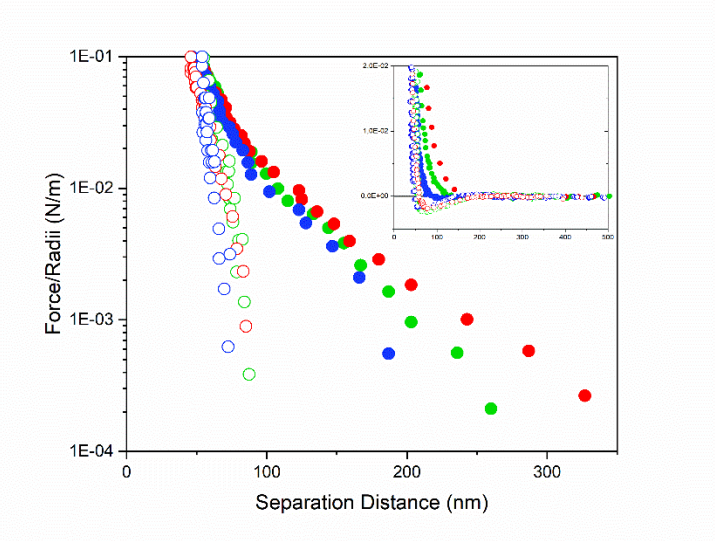

(C)

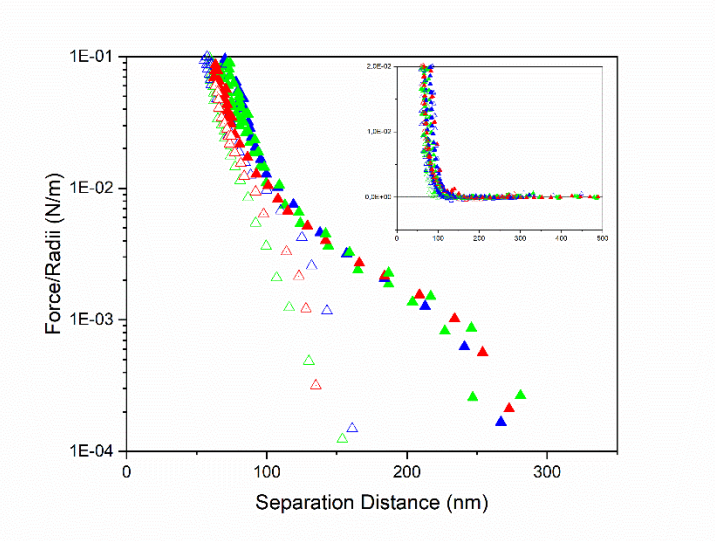

Figure 3.6. Interaction forces as a function of separation distance, D, measured on the approach and separation (insets) between two identical immobilized bare microgel (A, ■), microgel-co-PDMAEMA (B, ●) and microgel-co-PEG (C, ▲) layers at pH 4 (red), pH 7 (green) and pH 10 (blue) at 23 ˚C (filled symbols) and 43 ˚C (open symbols). D = 0 corresponds to the adhesive mica – mica contact. Each curve corresponds to the most representative one of three independent and reproducible experiments (**Fig. 3.S.10**).

The unperturbed layer thicknesses of bare and functionalized microgels in neutral media range between 115 and 160 nm (**Fig. 3.6**), corresponding to ca. 50 % of the microgel diameter in suspension (**Fig. 3.2A**). These results show the large capacity of the microgels to deform once immobilized on a surface, as previously reported.[23,65,66] Successive force profiles on approach were determined at constant temperature and pH to assess the swelling reversibility and the stability of the grafting (**Fig. 3.S.11**). History effects could be observed between the first and second force profiles. These effects, often observed between polymer layers,[16,22] are most

probably due to a more favorable conformation of the microgels caused by their first compression as well as the possible expulsion of residual physisorbed microgels.

The interaction range for all immobilized microgel layers decreases with increasing temperature regardless of the pH. This shows that the characteristic ability of PNIPAM microgels to collapse at temperature above the VPTT was maintained on surfaces.

To evaluate the thermo-triggered swelling capacity of the immobilized microgels, the following arbitrary swelling ratio, $T\text{-}Q_{imm}$, was used:

$$T\text{-}Q_{imm} = D_{swollen}/D_{collapsed} \quad (3)$$

where $D_{swollen}$ and $D_{collapsed}$ are the separation distances at the onsets of interaction forces evaluated at F/R = 1mN/m at 23 °C and 43 °C, respectively. The swelling ratios are reported in **Table 3.1** for all microgels.

In general, the surface swelling response is as important as that observed in suspension. As the surface immobilized microgels are initially flattened on the surface (at neutral pH), this suggests a relatively important surface response due to the closely packed arrangement of the microgel layers as shown in **Fig. 3.5** and **Fig. 3.S.2 – 4**. Lateral compression arising from the close neighboring particles can lead to an anisotropic (perpendicular to the surface) swelling, which would give rise to a more important change in thickness compared to isotropic swelling in suspension. Similar anisotropic swelling behaviors for hydrogel and microgel nanoparticles have been reported in the past.[16,22]

The thermo-triggered swelling response appeared to depend on pH for bare microgel and microgel-co-PDMAEMA. Indeed, swelling is expected to arise with decreasing pH due to the

increase in the degree of ionization of the amino groups as observed in suspension (**Fig. 3.2B**). To evaluate the pH-triggered swelling capacity of the immobilized microgels, the following arbitrary swelling ratio, *pH-Q_{imm}*, was used:

$$pH\text{-}Q_{imm} = D_{pH\ 4}/D_{pH\ 10} \quad (4)$$

where $D_{pH\ 4}$ and $D_{pH\ 10}$ are the separation distances at the onsets of interaction forces evaluated at F/R = 1mN/m at pH4 and 10, respectively. *pH-Q_{imm}* values are reported in **Table 3.2** and compared with the *pH-Q_{susp}*. The slight dependence of pH-induced swelling for all microgel layers agrees with the pH-triggered swelling observed in aqueous suspension (**Table 3.2**). Nevertheless, the thermo-triggered swelling is more significant than pH-triggered swelling. This is particularly true for microgel-co-PEG, where *T-Q_{imm}* ranges from 1.61 to 1.86, depending on pH (**Table 3.1**), and *pH-Q_{imm}* is 1.02 (**Table 3.2**).

The ability to control the surface properties of the surface-immobilized microgels was assessed by measuring the adhesion force on separating two opposing microgel-bearing surfaces upon variation in pH and temperature. The surfaces were slowly separated stepwise after being brought into a relatively compressed regime (at a distance corresponding to ca. 30 % of the unperturbed layer thickness). No adhesion force could be measured below the VPTT (at 23 °C) for all microgels under all studied pH conditions (**Fig. 3.6**, insets). The absence of adhesion below the VPTT is explained by the good solvent conditions for the polymers and the presence of charged groups (at low pH) providing electrostatic repulsion. Above the VPTT, adhesion appeared to depend on the surface chemistry of the microgels (**Fig. 3.6**, insets). Indeed, adhesion was measured above the VPTT between immobilized microgel-co-PDMAEMA (for all pH) and bare

microgel (pH $>$ 4). These results suggest that at pH 4, the surface charges of the bare microgels above the VPTT (ca. 25 mV, **Fig. 3.3**) provide sufficient electrostatic repulsion to overcome the hydrophobic attractions caused by NIPAM/NIPAM interactions. On the contrary, the lower surface charge of the microgel-co-PDMAEMA at pH 4 (ca. 12 mV, **Fig. 3.3**) does not provide enough electrostatic repulsion to overcome the NIPAM/NIPAM attractions. These results can be compared with the aggregation of microgels observed in suspension (**Table 3.3**). All microgels in suspension aggregated above the VPTT only at high pH while adhesion could be measured at low pH (above the VPTT). This is explained by the fact that adhesion was assessed on separating the compressed microgels. As previously mentioned, force profiles in approaching the surfaces were purely repulsive (**Fig. 3.6**) and did not exhibit any attractive forces causing the aggregation in suspension. This is most probably associated with the limited resolution in measuring forces which is determined by the force measuring spring used in these experiments (i.e., a compromise had to be made for the selection of the spring stiffness to make the determination of the immobilized microgel thickness possible). In a compressed conformation, the polymers can rearrange so that interactions promoting attraction can prevail such as NIPAM/NIPAM segment interactions (attractive above the VPTT). However, no adhesion force was measured between microgel-co-PEG layers above the VPTT regardless of pH. These results suggest that grafting polymer chains, more particularly PEG, on surface-immobilized microgels may provide a way to tune the swelling behavior via temperature without affecting the surface properties as also observed in suspension.

Table 3.3. Zeta potential and adhesion of bare microgel, microgel-co-PDMAEMA and microgel-co-PEG at different pH above the VPTT.

T = 39 - 43 °C*	Bare Microgel		Microgel-co-PDMAEMA		Microgel-co-PEG	
pH	Zeta potential (mV)	Adhesion	Zeta potential (mV)	Adhesion	Zeta potential (mV)	Adhesion
2 – 4**	24.7	No	16.6	Yes	6.8	No
7	23.6	Yes	12.7	Yes	4.1	No
10	-1.9	Yes	2.0	Yes	1.9	No

* 39 °C and 43 °C correspond to the highest recorded temperatures of microgels in suspension and surface-immobilized, respectively.

**pH 2 corresponds to microgels in suspension and pH 4 to surface-immobilized microgels.

3.6 Conclusion

Cationic thermo-sensitive PNIPAM microgels were successfully surface-functionalized with PEG and PDMAEMA polymer chains to to enable the swelling of the microgels to be reversibly triggered independently of the surface property. The ability to independently control the swelling and surface properties using temperature and pH as triggers was investigated for microgels in aqueous suspension and microgels immobilized on substrates. Polymer chain grafting did not impede the ability of cationic PNIPAM microgels to undergo a volume phase transition above the VPTT, either in suspension or immobilized on a substrate. Due to the presence of amino groups throughout the entirety of the microgel polymer network, the swelling behavior was also pH-dependent. However, the thermo-responsive swelling was more significant than the pH-triggered one. The microgels functionalized with PEG exhibited the most promising behavior. Indeed, the

thermo-triggered swelling of microgel-co-PEG did not give rise to changes in the microgel surface properties (i.e. surface potential and adhesion) within a wide range of pH values. It was possible for the immobilized microgel-co-PEG to undergo a volume transition (swelling/shrinking) with no change in adhesion, suggesting that the surface of the thermo-responsive microgels remains rather hydrophilic above the VPTT. For the microgel-co-PDMAEMA, the unexpected pH-triggered surface-response suggests that the surface grafting density and thickness of the PDMAEMA corona was insufficient and should be further optimized. Nonetheless, this work confirms the possibility of tuning the swelling behavior of microgels without changing the adhesive properties. Responsive surfaces whose swelling properties can be reversibly and externally altered over space and time independently of the surface chemistry are very innovative and will enable revolutionary advances in technologies, particularly in biomedical surface engineering and microfluidics where advanced assembly of functional components are increasingly required.

3.7 Notes

The authors declare no competing financial interests.

3.8 Acknowledgments

Financial support from the Natural Sciences and Engineering Research Council of Canada and the Fonds de Recherche Nature et Technologie, Québec is acknowledged.

3.9 Supporting Information

ATR-FTIR spectra of bare and functionalized microgels; AFM images of bare and functionalized microgels covalently attached to carboxyl-functionalized mica surfaces; grafting stability of covalently attached bare and functionalized microgels with pH and ionic strength; grafting

stability of physisorbed bare and functionalized microgels with pH and ionic strength; hydrodynamic diameter of bare and functionalized microgels over a wider temperature range; variations in hydrodynamic diameter and zeta potential of microgel covered with end-grafted PEG chains of different molecular weights; water contact angle on bare and functionalized microgel-coated surfaces; variability of force profiles in the approach; history effects of consecutive contacts between bare microgel surfaces; onset distances from the force profiles; values of hydrodynamic diameters in **Fig. 3.2**.

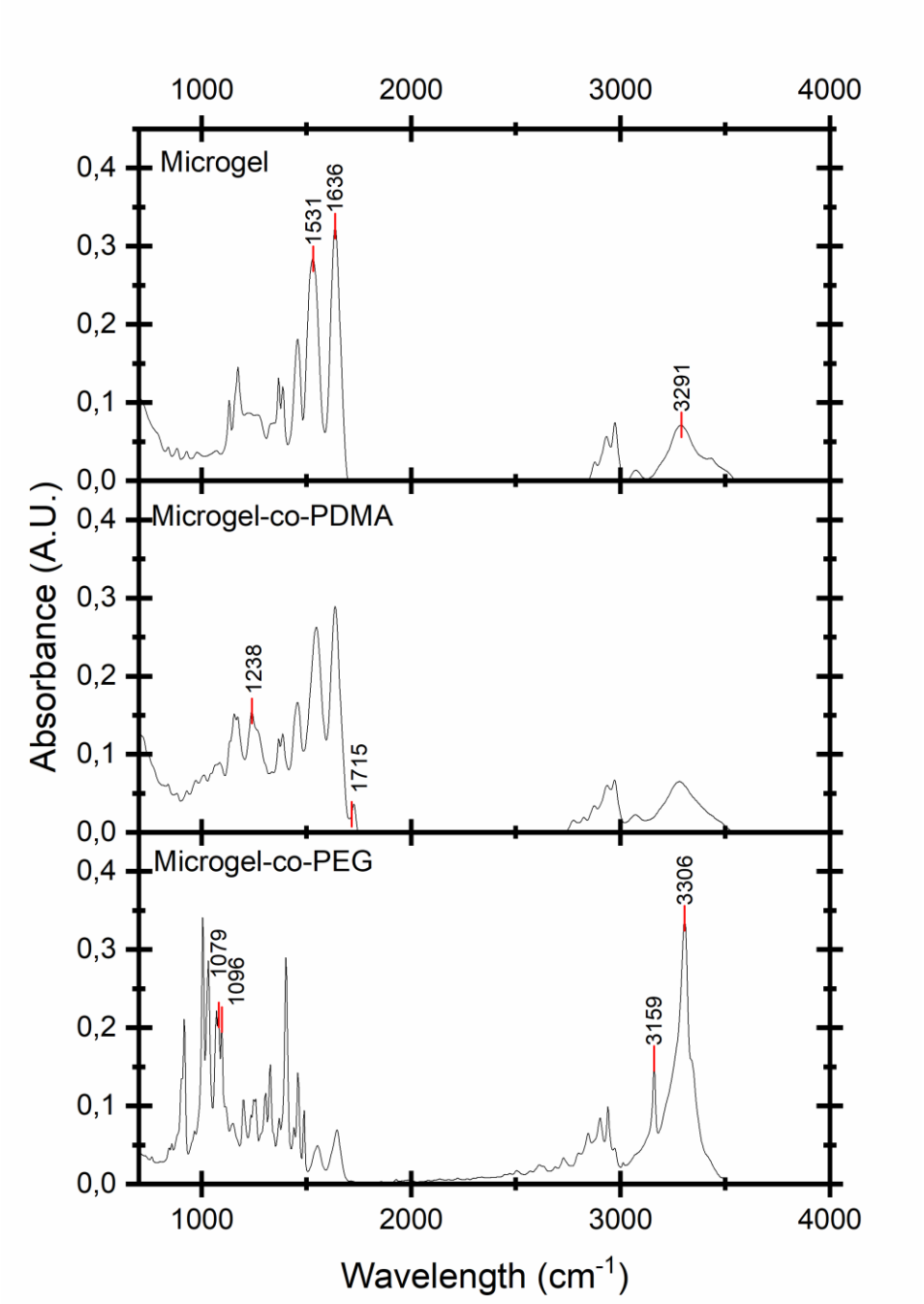

Figure 3.S.1. ATR-FTIR spectra of dried bare microgel, microgel-co-PDMAEMA and microgel-co-PEG.

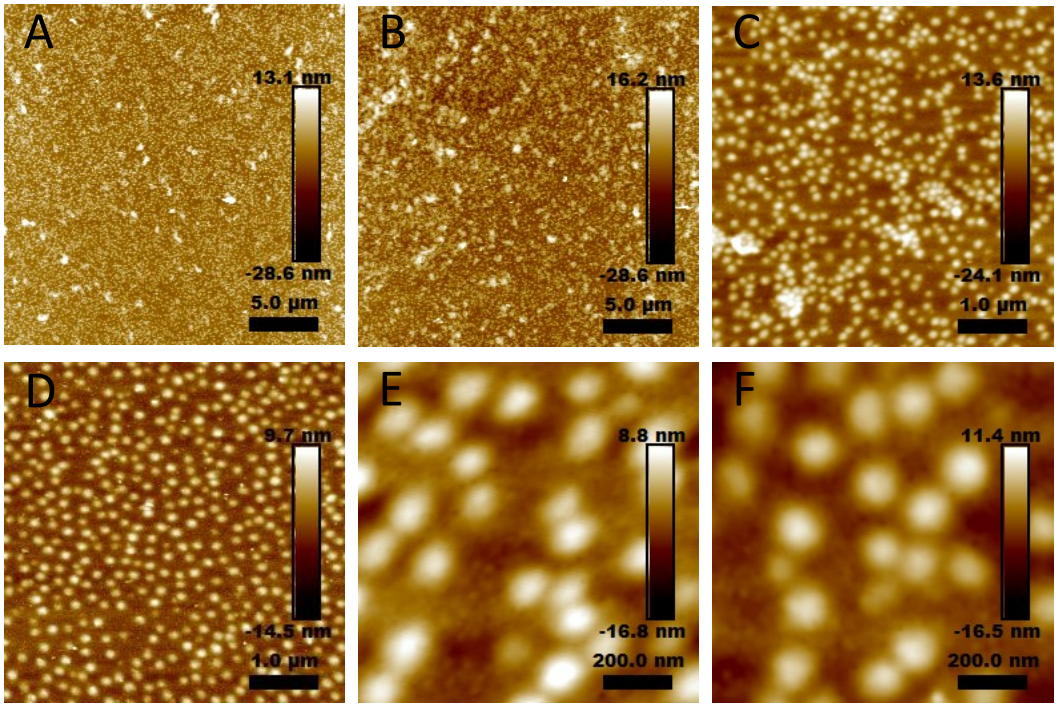

Figure 3.S.2. AFM images of bare microgels covalently attached to AUTES-GLA functionalized mica substrates, in duplicate, imaged 24 hours after grafting, in air at 25 °C and 30 % relative humidity. Obtained in the PeakForce tapping mode. Image scale, (A-B) 25 x 25 µm; (C-D) 5 x 5 µm and (E-F) 1 x 1 µm.

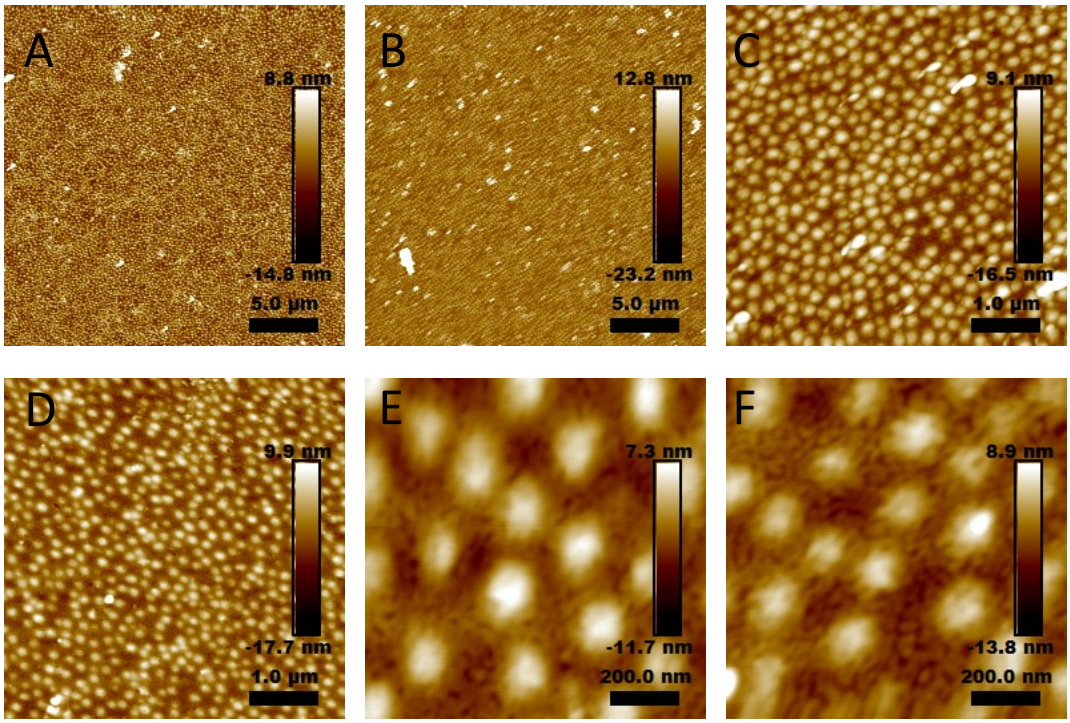

Figure 3.S.3. AFM images of microgel-co-PDMAEMA covalently attached to AUTES-GLA functionalized mica substrates, in duplicate, imaged 24 hours after grafting, in air at 25 °C and 30 % relative humidity. Obtained in the PeakForce tapping mode. Image scale, (A-B) 25 x 25 µm; (C-D) 5 x 5 µm and (E-F) 1 x 1 µm.

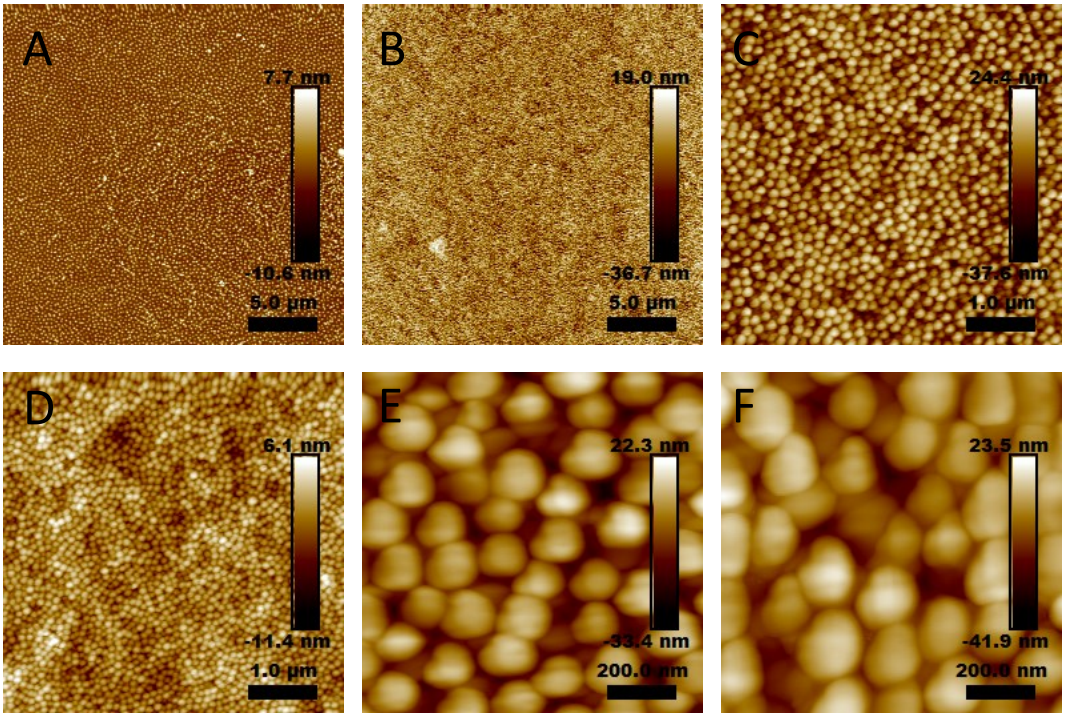

Figure 3.S.4. AFM images of microgel-co-PEG covalently attached to AUTES-GLA functionalized mica substrates, in duplicate, obtained 24 hours after grafting, in air at 25 °C and 30 % relative humidity obtained in the PeakForce tapping mode. Image scale, (A-B) 25 x 25 µm; (C-D) 5 x 5 µm and (E-F) 1 x 1 µm.

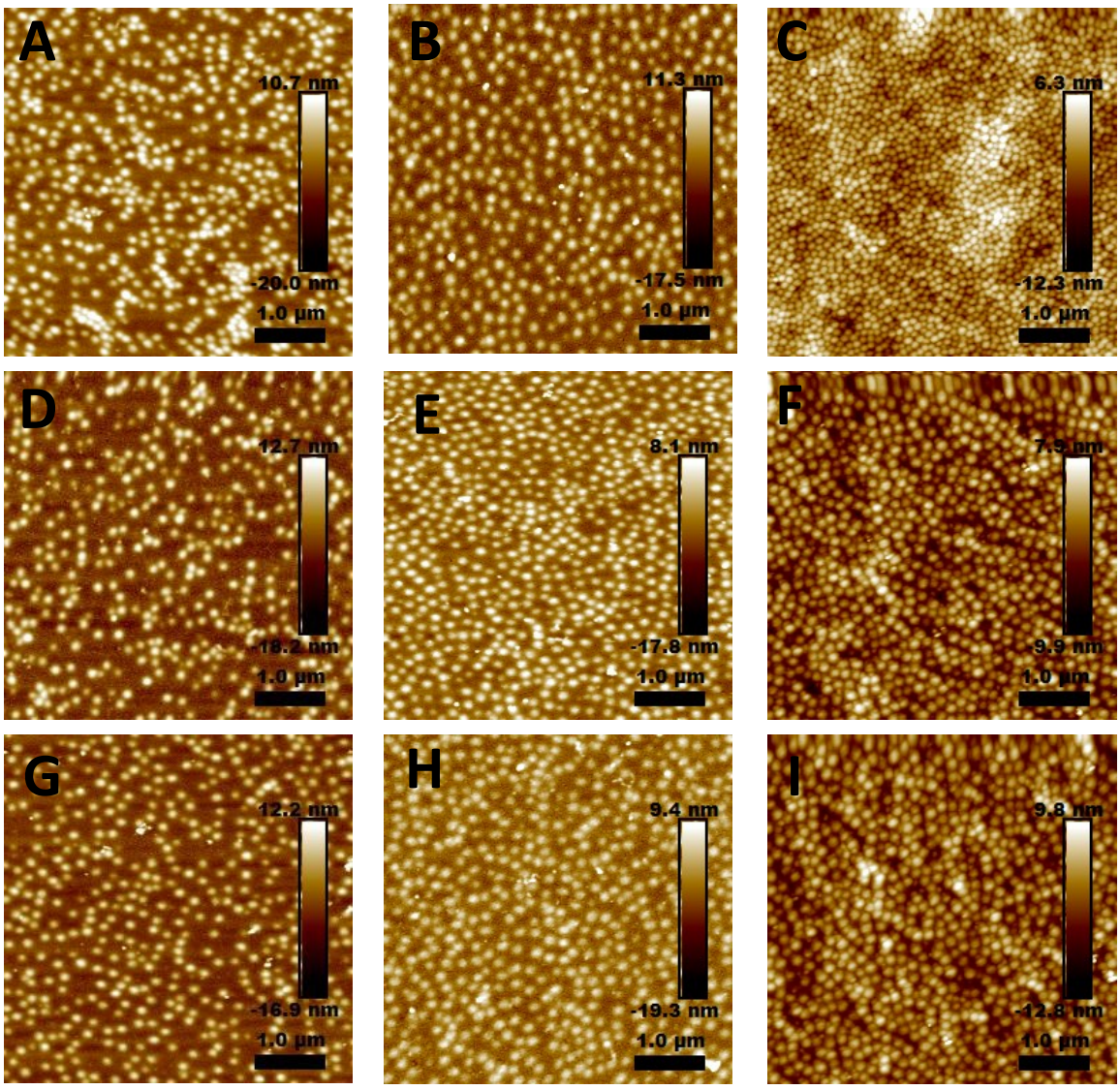

Figure 3.S.5. AFM images of bare microgel (A, D, G), microgel-co-PDMAEMA (B, E, H) and microgel-co-PEG (C, F, I) covalently attached to AUTES-GLA functionalized mica substrates obtained after 24 hours of immersion in aqueous 0.1 mM Na_2SO_4 pH 7 solution (A, B, C), pH 4 solution (D, E, F) and pH 10 solution (G, H, I) in the PeakForce tapping mode. Imaging was performed in air at 25 °C and 30 % relative humidity. Image scale, 1 x 1 µm.

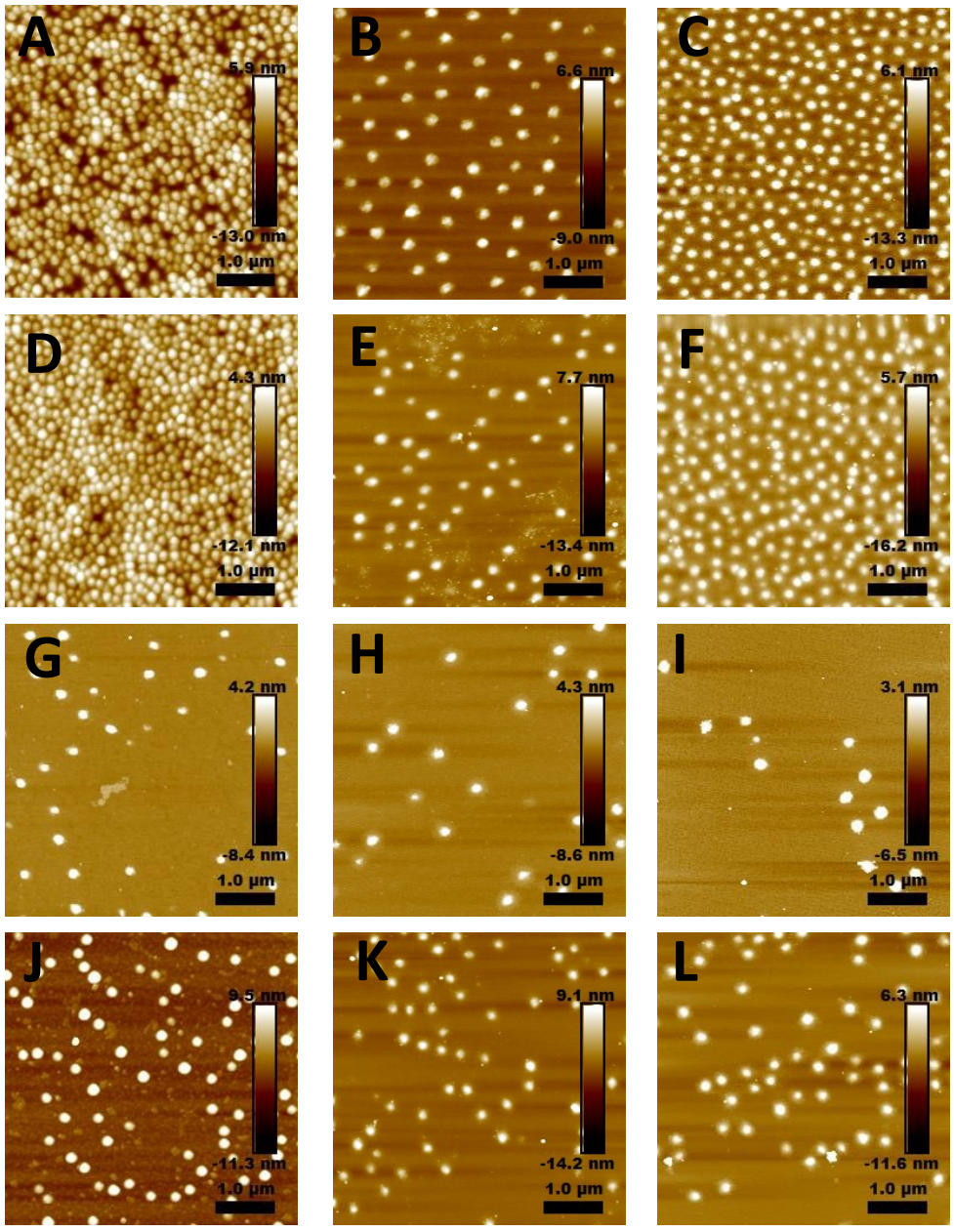

Figure 3.S.6. AFM images of bare microgel (A, D, G, J), microgel-co-PDMAEMA (B, E, H, K) and microgel-co-PEG (C, F, I, L) physisorbed on mica substrates obtained 24 hours after microgel physisorption (A, B, C) and after 24 hours of immersion in aqueous 0.1 mM Na_2SO_4 pH 7 solution (D, E, F), pH 4 solution (G, H, I) and pH 10 solution (J, K, L) in the PeakForce tapping mode. Imaging was performed in air at 25 °C and 30 % relative humidity. Image scale, 1 x 1 µm.

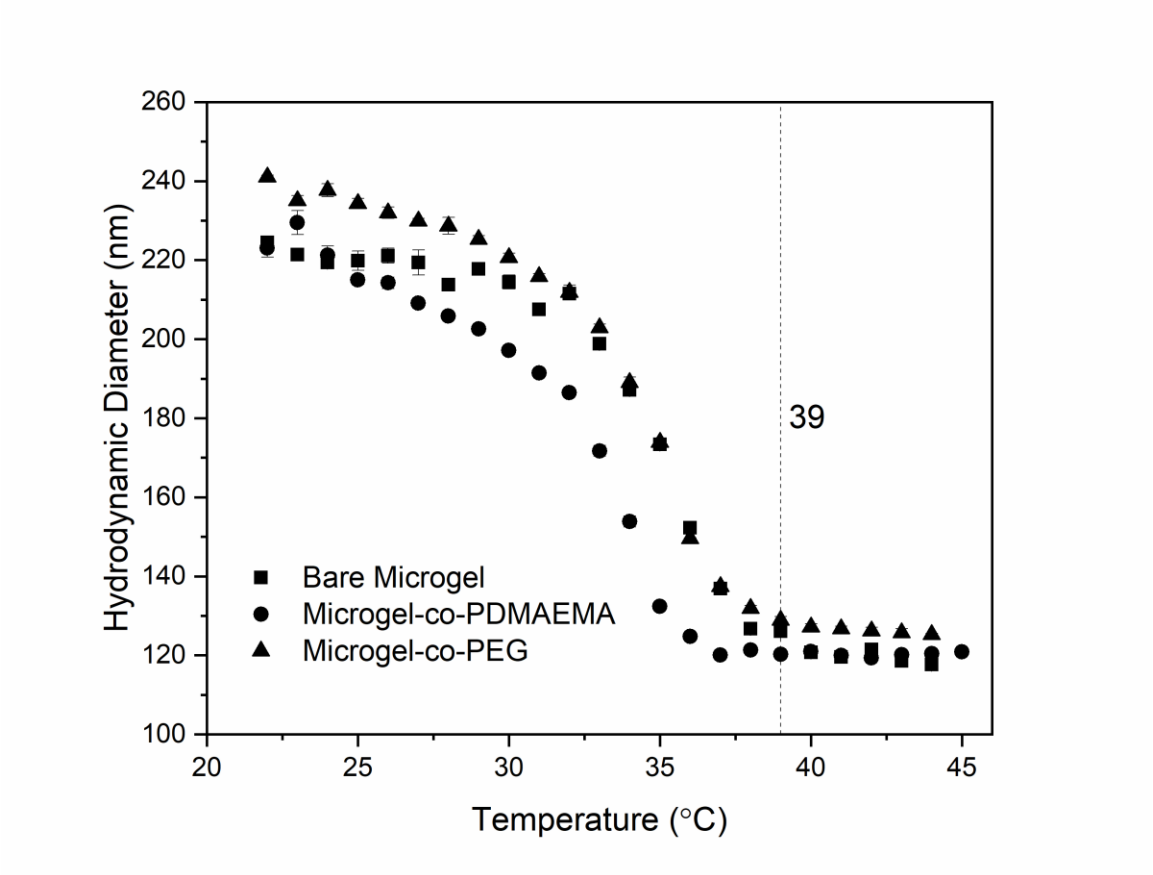

Figure 3.S.7. Variation in the hydrodynamic diameter as a function of temperature of bare microgel (■),microgel-co-PDMAEMA (●) and microgel-co-PEG (▲) in neutral media. Dashed line at 39 ˚C is a guide for the eyes. Error bars represent the standard deviation of three independent experiments.

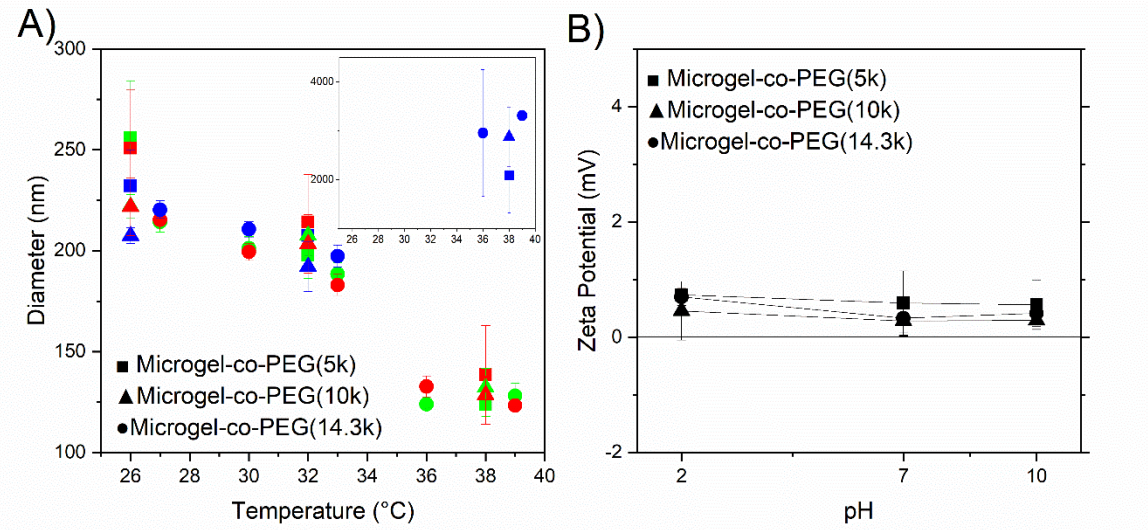

Figure 3.S.8. Variation in the hydrodynamic diameter as a function of temperature at different pH (A) and in zeta potential as a function of pH at 24 °C (B) of microgels grafted with PEG chains of mass 5k (■), 10k (▲) and 14.3k (●) at pH 2 (red), pH 7 (green) and pH 10 (blue). Inset shows the large size of most probably aggregated microgels at pH 10. Error bars represent the standard deviation of three independent experiments.

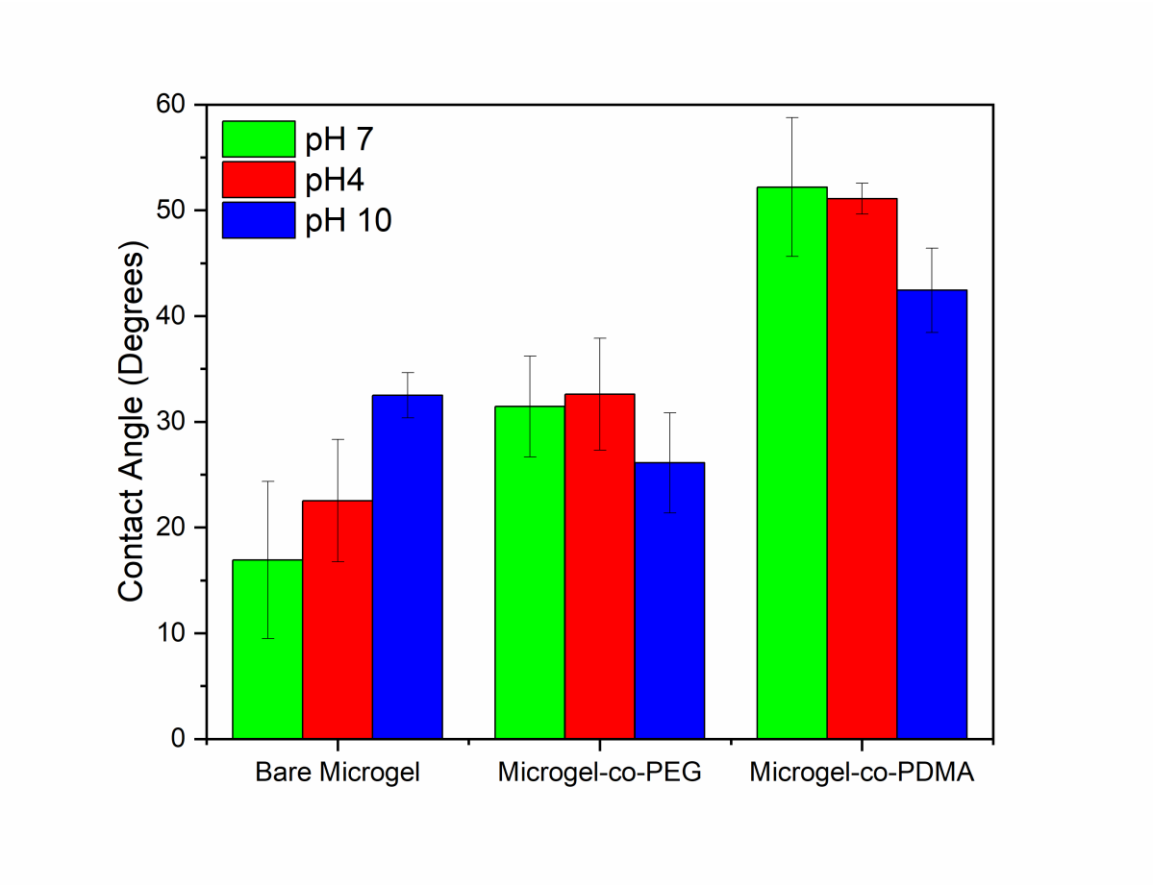

Figure 3.S.9. Variation of the water contact angle on AUTES-GLA functionalized substrates coated with chemisorbed bare and functionalized microgels with droplets (3 – 5 µL) at pH 7 (green), pH 4 (red) and pH 10 (blue).

(A)

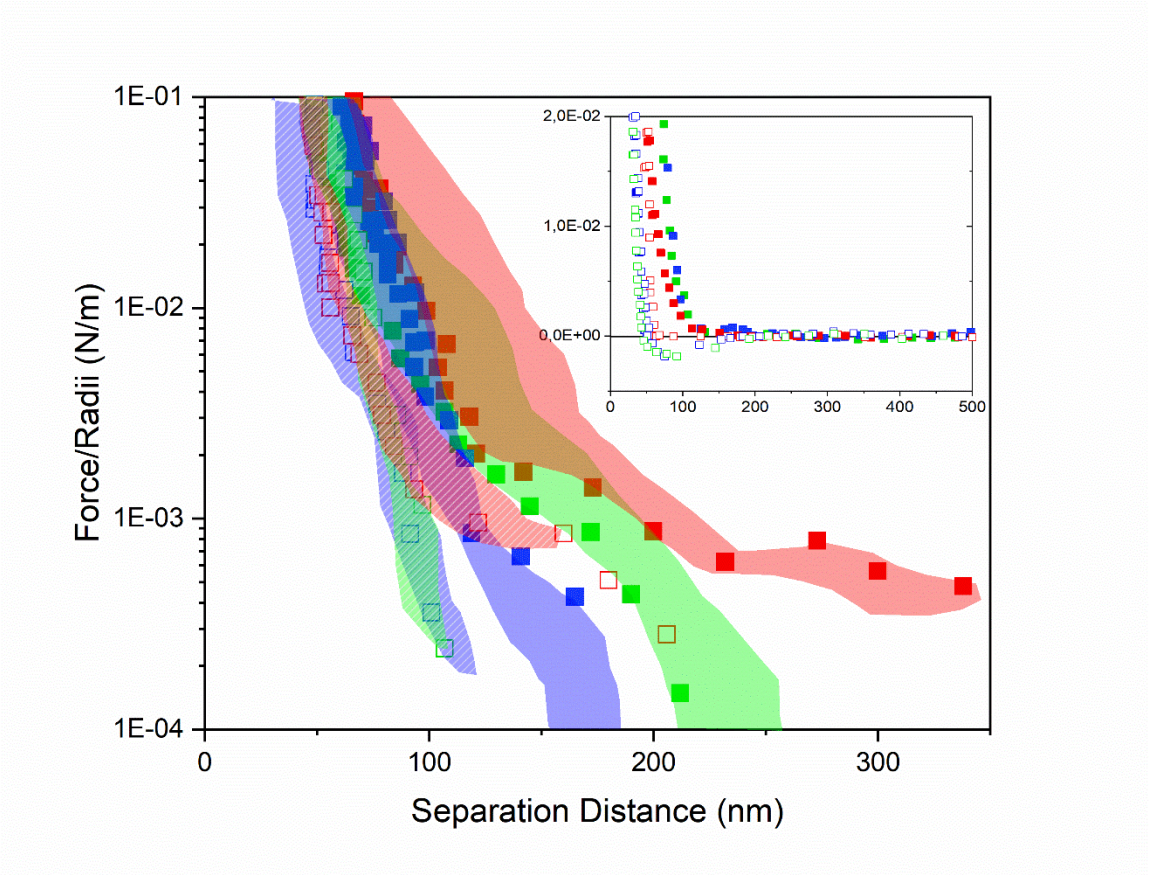
1E-01
1E-02
1E-03
1E-04
Force/Radii (N/m)
0
100
200
300
Separation Distance (nm)
2,0E-02
1,0E-02
0,0E+00
0
100
200
300
400
500

(B)

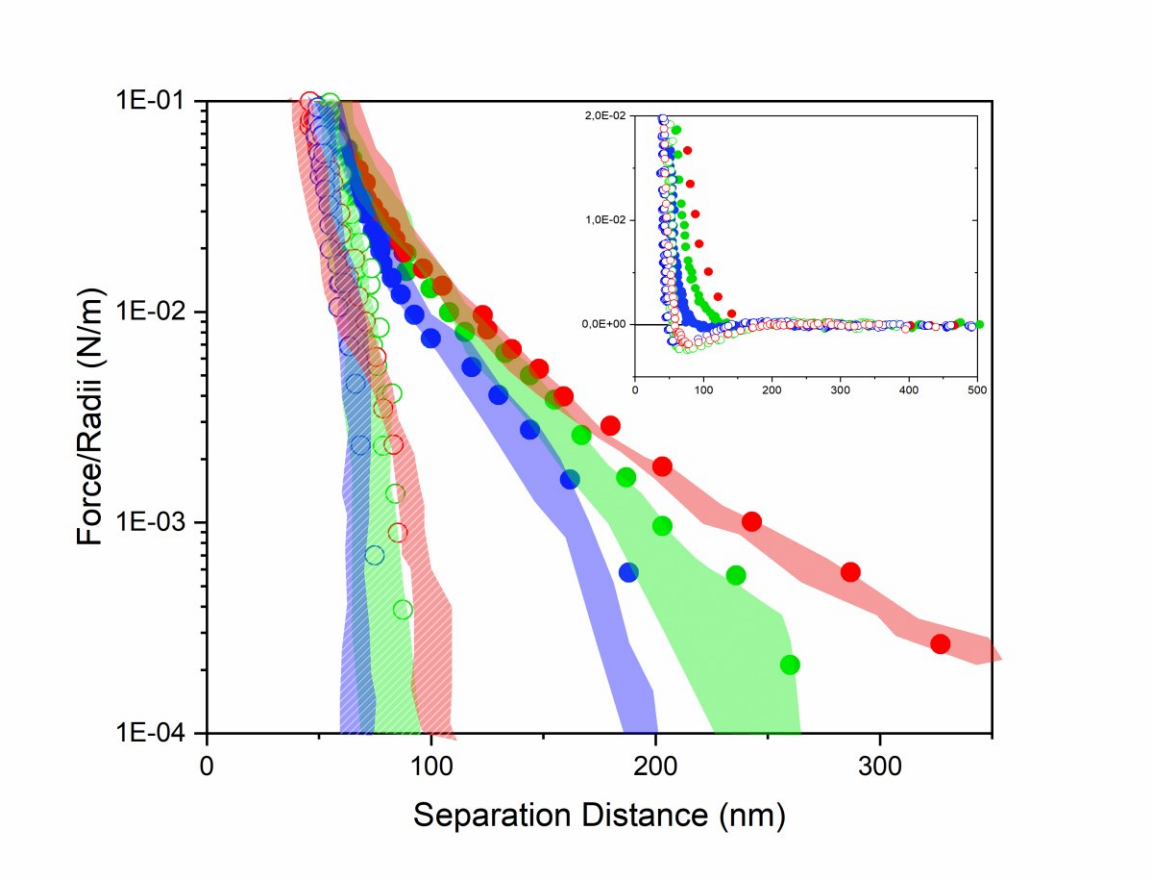
1E-01
1E-02
1E-03
1E-04
Force/Radii (N/m)
0
100
200
300
Separation Distance (nm)
2,0E-02
1,0E-02
0,0E+00
0
100
200
300
400
500

(C)

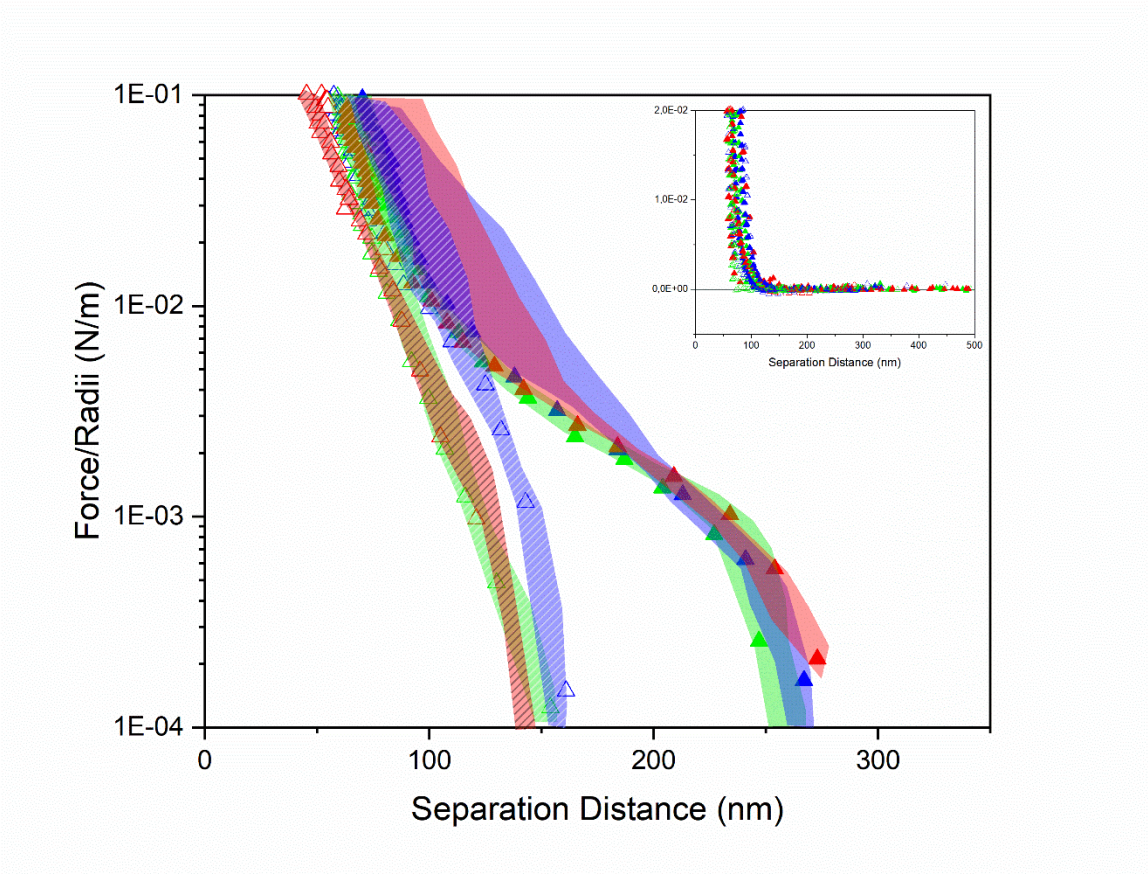

Figure 3.S.10. Interaction forces as a function of separation distance, D, measured on the approach and separation (insets) between two identical immobilized bare microgel (A, ■), microgel-co-PDMAEMA (B, ●) and microgel-co-PEG (C, ▲) layers at different pH values of 4 (red), 7 (green) and 10 (blue) at 23 ˚C (filled symbols) and 43 ˚C (open symbols). D = 0 corresponds to the adhesive mica – mica contact. The shaded areas represent the variability in the measured profiles. The reported results are from at least three independent experiments.

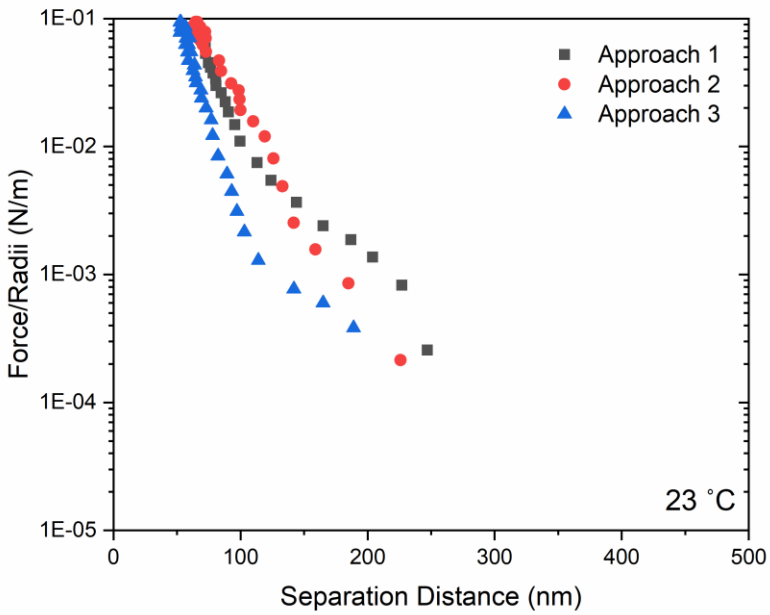

Figure 3.S.11. History effects on the force profiles, measured on three consecutive approaches on the same contact position for two layers of immobilized bare microgel at 23 ˚C in aqueous 0.1 mM Na_2SO_4. *D* = 0 corresponds to the adhesive mica – mica contact.

Table 3.S.1. Separation distance at the onset of the interaction forces measured in the approach for bare microgel, microgel-co-PDMAEMA and microgel-co-PEG as a function of temperature at different pH values.

Sample	Temperature (°C)	pH	Onset (nm)
Bare Microgel	23	4	189 ± 1
		7	155 ± 1
		10	108 ± 1
	43	4	106 ± 1
		7	87 ± 1
		10	88 ± 1
Microgel-co-PDMAEMA	23	4	201 ± 1
		7	179 ± 1
		10	158 ± 1
	43	4	90 ± 1
		7	75 ± 1
		10	68 ± 1
Microgel-co-PEG	23	4	216 ± 1
		7	210 ± 1
		10	211 ± 1
	43	4	116 ± 1
		7	119 ± 1
		10	131 ± 1

Table 3.S.2. Hydrodynamic diameter for bare microgel, microgel-co-PDMA and microgel-co-PEG as a function of temperature at different pH values.

Sample	Temperature (°C)	pH	Hydrodynamic diameter (nm)
Bare Microgel	24	2	250 ± 2
		7	224 ± 5
		10	204 ± 8
	39	2	132 ± 4
		7	129 ± 5
		10	1037 ± 134
Microgel-co-PDMAEMA	24	2	237 ± 1
		7	223 ± 1
		10	249 ± 8
	39	2	113 ± 2
		7	118 ± 1
		10	410 ± 19
Microgel-co-PEG	24	2	238 ± 6
		7	217 ± 7
		10	226 ± 1
	39	2	123 ± 3
		7	128 ± 6
		10	3309 ± 1103

3.10 References

(1) Liu, F.; Urban, M. Recent Advances and Challenges in Designing Stimuli-Responsive Polymers. *Prog. Polym. Sci.* **2010**, *35*, 3–23.

(2) Stuart, M.; Huck, W.; Genzer, J.; Muller, M.; Ober, C.; Stamm, M.; Sukhorukov, G.; Szleifer, I.; Tsukruk, V.; Urban, M.; Winnik, F.; Zauscher, S.; Luzinov, I.; Minko, S. Emerging Applications of Stimuli-Responsive Polymer-Materials. *Nat. Mater.* **2010**, *9*, 101–113.

(3) Leon-Lopez, T.; Ortega-Vinuesa, J.; Bastos-Gonzalez, D.; Elaissari, A. Cationic and Anionic Poly-(N-Isopropylacrylamide) Based Submicron Gel Particles: Electrokinetic Properties and Colloidal Stability. *J. Phys. Chem. B* **2006**, *110*, 4629–4636.

(4) Meunier, F.; Elaissari, A.; Pichot, C. Preparation and Characterization of Cationic Poly(n-Isopropylacrylamide) Copolymer Latexes. *Polym. Adv. Technol.* **1995**, *6*, 489–496.

(5) Pelton, R. Poly(N-Isopropylacrylamide) (PNIPAM) Is Never Hydrophobic. *J. Colloid Interface Sci.* **2010**, *348*, 673–674.

(6) Kieviet, B.; Schon, P.; Vancso, J. Stimulus-Responsive Polymers and Other Functional Polymers Surfaces as Components in Glass Microfluidic Channels. *Lab Chip.* **2014**, *21*, 4159–4170.

(7) Gao, Y.; Zago, G.; Jia, Z.; Serpe, M. Controlled and Triggered Small Molecule Release from a Confined Polymer Film. *ACS Appl. Mater. Interfaces* **2013**, *5*, 9803–9808.

(8) Kumashiro, Y.; Fukumori, K.; Takahashi, H.; Nakayama, M.; Akiyama, Y.; Yamato, M.; Okano, T. Modulation of Cell Adhesion and Detachment on Thermo-Responsive Polymeric Surfaces through Observation of Surface Dynamics. *Colloids Surf., B.* **2013**, *106*, 198–207.

(9) Guerron, A.; Giasson, S. Multiresponsive Microgels: Towards an Independent Tuning of Swelling and Surface Properties. *Langmuir* **2021**, *37*, 11212–11221.

(10) Kieviet, B. D.; Schön, P. M.; Vancso, G. J. Stimulus-Responsive Polymers and Other Functional Polymer Surfaces as Components in Glass Microfluidic Channels. *Lab Chip.* **2014**, *14*, 4159–4170.

(11) Cheng, R.; Meng, F.; Deng, C.; Klok, H.-A.; Zhong, Z. Dual and Multi-Stimuli Responsive Polymeric Nanoparticles for Programmed Site-Specific Drug Delivery. *Biomaterials* **2013**, *34*, 3647–3657.

(12) Gui, R.; Jin, H.; Guo, H.; Wang, Z. Recent Advances and Future Prospects in Molecularly Imprinted Polymers-Based Electrochemical Biosensors. *Biosens. Bioelectron.* **2018**, *100*, 56–70.

(13) Ma, Z.; Mao, Z.; Gao, C. Surface Modification and Property Analysis of Biomedical Polymers Used for Tissue Engineering. *Colloids Surf., B.* **2007**, *60*, 137–157.

(14) Faivre, J.; Shrestha, B.; Burdynska, J.; Xie, G.; Moldovan, F.; Delair, T.; Benayoun, S.; Laurent, D.; Matyjaszewski, K.; Banquy, X. Wear Protection without Surface Modification Using a Synergistic Micture of Molecular Brushes and Linear Polymers. *ACS Nano* **2017**, *11*, 1762–1769.

(15) Xia, W.; Adibnia, V.; Huang, R.; Murschel, F.; Faivre, J.; Xie, G.; Olszewski, M.; De Crescenzo, G.; Qi, W.; He, Z.; Matyjaszewski, K.; Banquy, X. Biomimetic Bottlebrush Polymer Coatings

for Fabrication of Ultralow Fouling Surfaces. *Angew. Chem.* **2018**, *131*, 1308–1314.
(16) Giraud, L.; Bazin, G.; Giasson, S. Lubrication with Soft and Hard Two-Dimensional Colloidal Arrays. *Langmuir* **2017**, *33*, 3610–3623.
(17) Gorelikov, I.; Field, L.; Kumacheva, E. Hybrid Microgels Photoresponsive in the Near-Infrared Spectral Range. *J. Am. Chem. Soc.* **2004**, *126*, 15938–15939.
(18) Perez-Fuentes, L.; Drummond, C.; Faraudo, J.; Bastos-Gonzalez, D. Anions Make the Difference: Insights from the Interaction of Big Cations and Anions with Poly(N-Isopropylacrylamide) Chains and Microgels. *Soft Matter* **2015**, *11*, 5077–5086.
(19) Liu, L.; Du, P.; Zhao, X.; Zeng, J.; Liu, P. Independent Temperature and PH Dual-Stimuli Responsive Yolk/Shell Polymer Microspheres for Controlled Release: Structural Effect. *Eur. Polym. J.* **2015**, *69*, 540–551.
(20) Wang, X.; Yan, S.; Song, L.; Shi, H.; Yang, H.; Luan, S.; Huang, Y.; Yin, J.; Khan, A. F.; Zhao, J. Temperature-Responsive Hierarchical Polymer Brushes Switching from Bactericidal to Cell Repellency. *ACS Appl. Mater. Interfaces* **2017**, *9*, 40930–40939.
(21) Vialar, P.; Merzeau, P.; Giasson, S.; Drummond, C. Compliant Surfaces under Shear: Elastohydrodynamic Lift Force. *Langmuir* **2019**, *35*, 15605–15613.
(22) Banquy, X.; Zhu, X. X.; Giasson, S. Mechanical and Frictional Properties of Nanoparticle Monolayers Grafted on Functionalized Mica Substrates. *J. Phys. Chem. B* **2008**, *112*, 12208–12216.
(23) Banquy, X.; Charrault, E.; Giasson, S. Normal and Lateral Interactions between Thermosensitive Nanoparticle Monolayers in Water. *J. Phys. Chem. B* **2010**, *114* (30), 9721–9728.
(24) Faivre, J.; Shrestha, B.; Xie, G.; Delair, T.; Laurent, D.; Matyjaszewski, K.; Banquy, X. Unraveling the Correlations between Conformation, Lubrication and Chemical Stability of Bottlebrush Polymers at Interfaces. *Biomacromolecules* **2017**, *18*, 4002–4010.
(25) Wang, C.-S.; Xie, R.; Liu, S.; Giasson, S. Tribological Behavior of Surface-Immobilized Novel Biomimicking Multihierarchical Polymers: The Role of Structure and Surface Attachment. *Langmuir* **2019**, *35*, 15592–15604.
(26) Stoychev, G.; Turcaud, S.; Dunlop, J.; Ionov, L. Hierarchical Multi-Step Folding of Polymer Bilayers. *Adv. Funct. Mater.* **2012**, *23*, 2295–2300.
(27) Odent, J.; Vanderstappen, S.; Toncheva, A.; Pichon, E.; Wallin, T.; Wang, K.; Shepherd, R.; Dubois, P.; Raquez, J.-M. Hierarchical Chemomechanical Encoding of Multi-Responsive Hydrogel Actuators via 3D Printing. *J. Mater. Chem. A* **2019**, *7*, 15395–15403.
(28) Yu, Q.; Zhang, Y.; Wang, H.; Brash, J.; Chen, H. Anti-Fouling Bioactive Surfaces. *Acta Biomater.* **2011**, *7*, 1550–1557.
(29) Zhao, C.; Hou, J.; Chen, R.; Xin, Z.; Shi, H.; Wong, S.-C.; Yin, J.; Shi, Q. Cell-Inspired Biointerfaces Constructed by Patterned Smart Hydrogels for Immunoassay in Whole Blood. *J. Mater. Chem. B* **2017**, *5*, 2315–2321.
(30) Karg, M.; Pastoriza-Santos, I.; Rodriguez-Gonzalez, B.; von Klitzig, R.; Wellert, S.; Hellweg, T. Temperature, PH, and Ionic Strength Induced Changes of the Swelling Behavior of PNIPAM-Poly(Allylacetic Acid) Copolymer Microgels. *Langmuir* **2008**, *24*, 6300–6306.
(31) Khan, A. Preparation and Characterization of N-Isopropylacrylamide/Acrylic Acid Copolymer Core-Shell Microgel Particles. *J. Colloid Interface Sci.* **2007**, *313*, 697–704.
(32) Bradley, M.; Vincent, B. Poly(Vinylpyridine) Core/Poly(N-Isopropylacrylamide) Shell

Microgel Particles: Their Characterization and the Uptake and Release of an Anionic Surfactant. *Langmuir* **2008**, *24*, 2421–2425.

(33) Chen, K.; Zhou, S.; Wu, L. Self-Healing Underwater Superoleophobic and Antibiofouling Coatings Based on the Assembly of Hierarchical Microgel Spheres. *ACS Nano* **2016**, *10*, 1386–1394.

(34) Wu, M.; Chen, J.; Huang, W.; Yan, B.; Peng, Q.; Liu, J.; Chen, L.; Zeng, H. Injectable and Self-Healing Nanocomposite Hydrogels with Ultrasensitive PH-Responsiveness and Tunable Mechanical Properties: Implications for Controlled Drug Delivery. *Biomacromolecules* **2020**, *21*, 2409–2420.

(35) Lu, T.; Zhu, S.; Ma, J.; Lin, J.; Wang, W.; Pan, H.; Tian, F.; Zhang, W.; Zhang, D. Bioinspired Thermoresponsive Photonic Polymers with Hierarchical Structures and Their Unique Properties. *Macromol. Rapid Commun.* **2015**, *36*, 1722–1728.

(36) Shang, S.; Liu, J.; He, Y.; Zhu, P. Smart Conducting PNIPAM-Co-AAc Microgels with Controllable Phase Transition and Stimuli Responsibility. *Mater. Lett.* **2020**, *272*, 127862–127866.

(37) Londe, G.; Chunder, A.; Wesser, A.; Zhai, L.; Cho, H. J. Microfluidic Valves Based on Superhydrophobic Nanostructures and Switchable Thermosensitive Surface for Lab-on-a-Chip (LOC) Systems. *Sens. Actuators, B* **2008**, *132*, 431–438.

(38) Chunder, A.; Etcheverry, K.; Londe, G.; Cho, H. J.; Zhai, L. Conformal Switchable Superhydrophobic/Hydrophilic Surfaces for Microscale Flow Control. *Colloids Surf., A* **2009**, *333*, 187–193.

(39) Bai, Y.; Zhang, Z.; Zhang, A.; Chen, L.; He, C.; Zhuang, X.; Chen, X. Novel Thermo- and PH-Responsive Hydroxypropyl Cellulose- and Poly (L-Glutamic Acid)-Based Microgels for Oral Insulin Controlled Release. *Carbohydr. Polym.* **2012**, *89*, 1207–1214.

(40) Raju, R.; Bandyopadhyay, S.; Sharma, A.; Villa Gonzalez, S.; Carlsen, P. H.; Gautun, O. R.; Glomm, W. R. Synthesis, Characterization and Drug Loading of Multiresponsive p[NIPAm-Co-PEGMA] (Core)/p[NIPAm-Co-AAC] (Shell) Nanogels with Monodisperse Size Distributions. *Polymers* **2018**, *10*, 309–323.

(41) Liu, L.; Zeng, J.; Zhao, X.; Tian, K.; Liu, P. Independent Temperature and PH Dual-Responsive PMAA/PNIPAM Microgels as Drug Delivery Systems: Effect of Swelling Behavior of the Core and Shell Materials in Fabrication Process. *Colloids Surf., A* **2017**, *526*, 48–55.

(42) Zeiser, M.; Freudensprung, I.; Hellweg, T. Linearly Thermoresponsive Core-Shell Microgels: Towards a New Class of Nanoactuators. *Polymer* **2012**, *53*, 6096–6101.

(43) Cors, M.; Wrede, O.; Genix, A.-C.; Anselmetti, D.; Oberdisse, J.; Hellweg, T. Core-Shell Microgel-Based Surface Coatings with Linear Thermoresponse. *Langmuir* **2017**, *33*, 6804–6811.

(44) Sabadasch, V.; Wiehemeier, L.; Kottke, T.; Hellweg, T. Core-Shell Microgels as Thermoresponsive Carriers for Catalytic Palladium Nanoparticles. *Soft Matter* **2020**, *16*, 5422–5430.

(45) Liberelle, B.; Banquy, X.; Giasson, S. Stability of Silanols and Grafted Alkylsilane Monolayers on Plasma-Activated Mica Surfaces. *Langmuir* **2008**, *24*, 3280–3288.

(46) Jirku, V.; Turkova, J. Cell Immobilization by Covalent Linkage. *Methods Enzymol.* **1987**, *135*, 341–357.

(47) Mansson, M.-O.; Mosbach, K. Immobilized Active Coenzymes. *Methods Enzymol.* **1987**,

136, 3–9.
(48) Israelachvili, J. Thin Film Studies Using Multiple-Beam Interferometry. *J. Colloid Interface Sci.* **1973**, *44*, 259–272.
(49) Israelachvili, J.; Adams, G. Measurement of Forces between Two Mica Surfaces in Aqueous Electrolyte Solutions in the Range 0-100 Nm. *J. Chem. Soc., Faraday Trans. 1* **1978**, *74*, 975–1001.
(50) Leon-Lopez, T.; Elaissari, A.; Ortega-Vinuesa, J.; Bastos-Gonzalez, D. Hofmeister Effects on Poly(NIPAM) Microgel Particles: Macroscopic Evidence of Ion Adsorption and Changes in Water Structure. *ChemPhysChem* **2006**, *8*, 148–156.
(51) Vialar, P.; Merzeau, P.; Barthel, E.; Giasson, S.; Drummond, C. Interaction between Compliant Surfaces: How Soft Surfaces Can Reduce Friction. *Langmuir* **2019**, *35*, 15723–15728.
(52) van de Wetering, P.; Zuidam, N. J.; van Steenbergen, M. J.; van der Houwen, O. A. G. J.; Underberg, W. J. M.; Hennink, W. E. A Mechanistic Study of the Hydrolytic Stability of Poly(2-(Dimethylamino)Ethylmethacrylate). *Macromolecules* **1998**, *31*, 8063–8068.
(53) Butun, V.; Armes, S. P.; Billingham, N. C. Synthesis and Aqueous Solution Properties of Near-Monodisperse Tertiary Amine Methacrylate Homopolymers and Diblock Copolymers. *Polymer* **2001**, *42*, 5993–6008.
(54) Hunter, R.; White, L.; Chan, D. *Foundations of Colloid Science*, 2nd ed.; Oxford University Press: New York, 2001.
(55) Grahame, D. The Electrical Double Layer and the Theory of Electrocapillarity. *Chem. Rev.* **1947**, *41*, 441–501.
(56) Gouy, M. Sur La Constitution de La Charge Électrique à La Surface d'un Electrolyte. *J. Phys. Théorique Appliquée* **1910**, *9*, 457–468.
(57) Chapman, D. L. A Contribution to the Theory of Electrocapillarity. *Philos. Mag.* **1913**, *25*, 475–481.
(58) Manouras, T.; Koufakis, E.; Anastasiadis, S.; Vamvakaki, M. A Facile Route towards PDMAEMA Homopolymer Amphiphiles. *Soft Matter* **2017**, *13*, 3777–3782.
(59) Patenaude, M.; Hoare, T. Injectable, Degradable Thermoresponsive Poly(N-Isopropylacrylamide) Hydrogels. *ACS Macro Lett.* **2012**, *1*, 409–413.
(60) Hoare, T.; Pelton. Functional Group Distributions in Carboxylic Acid Containing Poly(N-Isopropylacrylamide) Microgels. *Langmuir* **2004**, *20*, 2123–2133.
(61) Thompson, K.; Read, E.; Armes, S. Chemical Degradation of Poly(2-Aminoethyl Methacrylate). *Polym. Degrad. Stab.* **2008**, *93*, 1460–1466.
(62) Zhang, Q.; Xia, F.; Sun, T.; Song, W.; Zhao, T.; Liu, M.; Jiang, L. Wettability Switching between High Hydrophilicity at Low PH and High Hydrophobicity at High PH on Surface Based on PH-Responsive Polymer. *Chem. Commun.* **2008**, *10*, 1199–1201.
(63) Shangcong, H.; Haiying, W.; Daoshu, L.; Shutao, G.; Hongxu, D.; Jianhua, Z.; Liadong, D.; Ruming, L.; Hua, T.; Anjie, D. Contribution of Hydrophobic/Hydrophilic Modification on Cationic Chains of Poly(ε-Caprolactone)-Graft-Poly(Dimethylamino Ethylmethacrylate) Amphiphilic Co-Polymer in Gene Delivery. *Acta Biomater.* **2014**, *10*, 670–679.
(64) Shuanhong, M.; Jianxi, L.; Qian, Y.; Daoai, W.; Yongmin, L.; Feng, Z. A General Approach for Construction of Asymmetric Modification Membranes for Gated Flow Nanochannels. *J. Mater. Chem. A* **2014**, *2*, 8804–8814.

(65) Wiedemair, J.; Serpe, M.; Kim, J.; Masson, J.-F.; Lyon, A.; Mizaikoff, B.; Kranz, C. In-Situ AFM Studies of the Phase-Transition Behavior of Single Thermoresponsive Hydrogel Particles. *Langmuir* **2007**, *23*, 130–137.
(66) Tagit, O.; Tomczak, N.; Vancso, J. Probing the Morphology and Nanoscale Mechanics of Single Poly(N-Isopropylacrylamide) Microgels Across the Lower-Critical-Solution Temperature by Atomic Force Microscopy. *Small* **2008**, *4*, 119–126.

Chapter 4 – Tribological properties of PNIPAM microgels in the nano- and mesoscales

4.1 Introduction

The friction behavior of pH-responsive soft microgel particles indicates that the tribological properties are more closely dependant on nanoparticle swelling than on the degree of ionization or the surface charge.[1] In fact, increasing swelling of the particles was associated with a decrease in elasticity while the friction coefficient was observed to increase with elasticity. Similarly, the tribological behavior of thermosensitive microgels varies significantly with conformational changes associated with phase transitions above and below the VPTT as well as partial contributions from attractive forces between layers.[2,3] Further, polymer adhesion is one of the main mechanisms that controls the tribological behavior and it can be tuned via external stimuli such as temperature, pH, or ionic strength.[4–6] Results presented in chapter 3 showed that grafting polymer chains on the surface of the microgels does not inhibit the thermo-responsive behavior of PNIPAM. Further, it was shown that the surface properties, i.e. the surface potential and adhesion, could be modulated via surface-functionalization independently of the swelling.[7] For example, the surface-immobilized microgel-co-PEG underwent a thermo-triggered volume transition (swelling/shrinking) with no variation in the microgel-microgel adhesion. This is an important distinction between microgel-co-PEG and bare PNIPAM microgels, for which swelling behavior is closely associated to changes in surface wettability and adhesion.[2,7] On the other hand, even though adhesion between two opposing layers of covalently-immobilized PDMAEMA chains has been measured in basic pH as well as at temperatures above the VPTT (40 – 50 °C),[8–10]

no adhesion forces could be measured between microgel-co-PDMAEMA in basic media at 23 °C and only arose when heated to 43 °C regardless of pH.[7] This suggests that the grafting density or the molecular weight of PDMAEMA polymer chains on the microgel are insufficient to fully express their characteristic behavior.

This chapter investigates if the control of surface properties of bare and surface-functionalized microgels translates to changes in their respective tribological behavior. More specifically, the hypothesis of this section is that the friction behavior does not depend exclusively on particle swelling but also on surface chemistry. The tribological behavior of bare and surface-functionalized microgels in the nanoscale was determined under dynamic constrain using the SFA technique. Shearing is achieved by sliding the upper surface in reciprocating motion with the help of a digital encoder-controlled motor-driven micrometer and the friction force is measured with a Wheatstone Bridge connected to resistance strain gauges while the bottom surface is mounted on double-cantilever springs that remain stationary during sliding as shown in **Fig. 4.1** below.

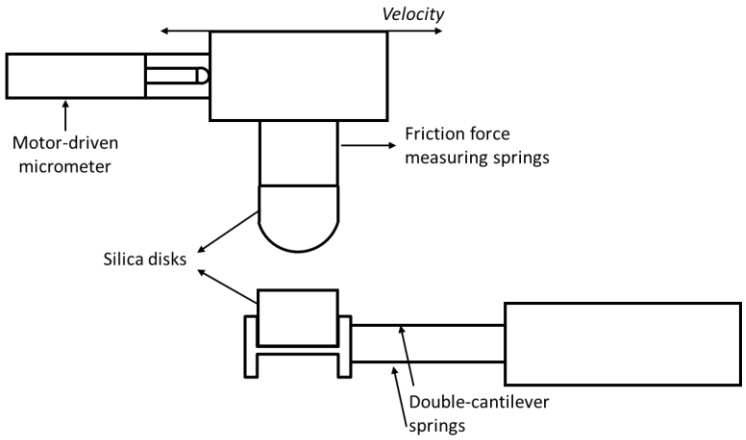

Figure 4.1. Scheme of the experimental setup for dynamic force measuring experiments in the nanoscale with the SFA.

The nanotribological properties of bare microgel with increasing normal applied load were studied in neutral media at 23 °C prior to modifying the pH of the medium surrounding the microgel layers. Then, microgel-co-PEG and microgel-co-PDMAEMA layers were studied under the same temperature and pH range. Previous work on similar microgels showed that the effect of sliding speed on the friction force is negligible at 25 °C.[2] Therefore, the sliding speed used in this study (3 μm/s) was chosen as a compromise between the time needed to perform sliding experiments and ensuring that sliding takes place over a distance that ranges several surface-immobilized microgel units. The friction force is often expressed as a function of the applied load to determine the coefficient of friction, μ, which is the ratio of the friction force and the applied normal load according to Amonton's law: $F_S = \mu F_N$.[1,11–13] The experimental curves used to calculate the coefficient of friction presented in this section are the most representative of two or more independent trials and the experimental error is not shown. The error in measuring friction forces is less than the resolution (of the friction gauges) in measuring friction forces, which is roughly 0.02 mN. Therefore, including identical error bars on all data points would hinder reading comprehension.

Lastly, the presence of an overlap of tribological properties measured in the nanoscale with the SFA and in the mesoscale with a custom-made tribometer (henceforth referred to as: tribo-brush)[14,15] was determined. When using two different tribometers, an overlap refers to two or more controlled parameters of each measuring technique. In this case, the overlap is between the applied normal forces that can be obtained in the SFA (nanoscale) and with the tribo-brush (mesoscale). This study was performed in collaboration with the tribology team of Dr. Sylvie

Descartes in the Contact and Structure Mechanics Laboratory (LamCoS) at the National Institute of Applied Sciences (INSA) in Lyon, France. This work seeks to provide an expanded knowledge of the tribological properties of bare and surface-functionalized microgel layers such as lubrication properties, load bearing capacity and resistance to wear and would permit to better envision potential applications for this type of material.

4.2 Tribological properties of bare and surface-functionalized microgels in the nanoscale

4.2.1 Effect of the normal applied load on covalently attached bare microgels

By measuring the strain on the springs supporting the upper surface in real time during shear it is possible to plot the friction traces that represent the strain on the lateral force gauges as a function of displacement (**Fig. 4.2**). These traces provide important insight into the friction properties of the microgel layers. A null trace means that no friction could be detected, this scenario may arise if the microgel layers are not in contact or if they slide against each other in a well lubricated manner. In the presence of friction, the friction traces depend on the nature and type of the friction. Particularly, the traces may adopt the shape of a pseudo-periodical wave, as illustrated in **Fig. 4.2**, which indicate that the corresponding friction is in the steady-state prior to changes in the direction of displacement. In this case, a very important value can be calculated from the traces: the friction force, which is obtained by calculating the average value of the plateaus of at least one cycle of the traces. For example, in **Fig. 4.2** the plateau averages are calculated from the traces between ca. 90 – 240 s, 250 – 390 s, and 400 – 500 s. Then, the absolute values of the plateau averages are calculated, and the mean of all absolute values is converted

from volts to Newtons by using the calibration of the gauges. Finally, stiction peaks may appear in the friction traces when the direction of the displacement is inverted. These sudden spikes in the friction force may arise from adhesion between the surfaces or the reorganization of the materials that compose them.

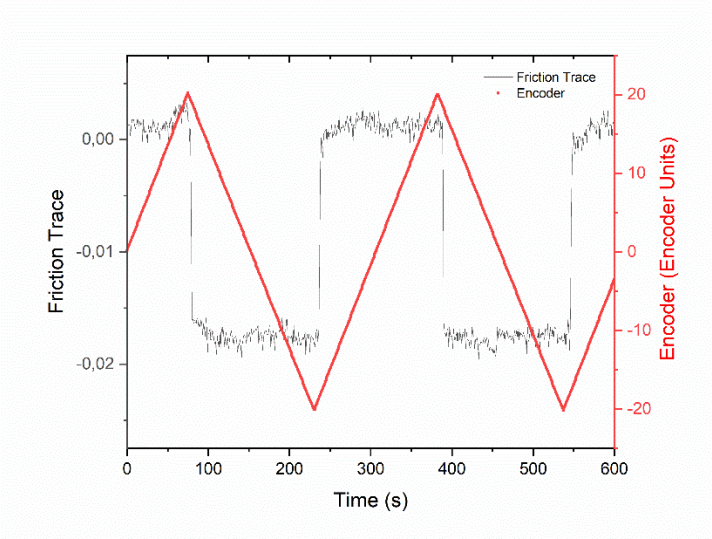

Figure 4.2. Friction traces (gray) and imposed displacement to the upper surface by the actuator (red), of covalently immobilized bare microgels in the presence of 0.1 mM Na_2SO_4 in neutral media at 23 °C, under a normal load of 23 mN and at a sliding velocity of 3 µm/s.

The friction force is positively correlated with the applied normal load on the surface. In other words, the friction force increases with the applied normal load. Such a graph was prepared for bare microgel layers sliding at a velocity of 3 µm/s in neutral aqueous media with 0.1 mM Na_2SO_4 at 23 °C (**Fig. 4.3**). Salt was added to enhance the screening of the electrostatic repulsion between the microgel-coated surfaces (the expected Debye length in the system is ca. 18 nm).[7] Several observations can be drawn from this graph. For applied normal loads between ca. 1 mN and 4 mN, a plateau in F_S vs. F_N can be observed. This phenomenon is attributed to uneven pressure

applied on the contact area between the microgel layers while sliding, which is discussed in detail later in this chapter.[2] The presence of a plateau in the F_S/F_N curve has been previously reported,[16] however, it is unusual and it disagrees with Amontons' law. On the contrary, the results herein suggest that a return to linearity is possible beyond the saturation in F_s. For applied loads between ca. 4 mN and 10 mN, F_S increases linearly with F_N according to Amontons' law.[17,18] In this regime, the slope provides the coefficient of friction which corresponds to $\mu = 0.31$ (**Fig. 4.3**). As comparison, the coefficient of friction of microgel particles in good solvent conditions can be roughly 10 times lower.[1,3] Indeed, the high water content of bare microgel particles as well as their non-negligible surface potential (ca. 12 mV) is expected to increase the osmotic pressure which decreases the mutual interpenetration between two polymer layers and helps to keep the sliding surfaces separated.[1,3,12,19,20] However, the first data point at which friction force was detected in **Fig. 4.3** took place at a separation distance (found in the static force mode) of ca. 106 nm. This separation distance is approximately halfway between the onset of interaction forces and the hardwall, which indicates that the microgel layers are in contact and in the compressed regime so that friction forces arise from boundary lubrication. Further, no friction force could be measured at normal applied loads lower than ca. 1 mN because of the low sensitivity of the strain gauges (123.7 N/V) in the friction device used for these experiments. In comparison, previous reports that utilize instrumentation with higher sensitivity are able to detect normal applied loads in the order of 10^{-2} mN.[16]

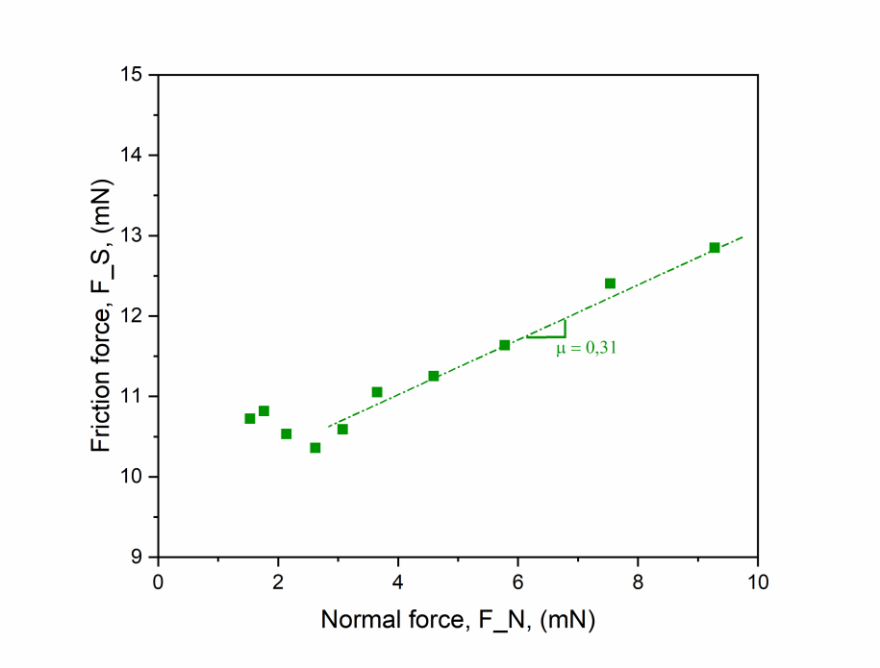

Figure 4.3. Friction force, F_S, measured between layers of bare microgels covalently attached on AUTES-GLA functionalized mica surfaces in the presence of 0.1 mM Na_2SO_4 in neutral media at 23 °C as a function of normal applied load and under a sliding velocity of the upper surface of 3 μm/s. Coefficient of friction corresponds to $\mu = F_S/F_N$. Dashed line is a guide for the eye.

Previous tribological studies involving cationic PNIPAM microgels performed with the SFA technique have reluctantly explored high applied loads due to the potential damage that may be imparted to the mica substrate.[16,21] Nevertheless, exploring the load-bearing capacity of these microgels is crucial to better understand the physical properties of this type of material as well as determining potential applications. At the risk of damaging the surfaces, normal loads ranging from 1 to 49 mN were applied to bare microgel surfaces in pH 10 aqueous solution at 23 °C and at a sliding speed of 3 μm/s and the quality of the contact was observed in real time by using Fringes of Equal Chromatic Order (FECO) interferometry. No damage to the surface was observed

at applied loads below 7 mN and small damage appeared exclusively on the edges of the contact area at ca. 9 – 10 mN as shown in **Fig. 4.4**. Fringes that show imperfections on the sides of the apex suggest that debris from sheared microgels begins to accumulate on the leading-edge during sliding and does not necessarily reflect permanent damage to the underlying mica surfaces. Further, as discussed in **Fig. 4.3**, for normal applied loads between 4 and 10 mN, the plateau in F_S vs. F_N is surpassed, thereupon a linear dependence is observed, and the coefficient of friction can be evaluated. Significant damage to the surface was recorded at the apex as well as on the edges of the contact area at normal applied loads of ca. 12 – 16 mN, indicating potential damage to the polymer layer as well as to the mica surfaces. Finally, at an applied load of ca. 49 mN, the quality of the optical fringes deteriorated significantly and the damage to both the polymer layers and the mica surfaces is clearly observed.

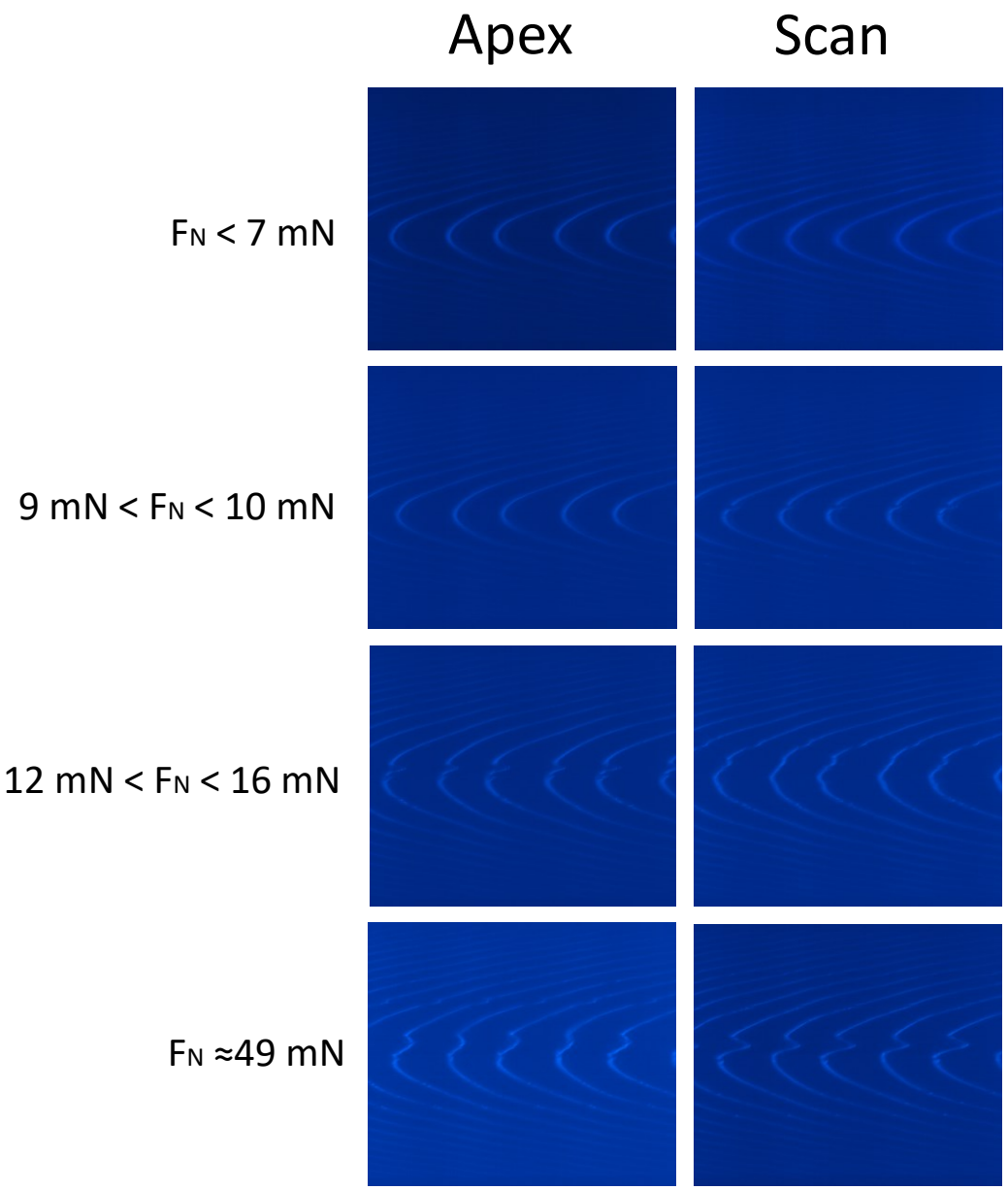

Figure 4.4. Fringes of equal chromatic order (FECO) obtained at the apex of the contact position and scanning to the sides of the apex of two similar bare microgel layers after sliding at a velocity of 3 μm/s for different applied loads. Deformations to the fringes correspond to microgels and/or surface deformations.

4.2.2 Effect of pH on the coefficient of friction of covalently attached bare microgels

Due to the presence of ionizable amine groups both on the surface of the microgels as well as throughout the polymer network, variations in the surface potential as well as the pH-induced swelling are expected to produce meaningful differences in the coefficient of friction. When microgels are in their swollen conformation, the diffusion of the free chains on the surface of the microgels is promoted by the favorable interactions between the polymer and the solvent which is expected to increase osmotic pressure and contribute to keeping the sliding surfaces separated and in the hydrodynamic lubrication regime. The purpose of changing the pH is to verify if at a given microgel conformation (i.e. swelling) at constant temperature, the friction behavior can be controlled by modulating the surface properties (i.e. surface potential). Nevertheless, the results presented in **Fig. 4.5** suggest that there is no significant change in the coefficients of friction of bare microgels immersed in water at pH 4 (μ = 0.52) and pH 10 (μ = 0.45) compared to that of bare microgels in neutral media (μ = 0.31) at 23 °C. The coefficient of friction of bare microgels in pH 4 media is higher than in neutral and basic media, which contradicts the expected trend, i.e., microgels in acid media exhibit a higher surface potential and a more important degree of swelling. For instance, the surface potential of bare microgels in pH 4 (11.8 ± 1.2 mV) is higher than in pH 10 (-0.2 ± 0.5 mV) and the pH-triggered swelling ratio of the microgel particles, pH-Q_{imm}, increased by 1.74 ± 0.24 between pH 10 and pH 4.[7] Previous studies have shown that pH-triggered swelling of core/shell microgels synthesized from polystyrene-poly(acrylic acid) showed a 4 to 10-fold increase in the coefficient of friction between pH 10 and pH 4 media.[1] Similarly, several tribological studies involving charged polymer brushes in different pH values revealed a

similar trend.[12,13,20] The higher coefficient of friction in acid media might be due to the overlap and entanglement of the pendant chains of bare microgel, which are likelier to be more extended when ionized in acid media compared to basic media. The change in elasticity of the polymer layer with pH was also studied to determine if it played a role in the friction forces.

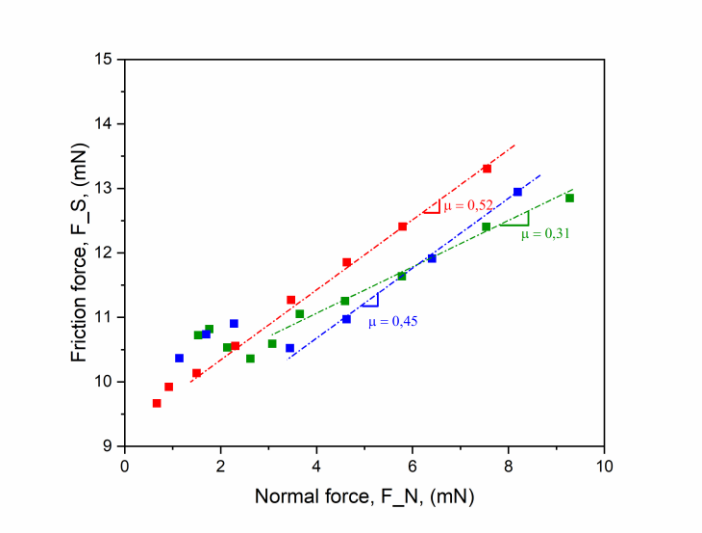

Figure 4.5. Friction forces, F_S, measured between layers of bare microgels covalently attached on AUTES-GLA functionalized mica surfaces in the presence of 0.1 mM Na_2SO_4 in neutral media (green), in water at pH 10 (blue) and in water at pH 4 (red) at 23 °C as a function of normal applied load and under a sliding velocity of the upper surface of 3 µm/s. Coefficients of friction correspond to $\mu = F_S/F_N$. Dashed lines are guides for the eye.

Increasing elasticity of polymer layers is associated with lower coefficients of friction between surfaces sliding past each other because it affects the energy dissipation during sliding.[3,22] To evaluate the role of elasticity in controlling friction, an arbitrary value of elasticity (E) was estimated from the slope of the force profiles (chapter 3) in the low load regime (<10 mN/m) by: $E = \Delta(F_N/R)/\Delta D$, where $\Delta(F_N/R)$ is the change in normal force obtained in the static mode,

F_N, normalized by the diameter of the silica disk, R, and ΔD is the variation in the separation distance. An increase in the pH-triggered swelling ratio of immobilized microgels, pH-Q_{imm}, is associated with a decrease in elasticity as can be observed in **Fig. 4.6A**. Although the coefficient of friction, μ, increases with elasticity, as expected, between pH 7 (μ = 0.31) and pH 10 (μ = 0.45), it increases with decreasing elasticity during the transition to pH 4 as illustrated in **Fig. 4.6B**. Indeed, friction results in pH 4 (μ = 0.52) are not in agreement with the trend towards lower coefficients of friction with higher degree of ionization, lower elasticity, particle swelling and higher water retention.[1,3] The lack of coherence in expected trends as well as the negligible variation in the coefficient of friction with changing physical and surface properties of the bare microgel layer indicate that the observed variations in the tribological properties are non-significant. As an example, an approximate increase in pH-Q_{imm} of 74 % between pH 10 and pH 4 (**Fig. 4.6**) is associated with a negligible variation in the coefficient of friction (**Fig. 4.5**). The lack of variation in μ with pH-Q_{imm} and pH-induced changes to the surface potential might arise from the fact that F_S is not significant before the microgels are largely confined, at separation distances below 110 nm, due to insufficient sensitivity of the strain gauges in the friction device. When the microgels are in the compressed regime, electrostatic repulsions do not have a meaningful contribution to the friction behavior.

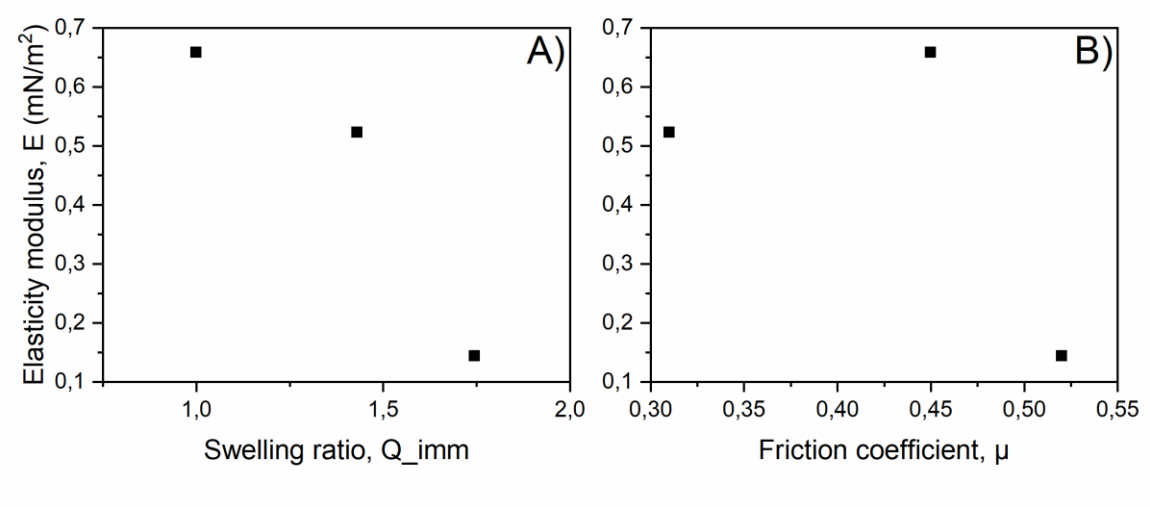

Figure 4.6. Effect of elasticity on the behavior of bare microgel layers in the presence of 0.1 mM Na_2SO_4 in neutral media at 23 °C and under a sliding velocity of the upper surface of 3 µm/s. A) Elastic modulus (E) as a function of the swelling ratio of immobilized microgels (pH-Q_{imm}) and B) coefficient of friction (µ) as a function of the elastic modulus between two identical opposing bare microgel layers.

4.2.3 Effect of functionalizing the microgel surface with PDMAEMA and PEG polymer chains

The tribological properties of surface-functionalized microgels, i.e. microgel-co-PDMAEMA and microgel-co-PEG, were studied to determine if the surface chemistry has an effect of the friction behavior. Specifically, surface potential measurements in suspension of microgel-co-PEG (chapter 3) revealed a negligible variation in zeta potentials between pH 2 and pH 10 media.[7] In addition, static force measurements of surface-immobilized microgel-co-PEG layers showed that the electrostatically induced swelling (1.02 ±0.04) is lower than that of bare microgel layers (1.74 ±0.24) between pH 10 and pH 4 media (chapter 3).[7] These observations suggest a finer-tuned

control of the surface properties of microgel-co-PEG which could potentially translate to a different tribological behavior than bare microgel layers.

The plateau in F_S/F_N that was observed for bare microgels for normal applied loads between ca. 1 and 4 mN (**Fig. 4.5**) is also present in microgel-co-PDMAEMA (< 4 mN) and microgel-co-PEG (<3 mN) layers (**Fig. 4.7A**). The emergence of the plateaus is independent of the pH of the medium and at friction forces similar in magnitude to that of bare microgel layers, as illustrated in **Fig. 4.7A**. The apparent saturation of F_S with F_N has been previously reported with the same type of bare microgels[16] as well as with core-shell microgels,[1] the latter particles offer a similar architecture to the surface-functionalized microgels presented in this work. However, this behavior is unusual as the general case is for F_S to increase with F_N. To better understand this behavior, the contact mechanics between microgel-coated surfaces was explored by visualizing the contact area in real-time through multiple beam interferometry.[16] Similarly, it is important to consider the multi-layered experimental set up used in SFA experiments (silica-glue-mica) and their respective deformation under applied normal loads. The deformation of the surface is expected to be determined by the epoxy glue used to bind the silica disk to the mica since the Young's modulus of the glue (7 GPa) is significantly lower than that of the silica disks (75 GPa) and of mica (170 GPa). At large separation distances (ca. 300 nm) and low normal applied loads, the microgels deform while the glue layer remains unaltered. On the contrary, at shorter separation distances the aspect of the contact region is increasingly deformed, with substantial deformation taking place far from the apex. In fact, it was observed that above a certain load, the point of closest approach barely changes with F_N.[16] The heterogeneity in the contact area and associated anisotropic applied pressure gives rise to the plateau observed in F_S. However, unlike the results

reported in previous work, here it was observed that F_S returns to a linear dependency with F_N at normal applied loads above ca. 5 mN for bare and surface-functionalized microgels independently of the pH of the media (**Fig. 4.7B**) and without imparting damage to the surface (**Fig. 4.4**), which makes it possible to calculate the coefficient of friction from their respective slopes.

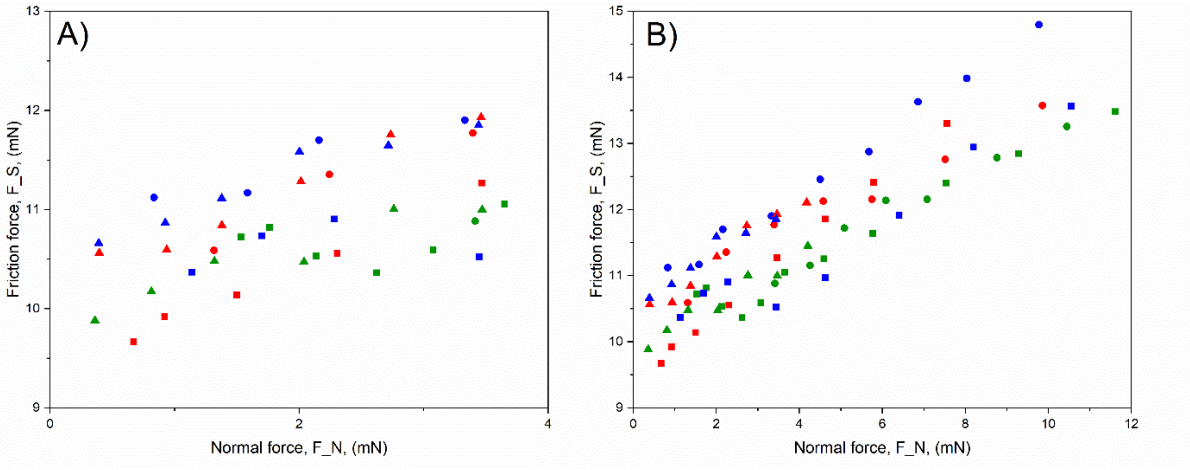

Figure 4.7. Friction forces, F_S, measured between layers of bare microgel (■), microgel-co-PDMA (●) and microgel-co-PEG (▲) covalently attached on AUTES-GLA functionalized mica surfaces in the presence of 0.1 mM Na_2SO_4 in neutral media (green), in water at pH 10 (blue) and in water at pH 4 (red) at 23 °C as a function of normal applied loads < 4 mN (A) and < 12 mN (B) and under a sliding velocity of the upper surface of 3 µm/s.

The coefficient of friction of surface-functionalized microgels was calculated from the slope of F_S/F_N curves in the linear regime. Microgel-co-PEG layers showed a linear dependency beyond the plateau in F_S/F_N at normal applied loads lower than microgel-co-PDMAEMA. Therefore, the maximum normal loads that were applied to microgel-co-PEG surfaces were also lower to prevent potential damage to these surfaces. The slope of the curves of microgel-co-PDMAEMA (**Fig. 4.8A**) and microgel-co-PEG (**Fig. 4.8B**) layers show that changes in pH do no produce meaningful

differences in the coefficient of friction and that the gap between the curves are similar to those observed for bare microgel layers as a function of pH (**Fig. 4.5**).

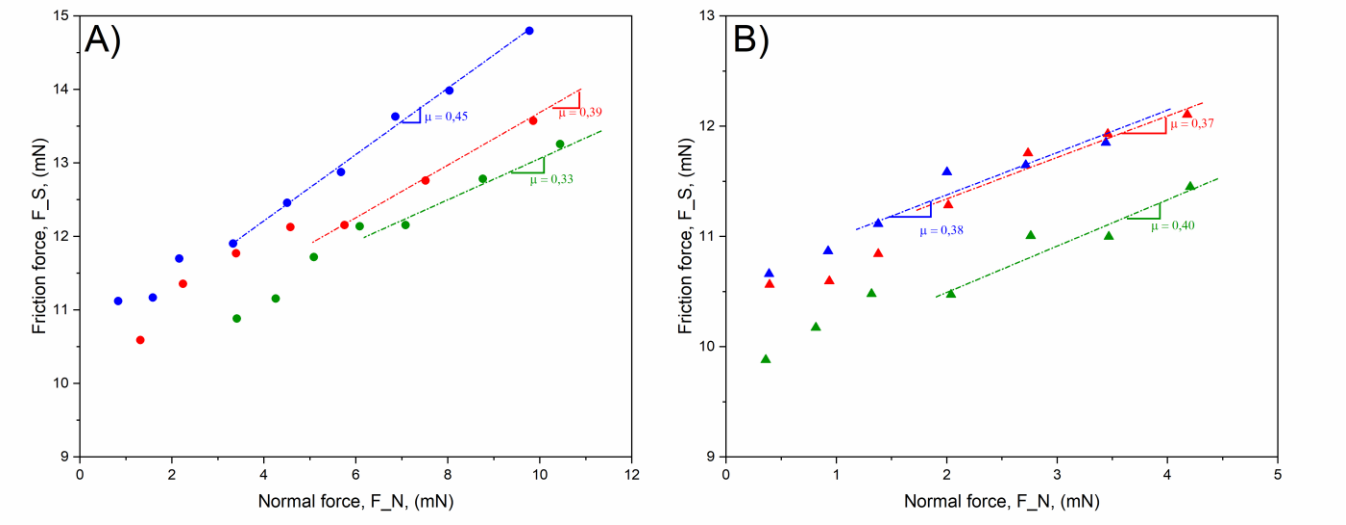

Figure 4.8. Friction forces, F_S, measured between layers of microgel-co-PDMA (A, ●) and microgel-co-PEG (B, ▲) covalently attached on AUTES-GLA functionalized mica surfaces in the presence of 0.1 mM Na_2SO_4 in neutral media (green), in water at pH 10 (blue) and in water at pH 4 (red) at 23 °C as a function of the normal applied load and under sliding velocity of the upper surface of 3 μm/s. Coefficients of friction correspond to $\mu = F_S/F_N$. Dashed lines are guides for the eye.

No clear trend is apparent in the coefficient of friction of either bare or surface-functionalized microgels with varying pH. To compare the relation between the coefficient of friction and the surface functionalization of microgels in different pH environments, the results are summarized in **Table 4.1**. For microgels bearing surface charges, i.e. bare microgel and microgel-co-PDMAEMA, the coefficient of friction increased slightly between pH 7 and 10. This behavior was

expected due to the decrease in particle swelling, decrease in the surface potential, and the increasing hydrophobicity caused by more favorable polymer-polymer interactions as opposed to polymer-solvent interactions. However, during the transition between pH 7 and 4 media, the coefficients of friction of bare microgel and microgel-co-PDMAEMA unexpectedly increased despite the previously reported swelling of the surface-immobilized microgels as well as increasing surface potentials.[7] This observation suggests that grafting PDMAEMA chains on the surface of bare microgels produces no measurable effect on the tribological behavior of the microgels. The relatively small variation in the coefficient of friction of microgel-co-PEG with pH could potentially suggest some degree of control of the tribological properties. However, the length of the PEG and PDMAEMA chains is insignificant compared to the hydrodynamic diameter of bare microgels and thus the chain lengths are likely insufficient to significantly alter the tribological properties of surface-functionalized microgels relative to bare microgels. In fact, the contour lengths of the PEG (ca. 22 nm)[23] and PDMAEMA (ca. 8 nm)[10] polymer chains are relatively small compared to the overall size of microgel-co-PEG and microgel-co-PDMAEMA particles, and represent roughly 9 % and 3 %, respectively, of the hydrodynamic diameters (chapter 3). The effect of the chain length is further diminished when the sliding happens in the compressed regime of the microgels. Because the friction forces were not measurable before the microgels are largely confined, the effect that the surface properties may have had in the tribological properties of surface-functionalized microgels is suppressed.

Table 4.1. Coefficients of friction of bare microgel, microgel-co-PDMAEMA and microgel-co-PEG at different pH at 23 °C.

	Bare microgel	Microgel-co-PDMAEMA	Microgel-co-PEG
pH 4	0.52	0.39	0.37
pH 7	0.31	0.33	0.40
pH 10	0.45	0.45	0.38

4.3 Tribological properties of covalently attached microgel layers in the mesoscale

The interest behind expanding the study of the friction behavior of microgel coated surfaces is to determine if a continuum in the friction forces exists between the nano- and meso-scales. Identifying such overlap could provide useful information such as load-bearing capacity and resistance to wear which could suggest potential applications for this type of material. For example, it is acknowledged that the elasticity of cell culture substrates plays a major role in cell adhesion, differentiation, and propagation.[24–26] Similarly, the study of the friction properties of PNIPAM polymer coatings may contribute to better understanding more complex systems, such as lubrication and wear mechanisms in synovial joints.[27–29] Friction experiments with the SFA revealed that the maximum normal applied force that could be generated was ca. 49 mN. At this pressure, significant damage to the microgel-coated layers and the mica substratum was observed (**Fig. 4.4**). Therefore, a different experimental set up is necessary to explore the friction behavior under normal applied loads greater than 49 mN and on a substrate more resistant than mica. Therefore, the results in this section were obtained in partnership with Dr. Sylvie Descartes whose laboratory is equipped with a custom-made tribometer, the tribo-brush, whose lower detection limit conveniently overlaps with the upper detection limit of the SFA and which can generated higher applied loads.[14,15] However, since the mica-bearing silica disks used in the SFA are not compatible with the tribo-brush, the methodology had to be modified to perform the experiments with microgel-coated silicon wafers sliding underneath a stationary, microgel-

coated, borosilicate lens as described in the methodology chapter. The sphere-on-a-plane spatial configuration in the tribo-brush is equivalent to the cross-cylinder configuration used in the SFA.

4.3.1 Topographical characterization of bare microgel and microgel-co-PEG covalently-immobilized on an ECHETES-functionalized silicon wafers and borosilicate lenses

To estimate the surface-covering of the microgels on the substrates, covalently attached microgels were analyzed using AFM. Chemically grafting polymers onto a surface depends on the properties of the substrate as well as the functional layer the polymer network forms bonds with.[30,31] The grafting densities of microgel and microgel-co-PEG on silicon wafers and borosilicate lenses functionalized with ECHETES are slightly higher to those on mica substrates functionalized with AUTES-GLA reported in chapter 3. All microgels formed dense and homogeneous coatings on both silicon wafers and on borosilicate lenses (**Fig. 4.9**). On borosilicate lenses, bare microgels showed a particle grafting density of 15.6 ± 1.2 particles/μm^2 while the density increased to 17.8 ± 1.4 particles/μm^2 for microgel-co-PEG (**Fig. 4.9A,B**). On silicon wafers, the particle grafting density was 16.6 ± 0.9 particles/μm^2 for bare microgels and 14.9 ± 1.5 particles/μm^2 for microgel-co-PEG (**Fig. 4.9C,D**). These results suggest that the difference in grafting densities between bare microgels and microgel-co-PEG are non-significant. In comparison, the particle grafting density on AUTES-GLA functionalized mica substrates reported in chapter 3 for bare microgels (22.5 ± 1.3 particles/μm^2) and microgel-co-PEG (24.0 ± 0.9 particles/μm^2) are slightly higher than on silicon wafers and borosilicate lenses. The relatively small increase in particle grafting density between ECHETES-functionalized silicon wafers and borosilicate lenses and AUTES-GLA mica substrates observed here is not expected to play a major role in the tribological behavior and therefore it is

possible to proceed with friction experiments using the tribo-brush and compare them to those obtained with the SFA.

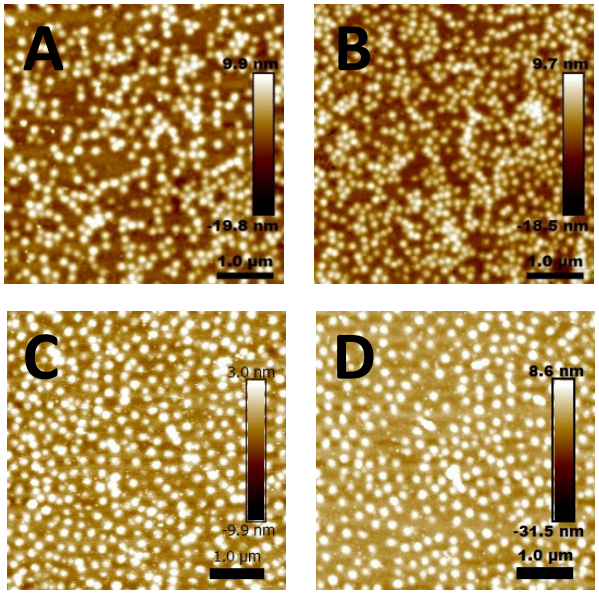

Figure 4.9. AFM images of bare microgels (A,C) and microgel-co-PEG (B,D) covalently attached to ECHETES functionalized borosilicate lenses (A,B) and silicon wafers (C,D) 24 hours after grafting in air at 25 °C and 30 % relative humidity. Peakforce tapping mode. Image scales 5 x 5 μm^2.

4.3.2 Effect of the sliding speed on covalently attached bare microgels

Sliding friction forces, F_S, between two similar microgel layers as a function of the normal applied load, F_N, were measured in the steady-state regime at sliding speeds ranging between 4 – 8 µm/s across milli-Q water at room temperature. Friction forces between two similar bare microgel layers showed that increasing the sliding speed did not significantly alter the measured friction force (**Fig. 4.10**). However, it appears that the shape of the friction traces became progressively deformed when the sliding speed increased from 4 to 6 µm/s (**Fig. 4.10B**) as well as from 6 to 8

μm/s (**Fig. 4.10C**). This is possibly due to the reconfiguration of the microgel coating during shear. Increasing the sliding speed did not have a significant impact on the coefficient of friction between bare microgel layers. The coefficient of friction decreased from 0.30 to 0.25 when the sliding speed increased between 4 and 6 μm/s (**Fig. 4.11A**). The increase in sliding speed is associated with a reconfiguration of the microgel layer which is evidenced by the more important standard deviation observed for normal applied loads of 0.3 N and 0.5 N at a sliding speed of 6 μm/s (**Fig. 4.11A**). However, when the sliding speed increased to 8 μm/s, the coefficient of friction does not decrease further (**Fig. 4.11A**), and the microgel-coated layer does not appear to experience additional reconfiguration because the standard deviation for normal applied loads between 0.2 – 0.5 N is lower than at 6 μm/s (**Fig. 4.11B**). In fact, Increasing the applied normal load showed a more significant impact on the magnitude of the measured friction forces than the sliding speed (**Fig. 4.11B**). These results suggest, as was observed in the nanoscale with the SFA, that the sliding speed does not have a major impact on the measured friction forces at 23 °C in the mesoscale.

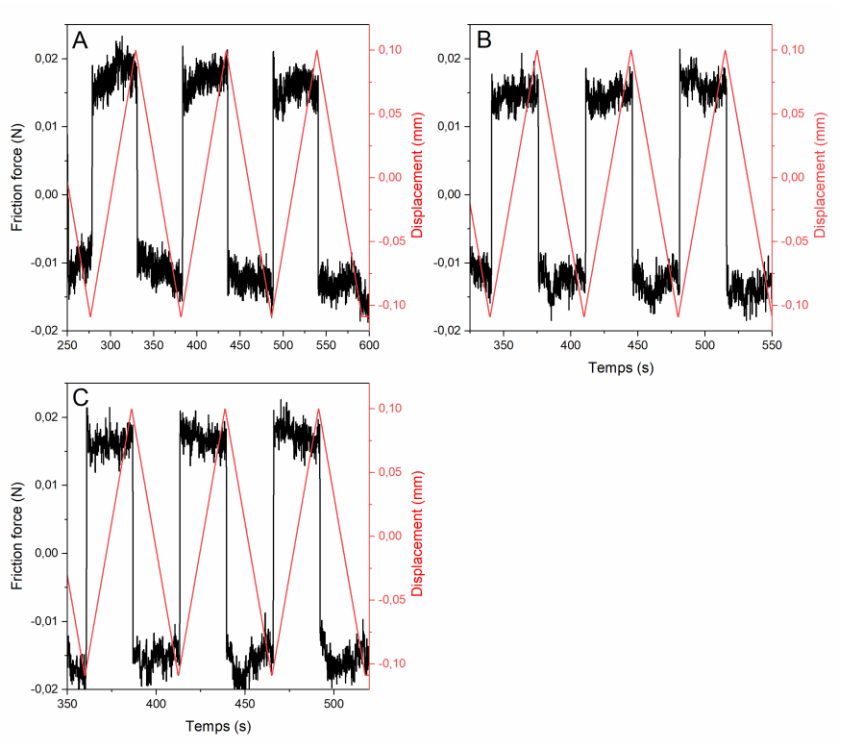

Figure 4.10. Friction forces, F_S, of two opposing layers of covalently-immobilized bare microgel at an applied normal load, F_N, of 0.05 N across milli-Q water and at a sliding speed of A) 4 µm/s, B) 6 µm/s and C) 8 µm/s.

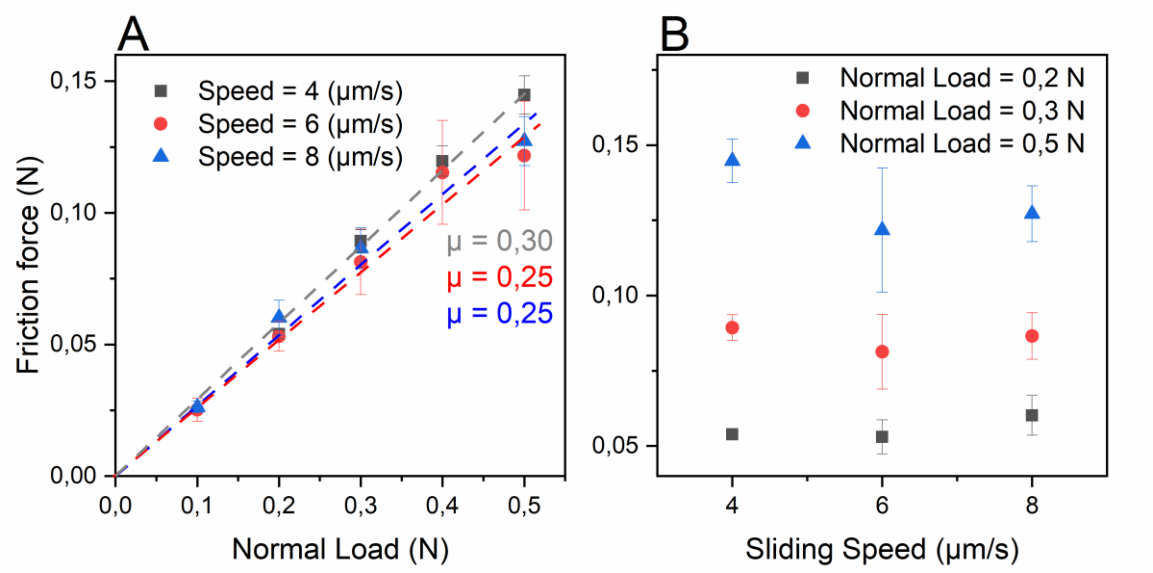

Figure 4.11. Variation in the friction force, F_S, with normal applied load at a sliding speed of 4 µm/s (grey), 6 µm/s (red) and 8 µm/s (blue) A) and with sliding speed at normal applied loads of 0.2 N (grey), 0.3 N (red) and 0.5 N (blue) B) of two opposing layers of covalently-immobilized bare microgel layers across milli-Q water at room temperature. Dashed lines are guides for the eye. Error bars correspond to the standard deviation of the friction force.

4.3.3 Effect of the normal applied load on covalently attached bare microgels and microgel-co-PEG

Friction forces for these microgel-coated surfaces were obtained at a sliding speed of 4 µm/s, which is the slowest speed available in the tribo-brush and the closest to the speed used in the SFA experiments (3 µm/s), allowing the comparison of the results between techniques in the nano- and meso-scales to be achieved. Typical friction traces between the bare microgel and microgel-co-PEG layers at a sliding speed of 4 µm/s are illustrated in **Fig. 4.12**. The friction traces of bare microgel and microgel-co-PEG layers exhibit smooth sliding friction forces up to 0.35 N for bare microgel (**Fig. 4.12A**) and 0.40 N for microgel-co-PEG (**Fig. 4.12C**). Beyond these normal

applied loads, stiction peaks appeared immediately prior to changes in the direction of the displacement (**Fig. 4.12B,D**). Stiction peaks may arise from some microgels being dragged during sliding at applied loads > 0.35 N. The evolution of the normal applied loads with time that was used to obtain the friction forces in **Fig. 4.12** are presented in **Fig. 4.13**. The normal applied loads are smooth and stable during sliding with bare microgel surfaces and exhibit a slight cyclical shape during sliding with microgel-co-PEG most likely due to a misalignment of the movable stage. Nevertheless, the alignment of the stage does not appear to impact the shape and periodicity of the friction traces of microgel-co-PEG, as can be observed over two independent experiments in **Fig. 4.14** for normal applied loads < 0.50 N.

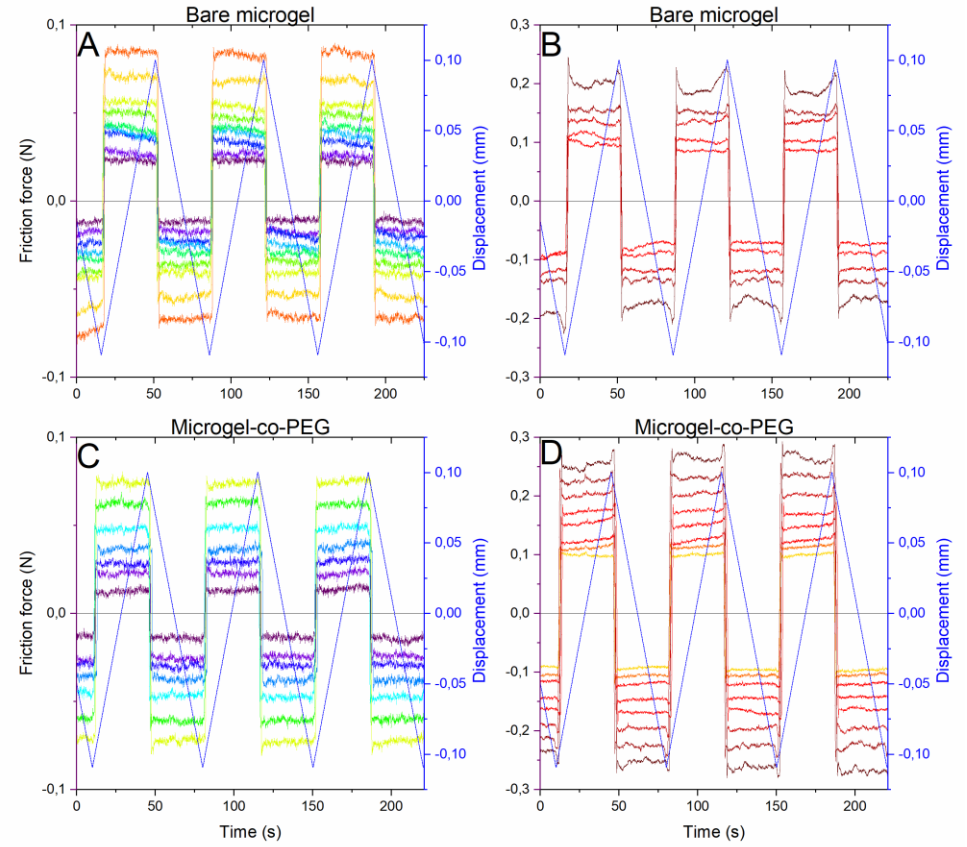

Figure 4.12. Friction force, F_S, and displacement traces of covalently attached bare microgel at low A) and high B) applied normal loads and microgel-co-PEG at low C) and high D) normal loads at room temperature and at a sliding speed of 4 µm/s across milli-Q water.

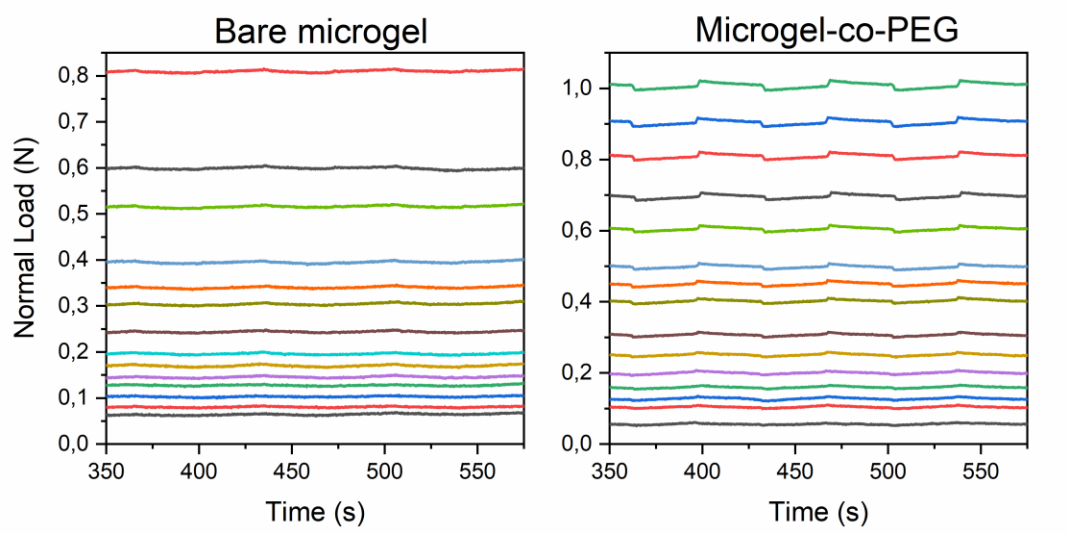

Figure 4.13. Variation in normal applied load, F_N, with time of covalently attached bare microgel and microgel-co-PEG used for friction measurements in **Fig. 4.12** at room temperature and at a sliding speed of 4 µm/s across milli-Q water.

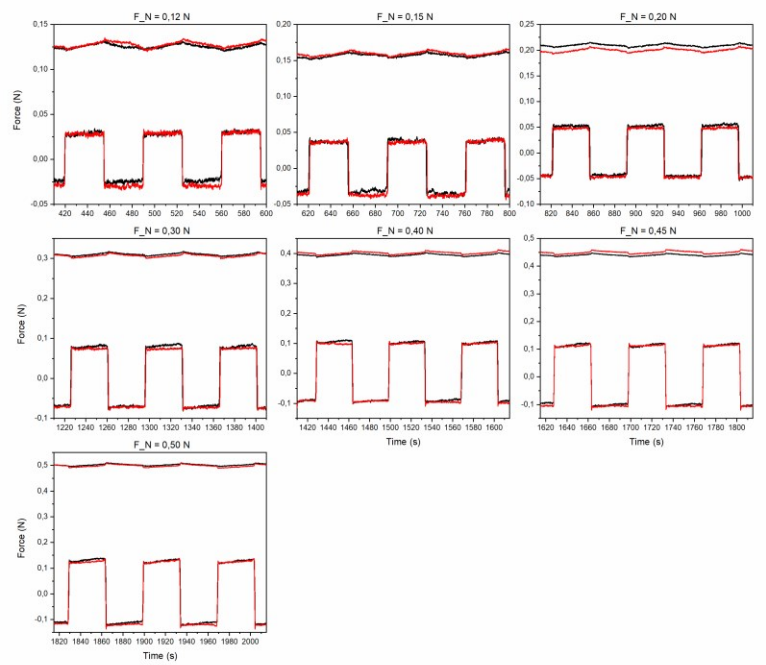

Figure 4.14. Friction forces, F_S, of two independent experiments with covalently attached microgel-co-PEG layers at room temperature and at sliding speed of 4 µm/s at seven progressively increasing normal applied loads across milli-Q water at room temperature.

To assess the cause of the stiction peaks, AFM and optical microscopy images of the microgel-co-PEG coated silicon wafers were obtained at the end of the experiment, i.e. following shearing under an applied load of 1.0 N. First, the wear track was highlighted as a continuous line on the silicon wafer surface by optical microscopy and the length was determined by comparing the wear track to the width of the AFM cantilever (provided by the manufacturer). The track length was ca. 213 µm, which corresponds to the displacement imposed on the movable stage which was set to 200 µm (**Fig. 4.15A**). AFM images of both extremities of the wear track confirmed that microgel debris accumulated at the ends of the track due to sliding. Further, the round contour at the extremities of the wear track corresponds to the shape of the microgel-coated borosilicate lens

(**Fig. 4.15B,C**). The centre of the wear track, shown in **Fig. 4.15D,E**, and which contains almost no microgels, was used to determine the width of the track which lies between 8 and 12 µm. For comparison, by using the Hertz equation for contact stress under the maximum normal applied load used in this study (1.0 N), the theoretical width of the friction trace corresponds to ca. 120 µm. The discrepancy between the hertzian and measured contact areas suggest that immobilizing microgel-co-PEG via covalent attachments improves the load bearing capacity and resistance to wear of the material. With both bare microgel and microgel-co-PEG coated surfaces, the friction behavior obtained with the tribo-brush follows Amonton's law and the small difference in the coefficients of friction of bare microgel (µ = 0.23) and microgel-co-PEG (µ = 0.25) suggests, as was observed in the nanoscale with the SFA, that the coefficient of friction does not depend on the surface properties of the immobilized microgel layers (**Fig. 4.16**).

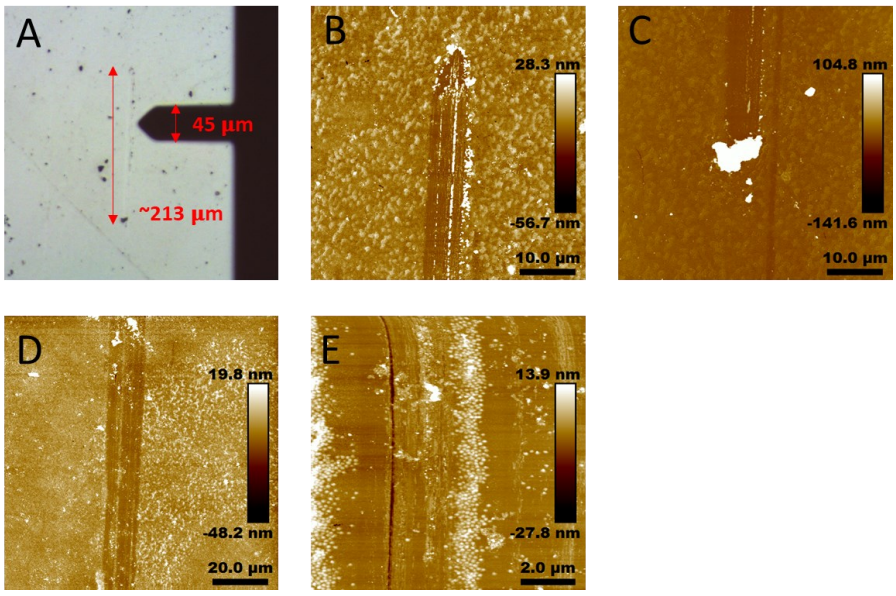

Figure 4.15. Microscopic characterization of the wear track on a silicon wafer surface with a covalently attached microgel-co-PEG layer following shear experiments at room temperature at a sliding speed of 4 um/s and under a maximum normal applied load of 1.0 N. A) optical

photograph of the wear track, B) top extremity of the wear track, C) bottom extremity of the wear track, D) centre of the wear track and E) amplification of the wear track in D). AFM images were obtained in the PeakForce tapping mode at room temperature and at 30 % relative humidity.

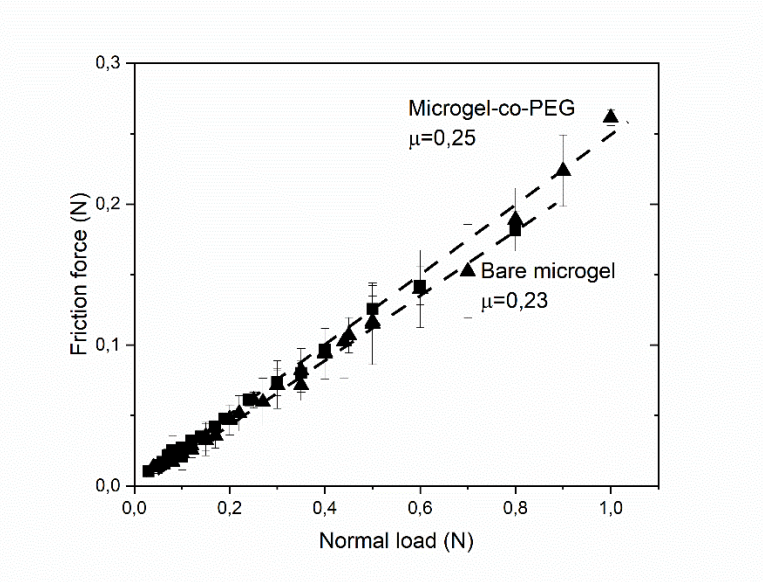

Figure 4.16. Friction force, F_S, as a function of the normal applied load, F_N, between two identical opposing layers of covalently attached bare microgel (■) and microgel-co-PEG (▲) at room temperature and at a sliding speed of 4 μm/s across milli-Q water. Dashed lines are guides for the eye. Error bars correspond to the standard deviation of the measured friction coefficients (n = 2).

4.3.4 Overlap of friction and normal forces of bare microgel layers on the nano and mesoscales

A continuum in the friction force (F_S) was identified across the overlap of normal forces (F_N) between tribological techniques, i.e., in the nanoscale (SFA) and the mesoscale (tribo-brush). A single friction experiment with bare microgel coated surfaces across pH 10 media at 23 °C was performed with the SFA and compared to a friction experiment with the tribo-brush at 25 °C

across milli-Q water (**Fig. 4.17**). The friction test with the SFA was done in pH 10 media for practical reasons: these were the conditions at the end of a set of friction experiments, therefore the maximum normal load possible with the double-cantilever spring of the SFA could be applied fully with the risk of damaging the surfaces. At normal applied loads < 3 mN, a plateau in the friction force with increasing normal applied load can be observed for bare microgels in the nanoscale (left inset, **Fig. 4.17**) as was also reported in **Fig. 4.5**. For normal applied loads between 5 and 50 mN a linear dependency of F_S with F_N can be observed for bare microgel layers in the nanoscale (right inset, **Fig. 4.17**) which obeys Amonton's law and from which the coefficient of friction, $\mu = 0.45$, can be calculated (**Table 4.1**). The friction behavior in the mesoscale, obtained with the tribo-brush, is linear within the range between 30 – 800 mN. A continuum of the measured friction was found between the lowest recorded normal applied load on the tribo-brush (30 mN) and the highest recorded normal applied load with the SFA, 50 mN (right inset, **Fig. 4.17**). According to the observations made of the contact through FECO interferometry, the integrity of the surface is maintained for normal applied loads < 16 mN and sharply deteriorates at normal applied loads of ca. 50 mN (**Fig. 4.4**). On the contrary, the friction traces between the bare microgels at the lowest recorded normal applied load with the tribo-brush, 30 mN (**Fig. 4.12A**), show no degradation in quality. In other words, the plateaus obtained in the steady-state sliding are smooth and no stiction peaks can be observed when the displacement changes direction. These observations suggest that a continuum exists in the detection of friction forces at the nano- and mesoscales which does not involve damage to the polymer surface or the underlying substrates.

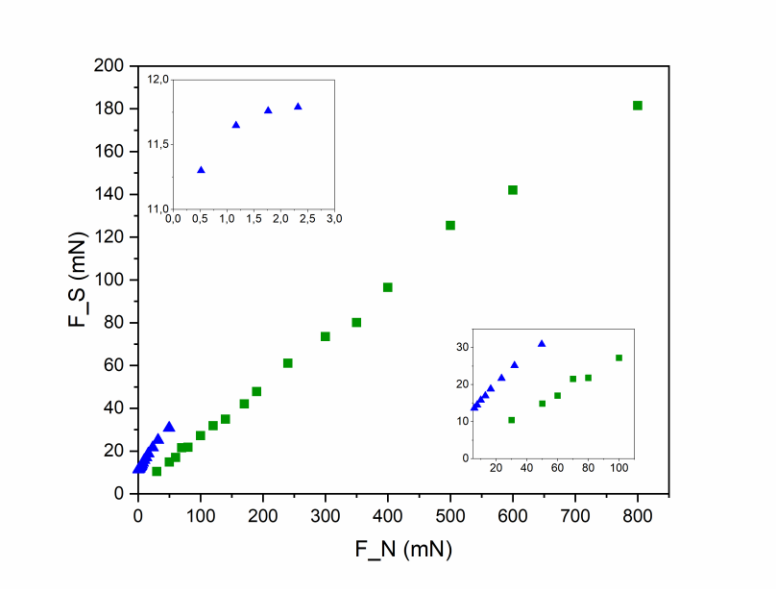

Figure 4.17. Overlap of the friction force, F_S, as a function of the normal force, F_N, between two identical opposing layers of covalently attached bare microgels on AUTES-GLA functionalized mica in the nanoscale (▲) and on ECHETES functionalized silicon wafer and borosilicate lens (■) in the mesoscale at pH 10 (blue) and in pH 7 (green) for sliding velocities of 3 and 4 µm/s, respectively. Insets depict amplifications of the friction behavior at denoted scales.

4.4 Challenges that limited the scope of the tribological properties of covalently attached microgels

Two technical challenges surrounding the experimental set up for tribological measurements in the nanoscale with the SFA severely impacted the scope of this study. First, the friction device used to measure the dynamic forces between sliding surfaces has its electronic components exposed to the environment and when the temperature is raised, the atmosphere inside of the SFA chamber becomes saturated with humidity which interferes with the circuits. Second, while attempting to overcome the challenges with humidity, one of the semiconductors making up the Wheatstone bridge of the friction device became damaged and resulted in a 16-fold loss in

sensitivity which prevented the detection of friction forces before the microgels were in the compressed regime.

4.4.1 Temperature-dependent tribological properties of microgel layers

It is acknowledged that the swelling and surface properties of PNIPAM-based microgels change with raising temperature as the microgel network transitions from highly swollen and hydrated to shrunken and rather hydrophobic across the VPTT.[32,33] Such a transformation is associated with more favorable NIPAM-NIPAM segment interactions above the VPTT, as opposed to more favorable NIPAM-solvent interactions below the VPTT. This behavior produces adhesion forces between two bare microgel layers separating in a step-wise fashion from the compressed microgel regime (chapter 3).[7] In fact, polymer adhesion is one of the main mechanisms through which the tribological properties of a polymer layer can be tuned through several stimuli such as temperature, pH or ionic strength.[4,5] For example, adhesion between PNIPAM-based cationic bare microgel layers above the VPTT depends on the pH and can be measured in pH 10 and 7 media, when the electrostatic repulsions are weaker due to a lower degree of ionization of the amine groups in the polymer network, but it is not detectable in pH 4 media due to higher surface potentials provided by the fully protonated surface amine groups.[7] Further, decoupling of the microgel swelling and associated transition to a rather hydrophobic network can be achieved by surface-functionalizing bare microgels with PEG chains (microgel-co-PEG).[7] These observations suggested that the tribological properties of bare and surface-functionalized microgels could potentially be regulated by modifying the conditions of the environment. The basis for this prediction are supported by previous work on the same type of microgels which demonstrated that when the temperature is raised above the VPTT, the friction force becomes closely

dependent on the sliding speed and a lift force tangential to the direction of shear arises due to elastohydrodynamic effects.[2] Similarly, the coefficients of friction of microgels synthesized from thermo-responsive *N,N*-diethylacrylamide increased 4-fold across the VPTT.[3]

Raising the temperature of the environment surrounding the surface-immobilized microgels created important interferences in the performance of the electronic components due to excess humidity and condensation. The microgel-bearing mica pieces, glued onto silica disks, are installed inside of a hermetically sealed chamber which provides a clean environment and precise control of the temperature and properties of the media surrounding the samples. A single drop of aqueous solution of defined ionic strength and pH is placed between the two opposing silica disks (**Fig. 4.1**), to maintain the microgels hydrated, and to provide a medium to regulate the ionization of the charged amino groups of the microgels through variations in pH. When the chamber was heated by means of two steel heating rods integrated into the bottom of the chamber, the atmosphere inside of the chamber became saturated with humidity originating from the water droplet between the silica disks and formed condensation beads on the interior surfaces. Humidity and condensation were not an issue when measuring normal forces in a heated environment because the upper disk support is made entirely of stainless steel and does not include any electronic components while the bottom disk support consists of a double cantilever force-measuring spring also made from stainless steel (**Fig. 4.1**). However, the circuitry of the friction device used to measure dynamic forces is exposed to the environment and is not protected by any isolation which makes it vulnerable to environmental humidity and condensation (**Fig. 4.18**). Excessive humidity on the circuits of the friction device was manifested through an overload of signal to the SFA amplifier which produced low quality friction traces. As

an example, a friction experiment of two mica surfaces in shear across a droplet of milli-Q water at 32 °C is shown in **Fig. 4.19**. Bare mica was chosen for this example because of its smooth surface, high surface energy leading to strong adhesion and ease of preparation. The friction output showed a considerable amount of noise in the signal, an almost imperceptible increase in the lateral force despite considerable increments in the normal applied loads, and absence of the square function before the highest applied normal load, at which point damage to the surface was observed (**Fig. 4.19**). Low quality friction data at high temperature is an important impediment to collecting useful and reliable results involving covalently-attached thermo-responsive microgels. A friction device with isolated circuitry that protects it from humidity is thus necessary before proceeding in this type of measurement. Unfortunately, coating the circuitry with an insulator implies a further decrease in the sensitivity of the whole device.

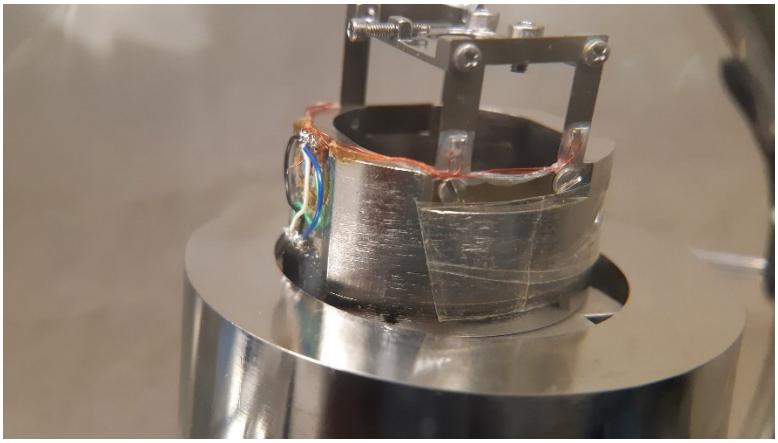

Figure 4.18. Photograph of the friction device with circuitry exposed to the environment used to collect friction forces in dynamic force experiments.

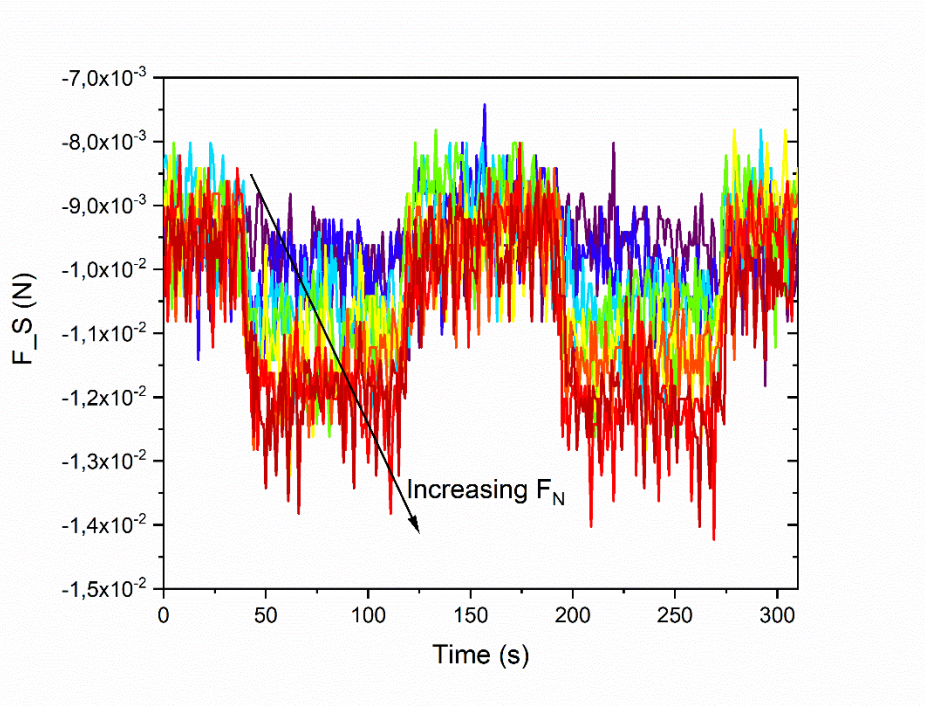

Figure 4.19. Evolution of friction forces, F_S, between two opposing mica surfaces with increasing normal applied load (colour of the traces in the direction of the arrow) at 32 °C and at a sliding speed of 3 µm/s across milli-Q water.

4.4.2 Damage to the friction device and resulting loss of instrumental sensitivity

During the friction experiments at high temperature one of the semiconductors in the friction device's Wheatstone bridge became damaged and an alternative circuit had to be fashioned. This solution, however, resulted in an important loss of sensitivity. Before the friction device was damaged, the sensitivity of the lateral force gauges was of 7.7 N/V which enabled the detection of lateral forces as low as 0.4 mN. Once the device was damaged and repaired, the sensitivity of the friction device decreased to 123.7 N/V which represents a 16-fold decrease in sensitivity. Such a loss proved to be detrimental to the study because friction forces could not be detected before a separation distance of ca. 106 nm, roughly halfway between the separation distance at the onset of the interaction forces and the hardwall (at 23 °C). At this separation distance, the microgels were largely compressed and the measured friction forces originated from osmotic

pressure at the boundary lubrication regime. Consequently, the effect of pH and of surface functionalization on the tribological properties of microgels could not be discerned because electrostically induced swelling and surface potential effects are detected in the hydrodynamic lubrication regime, when the microgel layers are barely in physical contact. The low instrumental sensitivity also explains the lack of effect that the pH and surface functionalization have on the coefficients of friction since no electrostatic or osmotic repulsion (the latter due to the presence of polymer chains) is expected when the microgels are in the compressed regime.

4.5 Conclusion

The tribological behavior of bare and surface-functionalized microgels immobilized on different substrates was determined using two different techniques, in the nanoscale with the SFA and in the mesoscale with the tribo-brush. With the SFA, the friction behavior was not affected by the nature of the surface-functionalization of the microgels or by variations in the surface potential of the polymer layers by adjusting the pH of the media at 23 °C. Similarly, no meaningful difference in the friction behavior of bare microgel and microgel-co-PEG layers was observed with the tribo-brush. However, it was possible to identify an overlap in the friction forces between the two scales. The objective to determine if the tribological properties of microgel-coated surfaces could be kept constant independently of the swelling degree of the polymer layer could not be accomplished. Significant improvements to the instrumentation coupled to the SFA, particularly involving the formation of condensation beads on the friction device at elevated temperatures, must be done prior to further investigation. The recommendation to future studies with microgel-coated surfaces in the mesoscale is to obtain AFM images of the friction trace after each increment in the normal applied load to precisely identify the wear resistance of the functional surfaces. Further, the inability to raise the temperature of the system above the VPTT of the microgels prevented the study of one the most promising characteristic of microgel-co-PEG vis-à-vis the bare microgel – keeping the polymer layer non-adhesive above the transition temperature.

4.6 References

(1) Giraud, L.; Bazin, G.; Giasson, S. Lubrication with Soft and Hard Two-Dimensional Colloidal Arrays. *Langmuir* **2017**, *33*, 3610–3623.

(2) Vialar, P.; Merzeau, P.; Giasson, S.; Drummond, C. Compliant Surfaces under Shear: Elastohydrodynamic Lift Force. *Langmuir* **2019**, *35*, 15605–15613.

(3) Banquy, X.; Charrault, E.; Giasson, S. Normal and Lateral Interactions between Thermosensitive Nanoparticle Monolayers in Water. *J. Phys. Chem. B* **2010**, *114* (30), 9721–9728.

(4) Friedrich, K. Polymer Composites for Tribological Applications. *Adv. Ind. Eng. Polym. Res.* **2018**, *1*, 3–39.

(5) Myshkin, N.; Kovalev, A. Adhesion and Surface Forces in Polymer Tribology - A Review. *Friction* **2018**, *6*, 143–155.

(6) Zheng, H. Adhesion and Friction Mechanisms of Polymer Surfaces and Thin Films. In *Polymer Adhesion, Friction and Lubrication*; John Wiley & Sons, Ltd, 2013; pp 391–442.

(7) Guerron, A.; Giasson, S. Multiresponsive Microgels: Towards an Independent Tuning of Swelling and Surface Properties. *Langmuir* **2021**, *37*, 11212–11221.

(8) Okubo, M.; Ahmad, H.; Suzuki, T. Synthesis of Temperature-Sensitive Micron-Sized Monodispersed Composite Polymer Particles and Its Applications as a Carrier for Biomolecules. *Colloid Polym. Sci.* **1998**, *276*, 470–475.

(9) Fournier, D.; Hoogenboom, R.; Thijs, H.; Paulus, R.; Schubert, U. Tunable PH- and Temperature-Sensitive Copolymer Libraries by Reversible Addition-Fragmentation Chain Transfer Copolymerization of Methacrylates. *Macromolecules* **2007**, *40*, 915–920.

(10) Nordgren, N.; Rutland, M. Tunable Nanolubrication between Dual-Responsive Polyionic Grafts. *Nano Lett.* **2009**, *9* (8), 2984–2990.

(11) Borozenko, O.; Machado, V.; Skene, W. G.; Giasson, S. Organophosphonic Acids as Viable Linkers for the Covalent Attachment of Polyelectrolyte Brushes on Silica and Mica Surfaces. *Polym. Chem.* **2014**, *5*, 5740–5750.

(12) Han, L.; Yin, J.; Wang, L.; Chia, K.-K.; Cohen, R.; Rubner, M.; Ortiz, C.; Boyce, M. Tunable Stimulus-Responsive Friction Mechanisms of Polyelectrolyte Films and Tube Forests. *Soft Matter* **2012**, *8*, 8642–8650.

(13) Liu, X.; Thormann, E.; Dedinaite, A.; Rutland, M.; Visnevskij, C.; Makuska, R.; Claesson, P. Low Friction and High Load Bearing Capacity Layers Formed by Cationic-Block-Non-Ionic Bottle-Brush Copolymers in Aqueous Media. *Soft Matter* **2013**, *9*, 5361–5371.

(14) Popa, M.; Peditto, F.; Sfarghiu, A.-M.; Berthier, Y.; Descartes, S. A Tribological Approach to Understand the Behavior of Oral-Care Silica during Tooth Brushing. *Biotribology* **2016**, *6*, 1–11.

(15) Trunfio-Sfarghiu, A. M.; Berthier, Y.; Meurisse, M.-H.; Rieu, J.-P. Multiscale Analysis of the Tribological Role of the Molecular Assemblies of Synovial Fluid. Case of a Healthy Joint and Implants. *Tribol. Int.* **2007**, *40*, 1500–1515.

(16) Vialar, P.; Merzeau, P.; Barthel, E.; Giasson, S.; Drummond, C. Interaction between Compliant Surfaces: How Soft Surfaces Can Reduce Friction. *Langmuir* **2019**, *35*, 15723–15728.

(17) Berman, A.; Drummond, C.; Israelachvili, J. Amontons' Law at the Molecular Level. *Tribol.*

Lett. **1998**, *4*, 95–101.
(18) Gao, J.; Luedtke, W. D.; Gourdon, D.; Ruths, M.; Israelachvili, J.; Landman, U. Frictional Forces and Amontons' Law: From the Molecular to the Macroscopic Scale. *J. Phys. Chem. B* **2004**, *108*, 3410–3425.
(19) Banquy, X.; Zhu, X. X.; Giasson, S. Mechanical and Frictional Properties of Nanoparticle Monolayers Grafted on Functionalized Mica Substrates. *J. Phys. Chem. B* **2008**, *112*, 12208–12216.
(20) Raviv, U.; Giasson, S.; Kampf, N.; Gohy, J.-F.; Jérôme, R.; Klein, J. Lubrication by Charged Polymers. *Nature* **2003**, *11* (425), 163–165.
(21) Vialar, P. Propriétés Mécaniques et Nanotribologiques de Monocouches Auto-Assemblées de Microgels de Poly(NIPAM) Cationique En Milieux Aqueux, Université de Bordeaux, 2018.
(22) Tambe, N.; Bhushan, B. Nanoscale Friction and Wear Maps. *Philos. Trans. R. Soc. A* **2007**, *366* (1869), 1405–1424.
(23) Devanand, K.; Selser, J. C. Asymptotic Behavior and Long-Range Interactions in Aqueous Solutions of Poly(Ethylene Oxide). *Macromolecules* **1991**, *24*, 5943–5947.
(24) Khademhosseini, A.; Langer, R. A Decade of Progress in Tissue Engineering. *Nat. Protoc.* **2016**, *11*, 1775–1781.
(25) Engler, A.; Sen, S.; Sweeney, L.; Discher, D. Matrix Elasticity Directs Stem Cell Lineage Specifications. *Cell* **2006**, *126*, 677–689.
(26) Swift, J.; Ivanovska, I.; Buxboim, A.; Harada, T.; Dingal, D.; Pinter, J.; Pajerowski, D.; Spinler, K.; Shin, J.-W.; Tewari, M.; Rehfeldt, F.; Speicher, D.; Discher, D. Nuclear Lamin-A Scales with Tissue Stiffness and Enhances Matrix-Directed Differentiation. *Science (80-.).* **2013**, *341*, 975–990.
(27) Wang, C.-S.; Xie, R.; Liu, S.; Giasson, S. Tribological Behavior of Surface-Immobilized Novel Biomimicking Multihierarchical Polymers: The Role of Structure and Surface Attachment. *Langmuir* **2019**, *35*, 15592–15604.
(28) Xia, W.; Adibnia, V.; Huang, R.; Murschel, F.; Faivre, J.; Xie, G.; Olszewski, M.; De Crescenzo, G.; Qi, W.; He, Z.; Matyjaszewski, K.; Banquy, X. Biomimetic Bottlebrush Polymer Coatings for Fabrication of Ultralow Fouling Surfaces. *Angew. Chem.* **2018**, *131*, 1308–1314.
(29) Banquy, X.; Burdynska, J.; Lee, D.-W.; Matyjaszewski, K.; Israelachvili, J. Bioinspired Bottle-Brush Polymer Exhibits Low Friction and Amontons-like Behavior. *J. Am. Chem. Soc.* **2014**, *136* (17), 6199–6202.
(30) Nedela, O.; Slepicka, P.; Svorcik, V. Surface Modification of Polymer Substrates for Biomedical Applications. *Materials (Basel).* **2017**, *10*, 1115–1137.
(31) Minko, S. Grafting on Solid Surfaces: "Grafting to" and "Grafting from" Methods. In *Polymer Surfaces and Interfaces*; Stamm, M., Ed.; Springer: Berlin, Heidelberg, 2008; pp 215–234.
(32) Leon-Lopez, T.; Ortega-Vinuesa, J.; Bastos-Gonzalez, D.; Elaissari, A. Cationic and Anionic Poly-(N-Isopropylacrylamide) Based Submicron Gel Particles: Electrokinetic Properties and Colloidal Stability. *J. Phys. Chem. B* **2006**, *110*, 4629–4636.
(33) Pelton, R. Poly(N-Isopropylacrylamide) (PNIPAM) Is Never Hydrophobic. *J. Colloid Interface Sci.* **2010**, *348*, 673–674.

Chapter 5 – Selectively triggered cell detachment from PNIPAM microgel functionalized substrates

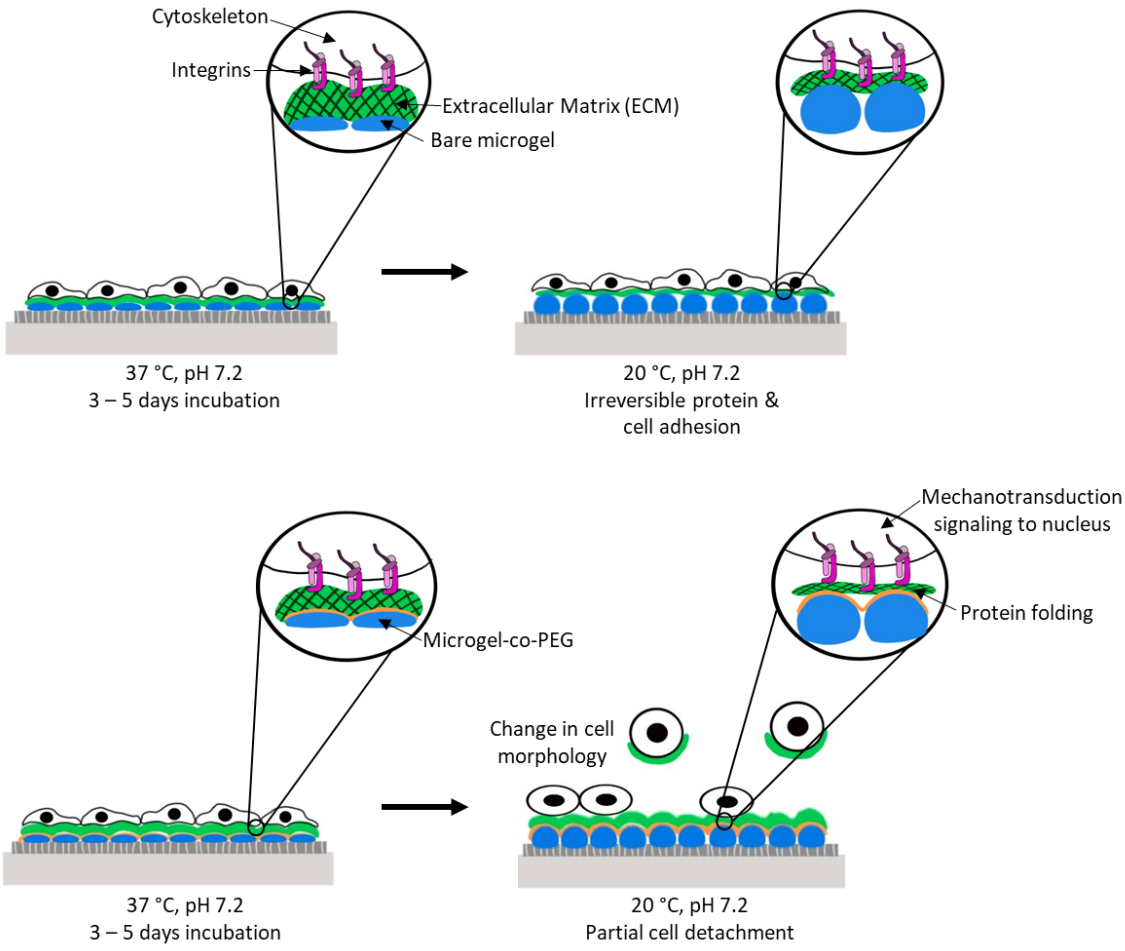

5.1 General Introduction to Chapter 5

PNIPAM-based substrates are widely applicable in the biomedical field. Indeed, because of the sharp coil-to-globule transition that PNIPAM undergoes across the LCST, conveniently situated close the physiological temperature, it has been used in a variety of drug delivery systems, to improve lubrication in artificial joints, as well as in biosensor platforms.[1–7] The change in the swelling degree that PNIPAM experiences with temperature is also closely associated to a drastic change in its surface properties; namely, surfaces coated with PNIPAM experience a transition from a highly hydrated and hydrophilic state to rather hydrophobic which has important repercussion on the surface wettability.[8–10] This characteristic behavior has been shown to effectively mediate cellular adhesion on a substrate and to provide a useful mean to detach cells from culture dishes without having to rely on enzymatic digestion or mechanical scrapping which can be harmful to cellular integrity and function.[11–13] Despite the clear advantages that PNIPAM-based substrates offer to cellular culture methodology, the broad variability in surface fabrication techniques, culture protocols and studied cell lines make it challenging to obtain comparative results. For instance, cell culture substrates functionalized with PNIPAM microgels have either succeeded,[14–16] or failed,[17,18] to produce a temperature-triggered cell detachment upon reducing the temperature.

The guiding hypothesis for this section of the thesis is that by using a hierarchical polymer structure, it is possible to promote the initial cell-substrate adhesion while favoring a temperature-triggered cell detachment. Underlying the hypothesis is the observation that microgel-co-PEG surfaces exhibit a superior hydrophilic character vis-à-vis bare PNIPAM microgels, which may positively contribute to cellular detachment.

In this chapter, we showed that microgel-co-PEG has the best ability to detach cancer cell lines when the temperature was reduced below the VPTT of the PNIPAM microgel. First, glass coverslips were functionalized with bare and surface-functionalized microgels according to the methodology described in chapter 3. The initial cellular attachment of the endothelial cell line bEnd.3 after 24 hours of incubation on bare and surface-functionalized surfaces was then verified by using two techniques: fluorescence microscopy to visualize and count cells stained with a fluorescent marker, and by counting with a haemocytometer after enzymatically detaching the cells from the substrate using trypsin-EDTA. The thermo- and pH-triggered cell detachment was evaluated with the same analytical techniques and by using bEnd.3 cells as well as with the cancerous cell lines MCF7 and U138. The superior ability of microgel-co-PEG to detach cells was attributed to its enhanced hydrophilicity which promotes protein and cellular detachment. To verify this assertion, the ability of microgel-co-PEG to prevent non-specific protein adsorption was assessed with surface plasmon resonance. The novelty of this work is that it normalizes experimental conditions to isolate the effect that the substrate may have on the cell detachment ability.

This study is the subject of a publication submitted to the Elsevier Publishing, Colloids and Surfaces B: Biointerfaces, and titled: *Selectively triggered cell detachment from PNIPAM microgel functionalized substrates*. Microgel synthesis, functionalization, and surface preparation was done in the laboratory of Pr. Suzanne Giasson while the cell culture as well as attachment/detachment experiments were done in the laboratories of the Medicament Formulation and Analysis Axis (AFAM) at the Faculty of Pharmacy of the University of Montreal. The majority of the experimental work was done by Alberto Guerron, with the exception of the

surface plasmon resonance experiments that were done by Huu Trong Phan. Carolina Peñaloza-Arias trained Alberto Guerron in cell culture techniques. All data processing and writing was done by Alberto Guerron, with the advice of Pr. Davide Brambilla, Pr. Valérie Gaëlle Roullin and Pr. Suzanne Giasson.

5.2 Abstract

Hypothesis

Stimuli-triggered cell attachment/detachment from responsive cationic poly(*N*-isopropylacrylamide) microgel-coated surfaces is influenced by electrostatic interactions, wettability, and the swelling of the polymer layer. Grafting non-responsive polymer chains to the microgel surface allows swelling and surface properties of the coating to be independently modulated. Such multi-responsive coatings promote initial cell adhesion and allow a stimuli-triggered cell detachment.

Experiments

Dual thermo- and pH-responsive cationic poly(*N*-isopropylacrylamide) microgels were surface-functionalized with polyethylene glycol (PEG) or poly-2-dimethylaminoethylmethacrylate (PDMAEMA) and covalently immobilized on glass coverslips to determine their stimuli-triggered cell detachment ability towards cultured bEnd.3, MCF7 and U138 cell lineages.

Findings

Microgels whose surface was functionalized with PEG chains presented cell adhesion and proliferation rates comparable to controls, while providing the best thermo-triggered detachment performance with MCF7 and U138 cells. This behavior was associated with a preserved hydrophilic character of the microgel surface regardless of the temperature and pH. Swelling behavior of all microgels tuned by pH gave rise to significant cellular detachment only for U138 cells. However, bEnd.3 cell detachment could not be triggered neither by temperature nor pH, regardless of the microgel surface coating.

5.3 Introduction

Cell culture is a fundamental technique in health sciences and biomedicine which intersects diverse fields such as cell biology, tissue engineering and regenerative medicine.[19] Cells are grown under controlled conditions and often need to be detached from their growth substrate to permit their passage or further testing. For several decades, the standard procedure to achieve this goal involved unspecific enzymatic digestion of binding proteins at the cell-substrate interface which are part of the extracellular membrane (ECM), using for instance trypsin-EDTA, or crude mechanical scrapping.[20,21] These methods, however, are known to be potentially harmful to cellular integrity and may compromise signaling pathways, adhesion, proliferation as well as cell survival.[22–24] For instance, cells detached by enzymatic treatment have shown to lose surface proteins in the ECM, such as collagens or glycoproteins like fibronectin, laminin and vitronectin, which increases the risk of inflammation and graft rejection when transplanted.[25–27] Further, the degradation of cell-cell junctions caused by trypsin-EDTA treatment prevents the harvesting of continuous tissue layers which limits tissue transplantation[28] or their collection following three-dimensional tissue printing.[29–32] To overcome these important challenges, stimuli-responsive polymer coatings have shown to be good alternatives for controlling cell detachment and beneficial for cell and tissue harvesting.[33,34]

Temperature- and pH-responsive polymer coatings are among the most widely used functional surfaces for cell culture.[35] pH-responsive substrates, such as chitosan-based polymer layers, can promote cellular detachment via pH variations which induce changes in the ionization degree of chitosan and therefore changes in the swelling and hydrophilicity of the polymer layer.[36,37] However, degradation of pH-sensitive polymer layers through changes in pH, such as those

occurring with poly (amino ester)-functionalized surfaces, may result in a non-controlled break down of the anchoring between cells and substrates.[38,39] Thermo-responsive surfaces based on poly(*N*-isopropylacrylamide) (PNIPAM) are extensively studied due to their sharp volume phase transition temperature (VPTT) around a lower critical solution temperature (LCST) of ca. 32 °C.[1,2] The temperature-triggered changes in the swelling and hydrophilicity of PNIPAM can be used to mediate protein and cellular adhesion. Indeed, conformational changes in PNIPAM-based substrates, when transitioning from a compact and rather hydrophobic state at physiological temperature (above the VPTT) to a highly hydrated structure (below VPTT), were shown to promote cellular detachment.[40] The thermo-triggered cell detachment ability of PNIPAM functionalized surfaces,[13] including PNIPAM brushes,[41] microgels[14,17] and hydrogels[42] have been exploited to develop responsive surfaces to recover various cell lines.[14,43–46] Diverse techniques have been used to fabricate PNIPAM-based substrates such as surface-initiated atom transfer radical polymerization[47] or electron beam polymerization[48] ("grafting-from" approaches) or by immobilizing PNIPAM gels ("grafting-to" approaches) via electrostatic interactions.[14,17] The main rationale for using PNIPAM-based surfaces for cell culture is generally based on the assumption that the polymer layer undergoes a hydrophilic – hydrophobic transition across the LCST, often justified by contact angle measurements.[10,40,49–55] Yet, contact angle measurements on PNIPAM report angles below 90° above the LCST[56] with a water content at 40 °C as high as 60 wt%.[57] High water content above the transition temperature is not the hallmark of a hydrophobic material and has prompted observations that PNIPAM is never truly hydrophobic.[8] Moreover, some studies report the absence of cell detachment triggered by temperature on PNIPAM substrates

suggesting that hydrophilic – hydrophobic transition is not solely responsible for controlling detachment. [17,18]

Herein, we present cell culture on dual thermo- and pH-responsive PNIPAM microgels, whose swelling behavior and surface properties can be independently tuned promoting cellular adhesion while maintaining stimuli-responsive detachment abilities. Unlike previous reported studies, experimental conditions were normalized for a more reliable comparison between different surfaces to better assess the role of wettability and surface charge on tuning the cell adhesion and detachment. The microgels are based on cationic thermosensitive poly(*N*-isopropylacrylamide) surface-functionalized with responsive or non-responsive polymers. Initial cellular adhesion was investigated with bEnd.3 cells, as this murine cell line, like most strongly adherent endothelial cell lines, is subjected to irreversible membrane damages during enzymatic cell detachment.[58] Further, thermo- and pH-triggered detachment ability was complemented with two widely-used cancerous cell lines, i.e. MCF7 and U138, to explore the impact of cell nature on the tunable detachment efficiency.

5.4 Materials and Methods

Milli-Q quality water was obtained from a Millipore Gradient A10 purification system (resistance 18.2 MΩcm, TOC $<$ 3 ppb). Square cover glass 22 mm in length No. 48366-067 was purchased from VWR (West Chester, PA, USA). Circular cover glass 15 mm in diameter No. 12-545-83 was obtained from Fisher Scientific (Saint Laurent, QC, Canada). 6-well plates Cellstar were purchased from Greiner Bio-One (Kremsmünster, Austria) and 24-well plates Costar from Corning Incorporated (Corning, NY, USA). *N*-isopropylacrylamide (NIPAM), 2-aminoethylmethacrylate

hydrochloride (AEMH), 2,2'-azobis-(2-methylpropylacrylamide) (V50), triethanolamine (TEA), *N*-hydroxysuccinimidyl (NHS), *N*-(3-dimethylaminopropyl)-*N*'-ethylcarbodiimide (EDC), glutaraldehyde (GLA), sodium cyanoborohydride ($NaBH_3CN$), dimethylsulfoxide (DMSO), Bovine Serum Albumin (BSA), 16-Mercaptohexadecanoic acid (16-MHA), 3-Mercaptopropionic acid (3-MPA), and Whatman 1 filter paper were purchased from Sigma-Aldrich (St. Louis, MO, USA). 11-aminoundecyltriethoxysilane (AUTES) was purchased from Gelest Inc. (Morrisville, PA, USA). *N,N'*-methylene-*bis*-acrylamide (MBA) were obtained from EMD Chemicals Inc. (Gibbstown, NJ, USA). Hydrochloric acid, sulphuric acid and hydrogen peroxide were purchased from Anachemia (Lachine, QC, Canada). Dimethylformamide (DMF) was obtained from ACP (Montreal, QC, Canada). Carboxy-terminated Poly(*N,N*-dimethylaminoethylmethacrylate) (PDMAEMA-COOH) 4800 g/mol, PI = 1.14 was purchased from Polymer Source (Dorval, QC, Canada). Methoxy polyethylene glycol succinimidyl carboxymethyl ester (PEG-NHS), 10000 g/mol, PI = 1.05, was obtained from JenKem (Plano, TX, USA). HyClone Dulbecco's Modified Eagle Medium (DMEM) with high glucose, L-Glutamine and Phosphate-Buffered Saline (PBS) were purchased from Cytiva (Mississauga, ON, Canada). Fetal Bovine Serum (FBS), trypsin-EDTA (trypsin) and penicillin-streptomycin were obtained from Gibco (Waltham, MA, USA). bEnd.3 cells (CLR-2299, passages 17 to 21), MCF7 cells (HTB-22, passages 2 to 5) and U138 cells (HTB-16, passages 125 to 129) were purchased from ATCC. Trypan blue solution was obtained from Wisent Inc. (St-Bruno, QC, Canada). Hoechst 33342 staining solution was purchased from Cayman Chemicals (Ann Arbor, MI, USA). Dialysis cellulose membranes were obtained from Spectrum Laboratories Inc. (Rancho Dominguez, CA, USA). Anhydrous and 95% ethanol were purchased from Commercial Alcohols

(Bramtpton, ON, Canada). All chemical products were used as received without further purification.

5.4.1 Microgel Synthesis

Synthesis of PNIPAM microgels was carried out according to a well established protocol described previously.[1] Briefly, NIPAM (7.10 mmol) was combined inside a three-necked round-bottomed flask with MBA (0.18 mmol) and AEMH (0.10 mmol). The reagents in the three-necked flask were diluted with 40 mL of milli-Q water, the flask was connected to a condenser and heated gently to 80 °C while degassing with a stream of nitrogen gas. V50 (0.06 mmol) was diluted separately in 10 mL of milli-Q water, heated gently to 80 °C and degassed with nitrogen gas. After thorough dilution and heating, the V50 solution was added to the three-necked flask and the reaction was monitored for 4 hours. Following polymerization, the resulting colloidal suspension was cooled down before filtering with a Whatman 1 filter paper. Then, it was transferred into a 6 – 8 kDa MWCO cellulose membrane and dialyzed against distilled water (ratio 1:100 v:v) for 72 hours, changing water every 12 hours. The microgel concentration in the resulting suspension (1 % w/v) was calculated by measuring the weight difference before and after drying. Microgel suspensions were stored at 7 °C prior to further use.

5.4.2 Surface functionalization of microgels

Microgels whose surfaces were functionalized with PDMAEMA (microgel-co-PDMA) were prepared from a 15 mL aqueous solution of 0.5 mM of PDMAEMA-COOH with 10 mM of NHS and 10 mM of EDC and stirred for 10 minutes at 7 °C inside a glass bottle covered in aluminium foil to block light out. After proper diluting and cooling, the microgel suspension was added to that solution to obtain a 0.1 % (w/v) microgel concentration. The suspension was left to react

overnight at 7 °C with constant stirring and protected from external light. Microgels with surfaces functionalized with PEG (microgel-co-PEG) were prepared from a 15 mL aqueous solution of 0.5 mM PEG-NHS with 100 mM TEA. The microgel suspension was added to the polymer solution to obtain a 0.1 % (w/v) microgel concentration and left to react overnight with constant stirring at room temperature. All functionalized samples were purified by dialysis following the coupling reaction using 25 kDa MWCO cellulose membranes against distilled water (ratio 1:100 v:v) for 72 hours, while changing water every 12 hours.

5.4.3 Microgel immobilization on gold and glass substrates

Microgels were immobilized onto functionalized gold and glass through amide coupling between amino groups in the microgel network and carboxyl groups of a functional layer coating the substrates as described hereafter.

For the preparation of gold substrates used in SPR experiments, dove BK7 prisms of 20 x 12 x 3 mm were sonicated in ethanol for 10 minutes and dried under nitrogen. Clean surfaces were then treated with piranha solution (H_2SO_4:H_2O_2 = 70:30 v:v) for 45 minutes at room temperature and thoroughly rinsed with anhydrous ethanol. Activated surfaces were then immediately coated with 1 nm Cr and 45 nm Au using a Cressington 308R sputter contact (Ted Pella Inc. Redding, CA). The SPR sensors were then immersed overnight in a solution consisting of 8:2, 16-MHA : 3-MPA, 1 mM in DMF to form a self assembled monolayer (SAM). Samples were then rinsed with ethanol and dried with a stream of nitrogen. Carboxyl groups in the SAM were activated with coupling agents (EDC 350 mM, NHS 110 mM) for 5 minutes. Activated surfaces were briefly rinsed with milli-Q water and immersed in an aqueous 0.1 % w/v microgel suspension and incubated in the

dark for 3 hours at room temperature. After microgel immobilization, sensor surfaces were rinsed with milli-Q water for 5 minutes.

Square and circular microscope glass cover slides were sonicated in ethanol for 10 minutes and dried under nitrogen before activating in a piranha solution (H_2SO_4:H_2O_2 = 70:30 v:v) for 45 minutes at room temperature. After activation, the surfaces were rinsed with ethanol and dried under nitrogen and were used immediately for surface functionalization with aminoalkylsilane AUTES.

Aminoalkylsilane monolayers were grafted to activated glass via self-adsorption from solution. A solution of 1 mM AUTES was prepared in anhydrous ethanol and stirred for 10 minutes. The freshly activated glass surfaces were immersed in the AUTES solution for 20 minutes. The resulting amino-functionalized surfaces were thoroughly rinsed with anhydrous ethanol. AUTES grafting was completed by annealing the surfaces for 1 hour at 120 °C under atmospheric pressure. Then, the surfaces bearing AUTES monolayers were immersed in a 0.1 % (w/w) aqueous solution of glutaraldehyde for 30 minutes, allowing the coupling reaction between the AUTES amine group and the glutaraldehyde carbonyl function to occur in the presence of $NaBH_3CN$.[59,60] After the coupling reaction, substrates were thoroughly rinsed with milli-Q water prior to microgel immobilization. Microgels were immobilized on glutaraldehyde-functionalized substrates via covalent bonds between the microgel amine groups and the surface glutaraldehyde carbonyl functions. A 0.1 % (w/v) aqueous suspension of bare or functionalized microgels was prepared and heated gently to 37 °C in a water bath. Glutaraldehyde-functionalized substrates were then immersed in the microgel suspension and kept in solution for 1 hour. Then, the

substrates were thoroughly rinsed with milli-Q water and dried under nitrogen. Microscope glass slides used as controls were sonicated in ethanol and dried under nitrogen prior to use.

5.4.4 Topographical characterization by Atomic Force Microscopy

Atomic Force Microscopy (AFM) imaging was done using a Multimode microscope equipped with a Nanoscope V extend controller (Digital Instruments, Santa Barbara, CA). The imaging was performed in dry air (30 % relative humidity) at 25 °C and 24 hours after the surface preparation. The PeakForce tapping-mode was employed using an ACTA silicon probe from APP Nano with a resonance frequency of 200 – 400 kHz. AFM images were treated and analyzed using Nanoscope Analysis software (version 1.4). The surface density of immobilized microgels was determined using Particle Analysis mode of the Nanoscope Analysis software.

5.4.5 Cell culture

bEnd.3 (ATCC CRL-2299, passages 17 to 21), MCF7 (ATCC HBT-22, passages 2 to 5) and U-138 (ATCC HBT-16, passages 125 to 129) cell lines were cultivated in DMEM containing 10% FBS, 1% penicillin/streptomycin and 2 mM L-glutamine at 37 °C and 5% CO_2 according to previously established culture protocols.[14,17,61] Initial cell attachment experiments were performed 24 hours after seeding in 6-well plates of 34.8 mm well diameter and on 22-mm square glass slides. Cell detachment experiments were conducted 3 and 5 days after seeding using 24-well plates of 16 mm well diameter and on circular microscope glass slides of 15-mm diameter.

5.4.6 Initial cellular attachment

The efficiency of the initial attachment of cells on the substrates was verified with the bEnd.3 cell line 24 hours after seeding. Bare and functionalized glass slides were sterilized by immersion in

70% ethanol for 10 minutes and kept inside a sterile biological hood for drying. About 52 $\times 10^4$ cells were seeded on glass, microgel-functionalized glass or the PDMS flat-bottom of the well plates, in duplicate, and left in the incubator for 1 hour. Thereafter, 3 mL of medium were added and plates were incubated for an additional 24 hours. After this time, the medium in each well was replaced with 3 mL of warm medium containing 1 $\mu g \times mL^{-1}$ Hoechst 33342 staining solution and plates were left in the incubator for 15 minutes. Plates were then immediately imaged by fluorescence microscopy (Zeiss Axio Observer equipped with a Zeiss LD Plan-Neofluar 20x 0.4 Ph 2 Korr lens) and the cells captured on the images (n = 4 per substrate) were automatically counted using ImageJ software equipped with an automatic nuclei counter plugin (ITCN). Afterwards, each well was rinsed twice using warm PBS. The glass microscope slides, with and without microgel-functionalization, were carefully transferred to individual polystyrene petri dishes (35 x 10 mm, Falcon) and 3 mL of trypsin were added to completely submerge the glass substrates in the cell-detaching solution. Three mL of trypsin were also added to the wells containing cells seeded directly on the bottom of the wells. Plates and petri dishes were then kept in the incubator for 5 minutes before transferring the cell suspensions to individual Eppendorf tubes for centrifugation (125 g for 5 minutes) and careful resuspension in 1 mL of warm medium. 50 µL aliquots of each cell suspension were diluted with the same volume of trypan blue staining solution and cells were counted, in triplicate, using a Neubauer haemocytometer (Hausser Scientific) and a Leica CME optical microscope.

5.4.7 Stimuli-triggered cellular detachment

The ability of microgel-functionalized surfaces to provide stimuli-triggered cellular detachment was verified using bEnd.3, MCF7 and U138 cell lines 3 and 5 days after seeding. Bare and

functionalized glass slides were sterilized by immersion in 70% ethanol for 10 minutes and kept inside a sterile biological hood for drying. About 16,000 cells were seeded on glass, microgel-functionalized glass and the PDMS flat-bottom of the well plates, in triplicate, and left in the incubator for 1 hour before adding 1 mL of DMEM medium (pH = 7.2) and incubated for the desired time while replacing the medium by a fresh one every 48 hours. After the prescribed time had elapsed, the medium in each well was replaced with 1 mL of warm medium containing 1 $\mu g \times mL^{-1}$ Hoechst 33342 staining solution and plates were left in the incubator for 15 minutes. They were immediately imaged by using fluorescence microscopy. Afterwards, one set of wells, including the bare PDMS ones and those containing bare glass and microgel-functionalized glass substrates, was rinsed twice with warm PBS and treated with 1 mL of warm trypsin cell-detaching solution. Each cell suspension was transferred to individual Eppendorf tubes for centrifugation (125 g for 5 minutes) followed by careful resuspension in 1 mL of fresh medium. 50 µL aliquots of each suspension were diluted in the same volume of trypan blue staining solution and the cells were counted, in triplicate, using a Neubauer haemocytometer. Meanwhile, the remaining two sets of wells were rinsed twice with warm PBS; 1 mL of test medium at 20 °C (pH = 7.2) was added to one set and 1 mL of medium at 20 °C and pH 5 was added to the second set. Both sets of wells were left to stand at 20 °C. After, the media were replaced with similar ones but containing 1 $\mu g \times mL^{-1}$ Hoechst 33342 staining solution. The wells were left to stand for an additional 15 minutes before imaging by using fluorescence microscopy. After imaging, each well was rinsed with warm PBS twice before treating with 1 mL of warm trypsin. All cell suspensions were collected in individual Eppendorf tubes for centrifugation (125 g for 5 minutes) and resuspension in 1 mL of

fresh medium. 50 µL aliquots of each suspension were diluted in the same volume of trypan blue staining solution and cells counted using a Neubauer haemocytometer.

5.4.8 Non-specific protein adsorption on microgel-functionalized surfaces

Non-specific protein adsorption on surfaces bearing immobilized bare microgel and microgel-co-PEG was assessed by using Surface Plasmon Resonance (SPR).

Adsorption of BSA and FBS on surfaces bearing immobilized bare microgels and microgel-co-PEG was measured with a portable 4-channel SPR instrument based on a dove prism design previously reported[62] at different temperatures (25, 32 and 40 °C). The microgel-functionalized SPR sensors were mounted in the SPR system placed in a room equipped with a temperature controller. The temperature of the system was allowed to stabilize for 3 hours. A baseline signal was established by injecting PBS buffer (137 mM NaCl, 2.7 mM KCl, 2 mM KH_2PO_4, and 10 mM Na_2HPO_4, pH 7.4) through the sensor until the output signal was stable. Protein solution (BSA or FBS, 1 $mg \times mL^{-1}$ in PBS buffer) was injected for 10 min, then the channel was rinsed with PBS buffer to remove unbound protein molecules. The protein adsorption was reported as λ_{SPR} shift. Data were acquired in real-time with the P4SPR control software. In all cases, the solution was injected using a 1-mL syringe and reacted in the PDMS fluidic cell under static flow conditions.

5.4.9 Statistical Analysis

Data were collected in triplicate and significant difference was determined by performing a two-way analysis of variance (ANOVA) followed by Tukey tests to compare experimental conditions using GraphPad Prism 7 software.

5.5 Results and Discussion

5.5.1 Initial cellular adhesion is similar on all microgel-functionalized substrates.

Initial cellular adhesion (observed after 24 hours of incubation) took place on all surface-immobilized microgels to a similar extent relative to the controls (**Fig. 5.1 – 5.2**). Initial cellular-substrate adhesion is known to occur within the first hours of contact between cells and substrates.[63,64] This initial adhesion is mediated by complex physicochemical interactions including hydrophobic, coulombic, and van der Waals forces.[65,66] Cells adhere and grow more easily on hydrophobic surfaces than on hydrophilic ones, due to the difficulty to displace adsorbed water molecules on hydrophilic surfaces.[67,68] Accordingly, it has been widely reported that PNIPAM-functionalized surfaces, exhibiting a hydrophobic character under physiological conditions (which correspond to temperature above the VPTT), readily support the adhesion and growth of a variety of cell lineages to a comparable extent than typical hydrophobic cell-culture surfaces such as polystyrene or polydimethylsiloxane (PDMS).[17,35,40,61,66] Fluorescence and atomic force microscopy images included in **Fig. 5.1** show dense and homogeneous microgel coatings on glass as well as the ability of bEnd.3 cells to adhere and proliferate on them. The unperturbed thickness of a single layer of bare and surface-functionalized microgels in neutral medium at 23 °C was determined by using the Surface Forces Apparatus (SFA) technique in our previous work and was found to be of approximately 25 – 30 nm above the VPTT (43 °C) and of 57 – 80 nm below the VPTT (23 °C).[69] Previous studies have suggested that the required thickness of a PNIPAM layer enabling efficient cell attachment and proliferation ranges between 20 – 45 nm[65,70] which agrees

well with results observed in **Fig. 5.1**. No change in the microgel grafting density and particle morphology was observed for neither bare nor surface-functionalized microgels before and after sterilisation by immersion in 70% ethanol for 5 minutes and subsequently dried in air as shown in **Fig. 5.SM1** in the Supporting Material section. This indicates that the covalent attachment of the microgels on the glass substrates guarantees a robust coating unlike the electrostatic interactions previously reported.[15–17] In addition, we previously showed that these surface-immobilized microgels are robust and stable in harsh pH environments (2 < pH < 10) and at elevated temperature (43 °C) during 24 hours.[69]

The initial cellular attachment of bEnd.3 cells on microgel-functionalized surfaces was quantitatively assessed by either fluorescence microscopy (**Fig. 5.2A**) or by counting them with a haemocytometer after enzymatic detachment using trypsin (**Fig. 5.2B**). The initial surface cell density measured on all microgel-functionalized substrates, PDMS and bare glass controls was not significantly different. This strongly suggests that the initial cell attachment was mediated by a combination of electrostatic and hydrophobic attractions. Above the VPTT, electrostatic attractions are possible between the positively charged microgels[69] and the negatively charged cells and hydrophobic attractions might arise between cells and the relatively hydrophobic bare microgel and microgel-co-PDMA layers above the VPTT (microgel-co-PEG layers were found to remain hydrophilic above the VPTT).[69]

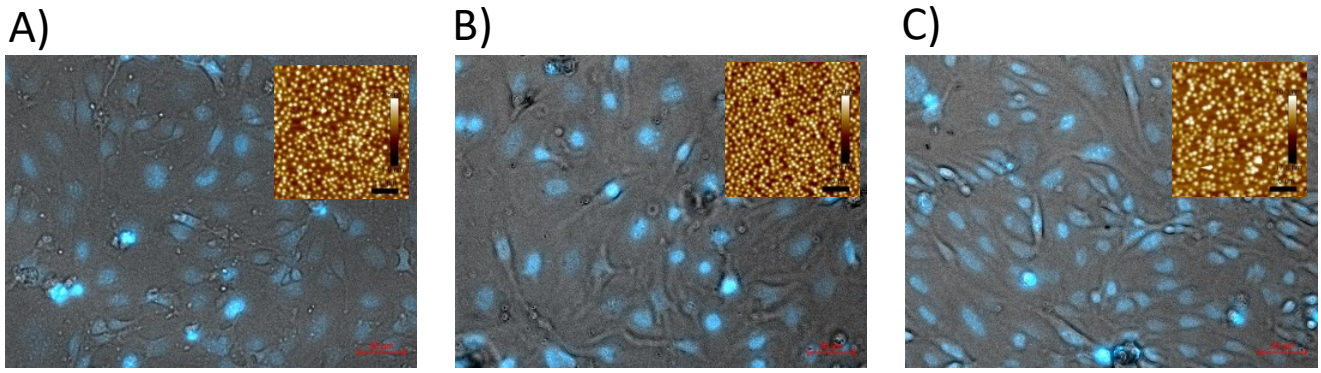

Figure 5.1. Merged fluorescence microscopy images (ca. 1.5 X 105 μm^2) of bEnd.3 cells grown on glass substrates functionalized with A) bare microgels, B) microgels-co-PDMA and C) microgels-co-PEG obtained after a 5-day incubation following seeding. Cell nuclei were stained with Hoechst 33342. Insets show AFM images (25 μm^2) of the corresponding microgel-functionalized substrates obtained in the PeakForce tapping mode following sterilization by immersion in 70% ethanol for 5 minutes and air dried for 40 minutes. AFM imaging was performed in air at 25 °C and 30% relative humidity.

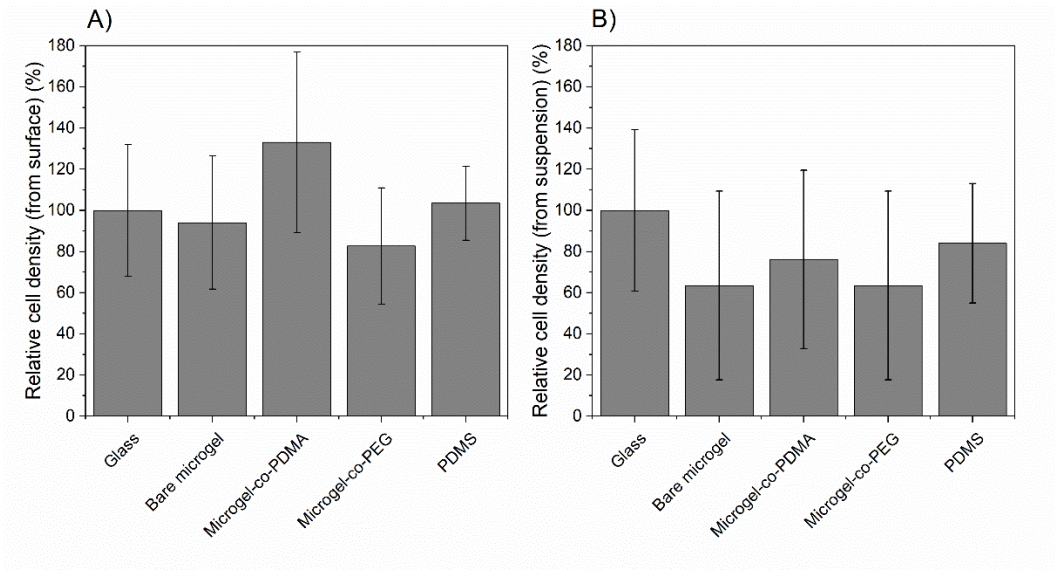

Figure 5.2. bEnd.3 relative cell density on microgel-functionalized substrates at 37 °C, compared to glass as a control, after a 24-hour incubation following cellular seeding and

calculated A) by fluorescence microscopy from surface-immobilized cells and B) from trypsin-detached suspensions using a haemocytometer chamber. Mean ± SD (n=3).

5.5.2 Substrate nature may temporarily alter cell proliferation kinetics for endothelial but not for cancer cell lines.

As previously mentioned, temperature-responsive PNIPAM coatings have been successfully exploited to induce cell detachment for a wide range of cell lineages.[14,43–46] Similarly, pH-responsive polymer coatings can be used to trigger cellular detachment from substrates.[36–39,71] However, comparing the efficiency of stimuli-responsive substrates to trigger cell detachment remains challenging due to the wide variety of polymer conformations (brushes, hydrogels, microgels), cell lineages and incubation protocols found in the literature. [14,42,56,72,73] For instance, it has been reported that PNIPAM microgels can either enable[14–16] or prevent[17,18] temperature-triggered cell detachment. To address these issues, experimental protocols in this work were normalized in order to provide comparative results.

The ability of cells to proliferate on bare and surface-functionalized microgel substrates under standard culture conditions (at 37 °C in neutral culture media) was investigated after 3 and 5 days of incubation by fluorescence microscopy and by counting trypsin-detached cells with a haemocytometer. All cell lines (U138, MCF7 and bEnd.3 cells) proliferated successfully on bare and surface-functionalized microgel-coated surfaces to a similar extent than the controls (**Fig. 5.3**, red bars). Unlike initial adhesion (**Fig. 5.2**), which is regulated by passive adhesion mechanisms and characterized by the initial cell-substrate contact and early cell spreading, these assays provide insight into the active cell adhesion mechanisms, which involve cell metabolism,

flattening (late spreading) and crawling.[74–76] After three days of incubation, no significant difference in the relative surface cell density (compared to cells grown on glass) was observed for MCF7 and U138 cells seeded on bare and surface-functionalized microgel substrates (**Fig. 5.3**, first and second rows). However, the surface density of bEnd.3 cells grown on bare microgels was significantly less than that on glass (ca. 40%) (**Fig. 5.3**, third row) while the initial (or passive) adhesion was similar to that of the controls (**Fig. 5.2**). On the contrary, bEnd.3 cells grown on microgels-co-PDMA and microgels-co-PEG showed no significant difference in proliferation compared to those grown on bare microgel and glass after 3 days of incubation (**Fig. 5.3**, third row). These observations suggested that electrostatic attractions between the negatively-charged cell membrane and the positively-charged bare microgel-coated substrate were beneficial for passive adhesion. However, the higher degree of hydrophobicity and surface charge of bare microgels, compared to that of surface-functionalized microgels, may have resulted in non-specific protein adsorption disfavoring cell proliferation. Indeed, the presence of proteins in the culture medium, able to partially adhere to the microgel-coated substrate through hydrophobic or electrostatic interactions, could slow down the formation of integrin bonding and subsequent focal adhesion during phases II and III of cellular proliferation.[35,77] On the contrary, MCF7 and U138 cells did not display a lower relative cell density after 3 days of incubation on bare microgel substrates despite a similar non-specific protein adhesion (**Fig. 5.3**, 1st and 2nd rows). This is most likely due to the characteristics of cancerous cell lineages able to spread and metastasize to distant sites through a process known as epithelial-mesenchymal transition (EMT). In this process E-cadherin proteins mediate the dissociation of adherens junctions, leading to the mesenchymal migratory phenotype which allows them to invade other tissues.[78–82] Nonetheless,

the possible steric impediment caused by non-specific protein adsorption on the bare microgel substrate diminishing bEnd.3 cell proliferation after 3 days of incubation appeared to be surmounted with time, as on day 5 of incubation, the surface density of bEnd.3 cells on bare microgels was statistically similar to that of the glass controls (**Fig. 5.3** and **5.4**).

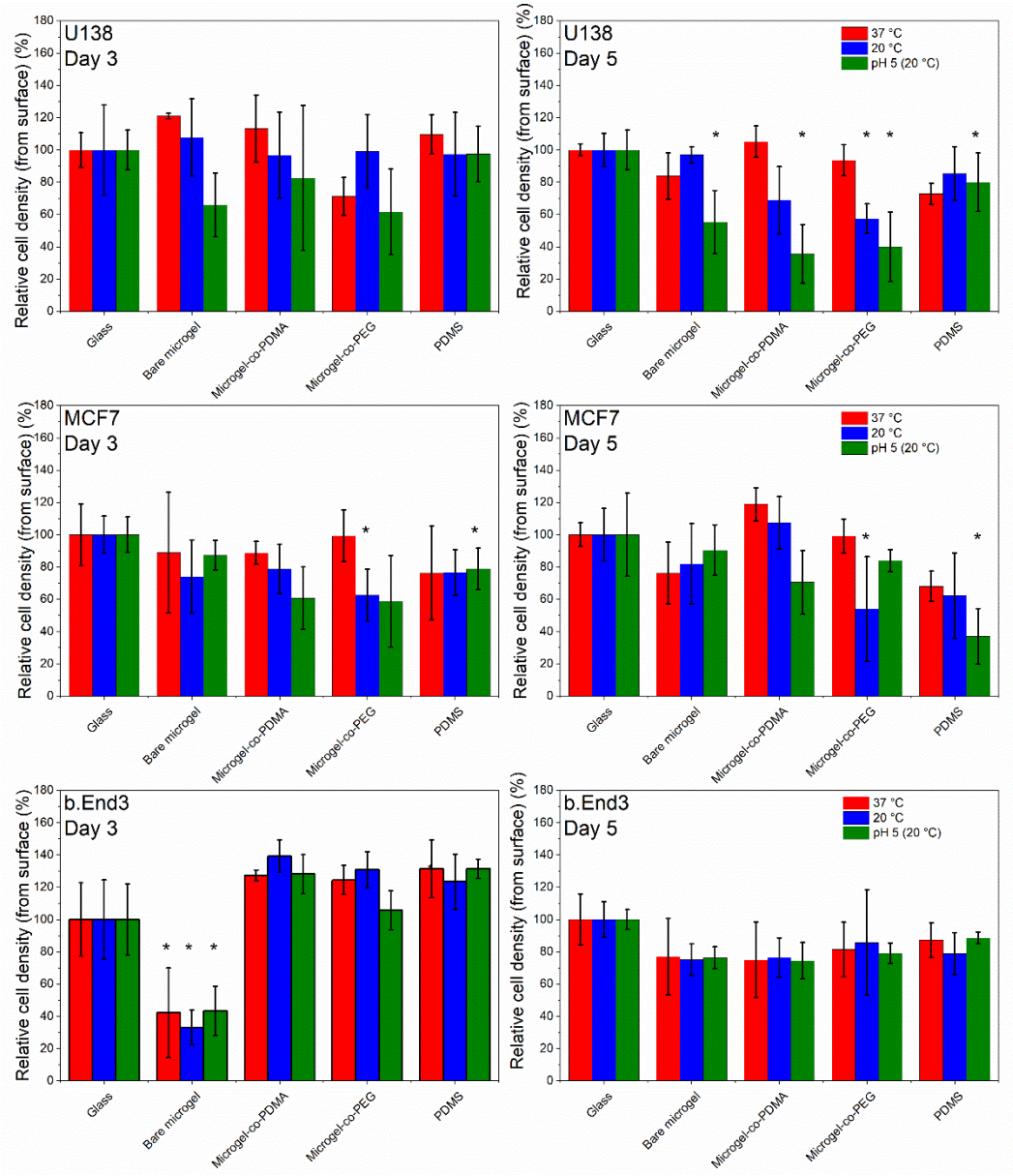

Figure 5.3. Relative cell density of U138 (first row), MCF7 (second row) and bEnd.3 (third row) cells obtained on day 3 (first column) and day 5 (second column) of incubation calculated by

fluorescence microscopy from surface-immobilized cells, at 37 °C (red) and after sequentially applying stimuli by decreasing temperature to 20 °C (blue) and then further adjusting the pH to 5 (green). *p<0.05 compared to glass control. Mean ± SD (n=3).

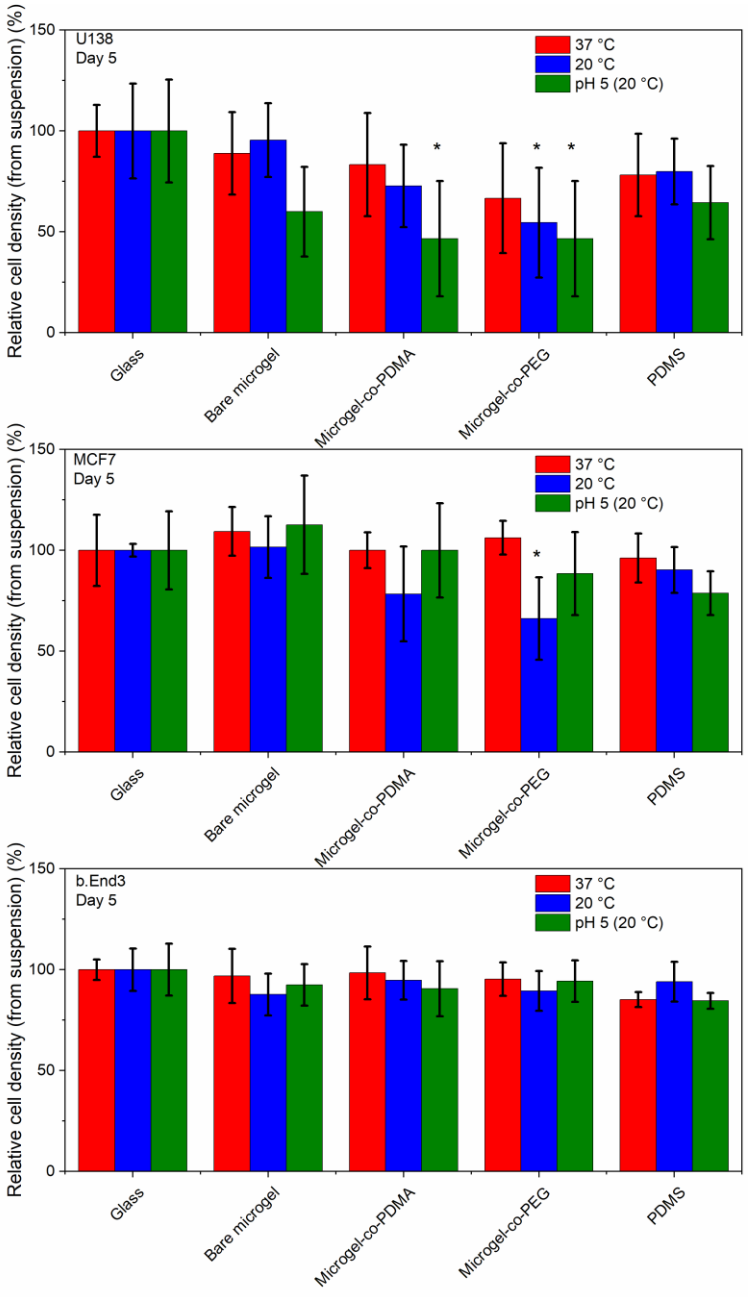

Figure 5.4. Relative cell density obtained on day 5 of incubation of U138 (first row), MCF7 (second row) and bEnd.3 (third row), at 37 °C (red) and after sequentially applying stimuli by

decreasing the temperature to 20 °C (blue) and further adjusting the pH to 5 (green). Cells were detached from their substrates using trypsin and counted using a haemocytometer. *p<0.05 compared to glass control. Mean ± SD (n=3).

5.5.3 Temperature, but not pH, triggers a significant cell detachment from functionalized substrates.

The relative cell densities of U138 and MCF7 cells grown on bare and surface-functionalized microgels decreased with temperature and the effect of temperature was more significant on day 5 compared to day 3 of incubation (**Fig. 5.3**). This behavior may be explained by the fact that after a few days of incubation, cells reach confluence and thus are more likely to detach from the substrate when a stimulus is applied.[83–85] U138 (day 5) and MCF7 (day 3 and 5) cells grown on microgels-co-PEG were the only ones displaying a significant decrease in the relative surface density upon decreasing the temperature (below the VPTT) (**Fig. 5.3**). This observation was supported by the number of trypsin-detached cells (measured with haemocytometer) after a 5-day incubation (**Fig. 5.4**). These results suggested that temperature-triggered cell detachment from PNIPAM microgel-coated functional substrates was improved by functionalizing the microgels with PEG chains which enhanced the hydrophilicity of the microgel surface even at temperatures above the VPTT, as previously observed.[69] As the temperature decreases (from above to below the VPTT), the PNIPAM polymeric network swells, becomes increasingly hydrated and more elastic. The variations in the surface and mechanical properties of the microgel layers during the transition are likely associated with conformational changes of the proteins in the ECM at the cell-substrate junction from unfolded to more globular configurations.[86–88] Consequently, the focal contacts formed during the active adhesion phase are disturbed and signals are relayed

downstream to the nucleus through either direct or indirect mechanotransduction, which may induce shape changes of the cells facilitating detachment from the surface.[89–92] Therefore, it is possible that the presence of PEG chains on the microgels improving hydrophilicity contributes to cell morphology changes promoting detachment to a greater extent than bare PNIPAM microgels. Okano *et al.* have previously demonstrated that hydration of PNIPAM did not completely govern cell detachment from culture surfaces but rather active cellular processes, i.e. consuming metabolic energy, enabled cell morphological changes essential to complete cell detachment.[66] The observation that thermo-responsive detachment of bEnd.3 was not achieved regardless of the substrate they were cultured on, number of days of incubation or the analytical technique used to evaluate the relative cell density (**Fig. 5.3** and **5.4**) can be explained by the fact that cell lineages demonstrate distinct metabolic rates at different environmental conditions. The fact that the bEnd.3 cells behaved differently than the U138 and MCF7 cells is not completely unexpected. Indeed, the absence of cellular detachment from PNIPAM microgels has also been reported in the past and attributed to irreversible and non-specific protein adsorption on the microgel-coated surfaces.[17,18] bEnd.3 cells express high levels of the platelet endothelial cell adhesion molecule-1 (PECAM-1) that makes them intrinsically more adherent[93–95] compared to U138 and MCF7 cancerous cell lineages which can migrate more easily through the EMT process. The absence of temperature-triggered detachment of bEnd.3 cells further supports previous observations that cell type is determinant in the cell detachment behavior.[14,42,56,72,73]

5.5.4 pH-triggered detachment only affected cell recovery to a minor extent.

Electrostatic effects provided by the polymer substrates can influence cellular detachment via changes in the degree of protonation mediating cellular adhesion through fibronectin adsorption.[36,37,71] Previous work confirmed the pH responsiveness (surface potential and swelling increase with decreasing pH) of the surface-immobilized microgels in their swollen state (below VPTT).[69] Accordingly, a certain decrease in the relative surface density of U138 and MCF7 cells grown on bare and surface-functionalized microgels with decreasing pH at 20 °C was observed after 5 days of incubation. However, this tendency was only statistically significant in the case of U138 cells (**Fig. 5.3**). These observations suggested that factors other than pH contributed to cellular detachment. The results show that cell lineage plays a critical role in the pH-triggered cell detachment ability of microgel-coated substrates given that bEnd.3 cells, which adhere more strongly to substrates than MCF7 and U138 cells, did not detach to a significant extent with decreasing pH (**Fig. 5.3** and **5.4**). Increasing surface potential (through pH changes) should promote electrostatic attractions between the microgel layers and cell membranes.[71] However, the simultaneous swelling of the polymer network with increasing pH also increases the layer thickness and hydrophilicity of the microgel layers, which are both contributing factors to cellular detachment.[65,70] These phenomena might be partially responsible for the observed detachment, via mechanotransduction, of U138 (statistically significant) and MCF7 (downward trend) on day 5 of incubation (**Fig. 5.3** and **5.4**). The extent of the surface potential variations upon pH changes could also explain the different pH-triggered cell detachments observed for a same cell line but on different substrates. For instance, a significant pH-triggered decrease in the relative surface

cell density of U138 and MCF7 incubated for 5 days on PDMS compared to glass (**Fig. 5.3**) might be partially due to the more important change in surface potential with pH ($\Delta\zeta \approx -46$ mV)[96] than that of glass within the same pH range ($\Delta\zeta \approx -4$ mV).[97] For the same reason, the temperature-triggered cell detachment (**Fig. 5.3** and **5.4**) can be partially due to the different temperature-triggered surface potential variations previously reported on the bare microgels ($\Delta\zeta \approx -11$ mV), microgel-co-PDMA ($\Delta\zeta \approx -7$ mV) and microgel-co-PEG ($\Delta\zeta \approx -4$ mV) between 39 °C and 24 °C in neutral media.[69] Hence, for bare and surface-functionalized microgels, the polymer layer thickness and hydrophilicity are probably more favorable to cellular detachment than variations in the surface potential.

5.5.5 Non-specific protein adsorption on functionalized coatings plays an important role in detachment ability.

Cellular adhesion and proliferation are mediated by the attachment between integrin proteins secreted by the extracellular membranes and the substrate.[65] The formation of integrin bonding enables cells to spread and flatten by forming focal attachments to the substrate that are subsequently strengthen by modifications of the cytoskeleton of the cells.[66] Wei *et al*. have previously established that the adsorption of BSA (a model protein) on surface-immobilized PNIPAM microgels could be irreversible with temperature, i.e. BSA adsorbed on PNIPAM microgel-coated surfaces at 37 °C, but failed to desorb from the surfaces once the temperature was reduced to 25 °C.[17] Therefore, the irreversible non-specific adsorption of BSA on microgel-coated surfaces could justify the inability of cells to detach by decreasing the temperature below the VPTT of the microgels.

To assess the role of non-specific protein adsorption in cell detachment, the non-specific adsorption of BSA or FBS proteins was studied by SPR (**Fig. 5.5**). On bare microgel substrates, the SPR response due to BSA adsorption was observed to increase roughly three-fold between 25 °C and 40 °C. This could be explained by the increasing hydrophobicity of microgel coating with temperature, leading to enhanced hydrophobic interactions between proteins and substrate (**Fig. 5.5**). Similarly, FBS (a more complex collection of proteins) gave rise to significant SPR signal shifts with increasing temperature, indicative of a more important protein adsorption on bare microgel-coated substrates (**Fig. 5.5**). However, neither BSA nor FBS incubated on microgel-co-PEG surfaces produced any significant SPR response within the same temperature range. These results strongly support the observation that the microgels-co-PEG remained hydrophilic above the VPTT[69] and are therefore capable of repelling most of serum proteins (**Fig. 5.5**). This may have facilitated cellular detachment when the temperature decreased from 37 to 20 °C, as illustrated in **Fig. 5.6**.

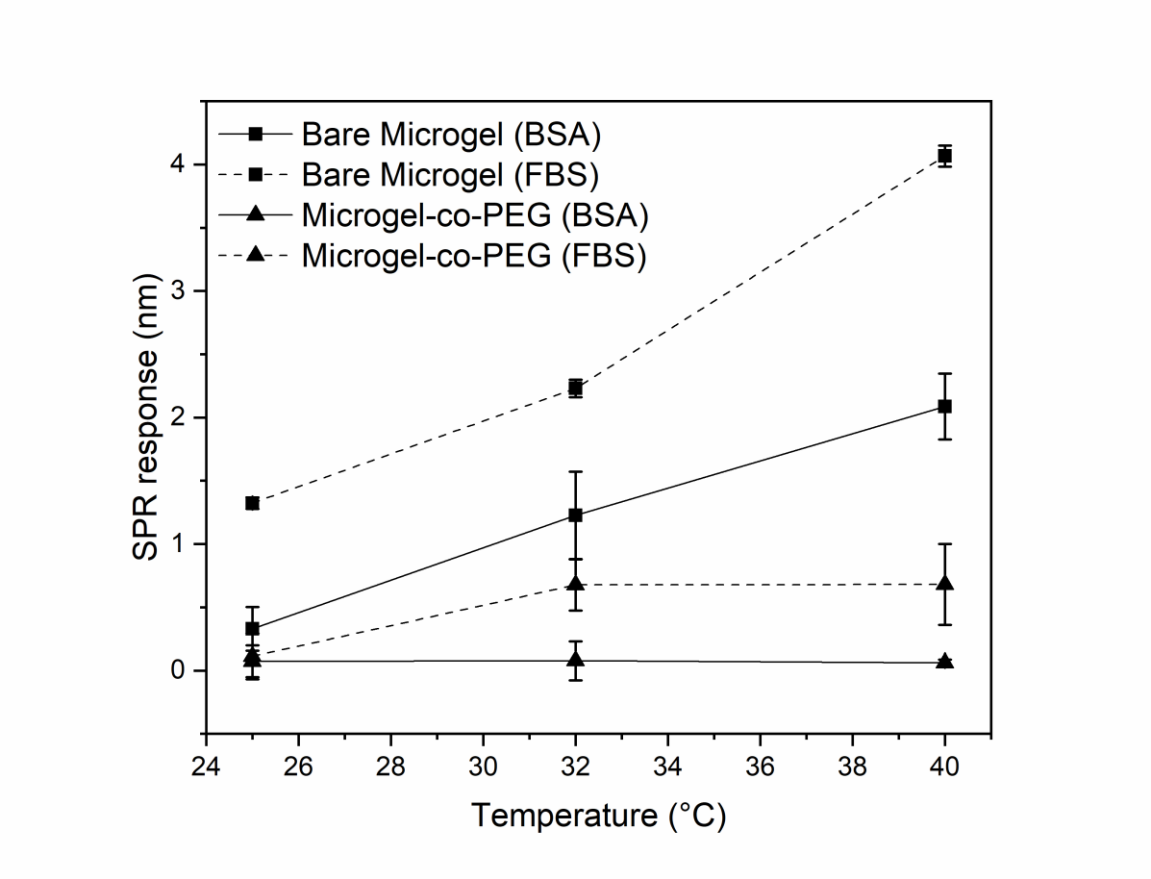

Figure 5.5. Non-specific protein adsorption with varying temperature evaluated using SPR on surfaces coated with bare microgel (■) and microgel-co-PEG (▲) interacting with BSA (solid lines) and with FBS (dashed lines). Mean ± SD (n=3).

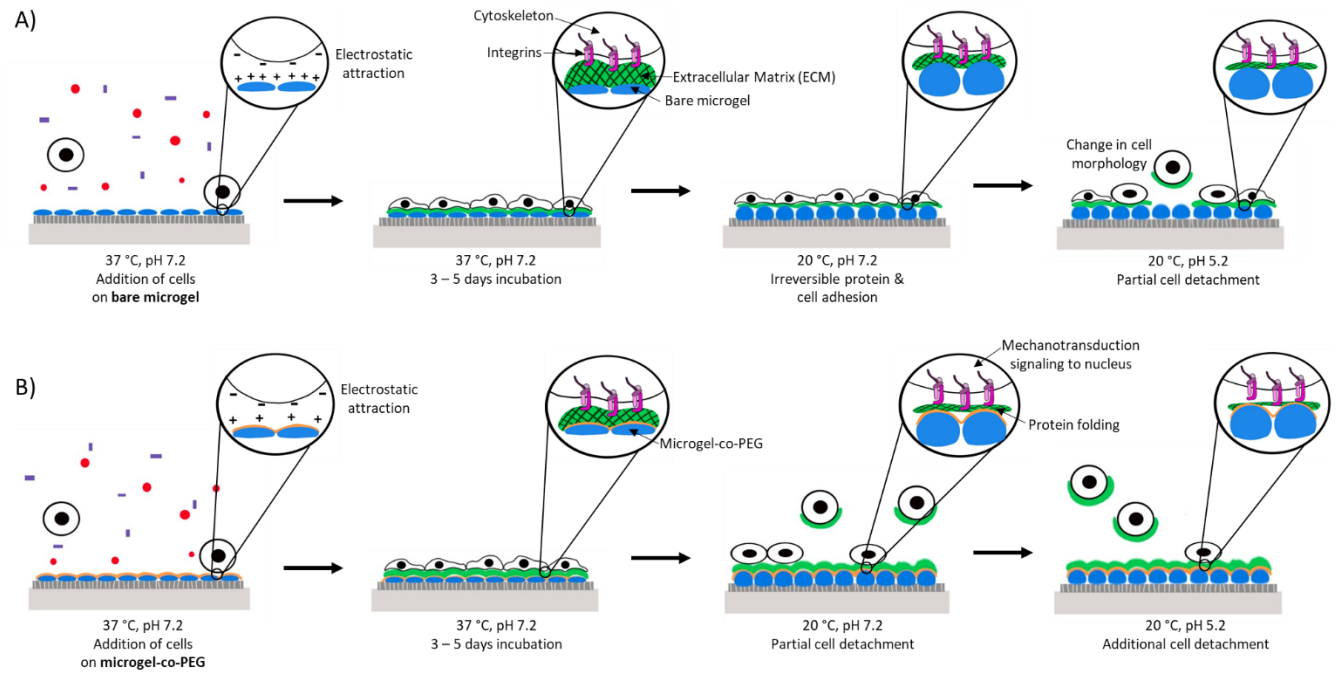

Figure 5.6. Schematic representation of cell adhesion and stimuli-triggered cell detachment using temperature and pH control from A) cationic PNIPAM bare microgels (bare microgel) and B) cationic PNIPAM microgels surface-functionalized with PEG (microgel-co-PEG). The presence of the PEG surface-functionalization (orange layers, row B) disfavors the interactions between the ECM and the flattened cells and promotes detachment at 20 °C.

5.6 Conclusion

The ability of dual temperature- and pH-responsive PNIPAM-based microgel coatings to trigger cellular detachment was studied. Promoting initial cellular attachment and triggering spontaneous cellular detachment from microgel-functionalized glass substrates was found possible via the swelling of the polymer layer through variations in temperature and medium pH. Nonetheless, the stimuli-triggered detachment was more efficient with cell lines whose phenotypes favor substrate detachment, such as cancerous lineages. As for more strongly

adherent cells, endothelial bEnd.3 cells adhered both onto bare and surface-functionalized microgel-coated surfaces to a similar extent than to the glass controls but were found the most difficult to detach. Microgel-co-PEG showed the best ability to detach MCF7 and U138 cells when the temperature was reduced below the VPTT of the PNIPAM microgel. It was proposed that the enhanced temperature-triggered cell-detaching ability of microgel-co-PEG was likely due to the microgels remaining hydrophilic and thus preventing non-specific protein adsorption regardless of the temperature. Once the pH of the media was adjusted to 5 from 7.2 (following a temperature decrease) the cell-detaching ability of all microgels improved, relative to the glass controls, for U138 cells. However, cellular detachment remained closely dependent on the cell type because no statistically significant temperature- or pH-triggered cellular detachment was observed with cultures involving strongly anastomosed and adherent bEnd.3 cells. These functional substrates could be useful in applications involving scarce, valuable cell lines susceptible to deterioration during enzymatic treatment or to prevent the development of biofilm on implanted medical devices.

5.7 Supporting Material

AFM images depicting grafting stability in ethanol of bare and functionalized microgels attached to carboxy-functionalized glass surfaces.

5.8 Credit authorship statement

A. Guerron: Conceptualization, Methodology, Validation, Formal analysis, Investigation, Data curation, Visualization, Writing – Original Draft; **H.T. Phan:** Investigation; **C. Peñaloza-Arias:** Resources; **D. Brambilla:** Conceptualization, Resources, Supervision, Writing – Review & Editing; **V.G. Roullin:** Conceptualization, Methodology, Resources, Supervision, Writing – Review &

Editing; **S. Giasson:** Resources, Supervision, Project administration, Funding acquisition, Writing – Review & Editing.

5.9 Declaration of competing interests

The authors declare that they have no known competing financial interests or personal relationships that could have appeared to influence the work reported in this paper.

5.10 Acknowledgements

The authors acknowledge funding from the Natural Sciences and Engineering Research Council of Canada (RGPIN-2016-06766) and the Fonds de Recherche Nature et Technologie, Québec.

5.11 Supplementary Information

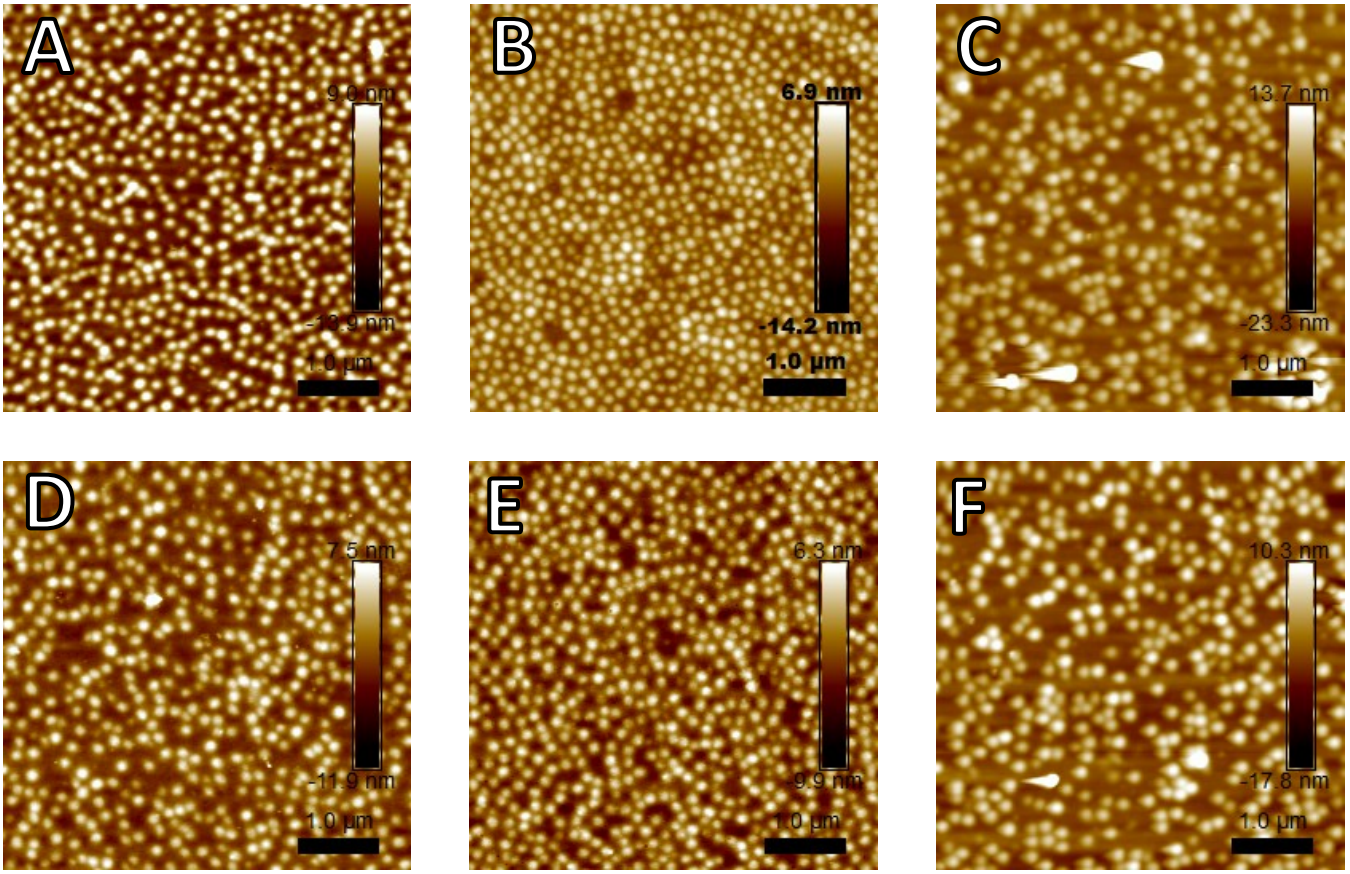

Figure 5.SM1. AFM images of bare microgel (A, D), microgel-co-PDMA (B, E) and microgel-co-PEG (C, F) covalently attached to AUTES-GLA functionalized glass substrates obtained before (A, B, C) and after (D, E, F) sterilization by immersion for 5 minutes in 70 % ethanol and air dried for 40 minutes in the PeakForce tapping mode. Imaging was performed in air at 25 °C and 30 % relative humidity. Image scale, 5 x 5 µm.

5.12 References

(1) Leon-Lopez, T.; Ortega-Vinuesa, J.; Bastos-Gonzalez, D.; Elaissari, A. Cationic and Anionic Poly-(N-Isopropylacrylamide) Based Submicron Gel Particles: Electrokinetic Properties and Colloidal Stability. *J. Phys. Chem. B* **2006**, *110*, 4629–4636.

(2) Meunier, F.; Elaissari, A.; Pichot, C. Preparation and Characterization of Cationic Poly(n-Isopropylacrylamide) Copolymer Latexes. *Polym. Adv. Technol.* **1995**, *6*, 489–496.

(3) Liu, L.; Zeng, J.; Zhao, X.; Tian, K.; Liu, P. Independent Temperature and PH Dual-Responsive PMAA/PNIPAM Microgels as Drug Delivery Systems: Effect of Swelling Behavior of the Core and Shell Materials in Fabrication Process. *Colloids Surf., A* **2017**, *526*, 48–55.

(4) Liang, G.; Li, L.; Xu, Q.; Tang, X.; Neoh, K. G.; Kang, E. T. Hairy Hollow Microspheres of Fluorescent Shell and Temperature-Responsive Brushes via Combined Distillation-Precipitation Polymerization and Thiol-Ene Click Chemistry. https://doi.org/10.1021/ma1008012.

(5) Kwon, Y.; Choi, Y.; Jang, J.; Yoon, S.; Choi, J. NIR Laser-Responsive PNIPAM and Gold Nanorod Composites for the Engineering of Thermally Reactive Drug Delivery Nanomedicine. *Pharmaceutics* **2020**, *12*, 204–222.

(6) Xu, Y.; Bao, Y.; Liu, Z.; Zheng, Q.; Dong, Y.; Song, R.; Yang, B. Temperature-Sensitive Tribological Performance of Titanium Alloy Lubricated with PNIPAM Microgels. *Appl. Surf. Sci.* **2022**, *572*, 151392–151406.

(7) Zhao, C.; Hou, J.; Chen, R.; Xin, Z.; Shi, H.; Wong, S.-C.; Yin, J.; Shi, Q. Cell-Inspired Biointerfaces Constructed by Patterned Smart Hydrogels for Immunoassay in Whole Blood. *J. Mater. Chem. B* **2017**, *5*, 2315–2321.

(8) Pelton, R. Poly(N-Isopropylacrylamide) (PNIPAM) Is Never Hydrophobic. *J. Colloid Interface Sci.* **2010**, *348*, 673–674.

(9) Zhang, Q.; Xia, F.; Sun, T.; Song, W.; Zhao, T.; Liu, M.; Jiang, L. Wettability Switching between High Hydrophilicity at Low PH and High Hydrophobicity at High PH on Surface Based on PH-Responsive Polymer. *Chem. Commun.* **2008**, *10*, 1199–1201.

(10) Fu, H.; Hong, X.; Wan, A.; Batteas, J.; Bergbreiter, D. Parallel Effects of Cations on PNIPAM Graft Wettability and PNIPAM Solubility. *ACS Appl. Mater. Interfaces* **2010**, *2*, 452–458.

(11) Kushida, A.; Yamato, M.; Konno, C.; Kikuchi, A.; Sakurai, Y.; Okano, T. Temperature-Responsive Culture Dishes Allow Nonenzymatic Harvest of Differentiated Madin-Darby Canine Kidney (MDCK) Cell Sheets. *J. Biomed. Mater. Res.* **2000**, *51*, 216–223.

(12) Akizuki, T.; Oda, S.; Komaki, M.; Tsuchioka, H.; Kawakatsu, N.; Kikuchi, A.; Yamato, M.; Okano, T.; Ishikawa, I. Application of Periodontal Ligament Cell Sheet for Periodontal Regeneration: A Pilot Study in Beagle Dogs. *J. Periodontal Res.* **2005**, *40*, 245–251.

(13) Yamada, N.; Okano, T.; Sakai, H.; Karikusa, F.; Sawasaki, Y.; Sakurai, Y. Thermo-Responsive Polymeric Surfaces; Control of Attachment and Detachment of Cultured Cells. *Die Makromol. Chemie, Rapid Commun.* **1990**, *11* (11), 571–576.

(14) Xia, Y.; Gu, Y.; Zhou, X.; Xu, H.; Zhao, X.; Yaseen, M.; Lu, J. R. Controllable Stabilization of Poly(N-Isopropylacrylamide)-Based Microgel Films through Biomimetic Mineralization of Calcium Carbonate. *Biomacromolecules* **2012**, *13*, 2299–2308.

(15) Uhlig, K.; Wegener, T.; He, J.; Zeiser, M.; Bookhold, J.; Dewald, I.; Godino, N.; Jaeger, M.; Hellweg, T.; Fery, A.; Duschl, C. Patterned Thermoresponsive Microgel Coatings for

Noninvasive Processing of Adherent Cells. *Biomacromolecules* **2016**, *17*, 1110–1116.
(16) Uhlig, K.; Wegener, T.; Hertle, Y.; Bookhold, J.; Jaeger, M.; Hellweg, T.; Fery, A.; Duschl, C. Thermoresponsive Microgel Coatings as Versatile Functional Compounds for Novel Cell Manipulation Tools. *Polymers* **2018**, *10* (6), 656–668.
(17) Wei, J.; Cai, J.; Li, Y.; Wu, B.; Gong, X.; Ngai, T. Investigation of Cell Behaviors on Thermo-Responsive PNIPAM Microgel Films. *Colloids Surf., B.* **2015**, *132*, 202–207.
(18) Cheng, X.; Canavan, H.; Graham, D.; Castner, D.; Ratner, B. D. Temperature Dependent Activity and Structure of Adsorbed Proteins on Plasma Polymerized N-Isopropylacrylamide. *Biointerphases* **2006**, *1* (1), 61–72.
(19) Alves, N.; Pashkuleva, I.; Reis, R.; Mano, J. Controlling Cell Behavior Through the Design of Polymer Surfaces. *Small* **2010**, *6* (20), 2208–2220.
(20) Zheng, Q.; Iqbal, S.; Wan, Y. Cell Detachment: Post-Isolation Challenges. *Biotechnol. Adv.* **2013**, *31*, 1664–1675.
(21) Canavan, H.; Cheng, X.; Graham, D.; Ratner, B.; Castner, D. Cell Sheet Detachment Affects the Extracellular Matrix: A Surface Science Study Comparing Thermal Liftoff, Enzymatic and Mechanical Methods. *J. Biomed. Mater. Res. Part A* **2005**, *75A* (1), 1–13.
(22) Waymouth, C. Autoclavable Medium AM 77B. *J. Cell Physiol.* **1979**, *100* (3), 548–550.
(23) Revel, J. P.; Hoch, P.; Ho, D. Adhesion of Culture Cells to Their Substratum. *Exp. Cell Res.* **1974**, *84* (1–2), 207–218.
(24) Osunkoya, B. O.; Frances, C.; Mottram, C.; Isoun, M. Synthesis and Fate of Immunological Surface Receptors on Cultured Burkitt Lymphoma Cells. *Int. J. Cancer* **1969**, *4* (2), 159–165.
(25) Vacanti, J. P. Beyond Transplantation: Third Annual Samuel Jason Mixter Lecture. *Arch. Surg.* **1988**, *123* (5), 545–549.
(26) Langer, R.; Vacanti, J. P. Tissue Engineering. *Science (80-.).* **1993**, *260*, 920–926.
(27) Vacanti, C.; Vacanti, J. P. The Science of Tissue Engineering. *Orthop. Clin. North Am.* **2000**, *31* (3), 351–355.
(28) Yang, J.; Yamato, M.; Kohno, C.; Nishimoto, A.; Sekine, H.; Fukai, F.; Okano, T. Cell Sheet Engineering: Recreating Tissues without Biodegradable Scaffolds. *Biomaterials* **2005**, *26*, 6415–6422.
(29) Wüst, S.; Müller, R.; Hofmann, S. Controlled Positioning of Cells in Biomaterials - Approaches Towards 3D Tissue Printing. *J. Funct. Biomater.* **2011**, *2*, 119–154.
(30) Zhou, F.; Hong, Y.; Liang, R.; Zhang, X.; Liao, Y.; Jiang, D.; Zhang, J.; Sheng, Z.; Xie, C.; Peng, Z.; Zhuang, X.; Bunpetch, V.; Zou, Y.; Huang, W.; Zhang, Q.; Alakpa, E. V.; Zhang, S.; Ouyang, H. Rapid Printing of Bio-Inspired 3D Tissue Constructs for Skin Regeneration. *Biomaterials* **2020**, *258*, 120287–120302.
(31) Haleem, A.; Javaid, M.; Khan, R. H.; Suman, R. 3D Printing Applications in Bone Tissue Engineering. *J. Clin. Orthop. Trauma* **2020**, *11*, S118–S124.
(32) Dogan, E.; Bhusal, A.; Cecen, B.; Miri, A. 3D Printing Metamaterials towards Tissue Engineering. *Appl. Mater. Today* **2020**, *20*, 100752–100765.
(33) Mano, J. Stimuli-Responsive Polymeric Systems for Biomedical Applications. *Adv. Eng. Mater.* **2008**, *10* (6), 515–568.
(34) Mendes, P. Stimuli-Responsive Surfaces for Bio-Applications. *Chem. Soc. Rev.* **2008**, *37* (11), 2361–2580.
(35) Chen, L.; Yan, C.; Zheng, Z. Functional Polymer Surfaces for Controlling Cell Behaviors.

Mater. Today **2018**, *21* (1), 38–59.
(36) Yen, C.-H.; Young, T.-H.; Huang, T.-W. Cell Detachment Ratio on PH-Responsive Chitosan: A Useful Biometric for Prognostic Judgment and Drug Efficacy Assessment in Oncology. *Carbohydr. Polym.* **2021**, *261*, 117911–117924.
(37) Yen, C.-H.; Young, T.-H.; Hsieh, M.-C.; Liao, L.-J.; Huang, T.-W. Increased Cell Detachment Ratio of Mesenchymal-Type Lung Cancer Cells on PH-Responsive Chitosan through the B3 Integrin. *Mar. Drugs* **2019**, *17* (12), 659–673.
(38) Lee, T.-J.; Wu, T.; Park, J. H.; Song, J.; Jeong, G.-J.; Hyun, J.; Lee, J. Y.; Lee, S.-H.; Lee, D. S.; Bhang, S. H. Enzyme Free Cell Detachment Using PH-Responsive Poly(Amino Ester) for Tissue Regeneration. *J. Ind. Eng. Chem.* **2020**, *88*, 373–381.
(39) Kim, Y.-J.; Lee, T.-J.; Jeong, G.-J.; Song, J.; Yu, T.; Lee, D. S.; Bhang, S. H. Development of PH-Responsive Polymer Coating as an Alternative to Enzyme-Based Stem Cell Dissociation for Cell Therapy. *Materials (Basel).* **2021**, *14*, 491–504.
(40) Nagase, K.; Yamato, M.; Kanazawa, H.; Okano, T. Poly(N-Isopropylacrylamide)-Based Thermoresponsive Surfaces Provide New Types of Biomedical Applications. *Biomaterials* **2018**, *153*, 27–48.
(41) Xue, C.; Choi, B.-C.; Choi, S.; Braun, P.; Leckband, D. Protein Adsorption Modes Determine Reversible Cell Attachment on Poly(N-Isopropyl Acrylamide) Brushes. *Adv. Funct. Mater.* **2012**, *22* (11), 2394–2401.
(42) Nash, M.; Carroll, W.; Foley, P.; Maguire, G.; O'Connell, C.; Gorelov, A.; Beloshapkin, S.; Rochev, Y. Ultra-Thin Spin Coated Crosslinkable Hydrogels for Use in Cell Sheet Recovery-Synthesis, Characterisation to Appliocation. *Soft Matter* **2012**, *8* (14), 3889–3899.
(43) Okano, T.; Yamada, N.; Sakai, H.; Sakurai, Y. A Novel Recovery System for Cultured Cells Using Plasma-Treated Polystyrene Dishes Grafted with Poly(N-Isopropylacrylamide). *J. Biomed. Mater. Res.* **1993**, *27*, 1243–1251.
(44) Yu, Q.; Zhang, Y.; Chen, H.; Zhou, F.; Wu, Z.; Huang, H.; Brash, J. Protein Adsorption and Cell Adhesion/Detachment Behavior on Dual-Responsive Silicon Surfaces Modified with Poly(N-Isopropylacrylamide)-Block-Polystyrene Copolymer. *Langmuir* **2010**, *26* (11), 8582–8588.
(45) Zhao, T.; Chen, H.; Zheng, J.; Yu, Q.; Wu, Z.; Yuan, L. Inhibition of Protein Adsorption and Cell Adhesion on PNIPAAm-Grafted Polyurethane Surface: Effect of Graft Molecular Weight. *Colloids Surf., B.* **2011**, *85* (1), 26–31.
(46) Pan, G.; Guo, Q.; Ma, Y.; Yang, H.; Li, B. Thermo-Responsive Hydrogel Layers Imprinted with RGDS Peptide: A System for Harvesting Cell Sheets. *Angew. Chemie Int. Ed.* **2013**, *52*, 6907–6911.
(47) Yu, Q.; Zhang, Y.; Chen, H.; Wu, Z.; Huang, H.; Cheng, C. Protein Adsorption on Poly(N-Isopropylacrylamide)-Modified Silicon Surfaces: Effects of Grafted Layer Thickness and Protein Size. *Colloids Surf., B.* **2010**, *76* (2), 468–474.
(48) Kumashiro, Y.; Fukumori, K.; Takahashi, H.; Nakayama, M.; Akiyama, Y.; Yamato, M.; Okano, T. Modulation of Cell Adhesion and Detachment on Thermo-Responsive Polymeric Surfaces through Observation of Surface Dynamics. *Colloids Surf., B.* **2013**, *106*, 198–207.
(49) Bischofberger, I.; Calzolari, D. C. E.; Trappe, V. Co-Nonsolvency of PNiPAM at the Transition between Solvation Mechanisms. *Soft Matter* **2014**, *10*, 8288–8295.
(50) Meng, T.; Xie, R.; Chen, Y.-C.; Cheng, C.-J.; Li, P.-F.; Ju, X.-J.; Chu, L.-Y. A Thermo-Responsive Affinity Membrane with Nano-Structured Pores and Grafted Poly(N-Isopropylacrylamide)

Surface Layer for Hydrophobic Adsorption. *J. Memb. Sci.* **2010**, *349*, 258–267.
(51) Burdukova, E.; Li, H.; Ishida, N.; O'Shea, J.-P.; Franks, G. Temperature Controlled Surface Hydrophobicity and Interaction Forces Induced by Poly(N-Isopropylacrylamide). *J. Colloid Interface Sci.* **2010**, *342*, 586–592.
(52) Kanidi, M.; Papagiannopoulos, A.; Matei, A.; Dinescu, M.; Pispas, S.; Kandyla, M. Functional Surfaces of Laser-Microstructured Silicon Coated with Thermoresponsive PS/PNIPAM Polymer Blends: Switching Reversibly between Hydrophilicity and Hydrophobicity. *Appl. Surf. Sci.* **2020**, *527*, 146841–146850.
(53) Gilcreest, V.; Carroll, W.; Rochev, Y.; Blute, I.; Dawson, K.; Gorelov, A. Thermoresponsive Poly(N-Isopropylacrylamide) Copolymers: Contact Angles and Surface Energies of Polymer Films. *Langmuir* **2004**, *20*, 10138–10145.
(54) de las Heras Alarcon, C.; Farhan, T.; Osborne, V.; Huck, W.; Alexander, C. Bioadhesion at Micro-Patterned Stimuli-Responsive Polymer Brushes. *J. Mater. Chem.* **2005**, *15*, 2089–2094.
(55) Liao, K.-S.; Fu, H.; Wan, A.; Batteas, J.; Bergbreiter, D. Designing Surfaces with Wettability That Varies in Response to Solute Identity and Concentration. *Langmuir* **2009**, *25*, 26–28.
(56) Cheng, X.; Canavan, H.; Stein, J.; Hull, J.; Kweskin, S.; Wagner, M.; Somorjai, G.; Castner, D.; Ratner, B. Surface Chemical and Mechanical Properties of Plasma-Polymerized N-Isopropylacrylamide. *Langmuir* **2005**, *21* (17), 7833–7841.
(57) Kujawa, P.; Segui, F.; Shaban, S.; Diab, C.; Okada, Y.; Tanaka, F.; Winnik, F. Impact of End-Group Association and Main-Chain Hydration on the Thermoresponsive Properties of Hydrophobically Modified Telechelic Poly(N-Isopropylacrylamides) in Water. *Macromolecules* **2006**, *39* (1), 341–348.
(58) Imashiro, C.; Hirano, M.; Morikura, T.; Fukuma, Y.; Ohnuma, K.; Kurashina, Y.; Miyata, S.; Takemura, K. Detachment of Cell Sheets from Clinically Ubiquitous Cell Culture Vessels by Ultrasonic Vibration. *Sci. Rep.* **2020**, *10*, 9468–9478.
(59) Jirku, V.; Turkova, J. Cell Immobilization by Covalent Linkage. *Methods Enzymol.* **1987**, *135*, 341–357.
(60) Mansson, M.-O.; Mosbach, K. Immobilized Active Coenzymes. *Methods Enzymol.* **1987**, *136*, 3–9.
(61) Fukumori, K.; Akiyama, Y.; Kumashiro, Y.; Kobayashi, J.; Yamato, M.; Sakai, K.; Okano, T. Characterization of Ultra-Thin Temperature-Responsive Polymer Layer and Its Polymer Thickness Dependency on Cell Attachment/Detachment Properties. *Macromol. Biosci.* **2010**, *10*, 1117–1129.
(62) Zhao, S.; Bukar, N.; Toulouse, J.; Pelechacz, D.; Robitaille, R.; Pelletier, J.; Masson, J.-F. Miniature Multi-Channel SPR Instrument for Methotrexate Monitoring in Clinical Samples. *Biosens. Bioelectron.* **2015**, *64*, 664–670.
(63) Garcia, A.; Gallant, N. Stick and Grip: Measurement Systems and Quantitative Analyses of Integrin-Mediated Cell Adhesion Strength. *Cell Biochem. Biophys.* **2003**, *39*, 61–73.
(64) Pierres, A.; Benoliel, A. M.; Bongrand, P. Cell Fitting to Adhesive Surfaces: A Prerequisite to Firm Attachment and Subsequent Events. *Eur. Cells Mater.* **2002**, *3*, 31–45.
(65) Kikuchi, A.; Okano, T. Nanostructured Designs of Biomedical Materials: Applications of Cell Sheet Engineering to Functional Regenerative Tissues and Organs. *J. Control. Release* **2005**, *101*, 69–84.

(66) Okano, T.; Yamada, N.; Okuhara, M.; Sakai, H.; Sakurai, Y. Mechanism of Cell Detachment from Temperature-Modulated, Hydrophilic-Hydrophobic Polymer Surfaces. *Biomaterials* **1995**, *16*, 297–303.
(67) Ratner, B. D.; Horbett, T.; Hoffman, A. Cell Adhesion to Polymeric Materials: Implications with Respect to Biocompatibility. *J. Biomed. Mater. Res.* **1975**, *9*, 407–422.
(68) Maroudas, N. G. Chemical and Mechanical Requierements for Fibroblast Adhesion. *Nature* **1973**, *244*, 353–354.
(69) Guerron, A.; Giasson, S. Multiresponsive Microgels: Towards an Independent Tuning of Swelling and Surface Properties. *Langmuir* **2021**, *37*, 11212–11221.
(70) Li, L.; Zhu, Y.; Li, B.; Gao, C. Fabrication of Thermoresponsive Polymer Gradients for Study of Cell Adhesion and Detachment. *Langmuir* **2008**, *24* (23), 13632–13639.
(71) Chen, Y.-H.; Chung, Y.-C.; Wang, I.-J.; Young, T.-H. Control of Cell Attachment on PH-Responsive Chitosan Surface by Precise Adjustment of Medium PH. *Biomaterials* **2012**, *33*, 1336–1342.
(72) Mizutani, A.; Kikuchi, A.; Yamato, M.; Kanazawa, H.; Okano, T. Preparation of Thermoresponsive Polymer Brush Surfaces and Their Interaction with Cells. *Biomaterials* **2008**, *29* (13), 2073–2081.
(73) Matsuzaka, N.; Nakayama, M.; Takahashi, H.; Yamato, M.; Kikuchi, A.; Okano, T. Terminal-Functionality Effect of Poly(N-Isopropylacrylamide) Brush Surfaces on Temperature-Controlled Cell Adhesion/Detachment. *Biomacromolecules* **2013**, *14* (9), 3164–3171.
(74) McGrath, J. Cell Spreading: The Power to Simplify. *Curr. Biol.* **2007**, *17*, R357–R358.
(75) Cuvelier, D.; Théry, M.; Chu, Y.-S.; Dufour, S.; Thiéry, J.-P.; Bornens, M.; Nassoy, P.; Mahadevan, L. The Universal Dynamics of Cell Spreading. *Curr. Biol.* **2007**, *17*, 649–699.
(76) Khalili, A. A.; Ahmad, M. R. A Review of Cell Adhesion Studies for Biomedical and Biological Applications. *Int. J. Mol. Sci.* **2015**, *16*, 18149–18184.
(77) Anselme, K.; Bigerelle, M. Modelling Approach in Cell/Material Interaction Studies. *Biomaterials* **2006**, *27*, 1187–1199.
(78) Abecassis, J.; Millon-Collard, R.; Klein-Soyer, C.; Nicora, F.; Fricker, J.-P.; Beretz, A.; Eber, M.; Muller, D.; Cazenave, J.-P. Adhesion of Human Breast Cancer Cell Line MCF-7 to Human Vascular Endothelial Cells in Culture. Enhancement by Activated Platelets. *Int. J. Cancer* **1987**, *40*, 525–531.
(79) Shtutman, M.; Levina, E.; Ohouo, P.; Baig, M.; Roninson, I. Cell Adhesion Molecule L1 Disrupts E-Cadherin-Containing Adherens Junctions and Increases Scattering and Motility of MCF7 Breast Carcinoma Cells. *Cancer Res.* **2006**, *66*, 11370–11382.
(80) McSherry, E.; Brennan, K.; Hudson, L.; Hill, A.; Hopkins, A. Breast Cancer Cell Migration Is Regulated through Junctional Adhesion Molecule-A-Mediated Activation of Rap1 GTPase. *Breast Cancer Res.* **2011**, *13*, R31–R45.
(81) Cordes, N.; Hansmeier, B.; Beinke, C.; Meineke, V.; van Beuningen, D. Irradiation Differentially Affects Substratum-Dependent Survival, Adhesion, and Invasion of Glioblastoma Cell Lines. *Br. J. Cancer* **2003**, *89*, 2122–2132.
(82) Thiery, J. P. Epithelial-Mesenchymal Transitions in Tumor Progression. *Nat. Rev. Cancer* **2002**, *2*, 442–454.
(83) Abercrombie, M. Contact Inhibition in Tissue Culture. *In Vitro* **1970**, *6*, 128–142.
(84) Martz, E.; Steinberg, M. The Role of Cell-Cell Contact in "Contact" Inhibition of Cell

Devision: A Review and New Evidence. *J. Cell. Physiol.* **1972**, *79*, 189–210.
(85) Puliafito, A.; Hufnagel, L.; Neveu, P.; Streitchan, S.; Sigal, A.; Fygenson, K.; Shraiman, B. Collective and Single Cell Behavior in Epithelial Contact Inhibition. *Proc. Natl. Acad. Sci.* **2012**, *109*, 739–744.
(86) Vogler, E. Structure and Reactivity of Water at Biomaterial Surfaces. *Adv. Colloid Interface Sci.* **1998**, *74*, 69–117.
(87) Norde, W.; Haynes, C. Reversibility and the Mechanism of Protein Adsorption. In *Proteins at Interfaces II: Fundamentals and Applications*; Horbert, T. A., Brash, J. L., Eds.; American Chemical Society: Washington, 1995; pp 26–40.
(88) Roach, P.; Farrar, D.; Perry, C. Interpretation of Protein Adsorption: Surface-Induced Conformational Changes. *J. Am. Chem. Soc.* **2005**, *127*, 8168–8173.
(89) Dalby, M. Topographically Induced Direct Cell Mechanotransduction. *Med. Eng. Phys.* **2005**, *27*, 730–742.
(90) Ingber, D. Cellular Tensegrity: Defining New Rules of Biological Design That Govern the Cytoskeleton. *J. Cell Sci.* **1993**, *104*, 613–627.
(91) Maniotis, A.; Chen, C.; Ingber, D. Demonstration of Mechanical Connections between Integrins, Cytoskeletal Filaments, and Nucleoplasm That Stabilize Nuclear Structure. *Proc. Natl. Acad. Sci.* **1997**, *94*, 849–854.
(92) Ge, C.; Xiao, G.; Jiang, D.; Franceschi, R. Critical Role of the Extracellular Signal-Regulated Kinase-MAPK Pathway in Osteoblast Differentiation and Skeletal Development. *J. Cell Biol.* **2007**, *176*, 709–718.
(93) Sheibani, N.; Frazier, W. Down-Regulation of Platelet Endothelial Cell Adhesion Molecule-1 Results in Thrombospondin-1 Expression and Concerted Regulation of Endothelial Cell Phenotype. *Mol. Biol. Cell* **1998**, *9*, 701–713.
(94) Booth, R.; Kim, H. Characterization of a Microfluidic in Vitro Model of the Blood-Brain Barrier (MBBB). *Lab Chip.* **2012**, *12*, 1784–1792.
(95) Omidi, Y.; Campbell, L.; Barar, J.; Connell, D.; Akhtar, S.; Gumbleton, M. Evaluation of the Immortalised Mouse Brain Capillary Endothelial Cell Line, b.End3, as an in Vitro Blood-Brain Barrier Model for Drug Uptake and Transport Studies. *Brain Res.* **2003**, *990*, 95–112.
(96) Song, Y.; Feng, A.; Liu, Z.; Li, D. Zeta Potentials of PDMS Surfaces Modified with Poly(Ethylene Glycol) by Physisorption. *Electrophoresis* **2020**, *41*, 761–768.
(97) Gu, Y.; Li, D. The ζ-Potential of Glass Surface in Contact with Aqueous Solutions. *J. Colloid Interface Sci.* **2000**, *226*, 328–339.

Chapter 6 – General Discussion of the Thesis

Discussions on Chapter 3: Multiresponsive Microgels: Towards an independent Tuning of Swelling and Surface Properties.

Objective (i): Preparation and characterization of surface-functionalized microgels.

The first step of this project was to functionalize the surface of PNIPAM microgels with polymer chains and to verify that the attachment was achieved. Previously, core/shell PNIPAM-based microgels have been synthesized using a two-staged seeding polymerization methodology that exhibit dual- or multi-stimuli responsive behaviors.[1–4] However, the choice to adopt a grafting to surface-functionalization approach was made to diminish the impact to the VPTT and the breadth of transition of the bare PNIPAM microgels.[5–7] Thus, PDMAEMA and PEG chains end-functionalized with carboxylic acid functions (see chapter 3) were selected to form a covalent amide attachment with the surface-amino groups on the microgels via peptide coupling using EDC and NHS that act as dehydration and addition promoters, respectively.[8,9] The formation of the peptide bond was evaluated either directly by spectroscopic characterization using NMR and ATR-FTIR, or indirectly using DLS to determine the surface potential of bare and surface-functionalized microgels and by ellipsometry.

Ideally, spectroscopic analysis was expected to reveal an increase in the intensity of the amide band in the spectra of surface-functionalized microgels relative to bare microgels and a proportional decrease in the primary amine band. However, two factors related to the chemical composition of the microgels prevented this observation. First, the concentration of primary amines, provided by the AEMH monomer copolymerized with PNIPAM during synthesis, is too

low (1.5 % w/w) to be able to discern any significant decrease in intensity after grafting polymer chains. Second, the amide coupling that is formed during conjugation of the end-functionalized polymer chains and the primary amines on the surface of the microgels can not be detected spectroscopically because the signal is buried by the much stronger amide band from PNIPAM. Previous reports have also discussed on the inability to identify significant changes in the amide band by using ATR-FTIR during the EDC/NHC mediated conjugation of folic acid and vinyl functions on PNIPAM microgels copolymerized with relatively higher concentrations (up to 5 % w/w) of poly acrylic acid (PAAC).[10,11] Nevertheless, the NMR and ATR-FTIR spectra reported in chapter 3 shows that additional bands corresponding to functional groups in PDMAEMA or PEG chains are added to the spectra of bare microgels after the grafting reaction. Further, because spectra were collected after the purification by dialysis step, it strongly suggests that the PDMAEMA or PEG chains that remain in the sample are covalently attached to the microgel. In addition, supplementary analysis was done to confirm indirectly that polymer chains were grafted on the surface of the microgels.

Intrinsic characteristics of bare microgels were modified upon grafting PDMAEMA or PEG chains on their surface. For instance, the surface potential of bare microgel at 24 °C in neutral media (12.4 ± 1.3 mV) decreased upon surface-functionalizing with PEG chains (0.3 ± 0.2 mV), which are not ionizable in suspension, and thus indicates that the primary amines on the bare microgel were neutralize during the coupling reaction. Variations in the surface charge have been used in the past to confirm that surface-functionalization of a charge-bearing PNIPAM microgel was successful.[10] Further evidence that surface-functionalization on PNIPAM microgels took place was shown in chapter 3 by measuring the surface potential of bare and surface-functionalized

microgels as a function of pH. It was observed that the surface charge of bare microgel and microgel-co-PDMAEMA, both charge bearing microgels, decreased between pH 2 and 10. On the contrary, the surface charge of microgel-co-PEG remained neutral within the same range of pH because PEG chains are insensitive to pH. Microgel-co-PEG also showed the ability to prevent non-specific protein adsorption at temperatures above the VPTT whereas bare microgel sustained considerable non-specific protein fouling above the VPTT (see chapter 5). Previous work reported a different indirect approach to validate surface functionalization of a PNIPAM-co-PAAC hydrogel, which involved grafting a fluorescent antibody using EDC/NHS and measuring the fluorescence by confocal laser microscopy.[12] This method showed that the antibody was grafted on the carboxylic functions but not on the underlying non-functional substrate. The final indirect method that was used to confirm that peptide coupling was possible was done by ellipsometry. A silicon wafer was functionalized with a molecule bearing primary amines (AUTES) to mimic the microgel surface and the peptide coupling was assessed by grafting PEG-COOH (see chapter 3). In the absence of coupling agents (EDC/NHS), no increase in the layer thickness was observed relative to that of the immobilized amino-functionalized layer. However, when the reaction took place in the presence of the coupling agents, an increase in the layer thickness of 2.8 ± 0.5 nm was measured. The considerable modifications to the surface properties and temperature-responsive behavior of bare microgels upon surface-functionalization with PDMAEMA or PEG chains strongly suggest that the coupling reaction was successful.

In addition to direct and indirect methods to confirm surface functionalization, a theoretical approximation was presented in chapter 3 to estimate the grafting density of the polymer chains on the microgels. Estimating the grafting density of a molecule surface-functionalized on

microgels is not a parameter usually reported in the literature, particularly when using the grafting to method, compared to core/shell which can be accomplished more easily.[1,3,4,10–12] The grafting density was estimated by first calculating the charge density on the surface of the microgels (4.6×10^{-4} C/m^2) from the zeta potential and using the Grahame equation derived from the Gouy-Chapman theory.[13–16] These results are in agreement with the published work on the same type of cationic microgels.[17] Because the zeta potential was observed to decrease upon surface-functionalization with PDMAEMA and PEG polymer chains, it was possible to estimate the change in charge densities. This led to the conclusion that the charge density decreased twofold for microgel-co-PDMAEMA and 35-fold for microgel-co-PEG. These calculations are rough approximations on the grafting density; however, it is possible that the charge density decreases for microgel-co-PDMAEMA is overestimated because PDMAEMA is itself charge-bearing in solution. In addition to grafting density approximation, further analytical measurements could have potentially supported that polymer chain grafting was successful.

Thermogravimetric analysis (TGA) and differential scanning calorimetry (DSC) could have provided supplementary evidence that PDMAEMA and PEG polymer chains were grafted on the microgels. However, these techniques were not used because they were not expected to conclusively determine that peptide coupling took place but rather add to the ensemble of indirect methods already reported in chapter 3. For example, the thermal stability of PNIPAM microgels increased significantly when surface-functionalized with folic acid.[10] Grafting PEG and PDMAEMA chains to PNIPAM has shown to decrease the thermal stability; however, these studies involved PEG and PDMAEMA polymer chains with molecular weights 1 – 2 orders of magnitude greater than those used in chapter 3.[18–22] Hence, the impact of surface functionalization on the

thermal stability, relative to bare microgels, is expected to be nonsignificant. DSC analysis of PNIPAM-co-PAA microgels surface-functionalized with folic acid revealed lower crystallization and melting points compared to PNIPAM-co-PAA microgels.[10] Similar changes to the DSC diagrams of PNIPAM with PDMAEMA or PEG incorporated in their structures have been reported;[18,22] yet, no significant impact is expected for DSC analysis of microgel-co-PDMAEMA and microgel-co-PEG due to the significant difference in the molecular weight of the polymer chains involved. Lastly, the advancing water contact angle has been used to demonstrate the thermo-triggered wettability switching of substrates functionalized with patterned PNIPAM hydrogels.[12] Extensive experimentation was done to investigate the wettability behaviors of surface-immobilized bare microgel, microgel-co-PDMAEMA and microgel-co-PEG coated-substrates. However, it was not possible to obtain significantly different results because immobilizing discrete microgel particles on a surface increases the rugosity and deteriorates the quality of the measurements.[23,24]

Sufficient evidence was gathered in chapter 3 to demonstrate that PEG and PDMAEMA polymer chains are grafted to the microgel surface. Through these results and observations, as well as those reported in the literature, it is possible to conclude that objective (i) was accomplished.

Objective (ii): Demonstration that physical and surface properties of the surface-functionalized microgels can be controlled independently in suspension and immobilized on a surface.

This objective explored the ability to control the swelling of the PNIPAM microgels independently from the surface properties provided by the grafted polymer chains. In other words, the

expectation is that by raising the temperature, the microgel particles will expel water and shrink without altering the surface potential (in suspension) or the adhesion forces (on a substrate), which is not usually the case with PNIPAM microgels.[25–27] On the other hand, it is expected that by changing the pH at constant temperature, to be able to control the surface potential or adhesion without altering the swelling degree of the underlying PNIPAM microgel.

In suspension, it was observed that the swelling behavior could be thermo-triggered independently of the surface-functionalization and that the surface potential of the microgels in a highly hydrated state (below the VPTT) can be tuned with pH via surface functionalization. For instance, the variation in swelling ratio (T-Q_{susp}, see chapter 3) of the bare and surface-functionalized microgels between 24 and 39 °C ranged from 1.70 to 2.10, depending on the pH of the media. The bare and surface-functionalized microgels in pH 10 media aggregated above the VPTT due to the deprotonation of the amine groups which leads to lower electrostatic repulsions between particles promoting NIPAM/NIPAM attractions. These results show that the surface functionalization of the microgels does not obstruct their thermo-responsiveness, a different behavior compared to what has been previously reported for PNIPAM core/shell microgels.[1,3,4] Further, unlike core/shell microgels, the results in suspension showed that the surface potential of microgel-co-PDMAEMA is pH-dependent at constant temperature while microgel-co-PEG was pH-insensitive. However, electrostatic-induced swelling (pH-Q_{susp}) was observed in bare and surface-functionalized microgels between pH 2 and 10 at constant temperature because the PNIPAM-network of the microgel was copolymerized with a pH-sensitive primary amine monomer (AEMH). This suggests that the swelling behavior is not entirely independent from pH-variations. Nevertheless, the pH-Q_{susp} reported in chapter 3 indicates that the pH-triggered

swelling was significantly less (maximum pH-Q_{susp} was 1.22) than the thermo-triggered swelling. This behavior contrasts observations obtained with core/shell microgels, where significant and interdependent variations in particle swelling and the surface potential were reported with pH modifications.[3,4] In suspension, it was observed that: i) the swelling can be controlled by the temperature regardless of the surface functionalization and, ii) that microgels surface-functionalized with pH-sensitive PDMAEMA allow for the surface potential to be tuned with pH while microgels with pH-insensitive PEG demonstrate no dependence on the surface potential or swelling with pH.

Microgels surface-functionalized with PDMAEMA or PEG and immobilized on a mica substrate demonstrated a similar independent control of the swelling and surface properties. The ability to control swelling was evaluated by raising the temperature above the VPTT of PNIPAM microgels. The swelling of the microgel-co-PDMAEMA and microgel-co-PEG layers (T-Q_{imm}, see chapter 3) shrunk to a similar extent than surface-functionalized microgel particles in suspension. Further, the temperature-induced swelling of immobilized microgels was more significant than the pH induced swelling of immobilized microgels (pH-Q_{imm}), as was also observed for microgels in suspension. The ability to control surface properties of the surface-immobilized microgels was assessed by measuring the adhesion force on separating two opposing microgel-bearing surfaces upon variation in pH and temperature. Below the VPTT no adhesion forces were measured when separating all microgel-coated surfaces regardless of the pH while above the VPTT adhesion appeared to depend on the surface chemistry of the microgels. For instance, above the VPTT adhesion forces were measured for microgel-co-PDMAEMA at all pH values and for bare microgels for pH > 4. This suggests that at pH 4, the surface charges of bare microgel above the

VPTT (25 mV) provide sufficient electrostatic repulsions to overcome hydrophobic attraction caused by NIPAM/NIPAM interactions. On the contrary, the lower surface charge of microgel-co-PDMAEMA at pH 4 (12 mV) does not provide enough electrostatic repulsions to overcome NIPAM/NIPAM attractions. More importantly, no adhesion force was measured between microgel-co-PEG layers above the VPTT regardless of pH. These results suggest that grafting polymer chains, and PEG in particular, on surface-immobilized microgels may provide a way to tune the swelling behavior via temperature without affecting the surface properties as was also observed in suspension. Control of adhesion between PNIPAM polymer layers independently of the swelling could represent a major advantage for controlling diverse surface behaviors. For instance, the friction forces between two surfaces in relative motion functionalized with PNIPAM or PNIPAM copolymerized with PEG increased significantly above the VPTT because of the desorption of the hydration layer on the polymer coating and increased adhesion forces due to NIPAM/NIPAM attractions.[25,28,29] In another study, PNIPAM microgels were decorated with hyaluronic acid motifs linked to the PNIPAM network via a photocleavable molecule and immobilized on a cell culture dish to promote cellular detachment through thermo- and irradiation stimulation.[30] Even though stimuli-triggered cellular detachment could be obtained by decreasing the temperature and exposing the surface to UV irradiation, only decreasing the temperature did not produce sufficient cellular detachment, which signals a lack of independent control of the swelling and surface properties. Shi et al. developed structured PNIPAM-co-PAA copolymer hydrogel substrates exhibiting thermo-responsiveness while minimizing the change in surface wettability.[12] However, the independent control of the swelling and wettability was not accomplished.

Polymer chain grafting on PNIPAM microgels are a promising way to independently tune the swelling and surface properties of a polymer layer. The thermo-responsive ability characteristic of PNIPAM was not compromised by surface-functionalization with polymer chains. In addition, the work presented in chapter 3 indicates that the surface properties can be tuned by changing the pH via grafting polymer chains on the PNIPAM microgels. Specifically, microgel-co-PEG exhibited the most promising behavior, it was possible to obtain a thermo-triggered swelling without affecting the surface properties, i.e. the surface potential and adhesion, within a wide range of pH values.

Within the framework of objective (ii) established at the beginning of this thesis, it can not be asserted that the goal was fully accomplished. Due to the presence of amino groups throughout the entirety of the microgel polymer network, the swelling behavior was also pH-dependent. However, the thermo-responsive swelling was more significant than the pH-triggered one, which indicates that further optimization may lead to a full dissociation in the control of the swelling and surface properties. It is important to point out that the scope of this work can be expanded beyond PNIPAM microgels grafted with PDMAEMA or PEG chains, which were selected as a proof of concept. In fact, a plethora of polymer compounds are available to develop customized applications that require responsive surfaces whose swelling properties can be altered regardless of their surface chemistry.

Discussions on Chapter 4: Tribological properties of PNIPAM microgels in the nano- and mesoscales.

Objective (iii): Application of the independent control of the swelling and surface properties to the control of the tribological properties in the nano- and mesoscales.

The results reported on chapter 3 of this thesis demonstrated that by functionalizing the surface of PNIPAM microgels with polymer chains, and particularly with PEG, it is possible to independently modulate the swelling of the microgel and the surface properties. More specifically, microgel-co-PEG demonstrated the ability to change its swellability with temperature, i.e. shrink above the VPTT, while maintaining its hydrophilic character and thus preventing the rise of adhesion forces. Similarly, it was observed that the surface potential of microgel-co-PEG remained constant as a function of pH of the surrounding environment at constant temperature. Polymer adhesion is one of the main mechanisms through which the tribological properties of a polymer layer can be tuned via variations in temperature, pH, or ionic strength.[31,32] Hence, the aim of objective (iii) was to verify if the independent tunability of swelling and surface properties of immobilized bare and surface-functionalized microgels translates into an independent control of their tribological properties. Further, the tribological behavior was expanded to the mesoscale using the tribo-brush to determine if a continuum of the friction forces exists and refine the knowledge on the load-bearing capacity and resistance to wear of this type of material.

No significant variations in the friction behavior of surface-immobilized bare and surface-functionalized microgels was measured while changing the surface potential of the microgels at 23 °C. The coefficient of friction, defined as the ratio between the friction force and the applied

normal load (chapter 4), was used as an indicator of the tribological properties of the microgel coatings. The coefficients of friction for all microgels ranged between 0.31 and 0.52 between pH 4 and 10, these values are roughly 10 times greater than those previously reported with similar soft polymeric particles in good solvent conditions.[33,34] Further, for charge-bearing microgel-co-PDMAEMA and bare microgel, the coefficients of friction between pH 10 and 4 (increasing surface charge) varied by a factor of 0.9 and 1.1, respectively. To put these values in perspective, pH-sensitive core/shell microgels have shown a 4 to 10-fold increase in the coefficient of friction within the same range of pH.[33] Tribological studies with charged polymer brushes in different pH values demonstrated a similar behavior.[29,35,36] This suggests that the magnitude of variation in the coefficients of friction with pH for the microgels reported in chapter 4 are nonsignificant. For example, a higher degree of ionization, a more important particle swelling, and lower elasticity of the polymer layer are expected to lead to lower coefficients of friction.[33,34] However, the coefficient of friction of bare microgel in chapter 4 increased during the transition to pH 4 from pH 7 despite a decrease in the elasticity of the polymer layer and an increase in the surface charge and swelling. Microgel-co-PEG layers showed the least variability in the coefficients of friction from pH 10 (0.38) to pH 4 (0.37), which hints at the possibility to control the tribological behavior by functionalizing the surface of the microgels. However, because of the lack of coherence in expected trends as well as the relatively small variation in the coefficients of friction with pH observed for charge bearing microgels, it is not possible to conclusively assert that microgel-co-PEG exhibits a superior control of tribological properties.

Technical problems related to the SFA prevented studying the friction behavior above the VPTT and resulted in a reduced sensitivity of the instrument. One of the key findings in chapter 3 was

that microgel-co-PEG remained hydrophilic and non-adhesive above the VPTT regardless of the pH of the media. Similarly, the adhesion forces between microgel-co-PDMAEMA layers could be modulated via the pH above the VPTT differently than with bare microgels. Moreover, the coefficient of friction of PNIPAM microgels has been shown to increase significantly, and become more closely dependent on the sliding speed, when the temperature is raised above the VPTT.[25] These results suggested that surface-functionalized microgels could reveal a distinct tribological behavior above the VPTT compared to bare microgels. Unfortunately, the friction device that was used during these experiments was fabricated such that the circuitry is exposed to the environment. Upon raising the temperature, the atmosphere within the SFA chamber saturates with humidity originating from the water placed between the microgel layers (see chapter 4). The humidity then forms condensation on the circuitry of the friction device which overloads the output signal and precludes the collection of useful data. While attempting to remediate the problems caused by the condensation, the Wheatstone bridge of the friction device was modified which resulted in a 16-fold decrease in detection sensitivity. Such a loss was detrimental to this section of the thesis because friction forces could no longer be detected before the microgels were largely confined and in a compressed regime. In other words, the friction forces were measured under a high applied load. This explains the higher coefficients of friction and the absence of effect of the surface functionalization. The response to pH variations in bare and surface-functionalized microgels were expected in the hydrodynamic lubrication regime, when the microgel layers are barely in physical contact with one another.

Tribological studies in the mesoscale revealed that there is no variation in the friction forces of bare and microgel-co-PEG layers and that a continuum of the friction forces exists between the

nano- and mesoscales. Experiments with the tribo-brush showed that the coefficients of friction of bare microgel (0.23) and of microgel-co-PEG (0.25) are equivalent. This result confirms the observations obtained in the nanoscale with the SFA; namely, that the friction does not depend on the surface properties of the immobilized microgel layers. Further, stiction peaks were observed in the friction traces during sliding at normal applied loads higher than 0.4 N for microgel-co-PEG and 0.35 N for bare microgel layers. Stiction peaks may arise from adhesion forces between the surfaces or due to the reorganization of the materials that compose them. Thus, the wear track on a bare microgel layer after sliding experiments was visualized by using the AFM technique and used to confirm that microgels were sheared away from the substrate (chapter 4) during sliding. These results suggest that microgel-co-PEG layers offer a higher resistance to wear than the bare microgel ones. However, to confirm that microgel particles are not sheared or damage at lower applied normal loads, further experimentation and imaging with the AFM are necessary. Finally, it was observed that a continuum in the friction forces exists between the nano- and the mesoscales and that the friction forces overlap within the range of roughly 30 – 40 mN of normal applied load. In addition, no substantial damage was imparted to the surface within the normal applied loads in which the overlap takes place. These results show that the load-bearing capacity and resistance to wear of these materials are suitable to applications in lubrication of artificial articulations.[28,29,37]

The most important condition for tribological studies with bare and surface-functionalized microgels, raising the temperature above the VPTT of PNIPAM, could not be explored due to technical difficulties. Moreover, the loss in sensitivity of the friction device prevented the study of the effect of pH, swelling and surface functionalization. Hence, objective (iii) established at the

beginning of this thesis was not successfully accomplished. Promising results were gathered in the mesoscale; particularly, there is some indications that microgel-co-PEG offers a better wear resistance than bare microgels. However, further experiments must be done in this regard to confirm it. Above all, given the importance that temperature has on PNIPAM microgels and its tribological properties, a suitable alternative to the current friction device must be developed. Unfortunately, the available options are either to replace it or to cover the whole device with an isolating coating. However, a new device requires a very significant investment while coating the device implies an additional loss of sensitivity, which has been shown in this section to be already insufficient for characterizing microgel layers.

Discussions on Chapter 5: Selectively triggered cell detachment from PNIPAM microgel functionalized substrates.

Objective (iv): Application of surface-functionalized microgels to promote initial cell-substrate adhesion while favoring a temperature-triggered cell detachment.

Thermo- and pH-responsive polymers are among the most widely used functional materials to trigger cell detachment from culture substrates during cell culture for applications in cancer therapy or regenerative medicine.[38] PNIPAM-based coatings arranged as brushes,[39] hydrogels[40,41] and microgels[42,43] are chief among them because of the sharp physical conformation transition that PNIPAM undergoes across the LCST/VPTT close to the physiological temperature and the associated variation in the wettability of the coating.[44–46] However, because of the variability in surface fabrication methods, cell lineages and culture protocols, reported results are difficult to

exploit comparatively. For example, cellular culture on substrates functionalized with PNIPAM microgels have either succeeded,[42,47,48] or failed,[43,49] to produce thermo-triggered cellular detachment. Hence, the rational behind objective (iv) was to normalize experimental conditions and isolate the effect of the substrate in order to elucidate its effect on the initial cellular attachment and subsequent stimuli-triggered detachment ability.

Initial cellular attachment on a substrate is a protein mediated process that happens within the first hours of contact between the cells and the substrate.[50–52] Protein adsorption on a substrate is a prerequisite to cellular adhesion and both are governed by complex physicochemical interactions including steric, hydrophobic, electrostatic and van der Waals forces.[53,54] In general, cells adhere and grow more easily on hydrophobic surfaces than on hydrophilic ones due the difficulty to displace water molecules adsorbed on hydrophilic surfaces.[55,56] The results reported in chapter 5 showed that the relative cell density for the initial attachment of the bEnd.3 cell line on substrates coated with bare and surface-functionalized microgels was statistically similar to the controls (glass, PDMS). This observation agrees with previously published work, which consistently show that a variety of cell lines are able to attach, proliferate and grow on PNIPAM-coated substrates to a similar extent than the controls.[43,54,57–59] In chapter 5, cellular attachment on substrates coated with bare microgels and microgel-co-PDMAEMA is promoted by the hydrophobic character and net positive charge of the polymer layers at 37 °C, above the VPTT (see chapter 3). Substrates coated with microgel-co-PEG remained hydrophilic above the VPTT (chapter 3), thus, cellular attachment is mediated by the net positive charge (4 mV) of microgel-co-PEG at 37 °C. There was no effect of the substrate on the initial cellular attachment of bEnd.3

cells. However, the nature of the polymer coating and of the cell lines played an important role during the stimuli-triggered cellular detachment experiments.

Microgel-co-PEG showed the best ability to detach MCF7 and U138 cancer cell lines when the temperature was reduced below the VPTT of the PNIPAM microgel. It has been shown that cell detachment from a functionalized substrate takes place through changes in the conformation and hydration state of the polymer layer.[50,51] Upon decreasing the temperature of the media surrounding the cells attached on functionalized substrates, a clear trend towards lower relative cell densities was observed for U138 and MCF7 cells (see chapter 5). The cellular detachment was more significant when the temperature was reduced on day 5 compared to day 3 probably because cells were near confluent after 5 days of incubation and more likely to detach when a stimulus is applied.[60,61] Further, U138 and MCF7 cells grown on microgel-co-PEG substrates were the only ones that displayed statistically significant lower cell densities when the temperature was decreased below the VPTT. These results indicate that the thermo-triggered cell detachment improved when the PNIPAM microgels were surface-functionalized with PEG chains which enhanced the hydrophilicity of the polymer coatings even above the VPTT (chapter 3). This observation is supported by the results obtained with SPR, which demonstrated that the non-specific protein adsorption on substrates functionalized with microgel-co-PEG was significantly lower than that on bare microgel coatings above the VPTT (chapter 5). In addition, previous publications have also reported on the outstanding anti-fouling properties of PEG-functionalized surfaces.[62–64] Nevertheless, no significant thermo-triggered detachment was observed for bEnd.3 cells regardless of the incubation time and the substrate functionalization. The lack of detachment is explained by the different nature of bEnd.3 cells compared to MCF7 and U138.

bEnd.3 are endothelial cells and thus express high levels of PECAM-1 that makes them more adherent[65–67] compared to U138 and MCF7 cancerous cell lines, which exhibit a greater ability to invade other tissues through the EMT process that facilitates the dissociation of adherens junctions.[68–70] Previous publications have also reported that strongly adhesive cell lines are unable to detach from PNIPAM-based coatings by decreasing the temperature due to irreversible protein adsorption on the substrate.[43,49] Hence, the behaviors observed with bEnd.3 cells in chapter 5 are not unusual and illustrate an important limitation of the PNIPAM-based coatings proposed in this section of the thesis; namely, that the contribution of PEG to the cell detachment ability is not applicable to strongly adhesive cell lines. An alternative to enhance cellular detachment could be to surface-functionalize the PNIPAM microgels with photocleavable motifs linked to receptors that target integrins in the ECM, for example RGD or CD44,[30,71–73] as well as PEG. In this manner, it might be possible to maximize the cell detachment without the need to employ enzymatic digestion or mechanical scraping.

Decreasing the pH of the environment at 20 °C produced a clear trend towards reduced cell densities of MCF7 and significantly lowered the cell density of U138 while no detachment was observed for bEnd.3 cells. Variations in pH may mediate cellular detachment from a pH-responsive surface by decreasing the electrostatic interactions between a positively charged polymer coating and the negatively charged ECM.[74] The changes in surface potential of bare and surface-functionalized microgels between pH 7 and 2 were small, but the bare microgel and microgel-co-PDMAEMA layers were observed to swell with decreasing pH, and did so to a greater extent than the microgel-co-PEG ones (chapter 3). Because at 20 °C the PNIPAM microgels are hydrated, the combined effect of additional pH-triggered swelling and associated increase in the

hydrophilicity of the polymer layers were likely the reason behind the observed cell detachment.[53,75] In fact, the thermo- and pH-triggered swelling and increasing hydration of the microgel layers change the conformation of the proteins in the ECM which disturbs the tension forces of actin-based fibers that link the cytoskeleton of the cells to focal adhesion points on the ECM.[76–78] The disruption in tension forces signals the cell nuclei through mechanotransduction and produces morphological changes in the cells, from spread and flattened when attached to spherical, which promotes detachment from the substrate.[76,77,79] Because the mechanotransduction process requires a metabolic energy input, the metabolism rate of each cell line determines the degree of detachment that is ultimately observed.[54,80] This reason justifies the difference in detachment behaviors between U138, MCF7 and bEnd.3 cell lines. Similarly, the ability of polymer coatings to alter their swelling and hydrophilicity in response to pH or temperature variations will determine the amount of modification sustained by the proteins in the ECM. Hence, mechanotransduction theory suggests that microgel-co-PEG layers possess a more efficient cell detachment ability because of their more hydrophilic nature.

The initial attachment of bEnd.3 cells on microgel-functionalized substrates was similar to that observed on the controls while thermo- and pH-triggered cell detachment was more significant when using substrates functionalized with microgel-co-PEG. Considering the objective (iv) proposed at the beginning of this thesis, it is reasonable to conclude that it was accomplished. However, given the inability to detach bEnd.3 cells, a highly adherent cell type, regardless of the stimulus applied or the properties of the substrate, the proposed functional surfaces do not represent a breakthrough. Rather, it indicates that these PNIPAM-based surfaces can be useful to obtain stimuli-triggered cell detachment during the culture of specific cell lines or potentially in

applications that require anti-fouling properties such as implantable biomedical devices to prevent the development of biofilm.

References

(1) Bradley, M.; Vincent, B. Poly(Vinylpyridine) Core/Poly(N-Isopropylacrylamide) Shell Microgel Particles: Their Characterization and the Uptake and Release of an Anionic Surfactant. *Langmuir* **2008**, *24*, 2421–2425.

(2) Bai, Y.; Zhang, Z.; Zhang, A.; Chen, L.; He, C.; Zhuang, X.; Chen, X. Novel Thermo- and PH-Responsive Hydroxypropyl Cellulose- and Poly (L-Glutamic Acid)-Based Microgels for Oral Insulin Controlled Release. *Carbohydr. Polym.* **2012**, *89*, 1207–1214.

(3) Raju, R.; Bandyopadhyay, S.; Sharma, A.; Villa Gonzalez, S.; Carlsen, P. H.; Gautun, O. R.; Glomm, W. R. Synthesis, Characterization and Drug Loading of Multiresponsive p[NIPAm-Co-PEGMA] (Core)/p[NIPAm-Co-AAC] (Shell) Nanogels with Monodisperse Size Distributions. *Polymers* **2018**, *10*, 309–323.

(4) Liu, L.; Zeng, J.; Zhao, X.; Tian, K.; Liu, P. Independent Temperature and PH Dual-Responsive PMAA/PNIPAM Microgels as Drug Delivery Systems: Effect of Swelling Behavior of the Core and Shell Materials in Fabrication Process. *Colloids Surf., A* **2017**, *526*, 48–55.

(5) Zeiser, M.; Freudensprung, I.; Hellweg, T. Linearly Thermoresponsive Core-Shell Microgels: Towards a New Class of Nanoactuators. *Polymer* **2012**, *53*, 6096–6101.

(6) Cors, M.; Wrede, O.; Genix, A.-C.; Anselmetti, D.; Oberdisse, J.; Hellweg, T. Core-Shell Microgel-Based Surface Coatings with Linear Thermoresponse. *Langmuir* **2017**, *33*, 6804–6811.

(7) Sabadasch, V.; Wiehemeier, L.; Kottke, T.; Hellweg, T. Core-Shell Microgels as Thermoresponsive Carriers for Catalytic Palladium Nanoparticles. *Soft Matter* **2020**, *16*, 5422–5430.

(8) Li, M.; Bresson, B.; Cousin, F.; Fretigny, C.; Tran, Y. Submicrometric Films of Surface-Attached Polymer Network with Temperature-Responsive Properties. *Langmuir* **2015**, *31*, 11516–11524.

(9) Roy, A.; Comesse, S.; Grisel, M.; Hucher, N.; Souguir, Z.; Renou, F. Hydrophobically Modified Xanthan: An Amphiphilic but Not Associative Polymer. *Biomacromolecules* **2014**, *15*, 1160–1170.

(10) Campora, S.; Mohsen, R.; Passaro, D.; Samir, H.; Ashraf, H.; Al-Mofty, S.; Diab, A.; El-Sherbiny, I.; Snowden, M.; Ghersi, G. Functionalized Poly(N-Isopropylacrylamide)-Based Microgels in Tumor Targeting Drug Delivery. *Gels* **2021**, *7*, 203–220.

(11) Sanzari, I.; Buratti, E.; Huang, R.; Tusan, C.; Dinelli, F.; Evans, N.; Prodromakis, T.; Bertoldo, M. Poly(N-Isopropylacrylamide) Based Thin Microgel Films for Use in Cell Culture Applications. *Sci. Rep.* **2020**, *10*, 6126–6140.

(12) Zhao, C.; Hou, J.; Chen, R.; Xin, Z.; Shi, H.; Wong, S.-C.; Yin, J.; Shi, Q. Cell-Inspired Biointerfaces Constructed by Patterned Smart Hydrogels for Immunoassay in Whole Blood. *J. Mater. Chem. B* **2017**, *5*, 2315–2321.

(13) Hunter, R.; White, L.; Chan, D. *Foundations of Colloid Science*, 2nd ed.; Oxford University Press: New York, 2001.

(14) Grahame, D. The Electrical Double Layer and the Theory of Electrocapillarity. *Chem. Rev.* **1947**, *41*, 441–501.

(15) Gouy, M. Sur La Constitution de La Charge Électrique à La Surface d'un Electrolyte. *J. Phys. Théorique Appliquée* **1910**, *9*, 457–468.

(16) Chapman, D. L. A Contribution to the Theory of Electrocapillarity. *Philos. Mag.* **1913**, *25*, 475–481.
(17) Meunier, F.; Elaissari, A.; Pichot, C. Preparation and Characterization of Cationic Poly(n-Isopropylacrylamide) Copolymer Latexes. *Polym. Adv. Technol.* **1995**, *6*, 489–496.
(18) Göktas, M. Synthesis and Characterization of Temperature-Responsive Block Copolymers Using Macromonomeric Initiator. *Chem. Pap.* **2020**, *74*, 2297–2307.
(19) Stawski, D.; Nowak, A. Thermal Properties of Poly(N,N-Dimethylaminoethyl Methacrylate). *PLoS One* **2019**, *14*, e0217441.
(20) Rossi, N.; Jadhav, V.; Lai, B.; Maiti, S.; Kizhakkedathu, J. Stimuli-Responsive Cationic Terpolymers by RAFT Polymerization: Synthesis, Characterization, and Protein Interaction Studies. *J. Polmer Sci. Part A* **2008**, *46*, 4021–4029.
(21) Ivanova, E.; Dimitrov, I.; Kozarova, R.; Turmanova, S.; Apostolova, M. Thermally Sensitive Polypeptide-Based Copolymer for DNA Complexation into Stable Nanosized Polyplexes. *J. Nanoparticle Res.* **2013**, *15*, 1358–1368.
(22) Oroojalian, F.; Jahanafrooz, Z.; Chogan, F.; Rezayan, A. H.; Malekzade, E.; Rezaei, S.; Nabid, M. R.; Sahebkar, A. Synthesis and Evaluation of Injectable Thermosensitive Penta-Block Copolymer Hydrogel (PNIPAAm-PCL-PEG-PCL-PNIPAAm) and Star-Shaped Poly(CL-CO-LA)-b-PEG for Wound Healing Applications. *J. Cell. Biochem.* **2019**, *120*, 17194–17207.
(23) Bracke, M.; Bisschop, F.; Joos, P. Contact Angle Hysteresis Due to Surface Roughness. In *Trends in Colloid and Interface Science II. Progress in Colloid & Polymer Science*; Degiorgio, V., Ed.; Steinkopff, 1988; pp 251–259.
(24) Schwartz, A. Contact Angle Hysteresis: A Molecular Interpretation. *J. Colloid Interface Sci.* **1980**, *75*, 404–408.
(25) Vialar, P.; Merzeau, P.; Giasson, S.; Drummond, C. Compliant Surfaces under Shear: Elastohydrodynamic Lift Force. *Langmuir* **2019**, *35*, 15605–15613.
(26) Leon-Lopez, T.; Ortega-Vinuesa, J.; Bastos-Gonzalez, D.; Elaissari, A. Cationic and Anionic Poly-(N-Isopropylacrylamide) Based Submicron Gel Particles: Electrokinetic Properties and Colloidal Stability. *J. Phys. Chem. B* **2006**, *110*, 4629–4636.
(27) Leon-Lopez, T.; Elaissari, A.; Ortega-Vinuesa, J.; Bastos-Gonzalez, D. Hofmeister Effects on Poly(NIPAM) Microgel Particles: Macroscopic Evidence of Ion Adsorption and Changes in Water Structure. *ChemPhysChem* **2006**, *8*, 148–156.
(28) Xu, Y.; Bao, Y.; Liu, Z.; Zheng, Q.; Dong, Y.; Song, R.; Yang, B. Temperature-Sensitive Tribological Performance of Titanium Alloy Lubricated with PNIPAM Microgels. *Appl. Surf. Sci.* **2022**, *572*, 151392–151406.
(29) Liu, X.; Thormann, E.; Dedinaite, A.; Rutland, M.; Visnevskij, C.; Makuska, R.; Claesson, P. Low Friction and High Load Bearing Capacity Layers Formed by Cationic-Block-Non-Ionic Bottle-Brush Copolymers in Aqueous Media. *Soft Matter* **2013**, *9*, 5361–5371.
(30) Schmidt, M.; Franken, A.; Wilms, D.; Fehm, T.; Neubauer, H.; Schmidt, S. Selective Adhesion and Switchable Release of Breast Cancer Cells via Hyaluronic Acid Functionalized Dual Stimuli-Responsive Microgel Films. *ACS Appl. Bio Mater.* **2021**, *4*, 6371–6380.
(31) Friedrich, K. Polymer Composites for Tribological Applications. *Adv. Ind. Eng. Polym. Res.* **2018**, *1*, 3–39.
(32) Myshkin, N.; Kovalev, A. Adhesion and Surface Forces in Polymer Tribology - A Review. *Friction* **2018**, *6*, 143–155.

(33) Giraud, L.; Bazin, G.; Giasson, S. Lubrication with Soft and Hard Two-Dimensional Colloidal Arrays. *Langmuir* **2017**, *33*, 3610–3623.
(34) Banquy, X.; Charrault, E.; Giasson, S. Normal and Lateral Interactions between Thermosensitive Nanoparticle Monolayers in Water. *J. Phys. Chem. B* **2010**, *114* (30), 9721–9728.
(35) Han, L.; Yin, J.; Wang, L.; Chia, K.-K.; Cohen, R.; Rubner, M.; Ortiz, C.; Boyce, M. Tunable Stimulus-Responsive Friction Mechanisms of Polyelectrolyte Films and Tube Forests. *Soft Matter* **2012**, *8*, 8642–8650.
(36) Raviv, U.; Giasson, S.; Kampf, N.; Gohy, J.-F.; Jérôme, R.; Klein, J. Lubrication by Charged Polymers. *Nature* **2003**, *11* (425), 163–165.
(37) Li, A.; Su, F.; Chu, P.; Sun, J. Articular Cartilage Inspired Bilayer Coating on Ti6Al4V Alloy with Low Friction and High Load-Bearing Properties. *Appl. Surf. Sci.* **2020**, *515*, 146065–146075.
(38) Alves, N.; Pashkuleva, I.; Reis, R.; Mano, J. Controlling Cell Behavior Through the Design of Polymer Surfaces. *Small* **2010**, *6* (20), 2208–2220.
(39) Xue, C.; Choi, B.-C.; Choi, S.; Braun, P.; Leckband, D. Protein Adsorption Modes Determine Reversible Cell Attachment on Poly(N-Isopropyl Acrylamide) Brushes. *Adv. Funct. Mater.* **2012**, *22* (11), 2394–2401.
(40) Nash, M.; Carroll, W.; Foley, P.; Maguire, G.; O'Connell, C.; Gorelov, A.; Beloshapkin, S.; Rochev, Y. Ultra-Thin Spin Coated Crosslinkable Hydrogels for Use in Cell Sheet Recovery-Synthesis, Characterisation to Appliocation. *Soft Matter* **2012**, *8* (14), 3889–3899.
(41) Haraguchi, K.; Takehisa, T.; Ebato, M. Control of Cell Cultivation and Cell Sheet Detachment on the Surface of Polymer/Clay Nanocomposite Hydrogels. *Biomacromolecules* **2006**, *7* (11), 3267–3275.
(42) Xia, Y.; Gu, Y.; Zhou, X.; Xu, H.; Zhao, X.; Yaseen, M.; Lu, J. R. Controllable Stabilization of Poly(N-Isopropylacrylamide)-Based Microgel Films through Biomimetic Mineralization of Calcium Carbonate. *Biomacromolecules* **2012**, *13*, 2299–2308.
(43) Wei, J.; Cai, J.; Li, Y.; Wu, B.; Gong, X.; Ngai, T. Investigation of Cell Behaviors on Thermo-Responsive PNIPAM Microgel Films. *Colloids Surf., B.* **2015**, *132*, 202–207.
(44) Bischofberger, I.; Calzolari, D. C. E.; Trappe, V. Co-Nonsolvency of PNiPAM at the Transition between Solvation Mechanisms. *Soft Matter* **2014**, *10*, 8288–8295.
(45) Meng, T.; Xie, R.; Chen, Y.-C.; Cheng, C.-J.; Li, P.-F.; Ju, X.-J.; Chu, L.-Y. A Thermo-Responsive Affinity Membrane with Nano-Structured Pores and Grafted Poly(N-Isopropylacrylamide) Surface Layer for Hydrophobic Adsorption. *J. Memb. Sci.* **2010**, *349*, 258–267.
(46) Burdukova, E.; Li, H.; Ishida, N.; O'Shea, J.-P.; Franks, G. Temperature Controlled Surface Hydrophobicity and Interaction Forces Induced by Poly(N-Isopropylacrylamide). *J. Colloid Interface Sci.* **2010**, *342*, 586–592.
(47) Uhlig, K.; Wegener, T.; He, J.; Zeiser, M.; Bookhold, J.; Dewald, I.; Godino, N.; Jaeger, M.; Hellweg, T.; Fery, A.; Duschl, C. Patterned Thermoresponsive Microgel Coatings for Noninvasive Processing of Adherent Cells. *Biomacromolecules* **2016**, *17*, 1110–1116.
(48) Uhlig, K.; Wegener, T.; Hertle, Y.; Bookhold, J.; Jaeger, M.; Hellweg, T.; Fery, A.; Duschl, C. Thermoresponsive Microgel Coatings as Versatile Functional Compounds for Novel Cell Manipulation Tools. *Polymers* **2018**, *10* (6), 656–668.
(49) Cheng, X.; Canavan, H.; Graham, D.; Castner, D.; Ratner, B. D. Temperature Dependent

Activity and Structure of Adsorbed Proteins on Plasma Polymerized N-Isopropylacrylamide. *Biointerphases* **2006**, *1* (1), 61–72.
(50) Garcia, A.; Gallant, N. Stick and Grip: Measurement Systems and Quantitative Analyses of Integrin-Mediated Cell Adhesion Strength. *Cell Biochem. Biophys.* **2003**, *39*, 61–73.
(51) Pierres, A.; Benoliel, A. M.; Bongrand, P. Cell Fitting to Adhesive Surfaces: A Prerequisite to Firm Attachment and Subsequent Events. *Eur. Cells Mater.* **2002**, *3*, 31–45.
(52) Andrade, J. D.; Hlady, V. Protein Adsorption and Materials Biocompatibility: A Tutorial Review and Suggested Hypotheses. In *Biopolymers/Non-Exclusion HPLC*; Springer Berlin Heidelberg, 1986; pp 1–63.
(53) Kikuchi, A.; Okano, T. Nanostructured Designs of Biomedical Materials: Applications of Cell Sheet Engineering to Functional Regenerative Tissues and Organs. *J. Control. Release* **2005**, *101*, 69–84.
(54) Okano, T.; Yamada, N.; Okuhara, M.; Sakai, H.; Sakurai, Y. Mechanism of Cell Detachment from Temperature-Modulated, Hydrophilic-Hydrophobic Polymer Surfaces. *Biomaterials* **1995**, *16*, 297–303.
(55) Ratner, B. D.; Horbett, T.; Hoffman, A. Cell Adhesion to Polymeric Materials: Implications with Respect to Biocompatibility. *J. Biomed. Mater. Res.* **1975**, *9*, 407–422.
(56) Maroudas, N. G. Chemical and Mechanical Requierements for Fibroblast Adhesion. *Nature* **1973**, *244*, 353–354.
(57) Chen, L.; Yan, C.; Zheng, Z. Functional Polymer Surfaces for Controlling Cell Behaviors. *Mater. Today* **2018**, *21* (1), 38–59.
(58) Nagase, K.; Yamato, M.; Kanazawa, H.; Okano, T. Poly(N-Isopropylacrylamide)-Based Thermoresponsive Surfaces Provide New Types of Biomedical Applications. *Biomaterials* **2018**, *153*, 27–48.
(59) Fukumori, K.; Akiyama, Y.; Kumashiro, Y.; Kobayashi, J.; Yamato, M.; Sakai, K.; Okano, T. Characterization of Ultra-Thin Temperature-Responsive Polymer Layer and Its Polymer Thickness Dependency on Cell Attachment/Detachment Properties. *Macromol. Biosci.* **2010**, *10*, 1117–1129.
(60) Abercrombie, M. Contact Inhibition in Tissue Culture. *In Vitro* **1970**, *6*, 128–142.
(61) Martz, E.; Steinberg, M. The Role of Cell-Cell Contact in "Contact" Inhibition of Cell Devision: A Review and New Evidence. *J. Cell. Physiol.* **1972**, *79*, 189–210.
(62) Dobrovolskaia, M.; McNeil, S. Immunological Properties of Engineered Nanomaterials. *Nat. Nanotechnol.* **2007**, *2*, 469–478.
(63) Banerjee, I.; Pangule, R.; Kane, R. Antifouling Coatings: Recent Developments in the Design of Surfaces That Prevent Fouling by Proteins, Bacteria, and Marine Organisms. *Adv. Mater.* **2010**, *23*, 690–718.
(64) Shih, Y.-J.; Chang, Y.; Quemener, D.; Yang, H.-S.; Jhong, J.-F.; Ho, F.-M.; Higuchi, A.; Chang, Y. Hemocompatibility of Polyampholyte Copolymers with Well-Defined Charged Bias in Human Blood. *Langmuir* **2014**, *30*, 6489–6496.
(65) Sheibani, N.; Frazier, W. Down-Regulation of Platelet Endothelial Cell Adhesion Molecule-1 Results in Thrombospondin-1 Expression and Concerted Regulation of Endothelial Cell Phenotype. *Mol. Biol. Cell* **1998**, *9*, 701–713.
(66) Booth, R.; Kim, H. Characterization of a Microfluidic in Vitro Model of the Blood-Brain Barrier (MBBB). *Lab Chip.* **2012**, *12*, 1784–1792.

(67) Omidi, Y.; Campbell, L.; Barar, J.; Connell, D.; Akhtar, S.; Gumbleton, M. Evaluation of the Immortalised Mouse Brain Capillary Endothelial Cell Line, b.End3, as an in Vitro Blood-Brain Barrier Model for Drug Uptake and Transport Studies. *Brain Res.* **2003**, *990*, 95–112.
(68) Thiery, J. P. Epithelial-Mesenchymal Transitions in Tumor Progression. *Nat. Rev. Cancer* **2002**, *2*, 442–454.
(69) Puliafito, A.; Hufnagel, L.; Neveu, P.; Streitchan, S.; Sigal, A.; Fygenson, K.; Shraiman, B. Collective and Single Cell Behavior in Epithelial Contact Inhibition. *Proc. Natl. Acad. Sci.* **2012**, *109*, 739–744.
(70) Vogler, E. Structure and Reactivity of Water at Biomaterial Surfaces. *Adv. Colloid Interface Sci.* **1998**, *74*, 69–117.
(71) Pan, G.; Guo, Q.; Ma, Y.; Yang, H.; Li, B. Thermo-Responsive Hydrogel Layers Imprinted with RGDS Peptide: A System for Harvesting Cell Sheets. *Angew. Chemie Int. Ed.* **2013**, *52*, 6907–6911.
(72) Kohler, N.; Sun, C.; Fichtenholtz, A.; Gunn, J.; Fang, C.; Zhang, M. Methotrexate-Immobilized Poly(Ethylene Glycol) Magnetic Nanoparticles for MR Imaging and Drug Delivery. *Small* **2006**, *2*, 785–792.
(73) Liong, M.; Lu, J.; Kovochich, M.; Xia, T.; Ruehm, S. G.; Nel, A. E.; Tamanoi, F.; Zink, J. I. Multifunctional Inorganic Nanoparticles for Imaging, Targeting, and Drug Delivery. *ACS Nano* **2008**, *2*, 889–896.
(74) Cuvelier, D.; Théry, M.; Chu, Y.-S.; Dufour, S.; Thiéry, J.-P.; Bornens, M.; Nassoy, P.; Mahadevan, L. The Universal Dynamics of Cell Spreading. *Curr. Biol.* **2007**, *17*, 649–699.
(75) Li, L.; Zhu, Y.; Li, B.; Gao, C. Fabrication of Thermoresponsive Polymer Gradients for Study of Cell Adhesion and Detachment. *Langmuir* **2008**, *24* (23), 13632–13639.
(76) Dalby, M. Topographically Induced Direct Cell Mechanotransduction. *Med. Eng. Phys.* **2005**, *27*, 730–742.
(77) Ingber, D. Cellular Tensegrity: Defining New Rules of Biological Design That Govern the Cytoskeleton. *J. Cell Sci.* **1993**, *104*, 613–627.
(78) Ge, C.; Xiao, G.; Jiang, D.; Franceschi, R. Critical Role of the Extracellular Signal-Regulated Kinase-MAPK Pathway in Osteoblast Differentiation and Skeletal Development. *J. Cell Biol.* **2007**, *176*, 709–718.
(79) Maniotis, A.; Chen, C.; Ingber, D. Demonstration of Mechanical Connections between Integrins, Cytoskeletal Filaments, and Nucleoplasm That Stabilize Nuclear Structure. *Proc. Natl. Acad. Sci.* **1997**, *94*, 849–854.
(80) Chen, G.; Imanishi, Y.; Ito, Y. Effect of Protein and Cell Behavior on Pattern-Grafted Thermoresponsive Polymer. *J. Biomed. Mater. Res.* **1998**, *42*, 38–44.

Chapter 7 – Conclusions and Perspectives

The objective of this thesis was to propose an innovative solution to a common challenge associated to stimuli-responsive polymeric coatings: changes to the physical conformation or swelling are inexorably linked to variations to the surface properties. To confront this obstacle, a hierarchical structure was developed composed of a thermo-responsive microgel surface-functionalized with either pH-responsive or pH-insensitive polymer chains. Additionally, their application to cellular culture was studied. The steps taken to achieve our goal were (i) functionalizing the microgels with polymer chains, (ii) studying the independent tunability of the hierarchical microgels in suspension as well as immobilized on a substrate, (iii) determining if the independent control of swelling and surface properties influence the tribological behavior and (iv) investigating the performances of the developed coatings as substrates for cellular culture.

PEG and PDMAEMA polymer chains were successfully immobilized on the surface of the PNIPAM microgels using a "grafting to" methodology. The functionalization was confirmed spectroscopically by identifying the functional groups characteristic of the PEG and PDMAEMA chains on the spectra of the PNIPAM microgels by using NMR and ATR-FTIR after the purification by dialysis step. These techniques are commonly employed to confirm surface grafting. It was also observed that some surface properties specific to the PNIPAM microgel, such as the surface potential and non-specific protein adsorption, changed upon grafting the polymer chains and these results were used to support the spectroscopic analysis. Further, a theoretical approximation was applied to estimate the grafting density of the polymer chains on the microgels. Beyond the techniques presented in this thesis, TGA and DSC could provide additional

information that confirms the functionalization of the polymer chains on the microgels. However, due to the low concentration of the primary amines and the polymer chains relative to PNIPAM, the effect of functionalizing might not be significant. Previous work has shown that concentrations as high as 5 wt% in the reaction site are not sufficient to demonstrate that covalent bonding takes place.[1] To improve the signal of the polymer chains, the concentration of primary amines, and therefore the amount of polymer chains that are grafted to the microgels, should be significantly increased. Therefore, the concentration in primary amines should be increased to 15 – 20 wt% relative to PNIPAM. This alternative would, unfortunately, drastically alter the thermoresponsive and surface properties of the microgels reported in this thesis.

In suspension and on a substrate, it was shown that surface-functionalization allows to modulate the surface properties separately from the swelling and with no hindrance to the thermo-response of the PNIPAM microgels. Specifically, it was observed that with microgel-co-PEG the thermo-triggered swelling can happen with no change in the surface potential or adhesion. This is an important difference compared to the usual response of PNIPAM microgels, i.e., the swelling behavior is associated with significant variations in surface properties. Nevertheless, no adhesion could be measured when separating microgel-co-PDMAEMA layers in pH 10 media at 23 °C even though the PDMAEMA chains are deprotonated and promote adhesion via the attraction between the polymer chain segments under these environmental conditions.[2] The lack of adhesion suggests that the grafting density and the length of the PDMAEMA chains were insufficient to adequately express their behavior and differentiate it from that of the PNIPAM microgels. Indeed, the molar mass of the PDMAEMA chains reported in this thesis was of 4,800 g/mol, which translates to a contour length of 8 nm, roughly 3 % of the hydrodynamic diameter

of the PNIPAM microgel. Therefore, the effect of grafting PDMAEMA chains of higher molecular weight to the PNIPAM microgels could eventually be investigated to determine if the characteristic behavior of PDMAEMA can be enhanced without changing the VPTT of PNIPAM.

No significant impact to the tribological properties of bare and surface-functionalized microgels was measured by changing the pH of the media at 23 °C. The coefficients of friction calculated for all microgels were roughly 10 times higher than expected and did not vary significantly with the pH. Further, two critical technical challenges severely limited the quality of the gathered data as well as the scope of this section of the thesis. Namely, the inability to raise the temperature of the system above the VPTT of the PNIPAM microgels and a 16-fold loss in sensitivity of the friction device used to collect tribological data. Therefore, the results of this section are not conclusive, and are not complete enough for publication. The quickest options to overcome this problem involve, i) building a new friction device, which requires a significant investment, or ii) to cover the friction device with an insulating coating. However, the latter option is not recommended because it implies an additional loss in the sensitivity of the device. Another potential alternative is to perform the tribological studies using the AFM coupled to a thermostated liquid cell.[3–5] Even though the AFM is a powerful tool to characterize the nanotribological behavior of polymer materials, there is no precedent of it being used to study the tribological properties of PNIPAM microgels. At the moment, a viable option would be to collaborate (either by relocating or by sending samples) with laboratories equipped with the necessary instrumentation to perform this type of analysis. Similar tribological studies at elevated temperature and with adequate detection sensitivity are currently done by Dr. Hongbo Zeng at the University of Alberta in Edmonton or by

Dr. Carlos Drummond at the French National Centre for Scientific Research located at the University of Bordeaux.

The relevance that independently modulating the swelling and surface properties of surface-functionalized microgels to application in biomedicine was verified with cell culture studies. Initial cellular attachment was statistically similar between bare and surface-functionalized microgels compared to glass and PDMS controls. This suggests that surface functionalization does not impede cells to attach to a substrate. On the other hand, microgel-co-PEG showed the best ability to detach MCF7 and U138 cells when the temperature was reduced below the VPTT. The superior detachment ability of microgel-co-PEG was attributed to the enhanced hydrophilicity, which promotes detachment by increasing conformational changes of the proteins in the ECM that trigger morphological transitions of the cells via mechanotransduction mechanisms. The enhanced hydrophilicity of microgel-co-PEG was also exhibited in protein adsorption studies that revealed a higher anti-fouling ability above the VPTT relative to PNIPAM microgels. These results represent a significant improvement compared to cell culture substrates modified with PNIPAM, which is one of the most widely used polymers for thermo-responsive applications in biomedicine. However, bEnd.3 cells, a type of endothelial cells characterized by their strong adhesive abilities, were not observed to detach regardless of the applied stimulus or the nature of the substrate they were grown on. The absence of detachment ability represents a significant obstacle to widespread applicability of the developed surfaces and signals the need for further optimization. A simple way to improve the cell detachment ability involves increasing the length of the PEG chains surface-functionalized on the PNIPAM microgels to accentuate the hydrophilic character of the polymer network. It was reported in chapter 3 that the thermo-responsive ability

and surface potential could be independently modulated by using PEG chains of increasing molar mass (5,000 – 14,300 g/mol) and this might translate to an enhanced cell detachment ability. Nonetheless, it is vital to first determine that the initial cellular attachment does not decrease due to the additional steric repulsion caused by the longer PEG chains. A more complex approach would involve bi-functionalizing the surface of the PNIPAM microgels with PEG chains and with photocleavable molecules linked to a receptor that binds specifically to the proteins of the ECM. In this way, cellular detachment would be promoted by the increased hydrophilicity of PEG and amplified via external irradiation.

This thesis confirmed the possibility to obtain an independent control of the swelling ability and of the surface properties. The implications of this work are applicable to diverse technologies that require a fine-tuned control of the surface properties and particularly in the biomedical field as cell culture substrates, as additives to improve lubrication, to prevent biological fouling and prolong the lifetime of implantable devices, and as actuators in microfluidics. The motivation behind this work was to demonstrate the feasibility of a concept. It is not, however, limited to the polymers studied herein. A vast range of synthetic and biological macromolecules can be employed to develop surfaces like the ones presented in this work to further advance and refine the responsive surfaces that are currently in use and to create novel materials.

References

(1) Campora, S.; Mohsen, R.; Passaro, D.; Samir, H.; Ashraf, H.; Al-Mofty, S.; Diab, A.; El-Sherbiny, I.; Snowden, M.; Ghersi, G. Functionalized Poly(N-Isopropylacrylamide)-Based Microgels in Tumor Targeting Drug Delivery. *Gels* **2021**, *7*, 203–220.

(2) Nordgren, N.; Rutland, M. Tunable Nanolubrication between Dual-Responsive Polyionic Grafts. *Nano Lett.* **2009**, *9* (8), 2984–2990.

(3) Kim, S. H.; Marmo, C.; Somorjai, G. Friction Studies of Hydrogel Contact Lenses Using AFM: Non-Crosslinked Polymers of Low Friction at the Surface. *Biomaterials* **2001**, *22*, 3285–3294.

(4) Oguchi, T.; Sakai, K.; Sakai, H.; Abe, M. AFM Surface Morphology and Friction Force Studies of Microscale Domain Structures of Binary Phospholipids. *Colloids Surf., B.* **2010**, *79*, 205–209.

(5) Kienle, S.; Boettcher, K.; Wiegleb, L.; Urban, J.; Burgkart, R.; Lieleg, O.; Hugel, T. Comparison of Friction and Wear of Articular Cartilage on Different Length Scales. *J. Biomech.* **2015**, *48*, 3052–3058.